BRAIN ENERGY METABOLISM: DEVELOPMENT AND APPLICATION OF NOVEL LIVE METHODOLOGIES

A thesis submitted by

Rachel Bennett B.Sc. (Hons.)

to the

National University of Ireland, Maynooth

For the degree of Doctor of Philosophy

NUI MAYNOOTH

Ollscoil na hÉireann Má Nuad

Volume 1 of 1

Based on the research carried out in the

Department of Chemistry, Faculty of Science, National University of Ireland, Maynooth

under the supervision and direction of

Professor John P. Lowry

October 2012

TABLE OF CONTENTS

Declaration

I hereby certify that this thesis, which I now submit for assessment on the programme of study leading to the award of Ph.D., has not been submitted, in whole or part, to this or any other university for any degree, and is, except where otherwise stated the original work of the author. This thesis has not been submitted as an exercise for a degree at this or any other university and that it is entirely my own work.

Signed: _____

Rachel Bennett

This thesis is dedicated to my parents, with love.

Acknowledgements

First and foremost I would like to thank my supervisor Prof. John Lowry. Over the last number of years he has offered me support, patience, encouragement and guidance. Nothing is ever too much trouble and he has afforded me the opportunity to learn not from just him but from other research groups with numerous trips to other labs.

Funding from NUI Maynooth (John and Pat Hume Scholarship), Science Foundation Ireland (SFI) and the Centre of Applied Science for Health which is funded by the Higher Education Authority under the Programme for Research in Third Level Institutions (PRTLI) Cycle 4 is gratefully acknowledged.

A special thanks to Dr. Niall Finnerty, Dr. Fiachra Bolger and Dr. John Kealy. Niall, for his patience, kindness, knowledge, ability to make me laugh on a daily basis and numerous cups of tea. Nothing was ever too much trouble, his encouragement and understanding has helped me more than I can say over the past few years. Fiachra, for his knowledge, always being there for advice, encouragement and for the long hours spent on experiments, teaching and correcting. John, for everything over the past 2 years, his time in and out of the lab, encouragement, friendship and help whenever it was needed. I can never thank you all enough.

Thanks to the lads in the lab. Saidhbhe (for the years of friendship), Keeley and Andrea (for the music, criac and chats), Emma, Emer and new recruit Michelle. Ken (not just a lab mate but one of my closest friends) for always being there for me through thick and thin (and the Pierce family for the dinners, support and encouragement). Thanks to all the postgrads and post docs in the chemistry department for all the laughs, parties and tea room banter. I can't name everyone but I would like to mention Alanna, Laura, Louise Declan and Valaria for the friendship and chats. To the staff in the chemistry department for all their help over the years, especially Noel, who goes beyond and above the call of

duty for everyone. Thanks so much for the help over the years in particular the last few months.

Thank you to all my friends especially Aisling (the best housemate ever) and Donagh, Wayne, Theresa, Lisa, Naomi and Sinéad for always being there for me. To Keith, Ciaran, Paul, Martina, Joanne, Ronan, Natalie and Chris for the friendship, support and encouragement over the years. A special thank you to Brian, although we only met post-thesis showed me the enjoyment and fun to be had in life as well as the meaning of true friends.

Thank you to David Whelan for filling my life with love, happiness and joy.

Most importantly, I would like to thank my family who supported me throughout my studies. My parents, David and Cornelia, and brother John for their love and support. Aunty Gen, Uncle Andrew and Grandma for chats, help and for taking an interest. I'm finally finished!

"Remember to look up at the stars and not down at your feet….Be curious. And however difficult life may seem, there is always something you can do and succeed at.

It matters that you don't just give up."

-Stephen Hawking

Abbreviations

AA	Ascorbic Acid
aCSF	Artificial Cerebrospinal Fluid
Ag	Silver
ANLS	Astrocyte-Neuron Lactate Shuttle
ANOVA	Analysis of Variance
AUC	Area Under the Curve
BOLD	Blood Oxygen Level Dependent
BSA	Bovine Serum Albumin
CNS	Central Nervous System
CPA	Constant Potential Amperometry
CF	Carbon Fibre
CFE	Carbon Fibre Electrode
CPE	Carbon Paste Electrode
CPU	Central Processing Unit
CRCE	Carbon Rhoplex® Composite Electrode
CV	Cyclic Voltammetry

DPA	Differential Pulse Amperometry
ECF	Extracellular Fluid
FAD	Flavin Adenine Dinucleotide
fMRI	Functional Magnetic Resonance Imaging
FSV	Fast Scan Voltammetry
GOx	Glucose Oxidase
H_2O_2	Hydrogen Peroxide
HPLC	High Performance Liquid Chromatography
HVA	Homovanillic Acid
IVV	*In Vivo* Voltammetry
K_M	Michaelis-Menten Constant
LIVE	Long-Term *In Vivo* Electrochemistry
MMA	Methyl Methacrylate
NADH	Nicotinamide Adenine Dinucleotide
NMR	Nuclear Magnetic Resonance
O_2	Oxygen
PEA	L-α-phosphatidylethanolamine
PET	Positron Emission Tomography
PNS	Peripheral Nervous System
PPD/*o*-PD	Poly (*o*-Phenyldiamine)

Pt	Platinum
Pt/Ir	Platimun/Iridium
PVA	Polyvinyl Acetate
rCBF	regional Cerebral Blood Flow
SCE	Saturated Calomel Electrode
SEM	Standard Error of the Mean
TCNQ	Tetracyanoquinodimethane
TTF	Tetrathiafulvalene
UA	Uric Acid
V_{max}	Maximum enzymatic velocity

Abstract

This thesis investigates methods of studying brain energy metabolism with a specific focus on the substrates oxygen and glucose. It details the *in vitro* development and *in vivo* characterisation of microelectrochemical sensors for the detection of brain tissue oxygen, and the *in vivo* characterisation of oxygen and glucose electrodes in the hippocampus utilising the technique of long-term *in vivo* electrochemistry (LIVE).

Chapter 1 introduces the brain, energy metabolism and neurochemical analysis focusing on oxygen and glucose monitoring in the brain. Chapter 2 discusses the theory relevant to the studies performed in this work, whilst Chapter 3 is a detailed description of sensor construction and techniques used for the *in vivo* and *in vitro* characterisation of the sensors utilised in this thesis.

The results are divided into five sections. The first of these, Chapter 4, details the *in vitro* characterisation of carbon paste electrodes (CPEs) and a Pt-based electrode modified with a membrane, methyl methacrylate (Pt-MMA) and makes comparisons between these two types of electrodes for use *in vivo*. Following on from the *in vitro* characterisation chapter, Pt-MMA electrodes were fully characterised *in vivo* and comparisons were made with previously published CPE data detailed in Chapter 5.

The development and standardisation of a metal-free electrode for use in conjunction with fMRI studies for the detection of brain tissue oxygen is presented in Chapter 6. The complete *in vivo* characterisation of the fully characterised fMRI compatible O_2 electrode developed in the previous chapter is detailed in Chapter 7.

Chapter 8 demonstrates and characterises the simultaneous recording of oxygen and glucose using CPEs and a Pt-based glucose biosensor (Pt/PPD/GOx) in the hippocampus of freely-moving animals, and utilises these sensors to monitor brain energy metabolism in conjunction with a behavioural task. Finally, overall conclusions in relation to the work presented in this thesis are discussed in Chapter 9.

1. INTRODUCTION

1.1 Introduction

The complexity of the mammalian brain and its function has been of interest for hundreds of years. The brain and spinal cord make up the central nervous system (CNS) and the peripheral nervous system (PNS). The PNS and CNS work in conjunction to regulate homeostasis whilst the PNS is responsible for maintaining it. The brain has a multitude of roles such as sensory input and processing, movement coordination, sensation, behaviour (Campbell N, 1990), as well as higher cognitive functions such as emotions (anxiety, reward), imaginative thought, memory and language (Reinis & Goldman, 1982). The human brain has been divided into 3 main regions: The forebrain, midbrain and hindbrain. A brief summary of these regions and their functions is listed below.

- **Forebrain:** The forebrain is the largest part of the brain, most of which is made up of the cerebrum. Other important structures found in the forebrain include the thalamus, the hypothalamus and the limbic system.
    - ***Cerebrum;*** divided into 2 hemispheres connected by a mass of white matter, divided into 4 lobes:
        - Frontal lobe; Cortex (motor cortex).
        - Parietal lobe; Cortex (somatosensory cortex).
        - Temporal lobe; Cortex (auditory cortex).
        - Occipital lobe; Cortex (visual cortex).
    - ***Cerebral Cortex;*** grey matter, makes up the surface of each hemisphere of the cerebrum.
    - ***Limbic system;*** a collection of structures within the forebrain, is important in the formation of memories and in controlling emotions, decisions, motivation and learning:
        - Amygdala; memory and emotions.
        - Hippocampus; memory and spatial navigation.
    - ***Thalamus;*** relays sensory information to the cerebral cortex.

  - ***Hypothalamus;*** regulates visceral functions, such as temperature, reproductive functions, eating, sleeping (circadian rhythm) and the display of emotion.

- **Midbrain:** The midbrain sits between the forebrain and the hindbrain. It forms a major part of the brainstem; the name given to the part of the brain which connects the spinal cord and the forebrain.
  - ***Dorsal surface (tectrum).***
  - ***Ventral surface;*** cerebral peduncles, fibre bundles that contain axons that travel between the cerebral cortex, brainstem and spinal cord. These divide the brain into two halves and each half is divided by a band of grey matter, known as the substantia nigra into anterior and posterior regions. These structures are important in sensory processes such as vision and movement.
- **Hindbrain:** The hindbrain includes the cerebellum, the pons and the medulla oblongata which all function to collectively support vital processes in the body.
  - ***Cerebellum;*** co-ordination and error-checking during motor, perceptual and cognitive tasks.
  - ***Medulla oblongata;*** joined to the spinal cord and controls unconscious, essential, bodily functions such as breathing, swallowing, blood circulation and muscle tone.
  - ***The Pons;*** Located above the medulla, serves as a bridge to connect the brainstem and the cerebellum. The pons receives information from visual areas to control eye and body movements and also plays a role in controlling patterns of sleep and arousal. Information is relayed from the pons to the cerebellum to control the co-ordination of muscular movements and maintain equilibrium.

The brainstem is made up of the pons, medulla and midbrain. The medulla connects the brain to the spinal cord and its motor and sensory tracts allow communication between the brain and the rest of the body. A schematic of the brain can be seen in Figure 1.1.

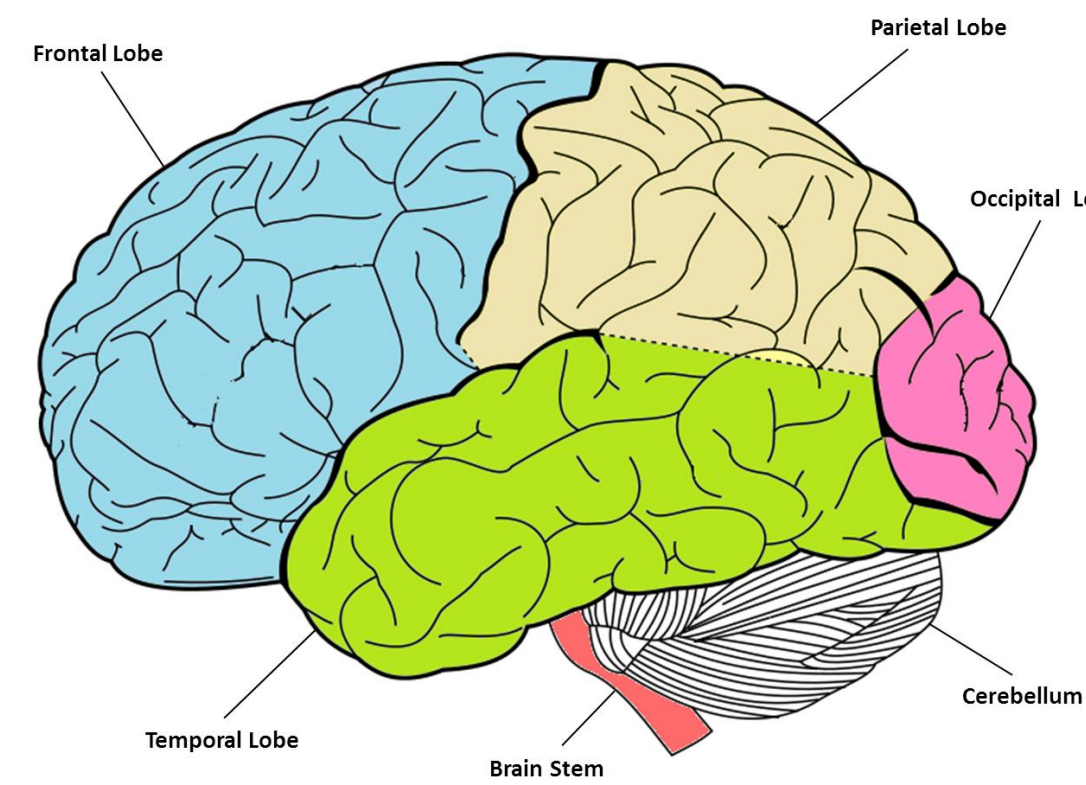

Figure 1.1: Schematic of the human brain detailing the four lobes of the cerebral cortex, the cerebellum and the brain stem.

The two main types of cell found in the brain are neurons and glial cells. Neurons are electrically excitable cells that are the functioning units in the brain which processes and transmits information through electrical and chemical signals (Figure 1.2). Glial cells provide support, protection and electrical insulation for neurons. Activation of neurons involves a stimulus which causes an electrical impulse (K^+, Na^+, Ca^{2+}) known as an action potential to pass through the axon to the axon terminal. The axon terminal contains synapses, where neurotransmitter release takes place. The neurotransmitters diffuse across the synaptic cleft and bind to receptors embedded in the postsynaptic membrane. The neurotransmitter molecules are either taken up by another neuron or quickly degraded by enzymes, terminating the synaptic response.

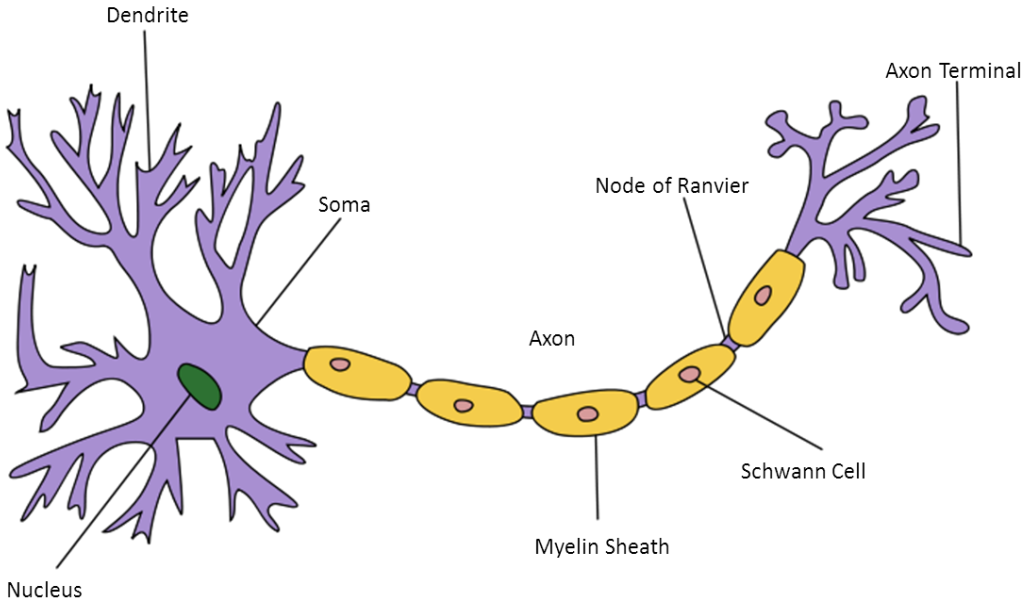

Figure 1.2: Schematic of a neuron.

This brief outline of the brain regions and their roles show the high complexity of the brain not just on an anatomical level but also on a functional and cellular level. A large amount of research has been conducted exploring the structure of the brain as well as the roles of neurochemicals in brain metabolism and signalling.

1.2 Analytical Techniques

A number of techniques are used to investigate structures, metabolism and neurochemicals in the brain ranging from non-invasive techniques such as blood oxygenation dependent (BOLD) functional magnetic imaging (fMRI) (Ogawa *et al.*, 1990; Ogawa *et al.*, 1992), positron emission tomography (PET) (Weaver *et al.*, 2007), two-photon fluorescence imaging of NADH (Kasischke *et al.*, 2004), spectroscopic analyses, ^{1}H-NMR (Mangia *et al.*, 2003) and ^{13}C-NMR (Rothman *et al.*, 1992), to invasive techniques such as microdialysis (Ungerstedt & Pycock, 1974; Fray *et al.*, 1996; McNay & Gold, 1999) and *in vivo* voltammetry (O'Neill *et al.*, 1998; O'Neill & Lowry, 2000).

1.3 *In Vivo* Neurochemical Analysis

1.3.1.1 *In Vivo* Voltammetry (IVV)

IVV allows for the direct monitoring of chemicals in the brain's extracellular fluid (ECF). The first reports of voltammetry in the brain date back as far as 1958 (Clark *et al.*, 1958; Clark Jr & Lyons, 1965) where oxygen and ascorbic acid were monitored. However, Adams and co-workers (Kissinger *et al.*, 1973; Adams, 1976) are credited with pioneering the technique. Many different methodologies have been developed such as constant potential amperometry (CPA), cyclic voltammetry (CV), differential pulse amperometry (DPA), fast scan voltammetry (FCV) and chronoamperometry. The basis of voltammetric techniques is that a chemical is either oxidised or reduced at the sensor's surface by applying a potential. The measured faradaic current is proportional to the concentration of the chemical at the active surface of the sensor (Marsden *et al.*, 1988; Adams, 1990). IVV is a popular choice for neurochemical monitoring and there are a number of electroactive species present in the ECF that have been detected using this technique such as ascorbic acid (O'Neill & Fillenz, 1985a; Boutelle *et al.*, 1989; O'Neill, 1995), homovanillic acid (HVA) (O'Neill & Fillenz, 1985b), uric acid (UA) (O'Neill, 1990), nitric oxide (Brown *et al.*, 2005; Finnerty *et al.*, 2012a; Finnerty *et al.*, 2012b) and oxygen (Lowry *et al.*, 1996; Bolger & Lowry, 2005; Bolger *et al.*, 2011b). However, the detection of non-electroactive species such as enzymatic substrates and amino acids are not possible without the use of modified electrodes discussed in Section 1.4. Biosensors have been developed to monitor substrates such as glucose (Lowry *et al.*, 1994b; Hu & Wilson, 1997a; Fillenz & Lowry, 1998; Lowry *et al.*, 1998a; Lowry *et al.*, 1998b; Dixon *et al.*, 2002), glutamate (Kulagina *et al.*, 1999; McMahon *et al.*, 2006a, b; McMahon *et al.*, 2007; Qin *et al.*, 2008; Tian *et al.*, 2009) and lactate (Hu & Wilson, 1997b).

IVV is superior to microdialysis (Section 1.3.1.2) in terms of temporal resolution with real-time data acquisition, minimal ECF depletion, smaller probe size and IVV is now possible using wireless technology (Serra *et al.*, 2007; Bazzu *et al.*, 2009; Calia *et al.*, 2009; Russell *et al.*, 2012). However, the disadvantages of this technique are issues with

selectivity and sensitivity, therefore limiting the amount of analytes it is possible to measure. The differences in behaviour of the sensors in a tissue matrix and buffer solution (Cheng *et al.*, 1979; Dayton *et al.*, 1983; Nicholson & Syková, 1998) can also cause disparities between the sensitivity, stability and selectivity of the sensors.

1.3.1.2 Microdialysis

Microdialysis is a popular technique for *in vivo* neurochemical analysis. It allows for the sampling of metabolites and neurochemicals. The technique was developed in 1974 (Ungerstedt & Pycock, 1974) and uses the principle of dialysis. A membrane in the form of a microdialysis probe (Figure 1.3) is implanted into the brain tissue and is perfused with a liquid know as the perfusate (i.e. aCSF). The perfusate equilibrates with the ECF by means of diffusion. The extent of equilibration is dependent on factors such as flow rate, membrane length and molecular size. The dialysate is collected and analysed usually by high performance liquid chromatography (HPLC).

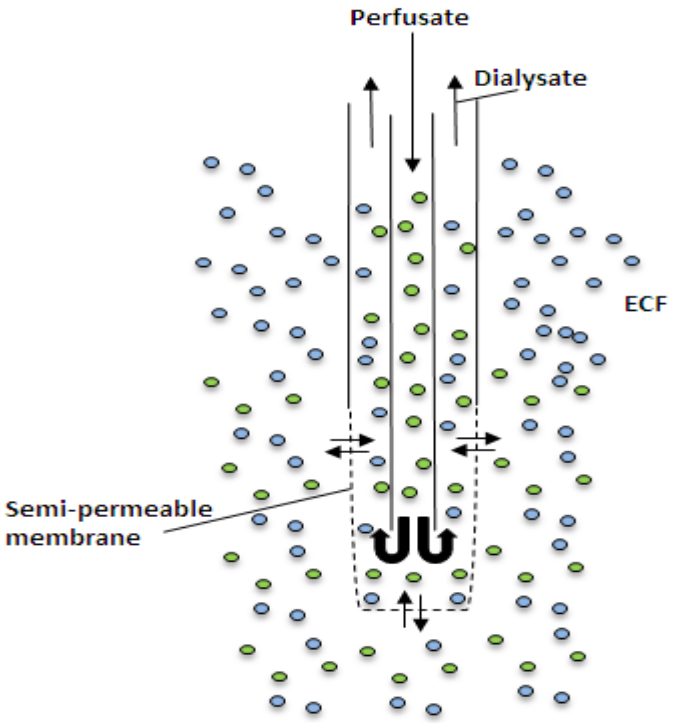

Figure 1.3: Schematic of a microdialysis probe.

Microdialysis in combination with a suitable detection technique allows for the monitoring of time-dependent changes in local tissue chemistry (neurotransmitter release and reuptake, drug delivery and energy metabolism) in particular brain regions. Microdialysis also allows for the detection of basal concentrations of particular analytes as well as physiologically or pharmacologically stimulated release. The technique has proven to be useful in the clinical environment where it has been used to routinely monitor head injury patients (Goodman *et al.*, 1999; Hutchinson *et al.*, 2000; Glenn *et al.*, 2003) and allowed for the detection of ischemia and secondary brain injury via the identification of markers (Zauner *et al.*, 1997; Sarrafzadeh *et al.*, 2003; Vespa *et al.*, 2003). The main disadvantages of microdialysis (classical) is its poor temporal resolution (30-60 mins (Feuerstein *et al.*, 2010)), although recently reports of real-time (30 s) microdialysis with on-line electrochemical detection have been described (Parkin *et al.*, 2003; Hopwood *et al.*, 2005; Parkin *et al.*, 2005), depletion of ECF chemicals and

large probe size. However, it is by far superior to other techniques as it offers unlimited selectivity for analytes.

1.4 Electrochemical Sensors

The advantages of IVV have previously been discussed in Section 1.3.1.1. The analyses of specific substrates is dependent on whether a method of detection for that particular substrate has been developed and if so can it be reliably detected without interference from other species present in the ECF. The specificity and selectivity of microelectrochemical sensors will be discussed in the subsequent sections. A chemical sensor is a device that transforms chemical information into an analytically useful signal. Chemical sensors contain usually two basic components connected in series: a chemical (molecular) recognition system (receptor) and a transducer. Biosensors are chemical sensors in which the recognition system utilises a biochemical mechanism (Cammann, 1977; Clark *et al.*, 1987).

1.4.1 *Biosensors*

There are three sub-divisions of amperometric biosensors (Thévenot *et al.*, 2001). They are categorised by the means by which the electrons reach the electrode surface and are defined by the term generation of amperometric biosensors (Wang, 1993).

- **First-generation:** Monitor the consumption of oxygen (McArthur *et al.*, 1962) or the production of hydrogen peroxide (H_2O_2) (Updike & Hicks, 1967). For the oxidation of H_2O_2 to occur a large over-potential is required which potentially results in interference from other oxidisable species such as ascorbic acid.
- **Second-generation:** Include a mediator species which acts as an electron transfer agent. This eliminates the biosensor's dependence on oxygen which removes the need for the high over-potential (El Atrash & O'Neill, 1995). However, leaching of potentially toxic mediators from the immobilisation matrix (O'Neill & Lowry, 2000) have been reported.

- **Third-generation:** Involve direct electron transfer between the redox site of the enzyme and the active surface of the electrode. Examples of these biosensors include the organic-conducting-salts, examples being tetrathiafulvalene (TTF) and tetracyanoquinodimethane (TCNQ) (Albery *et al.*, 1985). The presence of these salts make the surface highly reversible and stable to enzymes (Bartlett, 2003). These biosensors have been shown to involve a mediated mechanism implying second-generation behaviour (O'Neill & Lowry, 2000).

This body of work employs first-generation biosensors. The immobilisation of the biological recognition unit of the electrode is one of the main challenges of biosensor construction. The amount of enzyme present on the surface of the electrode has a direct effect on the sensitivity of the electrode. Enzyme immobilisation can be achieved using a number of techniques such as physisorption, cross-linking or entrapment in or behind a membrane or a mixture of these methods (Pantano & Kuhr, 1995; Eggins, 2002).

One of the principal difficulties with IVV is the presence of endogenous electroactive species. For first-generation biosensors the principal interferent is ascorbic acid (AA). AA oxidises at similar potentials to that of H_2O_2. Polymer membranes have been employed for interference rejection. These polymer layers which have a low permeability to interferents but still remain permeable to H_2O_2 are deposited on the surface of the electrode. 1,2-diaminobenzene (*o*-phenylenediamine) has these characteristics when electropolymerised onto the electrode surface (Chiba *et al.*, 1987; Almeida *et al.*, 1990; Sasso *et al.*, 1990; Lowry & O'Neill, 1994; Losito *et al.*, 2003). *o*-PD also allows incorporation of enzymes into the structure which allowed for the successful development of the glucose biosensor containing the enzyme glucose oxidase (Lowry *et al.*, 1998b).

1.5 Oxygen

Brain tissue oxygen (O_2) is one of the most important energy substrates for brain energy metabolism with brain cells critically dependent on a continuous supply. It is thought that at any given time the brain consumes approximately 20% of the total O_2 used by the

body. O_2 is delivered by the blood and the tissue concentration is determined by the balance of supply and utilisation (Magistretti *et al.*, 2000). Molecular O_2 was one of the first substances to be detected voltammetrically *in vivo* in the brain (Clark *et al.*, 1958; Clark Jr & Lyons, 1965) and in peripheral tissue (Clark Jr & Clark, 1964). In different brain regions the O_2 turnover rate varies and it has been established that the cerebral cortex has a higher turnover rate than others (Nair *et al.*, 1987). The concentration of O_2 in the brain varies as supply is altered in different layers of the brain tissue (Baumgärtl *et al.*, 1989) and is dependent on the tissue heterogeneity (Murr *et al.*, 1994; Lubbers & Baumgärtl, 1997). O_2 tissue concentrations have been reported to range from 40 µM (Murr *et al.*, 1994), 50 µM (Zimmerman & Wightman, 1991), 60 µM (Zauner *et al.*, 1995) to 80 µM (McCreery *et al.*, 1990).

Carbon-based electrodes such as glassy carbon (Clark Jr & Clark, 1964), carbon fiber electrodes (Zimmerman & Wightman, 1991; Zimmerman *et al.*, 1992; Venton *et al.*, 2003), carbon epoxy (Bazzu *et al.*, 2009) and carbon paste electrodes (Lowry *et al.*, 1996; Lowry *et al.*, 1997; Bolger & Lowry, 2005; Bolger *et al.*, 2011b) are commonly used for detecting changes in tissue O_2. Carbon electrodes have their advantages and disadvantages over noble metal electrodes. The main advantage of carbon fibre electrodes (CFEs) and carbon paste electrodes (CPEs) for use *in vivo* are that they are less susceptible to surface poisoning than noble metal electrodes, which usually require the addition of a protective membrane (Wisniewski *et al.*, 2000; Zhao *et al.*, 2001; Gifford *et al.*, 2006). CFEs (Zimmerman & Wightman, 1991) are advantageous due to their small diameter (5-50 µm), however if placed closely to blood vessels or metabolically active sites the O_2 concentration can vary (Lowry *et al.*, 1997). CPEs are advantageous as *in vivo* they are stable over long periods (O'Neill, 1993; O'Neill & Lowry, 1995; O'Neill, 2005; Bolger *et al.*, 2011b). CPEs have a diameter of 200 µm greater than the scale of the capillary zone (<100 µm) (Silver, 1965) which allows detection of average tissue O_2 levels. However due to their size they do cause greater tissue damage than noble metal electrodes.

Platinum(Pt)-based electrodes have been shown to be a potential alternative to CPEs to monitor brain tissue O_2 (Bolger *et al.*, 2011a). Pt electrodes are easier to manufacture

than CPEs and have a smaller diameter (125 µm) resulting in less tissue damage which makes them more desirable for use. However, they are prone to surface poisoning characteristic of metal-based electrodes and therefore require protective membranes making them only suitable for use in short-term experiments.

1.6 Brain Energy Metabolism

Increases in brain energy metabolism requirements are thought to have been met by an increase in blood flow that delivers glucose and oxygen to the extracellular compartment, according to the classical model of brain energy metabolism (Siesjö, 1978). In this model there is close coupling between blood flow and the delivery and utilisation of glucose and oxygen. This theory has been replaced by the compartmentalisation model known as the astrocyte-neuron-lactate shuttle (ANLS) theory (Pellerin & Magistretti, 1994). This theory hypothesises that lactate produced by the astrocytes is used as an energy source by activated neurons. A causal sequence of events is postulated to lead to the uptake of lactate by the neurons, beginning with the release of glutamate from nerve terminals upon stimulation whereupon it enters the astrocytes surrounding the synaptic complex. The uptake of glutamate is Na^+-dependent and stimulates Na/K ATPase leading to the uptake of glucose into the astrocytes. This glucose undergoes glycolysis which results in the production of lactate which is exported into the extracellular space whereupon it is subsequently taken up by the neurons for its ultimate oxidative phosphorylation. In summary this model suggests that increased energy requirements of activated neurons are met by the utlisation of lactate not glucose by these neurons and the lactate is being provided by astrocytic glycolysis, stimulated by the uptake of glutamate. This model has been supported by experiments using brain slices (Schurr *et al.*, 1988), cell cultures (Tsacopoulos & Magistretti, 1996) and NMR (Sibson *et al.*, 1998), however this theory has had many challenges as discussed by Fillenz (2005). The temporal relationships between these processes cannot be examined using these techniques therefore *in vivo* neurochemical analysis has been used to monitor changes in metabolic substrates. As these techniques can be utilised in freely-moving animals it is possible to related changes in neuronal activity to specific brain regions.

Microdialysis has been employed to examine brain energy metabolism. Using this technique it has been demonstrated that there is a stimulation-dependent increase in lactate correlated to glutamate uptake (Fray *et al.*, 1996; Demestre *et al.*, 1997) and it has been shown that there is a dissociation between increases in regional cerebral blood flow (rCBF) and increases in ECF glucose (Fray *et al.*, 1996). These results support employment of lactate as an energy substrate and they also propose that glucose in the EC compartment is not directly resulting from the blood vascular compartment. The immediate source of EC glucose has led to debate amongst advocates of the compartmental model as it has been found that astrocytes in cell culture export lactate and not glucose (Dringen *et al.*, 1993) which has led to Magistretti and Pellerin (1996) suggesting that glucose enters the EC space directly from the blood stream.

As discussed previously IVV allows for investigations of the functions and roles of specific neurochemicals in neuronal signalling, drug actions, and well-defined behaviours in real-time. A glucose biosensor for use *in vivo* has been developed for the detection of brain glucose (Lowry *et al.*, 2002). The Pt/PPD/GOx electrode is an amperometric biosensor and was constructed by immobilising the enzyme glucose oxide (GOx) onto a platinum microelectrode via the polymererisation of poly (*o*-phenylenediamine) (PPD) on the electrode surface. This biosensor was characterised *in vitro* (Lowry *et al.*, 1994a; Lowry *et al.*, 1994b) and subsequently modified, implanted and characterised *in vivo* in freely-moving rats (Lowry *et al.*, 1998b). The characterisation of the Pt/PPD/GOx electrode established the electrode had a high sensitivity, selectivity and was not hindered by endogenous species in the brain resulting in fowling. This sensor has been utilised to study brain energy metabolism (Fillenz & Lowry, 1998; Lowry & Fillenz, 2001) and is used in conjunction with and oxygen (carbon paste) electrodes to simultaneously monitor glucose and oxygen levels in the hippocampus (Chapter 8).

1.7 Conclusions

In summary, the use of *in vivo* voltammetry (IVV) and microelectrochemical sensors provides advancements in the exploration of metabolic processes such as neurovascular

coupling present in the mammalian brain. IVV can provide real-time monitoring of metabolic substrates and neurotransmitters which can translate as a useful tool for a better understanding of the metabolic and chemical processes in the healthy brain, disease states and aid in the development of therapeutic applications such as drug discovery. It also has the potential to be an invaluable clinical tool for the monitoring of brain metabolism.

This thesis details the *in vitro* development and *in vivo* characterisation of microelectrochemical sensors for the detection of brain tissue oxygen and the *in vivo* characterisation of oxygen and glucose electrodes in the hippocampus. This chapter (Chapter 1) introduces the brain, brain energy metabolism and neurochemical analysis focusing on oxygen and glucose monitoring in the brain. Chapter 2 discusses the theory relevant to the studies performed in this work, whilst Chapter 3 is a detailed description of sensor construction and techniques used for the *in vivo* and *in vitro* characterisation of the sensors utilised in this thesis. The *in vitro* characterisation of CPEs and a Pt-based electrode modified with a membrane (MMA) which is potentially suitable for use in the clinical environment, and the comparisons between these two types of electrodes are presented in Chapter 4. Chapter 5 details the *in vivo* characterisation of the Pt-MMA electrode characterised in the previous chapter. The development and standardisation of a metal-free electrode for use in conjunction with fMRI studies for the detection of brain tissue oxygen is presented in Chapter 6 and the full *in vivo* characterisation of this electrode is described in Chapter 7. Chapter 8 demonstrates and characterises the simultaneous recording of oxygen and glucose in the hippocampus of freely-moving animals and the use of these sensors to monitor brain energy metabolism in conjunction with a behavioural task. Overall conclusions in relation to the work presented in this thesis are discussed in Chapter 9.

References

Adams RN. (1976). Probing brain chemistry with electroanalytical techniques. *Analytical chemistry* **48,** 1126A.

Adams RN. (1990). *In vivo* electrochemical measurements in the CNS. *Progress in Neurobiology* **35,** 297.

Albery WJ, Bartlett PN & Cranston DH. (1985). Amperometric enzyme electrodes. Part II. Conducting salts as electrode materials for the oxidation of glucose. *Electroanalytical Chemistry* **194,** 223-235.

Almeida NF, Wingard J & Malmros MK. (1990). Immobilization of Glucose Oxidase by Electropolymerization of Monomers: Influence of Polymerization Conditions. *Annals of the New York Academy of Sciences* **613,** 448-451.

Bartlett PN. (2003). Conducting Organic Salt Electrodes. In *Biosensors: A Practical Approach*, ed. Cass AEG, pp. 47-95. Oxford University Press, Oxford.

Baumgärtl H, Heinrich U & Lübbers D. (1989). Oxygen supply of the blood-free perfused guinea-pig brain in normo-and hypothermia measured by the local distribution of oxygen pressure. *Pflügers Archiv European Journal of Physiology* **414,** 228-234.

Bazzu G, Puggioni GGM, Dedola S, Calia G, Rocchitta G, Migheli R, Desole MS, Lowry JP, O'Neill RD & Serra PA. (2009). Real-Time Monitoring of Brain Tissue Oxygen Using a Miniaturized Biotelemetric Device Implanted in Freely Moving Rats. *Analytical chemistry* **81,** 2235-2241.

Bolger F & Lowry J. (2005). Brain Tissue Oxygen: *In Vivo* Monitoring with Carbon Paste Electrodes. *Sensors* **5,** 473-487.

Bolger FB, Bennett R & Lowry JP. (2011a). An *in vitro* characterisation comparing carbon paste and Pt microelectrodes for real-time detection of brain tissue oxygen. *The Analyst* **136,** 4028-4035.

Bolger FB, McHugh SB, Bennett R, Li J, Ishiwari K, Francois J, Conway MW, Gilmour G, Bannerman DM, Fillenz M, Tricklebank M & Lowry JP. (2011b).

Characterisation of carbon paste electrodes for real-time amperometric monitoring of brain tissue oxygen. *Journal of neuroscience methods* **195,** 135-142.

Boutelle M, Svensson L & Fillenz M. (1989). Rapid changes in striatal ascorbate in response to tail-pinch monitored by constant potential voltammetry. *Neuroscience* **30,** 11-17.

Brown FO, Finnerty NJ, Bolger FB, Millar J & Lowry JP. (2005). Calibration of NO sensors for *in-vivo* voltammetry: laboratory synthesis of NO and the use of UV-visible spectroscopy for determining stock concentrations. *Analytical and bioanalytical chemistry* **381,** 964-971.

Calia G, Rocchitta G, Migheli R, Puggioni G, Spissu Y, Bazzu G, Mazzarello V, Lowry JP, O'Neill RD, Desole MS & Serra PA. (2009). Biotelemetric Monitoring of Brain Neurochemistry in Conscious Rats Using Microsensors and Biosensors. *Sensors* **9,** 2511-2523.

Cammann K. (1977). Bio-sensors based on ion-selective electrodes. *Fresenius' Journal of Analytical Chemistry* **287,** 1-9.

Campbell N A. (1990). Biology. *The Benjamin/Cummings Publishing Company, Inc*.

Cheng HY, Schenk J, Huff R & Adams RN. (1979). *In vivo* electrochemistry: behavior of micro electrodes in brain tissue. *Journal of Electroanalytical Chemistry and Interfacial Electrochemistry* **100,** 23-31.

Chiba K, Ohsaka T, Ohnuki Y & Oyama N. (1987). Electrochemical Preparation Of A Ladder Polymer Containing Phenazine Rings. *Journal of Electroanalytical Chemistry* **219,** 117-124.

Clark Jr L & Clark E. (1964). Epicardial oxygen measured with a pyrolytic graphite electrode *The Alabama Journal of Medical Sciences* **1,** 142.

Clark Jr L & Lyons C. (1965). Studies of a glassy carbon electrode for brain polarography with observations on the effect of carbonic anhydrase inhibition. *The Alabama Journal of Medical Sciences* **2,** 353.

Clark L, Turner A, Karube I & Wilson G. (1987). Biosensors: Fundamentals and Applications. Oxford University Press, New York.

Clark LC, Misrahy G & Fox RP. (1958). Chronically implanted polarographic electrodes. *Journal of Applied Physiology* **13,** 85-91.

Dayton MA, Ewing AG & Wightman RM. (1983). Diffusion processes measured at microvoltammetric electrodes in brain tissue. *Journal of Electroanalytical Chemistry and Interfacial Electrochemistry* **146,** 189-200.

Demestre M, Boutelle M & Fillenz M. (1997). Stimulated release of lactate in freely moving rats is dependent on the uptake of glutamate. *The Journal of Physiology* **499,** 825-832.

Dixon BM, Lowry JP & O'Neill RD. (2002). Characterization *in vitro* and *in vivo* of the oxygen dependence of an enzyme/polymer biosensor for monitoring brain glucose. *Journal of neuroscience methods* **119,** 135-142.

Dringen R, Gebhardt R & Hamprecht B. (1993). Glycogen in astrocytes: possible function as lactate supply for neighboring cells. *Brain Research* **623,** 208-214.

Eggins BR. (2002). *Chemical Sensors and Biosensors*. John Wiley & Sons Ltd., Chichester, Uk.

El Atrash SS & O'Neill RD. (1995). Characterisation in vitro of a naphthoquinone-mediated glucose oxidase-modified carbon paste electrode designed for neurochemical analysis *in vivo*. *Electrochimica Acta* **40,** 2791-2797.

Feuerstein D, Manning A, Hashemi P, Bhatia R, Fabricius M, Tolias C, Pahl C, Ervine M, Strong AJ & Boutelle MG. (2010). Dynamic metabolic response to multiple spreading depolarizations in patients with acute brain injury: an online microdialysis study. *Journal of Cerebral Blood Flow & Metabolism* **30,** 1343-1355.

Fillenz M. (2005). The role of lactate in brain metabolism. *Neurochemistry international* **47,** 413-417.

Fillenz M & Lowry J. (1998). The relation between local cerebral blood flow and extracellular glucose concentration in rat striatum. *Experimental Physiology* **83,** 233-238.

Finnerty NJ, O'Riordan SL, Brown FO, Serra PA, O'Neill RD & Lowry JP. (2012a). *In vivo* characterisation of a Nafion®-modified Pt electrode for real-time nitric oxide monitoring in brain extracellular fluid. *Analytical Methods* **4,** 550-557.

Finnerty NJ, O'Riordan SL, Palsson E & Lowry JP. (2012b). Brain nitric oxide: Regional characterisation of a real-time microelectrochemical sensor. *Journal of neuroscience methods*.

Fray AE, Forsyth RJ, Boutelle MG & Fillenz M. (1996). The mechanisms controlling physiologically stimulated changes in rat brain glucose and lactate: a microdialysis study. *The Journal of Physiology* **496,** 49-57.

Gifford R, Kehoe JJ, Barnes SL, Kornilayev BA, Alterman MA & Wilson GS. (2006). Protein interactions with subcutaneously implanted biosensors. *Biomaterials* **27,** 2587-2598.

Glenn TC, Kelly DF, Boscardin WJ, McArthur DL, Vespa P, Oertel M, Hovda DA, Bergsneider M, Hillered L & Martin NA. (2003). Energy dysfunction as a predictor of outcome after moderate or severe head injury: indices of oxygen, glucose, and lactate metabolism. *Journal of Cerebral Blood Flow & Metabolism* **23,** 1239-1250.

Goodman JC, Valadka AB, Gopinath SP, Uzura M & Robertson CS. (1999). Extracellular lactate and glucose alterations in the brain after head injury measured by microdialysis. *Critical Care Medicine* **27,** 1965-1973.

Hopwood SE, Parkin MC, Bezzina EL, Boutelle MG & Strong AJ. (2005). Transient changes in cortical glucose and lactate levels associated with peri-infarct depolarisations, studied with rapid-sampling microdialysis. *Journal of Cerebral Blood Flow & Metabolism* **25,** 391-401.

Hu Y & Wilson GS. (1997a). Rapid Changes in Local Extracellular Rat Brain Glucose Observed with an *In Vivo* Glucose Sensor. *Journal of Neurochemistry* **68,** 1745-1752.

Hu Y & Wilson GS. (1997b). A Temporary Local Energy Pool Coupled to Neuronal Activity: Fluctuations of Extracellular Lactate Levels in Rat Brain Monitored with Rapid Response Enzyme Based Sensor. *Journal of Neurochemistry* **69,** 1484-1490.

Hutchinson P, Al-Rawi P, O'Connell M, Gupta A, Maskell L, Hutchinson D, Pickard J & Kirkpatrick P. (2000). On-line monitoring of substrate delivery and brain metabolism in head injury. *Acta neurochirurgica Supplement* **76,** 431.

Kasischke KA, Vishwasrao HD, Fisher PJ, Zipfel WR & Webb WW. (2004). Neural activity triggers neuronal oxidative metabolism followed by astrocytic glycolysis. *Science Signalling* **305,** 99.

Kissinger PT, Hart JB & Adams RN. (1973). Voltammetry in brain tissue - a new neurophysiological measurement. *Brain Research* **55,** 209-213.

Kulagina NV, Shankar L & Michael AC. (1999). Monitoring glutamate and ascorbate in the extracellular space of brain tissue with electrochemical microsensors. *Analytical Chemsitry* **71,** 5093-5100.

Losito I, Palmisano F & Zambonin PG. (2003). *o*-Phenylenediamine Electropolymerization by Cyclic Voltammetry Combined with Electrospray Ionization-Ion Trap Mass Spectrometry. *Analytical Chemsitry* **75,** 4988-4995.

Lowry JP, Boutelle MG & Fillenz M. (1997). Measurement of brain tissue oxygen at a carbon paste electrode can serve as an index of increases in regional cerebral blood flow. *Journal of neuroscience methods* **71,** 177-182.

Lowry JP, Boutelle MG, O'Neill RD & Fillenz M. (1996). Characterization of carbon paste electrodes *in vitro* for simultaneous amperometric measurement of changes in oxygen and ascorbic acid concentrations *in vivo*. *The Analyst* **121,** 761-766.

Lowry JP, Demestre M & Fillenz M. (1998a). Relation between Cerebral Blood Flow and Extracellular Glucose in Rat Striatum during Mild Hypoxia and Hyperoxia. *Developmental Neuroscience* **20,** 52-58.

Lowry JP & Fillenz M. (2001). Real-time monitoring of brain energy metabolism in vivo using microelectrochemical sensors: the effects of anesthesia. *Bioelectrochemistry* **54,** 39-47.

Lowry JP, McAteer K, Atrash SSE & O'Neill RD. (1994a). Efficient glucose detection in anaerobic solutions using an enzyme-modified electrode designed to detect H_2O_2: implications for biomedical applications. *Journal of the Chemical Society, Chemical Communications***,** 2483-2484.

Lowry JP, McAteer K, El Atrash SS, Duff A & O'Neill RD. (1994b). Characterization of Glucose Oxidase-Modified Poly(phenylenediamine)-Coated Electrodes *in vitro* and *in vivo*: Homogeneous Interference by Ascorbic Acid in Hydrogen Peroxide Detection. *Analytical Chemsitry* **66,** 1754-1761.

Lowry JP, Miele M, O'Neill RD, Boutelle MG & Fillenz M. (1998b). An amperometric glucose-oxidase/poly(*o*-phenylenediamine) biosensor for monitoring brain extracellular glucose: *in vivo* characterisation in the striatum of freely-moving rats. *Journal of neuroscience methods* **79,** 65-74.

Lowry JP & O'Neill RD. (1994). Partial Characterization In-Vitro of Glucose Oxidase-Modified Poly-(Phenylenediamine)-Coated Electrodes for Neurochemical Analysis *In-Vivo*. *Journal of Electroanalytical Chemistry* **6,** 369-379.

Lowry JP, O'Neill RD, Boutelle MG & Fillenz M. (2002). Continuous monitoring of extracellular glucose concentrations in the striatum of freely moving rats with an implanted glucose biosensor. *Journal of Neurochemistry* **70,** 391-396.

Lubbers DW & Baumgärtl H. (1997). Heterogeneities and profiles of oxygen pressure in brain and kidney as examples of the pO_2 distribution in the living tissue: Oxygen sensing on the cellular and molecular level. *Kidney International* **51,** 372-380.

Magistretti PJ & Pellerin L. (1996). Cellular bases of brain energy metabolism and their relevance to functional brain imaging: evidence for a prominent role of astrocytes. *Cerebral Cortex* **6,** 50-61.

Magistretti PJ, Pellerin L & JL. M. (2000). Brain Energy Metabolism: An Integrated Cellular Perspective.

Mangia S, Garreffa G, Bianciardi M, Giove F, Di Salle F & Maraviglia B. (2003). The aerobic brain: lactate decrease at the onset of neural activity. *Neuroscience* **118,** 7-10.

Marsden C, Joseph M, Kruk Z, Maidment N, O'NEILL R, Schenk J & Stamford J. (1988). *In vivo* voltammetry—present electrodes and methods. *Neuroscience* **25,** 389-400.

McArthur KT, Clark L, Lyons C & Edwards S. (1962). Continuous recording of blood oxygen saturation in open-heart operations. *Surgery* **51,** 121-126.

McCreery D, Agnew W, Bullara L & Yuen T. (1990). Partial pressure of oxygen in brain and peripheral nerve during damaging electrical stimulation. *Journal of Biomedical Engineering* **12,** 309-315.

McMahon CP, Rocchitta G, Kirwan SM, Killoran SJ, Serra PA, Lowry JP & O'Neill RD. (2007). Oxygen tolerance of an implantable polymer/enzyme composite glutamate biosensor displaying polycation-enhanced substrate sensitivity. *Biosensors and Bioelectronics* **22,** 1466-1473.

McMahon CP, Rocchitta G, Serra PA, Kirwan SM, Lowry JP & O'Neill RD. (2006a). Control of the oxygen dependence of an implantable polymer/enzyme composite biosensor for glutamate. *Analytical Chemsitry* **78,** 2352-2359.

McMahon CP, Rocchitta G, Serra PA, Kirwan SM, Lowry JP & O'Neill RD. (2006b). The efficiency of immobilised glutamate oxidase decreases with surface enzyme loading: an electrostatic effect, and reversal by a polycation significantly enhances biosensor sensitivity. *The Analyst* **131,** 68-72.

McNay EC & Gold PE. (1999). Extracellular Glucose Concentrations in the Rat Hippocampus Measured by Zero-Net-Flux. *Journal of Neurochemistry* **72,** 785-790.

Murr R, Berger S, Schuerer L, Peter K & Baethmann A. (1994). A novel, remote-controlled suspension device for brain tissue PO_2 measurements with multiwire surface electrodes. *Pflügers Archiv European Journal of Physiology* **426,** 348-350.

Nair PK, Buerk DG & Halsey J. (1987). Comparisons of oxygen metabolism and tissue PO_2 in cortex and hippocampus of gerbil brain. *Stroke* **18,** 616-622.

Nicholson C & Syková E. (1998). Extracellular space structure revealed by diffusion analysis. *Trends Neuroscience* **21,** 207-215.

O'Neill RD. (1990). Uric acid levels and dopamine transmission in rat striatum: diurnal changes and effects of drugs. *Brain Research* **507,** 267-272.

O'Neill RD. (1993). Sensor-tissue interactions in neurochemical analysis with carbon paste electrodes *in vivo*. *The Analyst* **118,** 433-438.

O'Neill RD. (1995). The measurement of brain ascorbate and its link with excitatory amino acid neurotransmission. In *Voltammetric Methods in Brain Systems*, ed. Boulton AA, Baker GB & Adams RN, pp. 221-268. Humana Press, Totowa, New Jersey.

O'Neill RD & Fillenz M. (1985a). Circadian changes in extracellular ascorbate in rat cortex, accumbens, striatum and hippocampus: correlations with motor activity. *Neuroscience Letters* **60,** 331-336.

O'Neill RD & Fillenz M. (1985b). Detection of homovanillic acid in vivo using microcomputer-controlled voltammetry: simultaneous monitoring of rat motor activity and striatal dopamine release. *Neuroscience* **14,** 753-763.

O'Neill RD & Lowry JP. (1995). On the significance of brain extracellular uric acid detected with *in-vivo* monitoring techniques: a review. *Behavioural brain research* **71,** 33-49.

O'Neill RD & Lowry JP. (2000). Voltammetry In Vivo for Chemical Analysis of the Living Brain. In *Encyclopedia of Analytical Chemistry*, ed. Meyers RA, pp. 676-709. John Wiley & Sons Ltd, Chichester.

O'Neill RD, Lowry JP & Mas M. (1998). Monitoring brain chemistry *in vivo*: voltammetric techniques, sensors, and behavioral applications. *Critical reviews in neurobiology* **12,** 69-127.

O'Neill RD. (2005). Long-term monitoring of brain dopamine metabolism *in vivo* with carbon paste electrodes. *Sensors* **5,** 317-342.

Ogawa S, Lee TM, Kay AR & Tank DW. (1990). Brain magnetic resonance imaging with contrast dependent on blood oxygenation. *Proceedings of the National Academy of Sciences* **87,** 9868-9872.

Ogawa S, Tank DW, Menon R, Ellermann JM, Kim SG, Merkle H & Ugurbil K. (1992). Intrinsic signal changes accompanying sensory stimulation: functional brain mapping with magnetic resonance imaging. *Proceedings of the National Academy of Sciences* **89,** 5951.

Pantano P & Kuhr WG. (1995). Enzyme-modified microelectrodes for *in-vivo* neurochemical measurements. *Journal of Electroanalytical Chemistry* **7,** 405-416.

Parkin M, Hopwood S, Jones DA, Hashemi P, Landolt H, Fabricius M, Lauritzen M, Boutelle MG & Strong AJ. (2005). Dynamic changes in brain glucose and lactate in pericontusional areas of the human cerebral cortex, monitored with rapid sampling on-line microdialysis: relationship with depolarisation-like events. *Journal of Cerebral Blood Flow & Metabolism* **25,** 402-413.

Parkin MC, Hopwood SE, Boutelle MG & Strong AJ. (2003). Resolving dynamic changes in brain metabolism using biosensors and on-line microdialysis. *TrAC Trends in Analytical Chemistry* **22,** 487-497.

Pellerin L & Magistretti PJ. (1994). Glutamate uptake into astrocytes stimulates aerobic glycolysis: a mechanism coupling neuronal activity to glucose utilization. *Proceedings of the National Academy of Sciences* **91,** 10625-10629.

Qin S, Van der Zeyden M, Oldenziel WH, Cremers TIFH & Westerink BHC. (2008). Microsensors for *in vivo* measurement of glutamate in brain tissue. *Sensors* **8,** 6860-6884.

Reinis S & Goldman JM. (1982). *The Chemistry of Behaviour*. Plenum Press, New York.

Rothman D, Novotny E, Shulman G, Howseman A, Petroff O, Mason G, Nixon T, Hanstock C, Prichard J & Shulman R. (1992). 1H-[13C] NMR measurements of [4-13C] glutamate turnover in human brain. *Proceedings of the National Academy of Sciences* **89,** 9603-9606.

Russell DM, Garry EM, Taberner AJ, Barrett CJ, Paton JFR, Budgett DM & Malpas SC. (2012). A fully implantable telemetry system for the chronic monitoring of brain

tissue oxygen in freely moving rats. *Journal of neuroscience methods* **204,** 242-248.

Sarrafzadeh A, Haux D, Sakowitz O, Benndorf G, Herzog H, Kuechler I & Unterberg A. (2003). Acute focal neurological deficits in aneurysmal subarachnoid hemorrhage relation of clinical course, CT findings, and metabolite abnormalities monitored with bedside microdialysis. *Stroke* **34,** 1382-1388.

Sasso SV, Pierce RJ, Walla R & Yacynych AM. (1990). Electropolymerized 1,2-Diaminobenzene as a Means To Prevent Interferences and Fouling and To Stabilize Immobilized Enzyme in Electrochemical Biosensors. *Analytical Chemsitry* **62,** 1111-1117.

Schurr A, West CA & Rigor BM. (1988). Lactate-supported synaptic function in the rat hippocampal slice preparation. *Science (New York, NY)* **240,** 1326.

Serra PA, Rocchitta G, Bazzu G, Manca A, Puggioni GM, Lowry JP & O'Neill RD. (2007). Design and construction of a low cost single-supply embedded telemetry system for amperometric biosensor applications. *Sensors and Actuators B: Chemical* **122,** 118-126.

Sibson NR, Dhankhar A, Mason GF, Rothman DL, Behar KL & Shulman RG. (1998). Stoichiometric coupling of brain glucose metabolism and glutamatergic neuronal activity. *Proceedings of the National Academy of Sciences* **95,** 316-321.

Siesjö BK. (1978). *Brain energy metabolism*. Wiley.

Silver I. (1965). Some observations on the cerebral cortex with an ultramicro, membrane-covered, oxygen electrode. *Medical and Biological Engineering and Computing* **3,** 377-387.

Thévenot DR, Toth K, Durst RA & Wilson GS. (2001). Electrochemical biosensors: recommended definitions and classification. *Biosensors and Bioelectronics* **16,** 121-131.

Tian F, Gourine AV, Huckstepp RTR & Dale N. (2009). A microelectrode biosensor for real time monitoring of L-glutamate release. *Analytica chimica acta* **645,** 86-91.

Tsacopoulos M & Magistretti P. (1996). Metabolic coupling between glia and neurons. *The Journal of Neuroscience* **16,** 877-885.

Ungerstedt U & Pycock C. (1974). Functional correlates of dopamine neurotransmission. *Bulletin der Schweizerischen Akademie der Medizinischen Wissenschaften* **30,** 44.

Updike S & Hicks G. (1967). The enzyme electrode. *Nature* **214,** 986-988.

Venton BJ, Michael DJ & Wightman RM. (2003). Correlation of local changes in extracellular oxygen and pH that accompany dopaminergic terminal activity in the rat caudate–putamen. *Journal of Neurochemistry* **84,** 373-381.

Vespa PM, McArthur D, O'Phelan K, Glenn T, Etchepare M, Kelly D, Bergsneider M, Martin NA & Hovda DA. (2003). Persistently Low Extracellular Glucose Correlates With Poor Outcome 6 Months After Human Traumatic Brain Injury Despite a Lack of Increased Lactate: A Microdialysis Study. *Journal of Cerebral Blood Flow & Metabolism* **23,** 865-877.

Wang J. (1993). Electroanalysis and biosensors. *Analytical Chemsitry* **65,** 450-453.

Weaver JD, Espinoza R & Weintraub NT. (2007). The utility of PET brain imaging in the initial evaluation of dementia. *Journal of the American Medical Directors Association* **8,** 150-157.

Wisniewski N, Moussy F & Reichert WM. (2000). Characterization of implantable biosensor membrane biofouling. *Fresenius' Journal of Analytical Chemistry* **366,** 611-621.

Zauner A, Bullock R, Di X & Young HF. (1995). Brain oxygen, CO_2, pH, and temperature monitoring: evaluation in the feline brain. *Neurosurgery* **37,** 1168.

Zauner A, Doppenberg EMR, Woodward JJ, Choi SC, Young HF & Bullock R. (1997). Continuous Monitoring of Cerebral Substrate Delivery and Clearance: Initial Experience in 24 Patients with Severe Acute Brain Injuries. *Neurosurgery* **41,** 1082-1093.

Zhao H, Zhang Y & Yuan Z. (2001). Electrochemical Behaviour of Norepinephrine at Poly(2,4,6-trimethylpyridine) Modified Glassy Carbon Electrode. *Journal of Electroanalytical Chemistry* **14,** 445-448.

Zimmerman JB, Kennedy RT & Wightman RM. (1992). Evoked Neuronal Activity Accompanied by Transmitter Release Increases Oxygen Concentration in Rat Striatum *In Vivo* But Not *In Vitro*. *Welcome to Journal of Cerebral Blood Flow & Metabolism* **12,** 629-637.

Zimmerman JB & Wightman RM. (1991). Simultaneous electrochemical measurements of oxygen and dopamine *in vivo*. *Analytical Chemsitry* **63,** 24-28.

2. THEORY

2.1 Introduction

This primary aim of this thesis is the *in vitro* development and subsequent *in vivo* characterisation of microelectrochemical sensors for the detection of brain tissue oxygen and the *in vivo* characterisation of oxygen and glucose electrodes in the hippocampus. In order to accomplish this, two voltammetric electrochemical techniques were employed during the course of this project, these being cyclic voltammetry (CV) and constant potential amperometry (CPA). The theory relating to these two techniques is described in Section 2.3 and Section 2.4.

The various oxygen electrodes were characterised using voltammetry by their sensitivity (nA/μM) to O_2 and R^2 value. The Pt-based glucose oxidase (Pt/PPD/GOx) electrodes were calibrated by means of their response to the substrate, using Michaelis-Menten kinetics (V_{max} and K_M) and interferent rejection.

The theory of mass transport is a major parameter in all of these techniques, the motion of reactants and products to and from the active surface of the electrode. This theory details the processes which take place in the bulk liquid medium; it is described in Section 2.2.

The second process which is involved in all electrochemical techniques is the electron transfer which takes places as a species is oxidised or reduced at the active surface. The general reaction for this process is detailed in Equation 2.1.

The generalised equation for the oxidation and reduction of a species at an electrode surface is:

$$O + ne^- \rightleftharpoons R$$

Equation 2.1

Where *O* is the oxidised species, *R* is the reduced species and *n* is the number of electrons involved in the reaction.

Mass transport of the reactant to the active surface of the electrode and electron transfer are the two main processes involved in this reaction.

2.2 Mass Transport

In order to react, a species at an electrode needs to be transported from bulk solution to the electrode surface.

There are three forms of mass transport that can influence an electrolysis reaction.

- Diffusion
- Convection
- Migration

Diffusion occurs in all solutions and arises from local uneven concentrations of reagents. Entropic forces act to adjust these uneven distributions of concentration and are therefore the main driving force for this process. Diffusion is described by Fick's first law (Equation 2.2):

$$J = -D\frac{\partial c}{\partial x}$$

Equation 2.2

Where J is the diffusional flux, D is the diffusion coefficient and $\frac{\partial c}{\partial x}$ is the concentration gradient in direction x. The negative sign signifies that material moves down a concentration gradient.

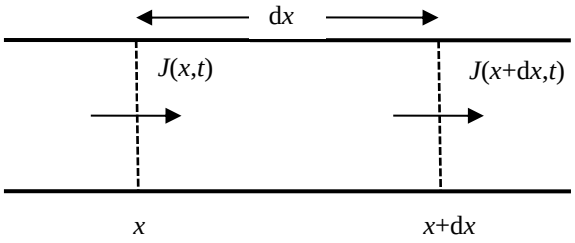

Figure 2.1: A volume segment *dx* of solution with a concentration gradient, where a flux *J* is flowing from the area of higher concentration to the area of lower concentration.

Fick's second law (Equation 2.3) describes how the concentration of material varies as a function of time (t) and this can be predicted from the first law

$$\frac{\partial c}{\partial t} = D\frac{\partial^2 c}{\partial x^2}$$

Equation 2.3

Where c is the concentration and t is time. The steeper the change in concentration, the greater the rate of diffusion. A steady-state current response is obtained: $\left(\frac{\partial c}{\partial t}\right) = 0$ (no change in c with t) for microelectrodes with diameter of between 5-300 μm (O'Neill *et al.*, 1998) where currents are small and minimal substrate is consumed.

For any co-ordinate system ∇ is substituted into Equation 2.2 to give Equation 2.4.

$$J = -D\nabla^2 c$$

Equation 2.4

For all geometries, a generalised version of Fick's second law (Equation 2.3) is:

$$\frac{\partial c}{\partial t} = D\nabla^2 c$$

Equation 2.5

∇ is the Laplace operator, which has varied forms depending upon the coordination of the systems. Electrodes with different geometries have dissimilar forms of the Laplace operator.

For planar (disk) electrodes the species can uniformly access the electrode from the bulk solution. The change in current with respect to time calculated using Fick's second law results in the Cottrell equation (Equation 2.6):

$$I = nFAJ = \frac{nFA\sqrt{D}c_\infty}{\sqrt{\pi}\sqrt{t}}$$

Equation 2.6

Where I is the current measured at the active surface of an area A at time t. The bulk concentration of the species is denoted by c_∞. D is the diffusion coefficient, J is the flux, n the number of electrons and F is Faraday's constant.

For an electrode of a cylindrical shape with a diameter greater than 50 µm the Laplacian Operator takes the form of (Brett & Brett, 1993):

$$\frac{\partial}{\partial r} + \left(\frac{1}{r}\right)\left(\frac{\partial}{\partial \varphi}\right) + \frac{\partial}{\partial x}$$

Equation 2.7

In order to solve Fick's 2nd Law, and thus find the flux variation in time and the diffusion limited current, it is necessary to define conditions for the system to obey. These conditions specify concentration and/or spatial characteristics, and are defined in relation to time, i.e. at t=0.

Fick's 1st Law, a species *R* at the surface of an electrode it is found that the flux, $J_R(0,t)$, is proportional to the current density $\frac{i}{A}$. This is because the total number of electrons transferred per unit time must be proportional to the quantity of R reaching the surface in that time *t.*

$$-J_R(0,t) = \frac{i}{nFA} = D_R\left[\frac{\partial c_R(x,t)}{\partial x}\right]_{x=0}$$

Equation 2.8

where i is the current, A is the surface area of the electrode, F is the Faraday constant and n is the number of electrons transferred per molecule that reacts at the surface.

2.3 Cyclic Voltammetry

Cyclic voltammetry (CV) is an electrochemical technique which involves the application of a triangular waveform potential to drive a redox reaction (Figure 2.2). An initial potential (E_i) where no oxidation occurs, is applied to the working electrode. The potential is increased at a constant scan rate (v) to the maximum potential (E_{max}). The scan is then reversed until the initial potential has been reached. As the potential is decreased back to the initial starting potential any species that was oxidised on the forward sweep is reduced. There is a delay between scans to prevent the previous scan influencing the next scan and

measurements are performed in quiescent solutions so that mass transport is diffusion controlled.

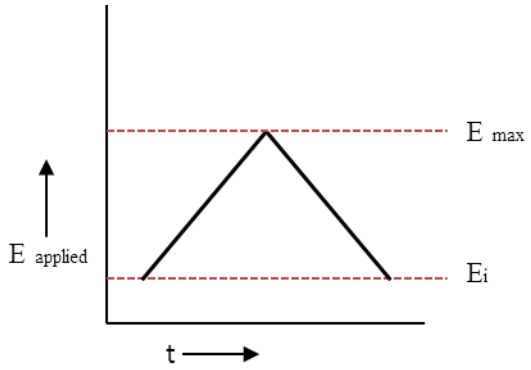

Figure 2.2: A cyclic voltammogram potential waveform.

Two types of current are generated when performing CV. Current generated from the electrochemical process is known as the Faradaic current, i_f. The capacitance current, i_c, know as the background current never dissipates, resulting in constant changes to the double layer charge. It is necessary to subtract the background current which is obtained before addition of an analyte to the buffer solution. This allows for observation of the Faradaic current resulting from electrochemical processes of specific analytes of interest.

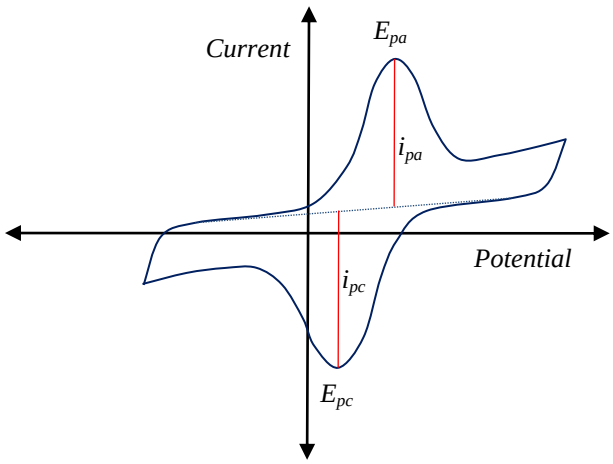

Figure 2.3: A typical current-potential profile for a CV of a reversible redox speices.

Considering the reversible system detailed in Figure 2.3 at E_i only *R* is present in the system so no electron transfere takes place. As the potential sweeps to positive potentials, electron transfer is induced as *R* is oxidised to *O*. Initially the rate of transfer, or the rate of oxidation, is limited by the potential. Once a sufficient potential is reached then all *R* reaching the surface is oxidised to *O*. Further increases in potential from this moment do not result in an increased rate of reaction. The process is now being controlled by diffusion resulting in larger currents. This occurs until the reverse potential commences. The maximum anodic current, i_{pa}, is a balance between the increasing electrochemical rate constant, k_{ox}, and decreasing surface concentration of *R*. Before E_{pa} is reached a rapidly increasing k_{ox} controls *i*, and at potentials higher than E_{pa} diffusion controls the rate of reaction, illustrated in Figure 2.3.

2.4 Constant Potential Amperometry

The voltammetric technique used most frequently throughout this project was constant potential amperometry (CPA). During CPA the current resulting from the oxidation or reduction of an analyte is recorded, occurring from the application of a fixed applied potential. Diffusion is the only form of mass transport considered to be occurring within the system (Section 2.2). After the initial application of a fixed potential the capacitance currents associated with the charged layers at the active surface of the electrode decay, resulting in steady-state diffusion-limited currents associated only with substrate reaction at the surface. The applied potentials used in this project were chosen so that all substrate reaching the surface of the electrode was oxidised/reduced which is known as overpotential. Therefore, amperometric current measured at the electrode is directly proportional to analyte concentration at all times. The current measured is the sum of two contributing factors (Equation 2.9); the Cottrell current (i_{cot}) and the steady-state current (i_{ss}).

$$I_{amp} = i_{cot} + i_{ss}$$

Equation 2.9

The Cottrell component disappears for large values of time, *t*, and the steady-state current predominates. It is these diffusion-limited steady-state currents which are reported in this work and for a reversible or irreversible reaction they are given by Equation 2.10 (Forster, 1994).

$$i_{ss} = \frac{nFAcD}{r}$$

Equation 2.10

where A is the surface area of the electrode, F is the Faraday constant, *D* is the diffusion coefficient, *c* is the concentration, *r* is the radius of the electrode and *n* is the number of electrons transferred.

However, additional factors such as the geometry or the insulation thickness of the electrode (Dayton *et al.*, 1980) have an effect on i_{ss}. As a result a geometric factor G is incorporated into the equation to consider these influences resulting in Equation 2.11.

$$i_{ss} = G\frac{nFADc}{r}$$

Equation 2.11

Despite theoretical reports of true steady-state behaviour not being reached by microelectrodes, a quasi-steady-state is achieved (Aoki, 1993). This is dependant on, and proportional to, the radius of the electrode.

2.5 Measurement of Dissolved Oxygen

Electrochemical oxygen electrodes are founded on the electrocatalytic reduction of oxygen at the working electrode surface. A number of mechanisms have been proposed for this reaction including a four-electron transfer Equation 2.12) which occurs in a single-step without the formation of intermediates (Damjanovic *et al.*, 1967).

$$O_2 + 4H^+ + 4e^- \rightarrow 2H_2O$$

Equation 2.12

A two-step process (Equation 2.13 Equation 2.14) has also been reported where hydrogen peroxide is formed as a measurable intermediate (Hoare, 1968).

$$O_2 + 2H^+ + 2e^- \rightarrow H_2O_2$$

Equation 2.13

$$H_2O_2 + 2H^+ + 2e^- \rightarrow 2H_2O$$

Equation 2.14

Equation 2.12 involves a $4e^-$ pathway, resulting in the reduction of O_2 to OH^- or H_2O. This reduction may involve a peroxide intermediate adsorbed on the electrode surface but does not result in peroxide being present in the solution phase. The two-step process involves the peroxide species, present in the solution phase. O_2 results from the decomposition of the peroxide species (Equation 2.15) and is recycled via the reaction (Equation 2.13) with the overall reaction being a $4e^-$ pathway.

$$2H_2O_2 \rightarrow 2H_2O + O_2$$

Equation 2.15

(Damjanovic *et al.*, 1967) proposed that oxygen reduction is a multi-electron process that involves a number of series-parallel pathways. These pathways are indicated by the rate constants k_1, k_2 and k_3 corresponding to the reactions in Equation 2.13, Equation 2.14 Equation 2.15 respectively.

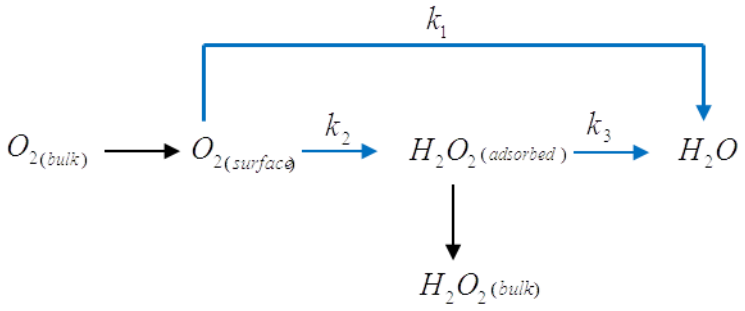

Figure 2.4: Proposed mechanism for reduction of oxygen in aqueous electrolytes for Pt electrodes (Damjanovic *et al.*, 1967).

2.6 Enzymes

Enzymes are biological catalysts which increase the rate of metabolic reactions. They are globular proteins, consisting of long chains of amino acids which are folded into a specific shape. The active site acts as the catalyst where the substrate binds and converts to a product. Enzymes are highly substrate specific and this specificity makes them extremely desirable in the fabrication of biosensors. Immobilisation of an enzyme on the electrode surface allows its corresponding substrates concentration to be monitored indirectly by electrochemical means.

Glucose oxidase, an oxidoreductase enzyme is used in this body of work. Oxidoreductase enzymes catalyse the oxidation and reduction of their respective substrates. In order for the oxidase enzymes to catalyse redox reactions, molecular oxygen (O_2) must be present. Flavin adenine dinucleotide (FAD) is the reactive redox site of these enzymes and it binds the O_2 after the enzyme and substrate reaction has taken place in order to convert the enzyme back to its original form thus enabling it to react with another substrate molecule.

The general scheme of an oxidase enzyme reaction process at the surface of a first generation biosensor is illustrated in Figure 2.5. H_2O_2 is produced when the FAD is oxidised and this reacts at the electrode surface to produce a current.

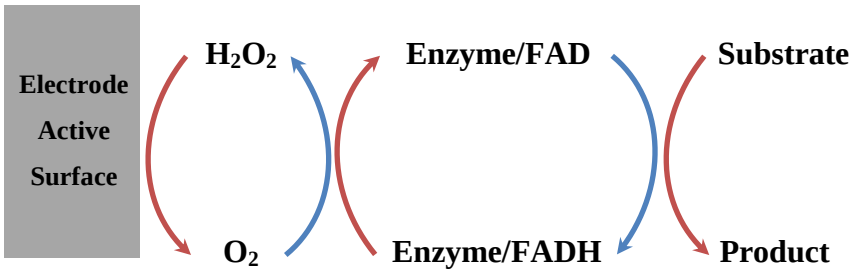

Figure 2.5: Generalised reaction mechanism of an oxidase enzyme on a first generation biosensor. The blue arrows represent reduction and red arrows indicate oxidation.

2.6.1 *Enzyme Kinetics*

The intricate nature of the active site of an enzyme is what allows it to selectively react with only one or a limited number of substrates, which leads to complex reaction mechanisms. The overall kinetic parameters of a specific reaction can be determined by examining these reactions in a generalised manner. A single substrate enzyme-catalysed reaction where one substrate-binding site is present results in the following general enzyme kinetic equation (Equation 2.16).

$$E + S \underset{k_{-1}}{\overset{k_1}{\rightleftharpoons}} ES \underset{k_{-2}}{\overset{k_2}{\rightleftharpoons}} E + P$$

Equation 2.16

where E is the enzyme, S is the substrate , ES is the enzyme-substrate complex, P is the resulting product of the reaction and k refers to the rate constants for each specific reaction

Initially it is found in a reaction that the concentration of the product is low and thus the reverse reaction of product to the enzyme-substrate complex, indicated by k_{-2} is negligible.

When experiments were limited to the initial period of the reaction, it follows that the product concentration is negligible and the formation of ES from product by pathway k_{-2} can be dismissed. As a result Equation 2.16 becomes Equation 2.17:

$$E + S \underset{k_{-1}}{\overset{k_1}{\rightleftharpoons}} ES \xrightarrow{k_2} E + P$$

Equation 2.17

Michaelis and Menten (1913) derived the rate equation for enzyme catalysis, in which the steady-state approximation can be applied to the formation and destruction of the enzyme-substrate complex, ES. The rate of change of the concentration of $[ES]$ with time is shown in the Equation 2.18.

$$\frac{d[ES]}{dt} = k_1[E][S] - k_{-1}[ES] - k_2[ES]$$

Equation 2.18

where $[E]$ is the concentration of unbound enzyme and $[ES]$ the concentration of the bound enzyme. Therefore, the total enzyme concentration $[E]_0$, can be substituted into Equation 2.18 by Equation 2.19.

$$[E] = [E]_0 - [ES]$$

Equation 2.19

Combining these two equations and applying the steady-state approximation, where, $\frac{d[ES]}{dt} = 0$, it is found:

$$k_1[E]_0[S] - k_1[ES][S] - k_{-1}[ES] - k_2[ES] = 0$$

Equation 2.20

From Equation 2.20 it is possible to isolate the concentration of the enzyme-substrate complex, giving:

$$[ES] = \frac{[E]_0[S]}{[S] + \frac{k_{-1} + k_2}{k_1}}$$

Equation 2.21

Replacing the constants $\frac{k_{-1} + k_2}{k_1}$ with K_M, the Michaelis constant, further simplifies the equation. Resulting in:

$$[ES] = \frac{[E]_0[S]}{[S] + K_M}$$

Equation 2.22

But the overall rate of reaction, *v*, is solely dependent on the concentration of the enzyme-substrate complex and the rate of formation of products, k_2, thus:

$$v = k_2[ES]$$

Equation 2.23

$[ES]$ has been isolated in order to allow its substitution into the following relationship where overall rate of reaction (the rate of formation of products), k_2 is solely dependent on it.

$$\nu = k_2[ES]$$

Equation 2.24

where ν is the overall rate of reaction. Substituting gives:

$$\nu = \frac{k_2[E]_0[S]}{[S] + K_M}$$

Equation 2.25

When substrate concentration is very high all the enzyme exists only as enzyme-substrate complex and the limiting initial velocity (rate), V_{max}, is reached. Hence, $[S] >> K_M$ and

$$V_{\max} = k_2[E]_0$$

Equation 2.26

and therefore,

$$\nu = \frac{V_{\max}[S]}{[S] + K_M}$$

Equation 2.27

Further assuming that substrate is present in a much higher concentration than the enzyme, then the initial substrate concentration, $[S]_0$, is much greater than the initial enzyme concentration, $[S]_0$ is much greater than the initial enzyme concentration $[E]_0$ then $[S] \cong [S]_0$ and as a result Equation 2.27 becomes the Michaelis-Menten equation:

$$\nu = \frac{V_{\mathbf{max}}\mathbf{[}S\mathbf{]}_0}{\mathbf{[}S\mathbf{]}_0 + K_M}$$

Equation 2.28

where ν is the rate of reaction, $V_{\mathbf{max}}$ is the maximal rate of reaction, $\mathbf{[}S\mathbf{]}_0$ is the initial substrate concentration and K_M is the Michaelis constant.

A rectangular hyperbola is observed when ν is plotted against $[S]_0$ as displayed in Figure 2.6. From this graph both $V_{\mathbf{max}}$ and K_M can be obtained as shown, with K_M being $\mathbf{[}S\mathbf{]}$ where $\nu = \frac{V_{\mathbf{max}}}{2}$.

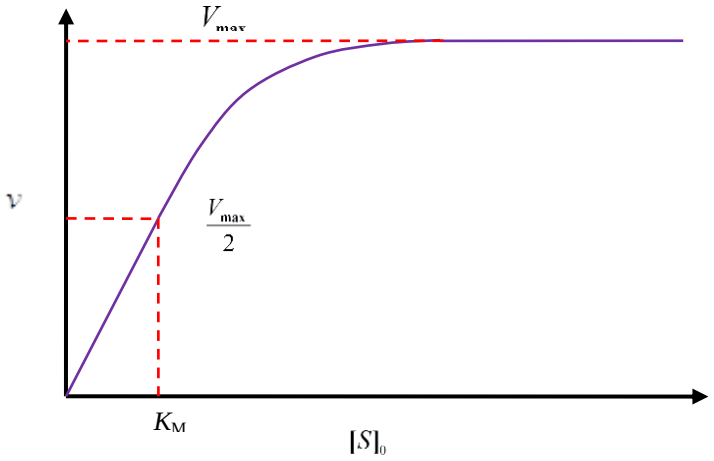

Figure 2.6: Graph of the reaction rate, v, against substrate concentration, $[S]_0$, for an enzyme concentration, $[E]_0$ for a single substrate enzyme catalysed reaction resulting from the Michaelis-Menten equation (Equation 2.28).

The hyperbolic response can be seen in Figure 2.6, when more than one molecule of substrate binds to a single molecule of enzyme. If each binding site on the enzyme is similar and independent the response observed will still be hyperbolic. If there is an increase in affinity to a binding site where the binding of a substrate to one active site on the enzyme increases the affinity of other sites on the enzyme to bind more molecules of substrate then sigmoidal kinetics are observed, known as the co-operative effect (Ricard & Cornish-Bowden, 1987). The Michaelis-Menten Hill-type equation (Lowry & O'Neill, 1992; Lowry *et al.*, 1994) is used to quantify the deviation from hyperbolic, idealised kinetics and the constants, V_{max} and K_M, in this body of work. It uses the constant α which was introduced following work on the aggregation of hæmoglobin and oxygen (Hill, 1910; Stryer, 1988).

$$i = \frac{V_{max}}{1 + \left(\frac{K_M}{[S]}\right)^{\alpha}}$$

Equation 2.29

where i indicates the current observed from the electro-oxidation of H_2O_2 at the surface of the electrode. α is used as a measure of deviation from the ideal Michaelis-Menten behaviour, with ideal behaviour α=1. An α value of 2 is indicative of sigmoidal kinetics.

2.7 Structures and Reactions

2.7.1 *Hydrogen Peroxide*

First generation biosensors (Section 1.4.1) utilising enzymes produce stoichiometrically equivalent amounts of H_2O_2 as the enzyme-substrate reaction occurs. Platinum is commonly used as the electrode material of choice to detect the production of H_2O_2 (Hall *et al.*, 1998). The process is well known and characterised as a two-electron process (Hickling & Wilson, 1951; Lingane *et al.*, 1963). It is based on a thin oxide film forming on the surface of the platinum, with which the H_2O_2 interacts, similar to that proposed for palladium (Gorton, 1985). The mechanism for the oxidation is outlined below in three equations (Hall *et al.*, 1998)

$$H_2O_2 \rightarrow O_2 + 2H^+ + 2e^-$$

Equation 2.30

$$Pt(OH)_2 + H_2O_2 \rightarrow Pt + 2H_2O + O_2$$

Equation 2.31

$$Pt + 2H_2O \rightarrow Pt(OH)_2 + 2H^+ + 2e^-$$

Equation 2.32

The complex formation between the oxide film and hydrogen peroxide is described in Equation 2.30 and Equation 2.31 describes the breakdown of this complex releasing water and oxygen and leaving behind an unoxidised metal surface. Finally in Equation 2.32 it is seen that the water recombines with the platinum surface to release two protons and two electrons. It is these electrons which produce the current that is measured and related directly to the concentration of substrate in solution.

2.7.2 *Glucose*

The enzyme glucose oxidase is an oxidoreductase enzyme discussed in Section 2.6. It catalyses the oxidation of β-D-glucose into D-glucono-1,5-lactone, which then hydrolyses to gluconic acid (Wilson & Turner, 1992) as can be seen in Figure 2.7. H_2O_2 is produced when the FAD is oxidised and this reacts at the electrode surface to produce a current.

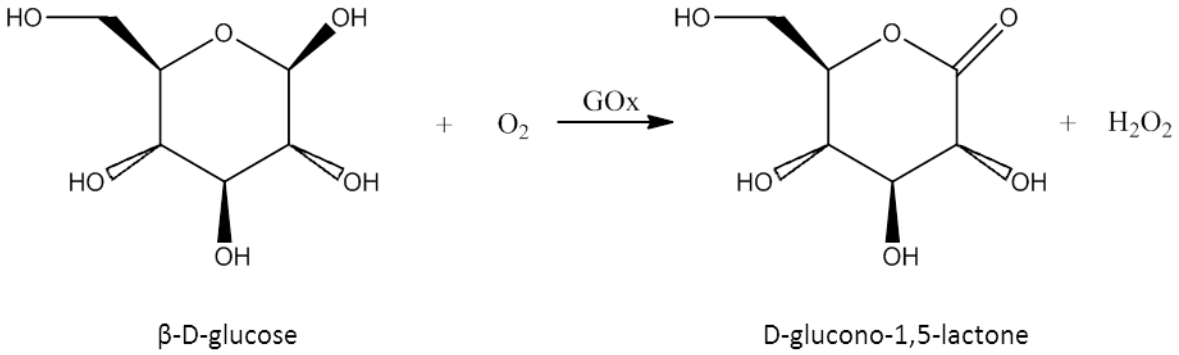

Figure 2.7: Reaction mechanism for the oxidation of β-D-glucose into D-glucono-1,5-lactone.

2.7.3 *Electropolymerisation of o-Phenylenediamine*

Poly-*o*-phenylenediamine (PPD) can be polymerised onto the active surface of the electrode by electropolymerisation in a neutral electrolyte to form an insulating polymer (Malitesta *et al.*, 1990). This insulating film of PPD prevents further electropolymerisation, thereby resulting in a reproducible coating. This coating blocks out any interferent species larger than the *o*-phenylenediamine monomer (Sasso *et al.*, 1990) and therefore it has been used as an interference rejection layer in biosensor design (Lowry *et al.*, 1994; Lowry & O'Neill, 1994; Rothwell *et al.*, 2010). Little is still known about the structure of PPD and the mechanism by which polyimerisation occurs, particularly under neutral conditions (Li *et al.*, 2002). Two different structures of PPD are proposed which appear to be dependent on polymerisation conditions. Under conditions of low pH (<1) it is believed that the structure is a phenazine-like 'ladder' structure, see Figure 2.8. This is the most commonly reported structure, supported by work on infrared, Raman and UV-Vis spectroscopy, quartz

microcrystal balance studies, radiometry and electrochemical techniques (Bilal *et al.*, 2011).

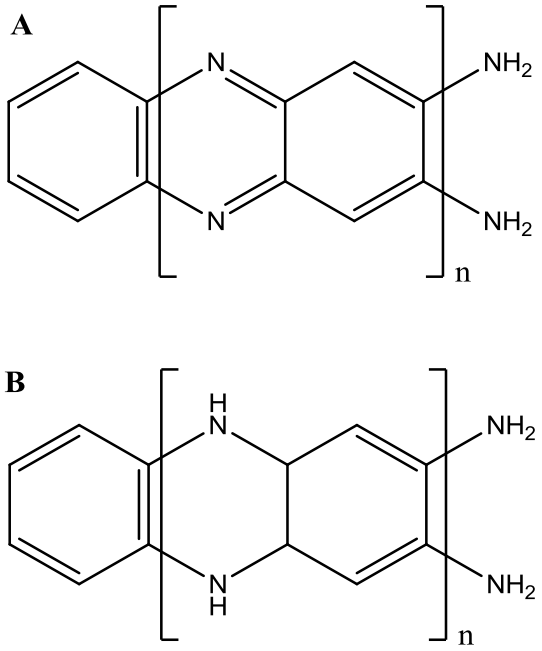

Figure 2.8: Proposed phenazine "ladder" like structures of PPD where A: the oxidised form (Sayyah *et al.*, 2009) and B: non-oxidised form (Bilal *et al.*, 2011).

The more 'open' or polyaniline-like 1,4-substituted benzenoid-quinoid structure (Yano, 1995) can be seen in Figure 2.9. A mechanism for the polymerisation of *o*-PD to PPD with the 'open' structure has been proposed (Sayyah *et al.*, 2009). In this project this 'open' polymer that self-insulates as it polymerises producing a film of *ca.*10 nm (Malitesta *et al.*, 1990) is hypothesised to be produced under neutral pH conditions.

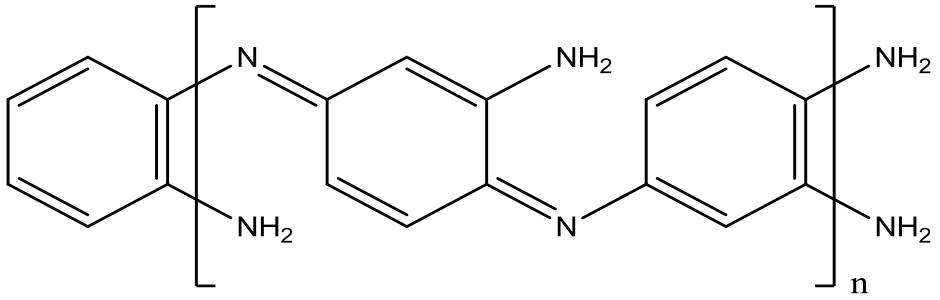

Figure 2.9: Proposed 1,4-substituted benzenoid-quinoid structure of PPD, 'open' structure (Losito *et al.*, 2001).

2.7.4 *Ascorbic Acid*

Ascorbic acid (AA) is one of the main endogenous interferents in electrochemical analysis as it's an electroactive species present in the ECF (Grunewald *et al.*, 1983) that is readily oxidised at metal electrodes, with an $E_{½}$ in the range -100 to +400 mV ***vs.*** SCE (O'Neill *et al.*, 1998). The oxidation of AA at the surface of a platinum electrode involves a $2H^+$, $2e^-$ mechanism resulting in the production of L-dehydroascorbic acid which rapidly forms an electro-inactive open chain product, L-2-3-diketogulonic acid. The reaction mechanism is shown in Figure 2.10.

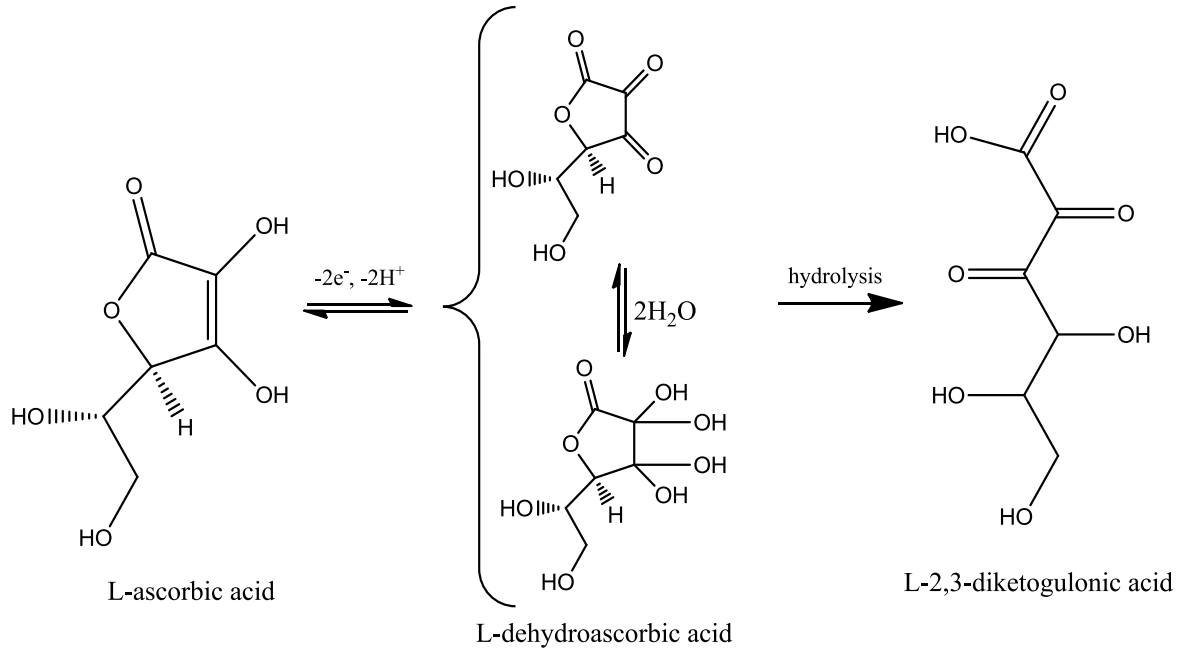

Figure 2.10: Reaction mechanism for the oxidation of AA to the electro-inactive product L-2,3-diketogulonic acid

2.8 Data Analysis

Constant potential amperometry (CPA) experiments were performed and relevant data was extracted using LabChart 6 software. Data was exported and either preliminarily processed in Microsoft® Excel® or directly analysed in GraphPad Prism® 5.

2.8.1 *Linear and Non-Linear Regression*

Linear regression fit was the most commonly used analysis in this body of work and was applied to O_2 calibrations performed *in vitro*. Non-linear regression fits taking the form of the Michaelis-Menten equation and the modified Hill-Type equation (see Section 2.6.1) were applied to *in vitro* glucose, enzymatic calibrations. Regression analyses allowed for comparisons and for further statistical analysis to be performed.

2.8.2 *Statistical Analysis*

Parametric *t*-tests allowed for the comparison of two data sets with a quantitative examination of the statistical difference between the results. Unpaired *t*-tests were performed on the mean of the data for the majority of analysis. However, paired *t*-tests were performed on individual data sets for particular analysis where appropriate. GraphPad InStat® as well as GraphPad Prism® 5 was used for *t*-tests. Area under the curve (AUC) analysis was performed on normalised *in vivo* data to determine the mean change from the baseline signal. For multiple comparisons, repeated-measures and mixed-factorial analysis of variance tests (ANOVA) with either standard Tukey-Kramer Multiple Comparison or Bonferroni *post-hoc* analysis used, where appropriate.

The *P* value is a probability, where $0 \leq P \leq 1$. It describes the statistical difference between two values and allows one to decide whether or not it is significantly different. Small *P* values indicate that the sampled populations have different means (i.e. difference is unlikely to be due to chance) and that the results are significantly different. The standard 95% confidence interval was used for these tests, so a *P*-value less than 0.05 would indicate

that there was a significant difference between the two sets of data analysed, whereas a *P*-value higher than 0.05 would indicate no significant difference.

For one-way ANOVA, the *F* value (*F*-test) is used to assess whether the expected values of a quantitative variable within several pre-defined groups differ from each other and *df* denotes the degrees of freedom.

The R^2 value is a measure of the goodness of fit of a data set to a regression (linear and non-linear), where $0 \leq R^2 \leq 1$. An R^2 value of 1 indicates a perfect fit, where all points lie directly on the line or curve which is proposed as the fit. A value of 0 indicates that there is no relationship between the X and Y values in the data set and that it is not possible to assign the chosen trend, linear or non-linear, to them.

2.8.3 *Current Densities*

For electrodes with varying physical dimensions to be compared it is necessary to convert current values into current density values (J). This allows for current per unit area, J ($\mu A.cm^{-2}$), to be calculated. Equation 2.33 gives the formula for calculation of the current density:

$$J = \frac{I}{A}$$

Equation 2.33

where J is the current density, I is the current and A is the area of the active surface of the electrode.

2.8.4 *Dissolved Oxygen – Temperature dependence*

For oxygen calibrations performed at 37°C the dissolved oxygen (Do) was determined to be 214 µM for air saturated solutions and 1020 µM for O_2 saturated solutions. These values were calculated using Do = 6.856 mg/L for an air saturated (21 % O_2) solution.

References

Aoki K. (1993). Theory of Ultramicroelectrodes. *Electroanalysis* **5,** 627-639.

Bilal S, Ali Shah A-u-H & Holze R. (2011). Spectroelectrochemistry of poly(*o*-phenylenediamine): Polyaniline-like segments in the polymer structure. *Electrochimica Acta* **56,** 3353-3358.

Brett CMA & Brett AMO. (1993). *Electrochemistry: Principles, Methods, and Applications*. Oxford University Press, New York.

Damjanovic A, Greenshaw MA & Bockris JOM. (1967). The Mechanism of Oxygen Reduction at Platinum in Alkaline Solutions with Special Reference to H_2O_2. *The Journal of The Electrochemical Society* **114,** 1107-1112.

Dayton MA, Brown JC, Stutts KJ & Wightman RM. (1980). Faradaic electrochemistry at micro-voltammetric electrodes. *Analytical chemistry* **52,** 946-950.

Forster RJ. (1994). Microelectrodes - New Dimensions In Electrochemistry. *Chem Soc Rev* **23,** 289-297.

Gorton L. (1985). A carbon electrode sputtered with palladium and gold for the amperometric detection of hydrogen peroxide. *Analytica chimica acta* **178,** 247-253.

Grunewald RA, O'Neill RD, Fillenz M & Albery WJ. (1983). The origin of circadian and amphetamine-induced changes in the extracellular concentration of brain ascorbate. *Neurochemistry international* **5,** 773-778.

Hall SB, Khudaish EA & Hart AL. (1998). Electrochemical oxidation of hydrogen peroxide at platinum electrodes. Part II: effect of potential. *Electrochimica Acta* **43,** 2015-2024.

Hickling A & Wilson WH. (1951). The anodic decomposition of hydrogen peroxide. *Journal of the Electrochemical Society* **98,** 425-433.

Hill AV. (1910). Proceedings of the Physiological Society: January 22, 1910. *Journal of Physiology-London* **40,** i-vii.

Hoare JP. (1968). *The Electrochemistry of Oxygen*. Interscience, New York.

Li XG, Huang MR, Duan W & Yang YL. (2002). Novel multifunctional polymers from aromatic diamines by oxidative polymerizations. *Chemical reviews* **102,** 2925-3030.

Lingane JJ, Lingane PJ & Morris MD. (1963). Gravimetric determination of cobalt as presumed $K_3CO(NO_2)_6$. *Analytica chimica acta* **29,** 10-&.

Losito I, De Giglio E, Cioffi N & Malitesta C. (2001). Spectroscopic investigation on polymer films obtained by oxidation of *o*-phenylenediamine on platinum electrodes at different pHs. *J Mater Chem* **11,** 1812-1817.

Lowry JP, McAteer K, El Atrash SS, Duff A & O'Neill RD. (1994). Characterization of Glucose Oxidase-Modified Poly(phenylenediamine)-Coated Electrodes *in vitro* and *in vivo*: Homogeneous Interference by Ascorbic Acid in Hydrogen Peroxide Detection. *Analytical Chemsitry* **66,** 1754-1761.

Lowry JP & O'Neill RD. (1992). Homogenous Mechanism of Ascorbic Acid Interference in Hydrogen Peroxide Detection at Enzyme-Modified Electrodes. *Analytical Chemsitry* **64,** 453-459.

Lowry JP & O'Neill RD. (1994). Partial Characterization In-Vitro of Glucose Oxidase-Modified Poly-(Phenylenediamine)-Coated Electrodes for Neurochemical Analysis *In-Vivo*. *Journal of Electroanalytical Chemistry* **6,** 369-379.

Malitesta C, Palmisano F, Torsi L & Zambonin PG. (1990). Glucose Fast-Response Amperometric Sensor Based on Glucose Oxidase Immobilized in an Electropolymerized Poly(*o*-Phenylenediamine) Film. *Analytical Chemsitry* **62,** 2735-2740.

Michaelis L & Menten ML. (1913). Die Kinetik Der Invertinwirkung. *Biochemische Zeitschrift* **49,** 333-369.

O'Neill RD, Lowry JP & Mas M. (1998). Monitoring brain chemistry *in vivo*: voltammetric techniques, sensors, and behavioral applications. *Critical reviews in neurobiology* **12,** 69-127.

Ricard J & Cornish-Bowden A. (1987). Co-operative and allosteric enzymes: 20 years on. *European Journal of Biochemistry* **166,** 255-272.

Rothwell SA, McMahon CP & O'Neill RD. (2010). Effects of polymerization potential on the permselectivity of poly(*o*-phenylenediamine) coatings deposited on Pt–Ir electrodes for biosensor applications. *Electrochimica Acta* **55,** 1051-1060.

Sasso SV, Pierce RJ, Walla R & Yacynych AM. (1990). Electropolymerized 1,2-Diaminobenzene as a Means To Prevent Interferences and Fouling and To Stabilize Immobilized Enzyme in Electrochemical Biosensors. *Analytical Chemsitry* **62,** 1111-1117.

Sayyah SM, El-Deeb MM, Kamal SM & Azooz RE. (2009). Electropolymerization of *o*-phenylenediamine on Pt-electrode from aqueous acidic solution: Kinetic, mechanism, electrochemical studies and characterization of the polymer obtained. *Journal of Applied Polymer Science* **112,** 3695-3706.

Stryer L. (1988). *Biochemistry*. W.H. Freeman and Co., New York.

Wilson R & Turner A. (1992). Glucose oxidase: an ideal enzyme. *Biosensors and Bioelectronics* **7,** 165-185.

Yano J. (1995). Electrochemical and structural studies on soluble and conducting polymer from *o*-phenylenediamine. *Journal of Polymer Science Part A: Polymer Chemistry* **33,** 2435-2441.

3. EXPERIMENTAL

3.1 Introduction

This experimental chapter details the design, fabrication and characterisation, *in vitro* and *in vivo*, of various sensors for the detection of energy substrates in the brain. The electrodes are based on previous sensor development work by the Lowry research group (O'Neill *et al.*, 1998). Carbon paste based electrodes were founded on work by (Lowry *et al.*, 1996), carbon composite electrodes on work by (Bazzu *et al.*, 2009), a standardised sensor for O_2 detection in an fMRI scanner based on a carbon fibre electrode (Lowry *et al.*, 2010) and platinum-based sensors on work by (Lowry *et al.*, 1994).

Sections 3.2 and 3.3 describe computer-based instrumentation, chemicals, enzymes and solutions. The preparation of various electrodes are detailed in section 3.4 as well as electrode modifications in section 3.5.

Electrochemical experiments *in vitro* are detailed in section 3.6 and all *in vivo* procedures and experiments in section 3.7.

3.2 Computer-Based Instrumentation, Equipment & Software

All electrochemical experiments throughout the course of this work involved the use of:

- A computer
- An interface: A Powerlab® or e-corder
- A potentiostat: A Biostat or Quadstat

3.2.1 *Potentiostat, CPU & Data Acquisition*

All *in vitro* electrochemical experiments (constant potential amperometry, CPA) and cyclic voltammetry, CV) were performed using a low noise potentiostat (Biostat IV, ACM Instruments, Cumbria, UK). Data acquisition was performed using a PowerLab® interface

system (ADInstruments Ltd; Oxford, UK) and a Logiq notebook computer (Clevo, Berkshire, UK) or an Apple iMac Computer. The software packages used were LabChart for Windows and iMac (Version 6) and EChem for Windows Version 1.5.2 (ADInstruments Ltd.).

In vivo freely-moving CPA experiments were performed using low noise potentiostats (Biostat IV, ACM Instruments, Cumbria, UK, and Biostat II, with a head-stage amplifier from Electrochemical and Medical Systems (EMS), Newbury,UK. Data acquisition was performed using a PowerLab® interface system (ADInstruments Ltd; Oxford, UK) and an Apple iMac Computer. The software package used was LabChart for Mac (Version 6.1).

In vivo +-maze based CPA experiments were performed using a QuadStat (Model EA164) and data acquisition was performed using an e-corder 410 (Model ED410). The software packages used was Edaq chart (Version 5) for Windows.

The graphical and statistical analysis of acquired data was performed using Microsoft Excel 2010, GraphPad InStat® and Prism® (Version 5.01) from GraphPad Software, Inc. California, USA.

3.2.2 *Additional Equipment*

Air pump: The air pump used for O_2 experiments was a Rena Air 200 from RENA®, France

Anaesthetic unit: A multi-system set-up consisting of a vaporiser for induction (Univentor 400 Anaesthesia unit), an air pump (Stellar S3), an induction chamber with a 1.4 L capacity, a gas routing switch and stereotaxic inhalation mask which were all supplied from Agnthos, Sweden.

Carbon fibre bundle wire: Goodfellow Cambridge Ltd; UK.

Carbon fibre wire (PVA coated 1mm): World Precision Instruments, Hertfordshire, UK.

Conducting silver epoxy: Circuit Works CW2400, RS Components Ltd; UK.

Electrode wire: All Teflon® coated platinum, silver and gold wire was obtained from Advent Research Materials, Suffolk, UK.

Electronic Balance: Sartorius LA230D, Sartorius Stedim UK Limited, Dublin.

Gold clips: *In vitro*- Fine Science Tools, UK. *In vivo* - Plastics One, VA, USA.

Hamilton syringe: Fisher Scientific Ireland, Dublin.

Heat shrink: RS Components Ltd; UK.

Incubator: The incubator used for animal recovery a Thermacage MKII supplied by Datesand Ltd; UK.

Insulated Copper wire: 1mm PVA insulated Copper wire, RS Components Ltd; UK.

Magnetic Stirring Plate: Yellowline IKA MST Mini Magnetic Stirrer, Lennox, Ireland.

Microscope: The microscope used for electrode preparation was an Olympus SZ51, Mason Technology, Dublin.

pH meter: S20 Seven Easy Multi pH Meter, Mason Technology, Dublin.

Silica tubing: SGE Analytical Science supplied by VWR International Ltd; Dublin, Ireland.

Solder and soldering iron: Weller - WTCP 51, Farnell, UK.

Sonicator: Fisherbrand, FB11002, Fisher Scientific Ireland, Dublin.

Stereotaxic frame: The stereotaxic frame used was sourced from Kopf, CA, USA.

Surgical Screws: Plastics One, VA, USA

Teflon® Pedestal: Plastics One, VA, USA.

Temperature Probe: For temperature experiments a magnetic stirrer/hotplate (IKA MST Basic C, Lennox Laboratory Supplies Ltd; Dublin, Ireland) was used. Solution temperature, were indicated was controlled using a TC1 temperature controller (IKA).

Vortex: The Vortex (Reax Control, Heidolph, Essex, UK) was used to uniformly mix solutions by agitation.

3.3 Chemicals, Enzymes, Composites and Solutions

3.3.1 *In Vitro Chemicals*

Acetone	Sigma-Aldrich Co.
Bovine Serum Albumin (Fraction V)	Sigma-Aldrich Co.
Collodion	Fluka
Conductive Carbon Paste	SPI Supplies Inc.
Epoxy Resin	Sigma-Aldrich Co.
Graphite Powder	Sigma-Aldrich Co.
L-α-phosphatidylethanolamine (PEA)	Sigma-Aldrich Co.
Methyl Methacrylate (MMA)	Sigma-Aldrich Co.
Nitrogen Gas	BOC, Ireland

o-Phenylenediamine	Sigma-Aldrich Co.
Oxygen Gas	BOC, Ireland
Rhoplex®	General Paints Ltd.
Silicone oil	Aldrich Chemical Co.
Sodium Chloride	Sigma-Aldrich Co.
Sodium Hydroxide	Sigma-Aldrich Co.
Sodium Phosphate	Sigma-Aldrich Co.

3.3.2 *In Vivo Chemicals*

Acetazolamide (Diamox)	Sigma-Aldrich Co.
Buprenorphine hydrochloride (Tamgestic)	Sigma-Aldrich Co.
Chloral Hydrate	Sigma-Aldrich Co.
Dental acrylate	Sigma-Aldrich Co.
Dimethylsulfoxide (DMSO) for molecular biology	Sigma-Aldrich Co.
Isoflurane	Abbott Laboratories.

3.3.3 *Enzymes*

Glucose oxidase (49180)	Sigma-Aldrich Co.
Glucose oxidase (Aspergillus niger)	Sigma-Aldrich Co.

Glucose oxidase (Aspergillus niger)	Genzyme Chemical Co.
Glucose oxidase (G2133 50KU)	Sigma-Aldrich Co.

3.3.3.1 Enzyme substrates

D-(+)-Glucose	Sigma-Aldrich Co.

3.3.4 *Solutions*

3.3.4.1 *In Vitro* Solutions

Artificial Cerebro Spinal Fluid (aCSF)

This was prepared by dissolving 8.9 g NaCl (0.15 M), 0.298 g KCL (0.004 M), 0.176 g $CaCl_2$ (0.0016 M) and 0.204 g $MgCl_2$ (0.021 M) in 1 L of H_2O.

Ascorbic Acid (AA)

A 0.1 M standard solution was prepared by dissolving 0.176 g in 10 ml H_2O. The solution was N_2 saturated and prepared freshly before use.

Bovine Serum Albumin (BSA)

A 10% (w/v) solution was prepared by dissolving 0.1g in 1 ml H_2O.

Glucose

A 1 M standard solution was prepared by dissolving 9.01g of glucose in 50 ml H_2O. The solution was prepared 24 hours before use and stored at room temperature to allow complete mutarotation of the anomers.

L-α-phosphatidylethanolamine (PEA)

A 10% solution was prepared by dissolving 0.140 g in 1 ml H_2O.

o-Phenylenediamine (o-PD)

A 300 mM (saturated) solution was prepared by dissolving 0.324 g in 10 ml of N_2 saturated PBS. A sonic bath was used for a minimum of 10 minutes to agitate the solution and ensure maximum dissolution.

o-Phenylenediamine /Glucose oxidase (o-PD/GOx)

A 300 mM solution of *o*-PD was prepared as previously described. 5 mg/ml of GOx was incorporated into 5 ml of *o*-PD solution.

Phosphate Buffer Saline (PBS) pH 7.4

This was prepared by dissolving 8.9 g NaCl (0.15 M), 1.76 g NaOH (0.044 M) and 6.86 g $NaH_2PO_4.2H_2O$ (0.044 M) in 1 L of H_2O. The pH was adjusted to 7.4 as required and the solution was N_2 saturated for a minimum of one hour.

PBS pH 6.5 & 8

This was prepared by dissolving 8.9 g NaCl (0.15 M), 1.76 g NaOH (0.044 M) and 6.86 g $NaH_2PO_4.2H_2O$ (0.044 M) in 1 L of H_2O. The pH was adjusted to pH 6.5 using NaH_2PO_4 and pH 8 using NaOH.

3.3.4.2 *In Vivo* Solutions

Chloral Hydrate

For systemic administration 350 mg/kg/1 ml was prepared in 0.9 % saline solution.

Acetazolamide (Diamox)

For systemic administration 50 mg/kg/1.5 ml was prepared in 0.5 ml 0.9 % saline solution and 1 ml DMSO.

Glucose soultion

For systemic administration 250 mg/kg/1 ml was prepared in 0.9 % saline solution.

Normal Saline Solution

A 0.9% solution was prepared by dissolving 0.9 g NaCl in 100 ml H_2O.

3.3.5 *Composites*

Carbon Paste

0.71 g of graphite powder was mixed with 250 µl of silicone oil. This was done by continuous mixing in a pestle and mortar for 3 hours to ensure that the two components were completely amalgamated.

Carbon Polyvinyl Acetate (PVA)

Three PVA based composites were used throughout this project with varying amounts of graphite powder.

0.05 g PVA/0.01 g carbon

0.05 g PVA/0.02 g carbon

0.05 g PVA/0.03 g carbon

The graphite powder was weighed and mixed with PVA using a needle on a non-absorbent acetate sheet.

Carbon Rhoplex®

Rhoplex® based composites were used throughout this project with varying amounts of graphite powder.

0.05 g Rhoplex®/0.01 g carbon

0.05g Rhoplex®/0.02 g carbon

0.05 g Rhoplex®/0.03 g carbon

0.01g Rhoplex®/0.05g carbon

0.005g Rhoplex®/0.0125g carbon

The graphite powder was weighed and mixed with Rhoplex® using a needle on a non-absorbent acetate sheet.

3.4 Electrode Preparation

3.4.1 *Carbon Paste Electrodes*

All carbon paste electrodes (CPE) were prepared by trimming approximately 4.5 cm lengths of 200 µm Teflon®- insulated silver wire (200 µm bare diameter, 270 µm coated diameter (8T), Advent Research Materials, Suffolk, UK). The wire was carefully cut at both ends using a sharp scalpel to create an even disk surface. 3 mm of the wire was exposed by removing the Teflon® from one end of the wire and the Teflon® was carefully pushed up the wire to create a 2 mm cavity. The cavity was then packed with carbon paste (Section 3.3.5) by dipping the tip of the electrode into a small amount of the paste which

was packed in using a bare silver wire as a plunger. This process was repeated until the cavity was completely packed. A flat active surface at the tip of the electrode was obtained by gently tapping the electrode off a hard, flat surface. The 3 mm of exposed wire was soldered into a gold clip for electrical conductivity and rigidity.

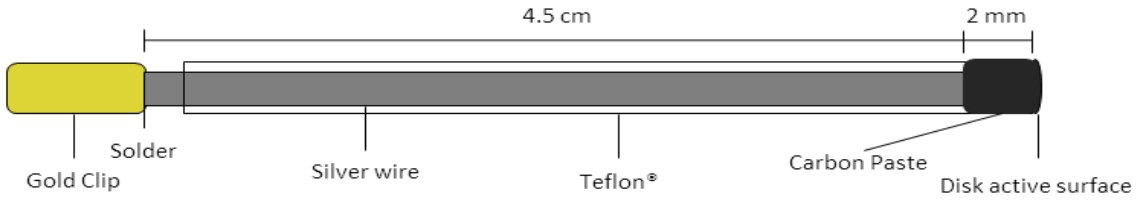

Figure 3.1: Schematic representation of a carbon paste electrode.

3.4.2 *Silver based carbon composite electrodes*

Carbon composite electrodes were prepared by trimming approximately 4.5 cm lengths of 200 µm Teflon®- insulated silver wire (200 µm bare diameter, 270 µm coated diameter (8T), Advent Research Materials, Suffolk, UK). The wire was carefully cut at both ends using a sharp scalpel to create an even disk surface. 3 mm of the wire was exposed by removing the Teflon® from one end of the wire and the Teflon® was carefully pushed up the wire to create a 2 mm cavity. The cavity was then packed with a carbon composite (section 3.3.5) by dipping the tip of the electrode into the paste. This process was repeated until the cavity was completely packed. A flat active surface at the tip of the electrode was obtained by gently tapping the electrode off a hard, flat surface. The 3 mm of exposed wire was soldered into a gold clip for electrical conductivity and rigidity.

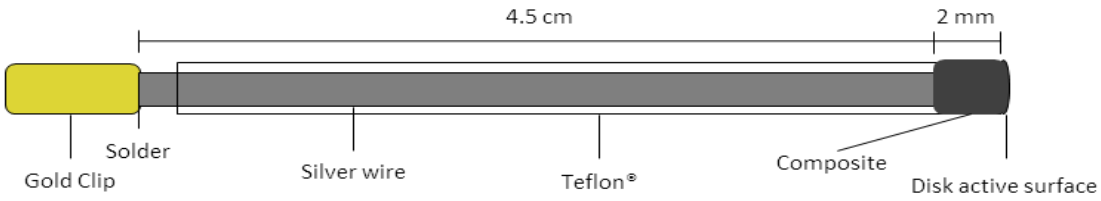

Figure 3.2: Schematic representation of a silver based carbon composite electrode.

3.4.3 *Carbon Rhoplex® composite electrodes fMRI design (CRCEs)*

A 4.5 cm length of 200 µm Teflon®-insulated silver wire (200 µm bare diameter, 270 µm coated diameter (8T), Advent Research Materials, Suffolk, UK) was cut at both ends using a sharp scalpel to create an even disk surface. The Teflon® was carefully removed from the wire and a bundle of carbon fibres was inserted into the Teflon®. The carbon fibres were trimmed at one end and pulled gently back through the Teflon® creating a cavity of ~ 1 mm. The opposite end was glued with a small amount of superglue and left to dry.

5 mm from both ends of a 20 cm length of coated copper was removed and a gold clip was soldered at one end for electrical contact and connection to the system. An 11 cm length of polyamide coated carbon fibre was cut and 5 mm of coating removed from either end of the wire. Using conductive silver epoxy the wire was adhered at one end to the Teflon® containing the carbon fibres and to the copper wire at the other. Both connections were carefully sealed avoiding the Teflon® with clear heat shrink and a small amount of superglue.

3.9 cm of polyamide coated carbon fibre was cut and the carbon fibre bundle was removed from the coating. The Teflon® containing the carbon fibres was then inserted into the polyamide coating and glued. This was then sealed with heat shrink and glued.

When dry a 1 cm length of silica (320 µm i.d./430 µm o.d.) was cut and both sides were polished with fine sandpaper. A silver wire was pushed through the silica tubing to remove any residue on the inside of the tube. The Teflon® coating the carbon fibres was then inserted into the silica, with a small amount of the fibres visible at the cavity end of the Teflon® and the silica was glued to the polyamide coating.

The carbon Rhoplex® composite was fabricated by mixing 0.03 g of carbon with 0.05 g of Rhoplex®. This was mixed thoroughly and carefully packed by gently dipping the Teflon® cavity into the mixture. The electrode was checked frequently through this process to ensure sufficient packing of the cavity. When completed the tip of the electrode was tapped off a clean dry surface to ensure the active surface was a uniformly flat, smooth disk shape.

The electrodes were left to dry for 24 hours with the active surface flat against a hard surface to prevent the glue from displacing. After 24 hours the packing was checked and any excess composite on the outer Teflon® was removed carefully using a needle.

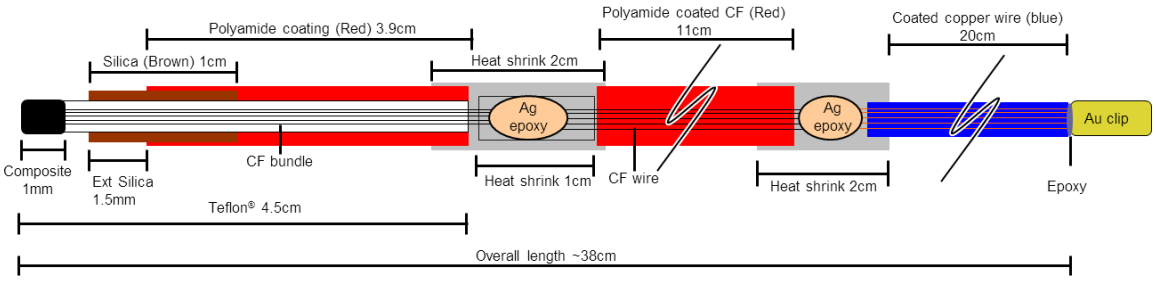

Figure 3.3: Schematic representation of a CRCE full fMRI design.

3.4.4 *Carbon Rhoplex® composite electrodes in vivo freely-moving design (CRCEs)*

A 3 cm length of 200 µm Teflon®-insulated silver wire wire (200 µm bare diameter, 270 µm coated diameter (8T), Advent Research Materials, Suffolk, UK) was cut at both ends using a sharp scalpel to create an even disk surface. The Teflon® was carefully removed from the wire and a bundle of carbon fibres was inserted into the Teflon®. The carbon fibres were trimmed at one end and pulled gently back through the Teflon® creating a cavity of ~ 1 mm. The opposite end was glued with a small amount of superglue and left to dry.

1 mm from both ends of a 3 cm length of coated copper was removed and a gold clip was soldered at one end for electrical contact and connection to the system.

Using conductive silver epoxy the copper wire was adhered to the carbon fibres. This connection was carefully sealed avoiding the Teflon® with clear heat shrink and a small amount of superglue. 3 cm of polyamide coated carbon fibre was cut and the carbon fibre bundle was removed from the coating. The Teflon® containing the carbon fibres was then inserted into the polyamide coating and glued to the heat shrink. This was then sealed with heat shrink and glued.

When dry a 1 cm length of silica (320 µm i.d./430 µm o.d.) was cut and both sides were polished with fine sandpaper. A silver wire was pushed through the silica tubing to remove any residue on the inside of the tube. The Teflon® coating the carbon fibres was then inserted into the silica, with a small amount of the fibres visible at the cavity end of the Teflon® and the silica was glued to the polyamide coating.

The carbon Rhoplex® composite was fabricated by mixing 0.03 g of carbon with 0.05 g of Rhoplex®. This was mixed thoroughly and carefully packed by gently dipping the Teflon® cavity into the mixture. The electrode was checked frequently through this process to ensure sufficient packing of the cavity. When completed the tip of the electrode was tapped off a clean dry surface to ensure the active surface was a uniformly flat, smooth disk shape. The electrodes were left to dry for 24 hours with the active surface flat against a hard surface to prevent the glue from displacing. After 24 hours the packing was checked and any excess composite on the outer Teflon® was removed carefully using a needle.

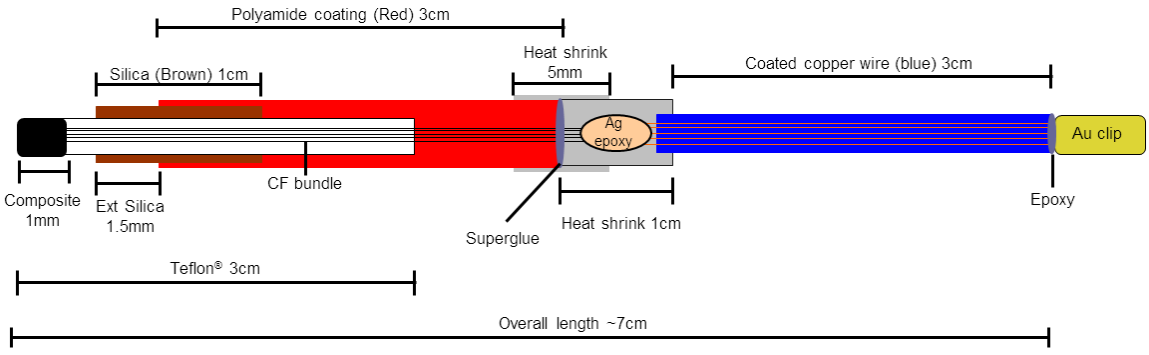

Figure 3.4: Schematic representation of a CRCE freely-moving design.

3.4.5 *Disk platinum electrodes*

Platinum based disk working electrodes were prepared by trimming approximately 4.5 cm lengths of 200 µm Teflon®-insulated Pt/Ir (90%/10%) wire (125 µm bare diameter, 175 µm coated diameter (5T), Advent Research Materials, Suffolk, UK). The wire was carefully cut at both ends using a sharp scalpel to create an even disk surface. 3 mm of the wire was

exposed by removing the Teflon® from one end of the wire and this was soldered into a gold clip for electrical conductivity and rigidity.

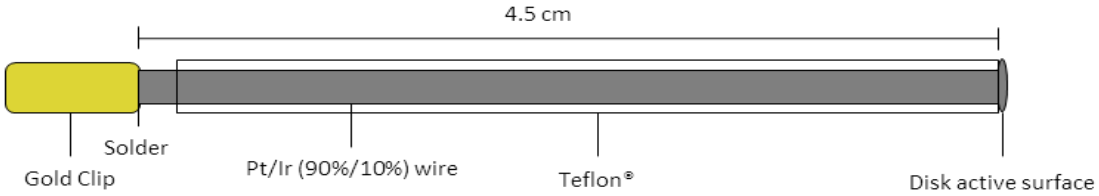

Figure 3.5: Schematic representation of a Pt-disk electrode.

3.5 Electrode Modifications

3.5.1 *Electropolymerisations*

To prevent interference from endogenous electroactive species such as ascorbic acid some electrodes were modified by generating a size exclusion polymer over the active surface of the electrodes.

The electrodes were electropolymerised using a standard three-electrode cell consisting of four working electrodes, a bare platinum wire as an auxiliary electrode and a SCE reference electrode. A nitrogen (N_2) atmosphere was maintained throughout the polymerisation as the solution is liable to oxidation in air. The cell was set up and N_2 saturated prior to the preparation of the monomer. The monomer solution was transferred to the cell and the lid replaced immediately. When the polymerisation was complete the working electrodes were instantly removed from the monomer solution, dipped in H_2O and allowed to dry for a minimum 1 hour before further use.

3.5.1.1 Poly-*o*-phenylenediamine Modified Electrodes (PPD)

A 300 mM solution of *o*-Phenylenediamine (*o*-PD) was prepared as described previously (section 3.3.4.1). The solution was placed in a previously set up N_2 saturated cell and a potential of +700 mV *vs.* SCE was applied to the working electrodes for 30 minutes. The

electrodes were removed from the monomer solution, rinsed in H_2O and allowed to dry for 1 hour before further use. The electrodes were stored in the refrigerator at 4 ˚C when not in use.

3.5.2 *Metal based modified O_2 electrodes*

3.5.2.1 MMA modified O_2 electrodes

A Pt disk electrode was placed in pure MMA monomer solution for a period of 5 s, removed and allowed to dry at room temperature for a minimum of 1 h before use. The electrode was stored in the refrigerator at 4 ˚C when not in use.

3.5.3 *Enzyme based Electrodes*

3.5.3.1 Poly-*o*-phenylenediamine/Glucose Oxidase Modified Electrodes

For the detection of the substrate glucose the enzyme glucose oxidase (GOx) was incorporated in to the PPD polymer by means of entrapment. A 300 mM solution of *o*-PD was prepared as described (Section 3.3.4.1). 5mg/ml of GOx was added to the *o*-PD solution which was agitated using a vortex to amalgamate the monomer and the enzyme. Pt disk electrodes were usually polymerised using 5 ml of monomer with 25 mg of GOx to minimise the amount of enzyme for cost effective purposes.

3.5.4 *Electrode treatments and stability*

To determine the electrode's viability in the *in vivo* environment the effects of proteins and lipids were investigated. The proteins and lipids naturally occurring in endogenous tissue can have an effect on the sensitivity of the electrodes (Ormonde & O'Neill, 1989, 1990) . To determine if the electrodes are liable to a reduction in sensitivity they were exposed to bovine serum albumin (BSA), L-α-phosphatidylethanolamine (PEA) and *ex-vivo* brain tissue samples.

Stability was examined to investigate the shelf-life of the electrodes with respect to time. Electrodes were calibrated, stored in the refrigerator at 4 ˚C and repeatedly recalibrated for specified amounts of time (see individual electrodes) to determine if there was a reduction in the sensitivity.

3.5.4.1 BSA treated electrodes

Previously calibrated electrodes were immersed in a BSA 10% (w/v) solution (Section 3.3.4.1). The electrodes remained in the solution for 12 or 24 hours and were recalibrated an hour following removal from the BSA solution. The electrodes were then re-immersed in the solution and calibrated after specified amounts of days.

3.5.4.2 PEA treated electrodes

Previously calibrated electrodes were immersed in a PEA 10% (w/v) solution (Section 3.3.4.1). The electrodes remained in the solution for 12 or 24 hours and were recalibrated an hour following removal from the PEA solution. The electrodes were then re-immersed in the solution and calibrated after specified amounts of days

3.5.4.3 Brain Tissue Treated Electrodes

Previously calibrated electrodes were placed in a sample of *ex-vivo* brain tissue. Small amounts of PBS, depending on the amount of sample present, were added to the tissue to prevent dehydration. The active surface of the electrodes remained in contact with the brain tissue for 12 or 24 hours and were recalibrated an hour following removal from the tissue. The electrodes were then re-immersed in the brain tissue sample and calibrated after a specified amount of days.

3.6 Electrochemical Experiments

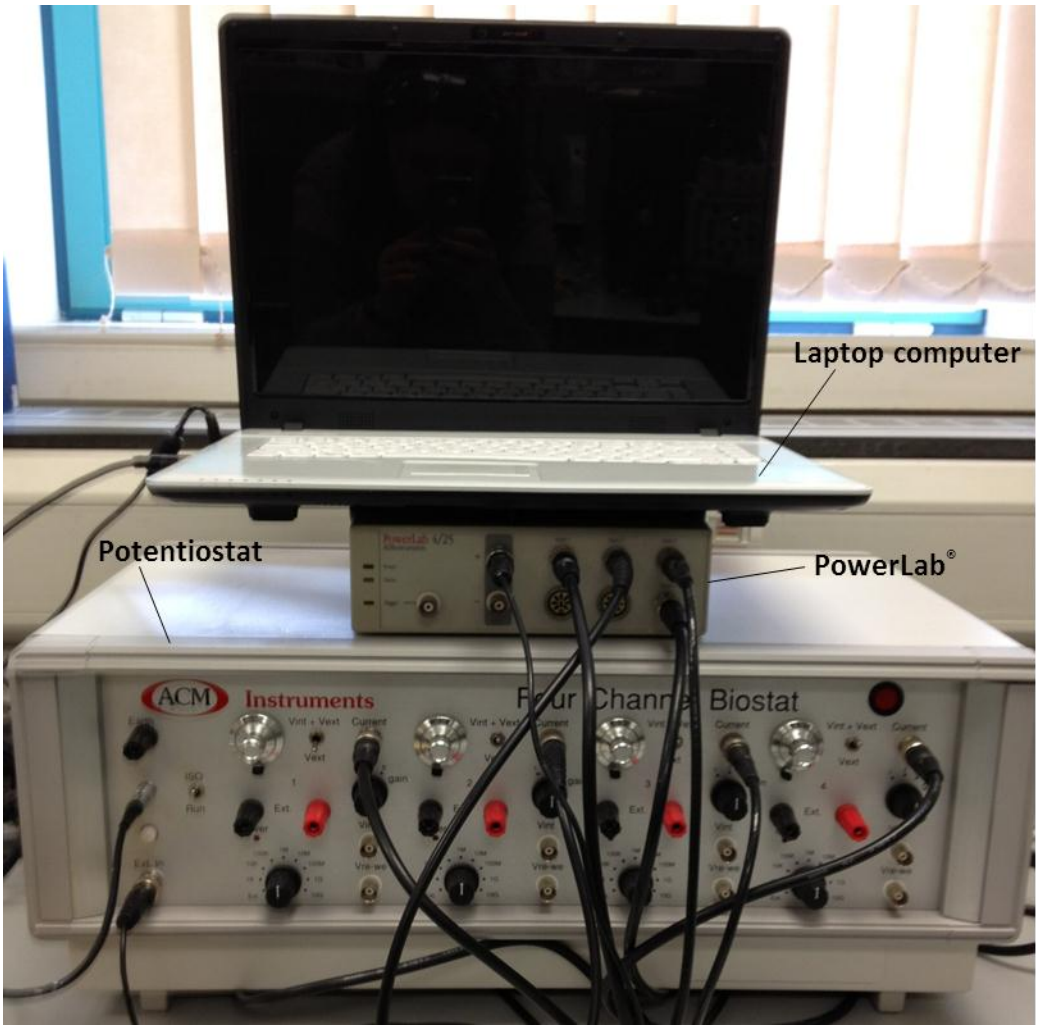

Figure 3.6: ***In vitro*** **electrochemical equipment set-up.**

3.6.1 *In Vitro Experiments*

3.6.1.1 Three- Electrode Electrochemical Cell

All of the *in vitro* experiments were performed using an in-house manufactured cell. The cell itself was made of glass and a custom lid was used which was constructed using Teflon®. The cap consisted of an opening for the reference, auxiliary and working electrodes. The cap also had openings which served as gas and injection inlets. A

magnetic stirring bead was also used when required and all experiments were performed at room temperature (21˚C) except when stated.

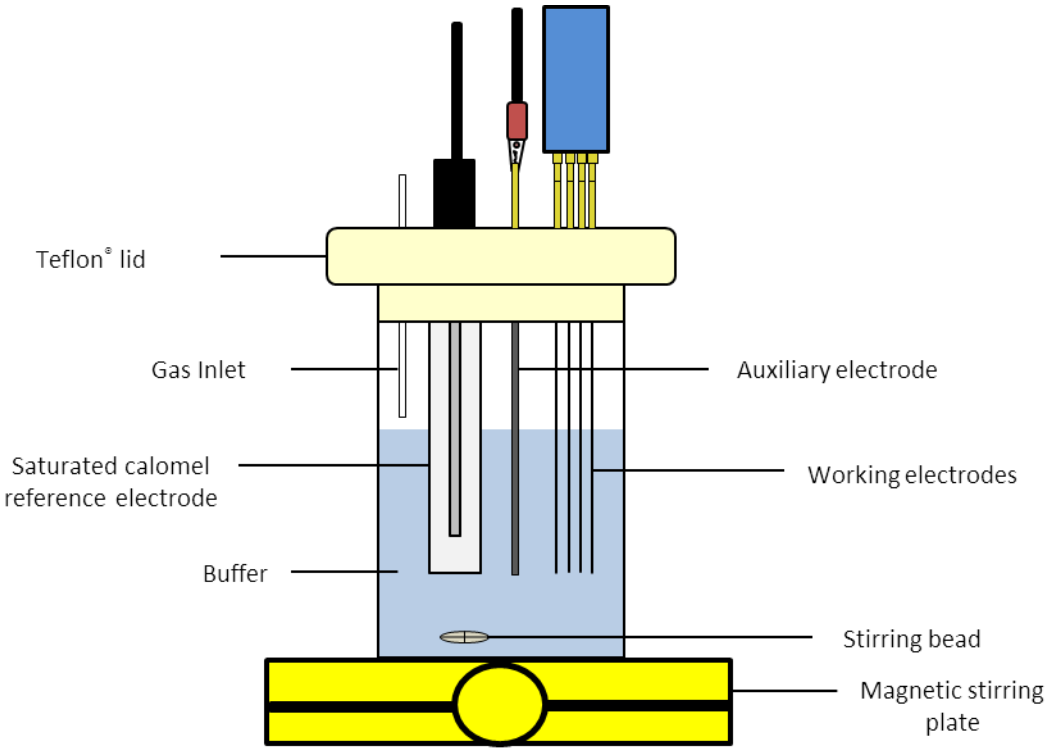

Figure 3.7: Schematic of a three-electrode cell set-up used in electrochemical experiments.

3.6.1.2 Cyclic Voltammetry (CV)

To determine the oxidation or reduction peak of a species CV is used. A potential sweep is applied to the working electrode from an initial potential to a maximum potential. The sweep is inverted and then scanned back to the initial potential. The parameters used for these experiments were between -1000 to +1000 mV *vs.* SCE at a scan rate of between 20 to 100 mV/s, however the range used varied between types of electrodes. All CV experiments were performed in a standard three-electrode electrochemical cell. The reference electrode used was a saturated calomel electrode (SCE) and the auxiliary was a bare Pt wire. CV experiments were performed in quiescent solution.

3.6.1.3 Constant Potential Amperometry (CPA)

To calibrate the various types of working electrodes, CPA was used. A fixed potential was applied throughout the experiment which varied according to each specific type of electrode and analyte. The applied potential was determined by CV.

All CPA experiments were performed in a standard three-electrode electrochemical cell. The reference electrode used was a saturated calomel electrode and the auxiliary was a bare Pt wire. The potential was applied to the working electrodes which were allowed to settle until a stable baseline was reached. The amount of time for a stable baseline to occur varied depending on the working electrodes used.

3.6.1.4 High concentration Oxygen (O_2) Calibrations

The potential applied to the O_2 electrodes was -650 mV *vs.* SCE (unless otherwise stated). The electrodes were allowed to settle before being calibrated. Various concentrations of O_2 were used. A 0 µM concentration of O_2 was firstly obtained by deoxygenating the cell with N_2 gas. A 240 µM concentration of O_2 was obtained by bubbling air through the buffer solution (Bourdillon *et al.*, 1982; Foster *et al.*, 1993). A 1200 µM concentration of O_2 was obtained by bubbling pure O_2 through the buffer solution until it was saturated (Bourdillon *et al.*, 1982). Each was bubbling and quiescent period was for approximately 40 minutes. The experiment was continuously recorded and in the absence of agitation steady states were chosen for analysis (unless otherwise stated).

3.6.1.5 Low concentration O_2 saturated PBS Calibrations

To determine the O_2 sensitivity of electrodes at low O_2 concentrations (0-125 µM) 100 % O_2 saturated PBS (1.2 mM) was used. A potential of -650 mV *vs.* SCE (unless otherwise stated) was applied to the electrodes and the PBS was deoxygenated by vigorously bubbling N_2 into the cell. When the electrodes had reached a steady state, standard aliquots (+416, +425, +434, +443 and +452 ml) of a saturated O_2 solution, each containing 25 mM O_2, were injected into the cell. The concentration range for the O_2 calibrations were:

0, 25, 50, 75, 100, 125 µM

3.6.1.6 Glucose Calibrations

A potential of +700 mV *vs.* SCE was applied to the glucose electrodes. The electrodes were allowed to reach a steady baseline. Aliquots of a 1 M glucose stock solution (section 3.3.4.1) were injected into the PBS solution in the cell. The PBS was briefly stirred using a magnetic stirring bead to uniformly mix the solution. The concentration range for the glucose calibrations were:

0, 1, 5, 10, 15, 20, 30, 50, 80, 100 mM

3.6.1.7 Ascorbic Acid (AA) Calibrations

Standard AA calibrations were performed at a potential of +700 mV *vs.* SCE. Aliquots of a 0.1 M AA stock solution was injected into the PBS solution in the cell. The PBS was briefly stirred using a magnetic stirring bead to uniformly mix the solution. The concentration range for the AA calibrations were:

0, 200, 400, 600, 800, 1000 µM

Calibrations involving a pre-injection of AA were performed at -650 mV *vs.* SCE. A 500 µM aliquot of 0.1 M AA stock solution was injected into the PBA solution in the cell once the electrodes had reached a steady-state. The PBS solution was briefly stirred using a magnetic stirring bead to uniformly mix the solution. The high concentration O_2 calibration was then performed in the presence of 500 µM AA.

3.6.1.8 Post- implantation Calibrations

Following removal of the headpiece the O_2 electrodes were calibrated in 20 ml PBS as described previously (Section 3.6.1.4). The headpiece was connected to the potentiostat via customised cables. Glucose electrodes could not be calibrated as the polymer does not

withstand the removal process. However pre-calibration data can be used with these electorodes (Lowry *et al.*, 2002). The post-calibration process allowed for *in vivo* currents to be converted into concentrations for analysis purposes.

3.7 *In Vivo* Experiments

3.7.1 *Animals*

Two strains of male rats were used during the course of this work. The Wistar strain was used for characterisation of various electrodes and the Sprague Dawley strain was used for hippocampal characterisation and behavioural experiments. Animals were obtained from Harlan (UK) and Charles River (UK) weighing between 200-300g. Animals were housed in a temperature (17-23˚C), humidity and light (on 08:00, off 20:00) controlled environment with food available *ad libitum* (unless otherwise stated).

3.7.2 *Surgery Protocol*

To implant electrodes into the brain for continuous monitoring a sterile surgery was performed. Firstly the rat was placed in an induction chamber connected to a vaporiser (Univentor) unit and anesthetised with the volatile anaesthetic Isoflurane. Once the animal was anesthetised its weight was recorded and the top of the animal's head was shaven. The animal was immediately placed in a sterotaxic frame ensuring that the head is completely levelled between bregma and lambda.

An Iodine solution was used as a pre-operative antiseptic and a midline incision of approximately 2 cm was made from the anterior to the posterior of the animal's skull. The skull was exposed by clamping the Periosteum at the top and bottom of each side of the incision. Minor epidural haemorrhages occasionally occur upon removal of the skin but these are quickly minimised by cauterising the affected area.

The steriotaxic coordinates used are from The Rat Brain in Steriotaxic Coordinates (Paxinos & Watson, 1998). Bregma is the anatomical point on the skull at which the

coronal suture is intersected perpendicularly by the sagittal suture, and used as the zero reference point. Bregma is used to obtain the anterior-posterior (A-P) and medial-lateral (M-L) coordinates where + A-P is anterior to bregma and + M-L is the right hemisphere. The dorsal-ventral (D-V) coordinates are obtained in respect to dura where - D-V is depth into the brain. The coordinates in mm used for various regions are listed in Table 3.1.

Brain Region	A-P	M-L	D-V
Striatum	+1.0	± 2.5	-5/-6
Dorsal Hippocampus	-5.6	± 4.6	-3.6

Table 3.1: Steriotaxic coordinated for electrode for various brain regions in mm.

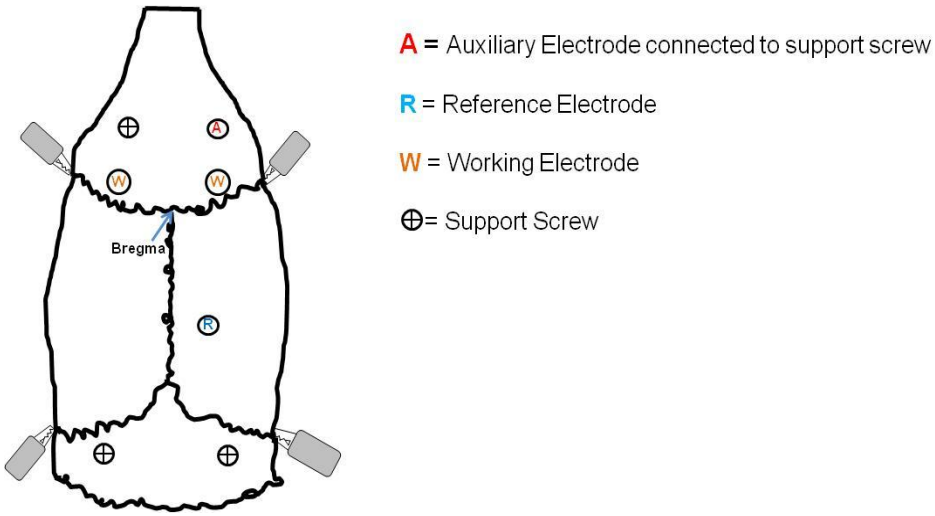

Figure 3.8: Schematic representation of the bilateral placement of two working electrodes in the striatum as well as the location of clamps, support screws, reference and auxiliary electrodes.

The location of bregma was confirmed and the working electrode's coordinates were marked. The skull was drilled to allow for the placement of four support screws, one of which was used for attachment of the auxiliary electrode (Figure 3.9(bottom)). These support screws were used to aid the adhesion of cement to the skull. The holes for the working electrodes were drilled next and the dura was pierced for a few seconds using a 25G hypodermic needle. Electrodes were implanted using D-V co-ordinates (Table 3.1), via the steriotaxic arm. A thin layer of cement was placed around the working electrodes to

ensure that the electrodes remained firmly in place. The reference electrode (Figure 3.9(top)) was then implanted into the cortex in the same way and secured in place with cement. The electrodes were carefully manoeuvred and bent against the cement layer and the gold clips were placed into a pedestal (Figure 3.10). The level of anaesthetic was adjusted according to the procedure i.e. increased during the drilling procedure and decreased whilst cementing.

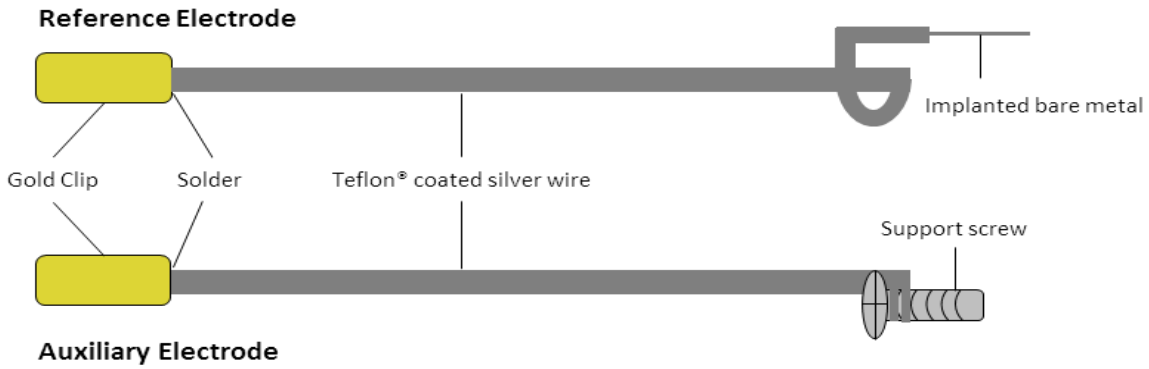

Figure 3.9: Schematic of a reference electrode (Top) and an auxiliary electrode (Bottom) for *in vivo* implantation.

The gold clips were carefully cemented into the pedestal and when fully dry the wires were bent carefully to compact them as much as possible. The electrodes were then completely covered using cement, this ensured that they were protected and gave support for the pedestal. Care was taken not to place cement too far up the pedestal so that the cables could be attached securely to it. When the cement was completely dry, the animal was removed from the sterotaxic frame and placed in an incubation unit for at least an hour to recover. Animals were post-surgically administered the analgesic Temgesic (Buprenorphine) via subcutaneous (s.c.) injection (0.1 mg/kg), and 1 ml normal saline to prevent dehydration.

Animals were assessed post-surgery and daily thereafter for good health and were allowed to recover for at least 24 hours before being connected to the equipment.

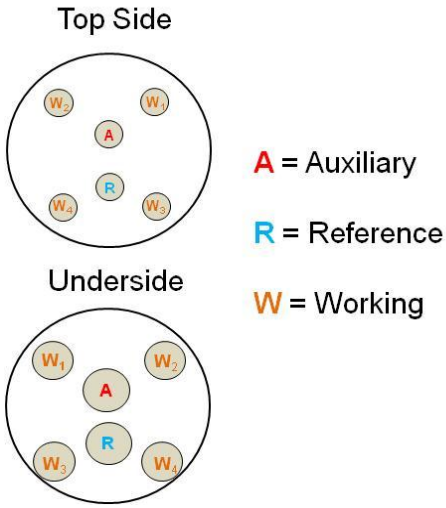

Figure 3.10: Schematic of a Teflon® pedestal used for in vivo experiments. The electrodes were placed in the corresponding holes to allow for connection to the recording equipment.

3.7.3 *Freely-moving continuous monitoring*

Animals were connected to a potentiostat at least 24 hours following surgery. The equipment was set up for constant potential amperometry and the animal was attached to an insulated cable via the pedestal. The cable was then connected to the potentiostat and the required potential was applied to each electrode individually. The electrodes were allowed to settle for the required amount of time which was dependent on the electrode type.

3.7.4 *Gaseous administrations*

O_2 and N_2 gases were administered to the animal to produce mild hyperoxic and hypoxic conditions. This was achieved via plastic tubing which was connected to the relative cylinder and held closely to the animal's snout for the required duration (3 or 5 min).

3.7.5 *Neuronal Activation*

3.7.5.1 Tail pinch

A tail pinch was performed using a paper clip or crocodile clip. The clip was attached to the animal's tail approximately 2 cm from the tip of the tail for 5 minutes. The animal was given a piece of wood to encourage gnawing. The gnawing action promoted by the stimulating tail pinch has been shown to increase motor activity (Antelman *et al.*, 1975). After 5 minutes the clip was carefully removed.

3.7.5.2 Restraint test

A restraint test was performed by holding down the animal in its home bowl to restrict movement. The animal was restrained this way for 5 minutes which induces a mild stress reaction.

3.7.6 *Drug administration via injection*

Drugs or drug vehicles were administered to the animal via two methods. A subcutaneous (s.c.) injection under the skin, and intraperitoneal (i.p.) injection into the abdominal cavity (Wolfensohn & Lloyd, 2008).

3.7.7 *+-maze experiments*

Animals were housed in a plastic home bowl and connected to a Quadstat as previously described (Section 3.7.3). Animals were administered via i.p. either saline or glucose solutions and after 30 mins animals were placed into the +-maze. Animals were allowed to explore the +-maze for a duration of 20 mins. All arm entries (the animal moved past the entry gate of any arm from the central region of the +-maze so that all four feet were in the arm) were recorded in the order in which they occurred and all +-maze experiments were recorded on a webcam to verify arm entry order.

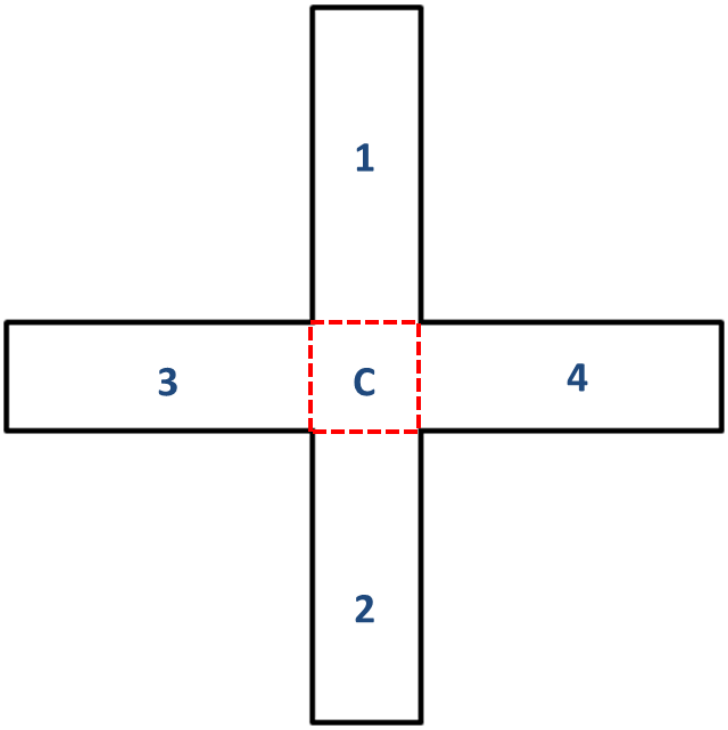

Figure 3.11: Schematic representation of a +-maze representing the four arms and the centre area.

3.7.8 *End of in vivo experiments*

In vivo experiments were terminated by euthanising the animal with a 1 ml i.p. injection of Euthatal. The brain was removed and stored in a solution of formaldehyde.

References

Antelman SM, Szechtman H, Chin P & Fisher AE. (1975). Tail pinch-induced eating, gnawing and licking behavior in rats: Dependence on the nigrostriatal dopamine system. *Brain Research* **99,** 319-337.

Bazzu G, Puggioni GGM, Dedola S, Calia G, Rocchitta G, Migheli R, Desole MS, Lowry JP, O'Neill RD & Serra PA. (2009). Real-Time Monitoring of Brain Tissue Oxygen Using a Miniaturized Biotelemetric Device Implanted in Freely Moving Rats. *Analytical chemistry* **81,** 2235-2241.

Bourdillon C, Thomas V & Thomas D. (1982). Electrochemical study of d-glucose oxidase autoinactivation. *Enzyme and Microbial Technology* **4,** 175-180.

Foster TH, Hartley DF, Nichols MG & Hilf R. (1993). Fluence Rate Effects in Photodynamic Therapy of Multicell Tumor Spheroids. *Cancer Research* **53,** 1249-1254.

Lowry JP, Boutelle MG, O'Neill RD & Fillenz M. (1996). Characterization of carbon paste electrodes *in vitro* for simultaneous amperometric measurement of changes in oxygen and ascorbic acid concentrations *in vivo*. *The Analyst* **121,** 761-766.

Lowry JP, Griffin K, McHugh SB, Lowe AS, Tricklebank M & Sibson NR. (2010). Real-time electrochemical monitoring of brain tissue oxygen: a surrogate for functional magnetic resonance imaging in rodents. *NeuroImage* **52,** 549-555.

Lowry JP, McAteer K, El Atrash SS, Duff A & O'Neill RD. (1994). Characterization of Glucose Oxidase-Modified Poly(phenylenediamine)-Coated Electrodes *in vitro* and *in vivo*: Homogeneous Interference by Ascorbic Acid in Hydrogen Peroxide Detection. *Analytical Chemsitry* **66,** 1754-1761.

Lowry JP, O'Neill RD, Boutelle MG & Fillenz M. (2002). Continuous monitoring of extracellular glucose concentrations in the striatum of freely moving rats with an implanted glucose biosensor. *Journal of Neurochemistry* **70,** 391-396.

O'Neill RD, Lowry JP & Mas M. (1998). Monitoring brain chemistry *in vivo*: voltammetric techniques, sensors, and behavioral applications. *Critical reviews in neurobiology* **12,** 69-127.

Ormonde DE & O'Neill RD. (1989). Altered response of carbon paste electrodes after contact with brain tissue: Implications for modified electrode use *in vivo*. *Journal of Electroanalytical Chemistry and Interfacial Electrochemistry* **261,** 463-469.

Ormonde DE & O'Neill RD. (1990). The oxidation of ascorbic acid at carbon paste electrodes: Modified response following contact with surfactant, lipid and brain tissue. *Journal of Electroanalytical Chemistry and Interfacial Electrochemistry* **279,** 109-121.

Paxinos G & Watson C. (1998). *The Rat Brain in Stereotaxic Coordinates*. Academic Press.

Wolfensohn S & Lloyd M. (2008). *Handbook of Laboratory Animal Management and Welfare*. John Wiley & Sons.

4. RESULTS: CHARACTERISATION OF SENSORS FOR THE DETECTION OF OXYGEN *IN VITRO*

4.1 Introduction

Carbon paste electrodes (CPEs) have been previously used successfully *in vitro* and *in vivo* for the detection and measurement of brain tissue oxygen in freely-moving animals (Lowry *et al.*, 1996; Lowry *et al.*, 1997; Bolger & Lowry, 2005; Bolger *et al.*, 2011a). CPEs are a popular choice due to their stability, are less prone to surface poisoning than metal-based electrodes and therefore do not require protective membranes, although CPEs generally have a longer construction time than metal-based electrodes. Pt-based electrodes have several advantages over CPEs including smaller probe size and ease of construction. Pt-based electrodes been shown to have the potential to provide a reliable alternative to CPEs to monitor brain tissue O_2 *in vivo* (Bolger *et al.*, 2011a). This chapter details comparisons between CPEs and a Pt-based electrode modified with methyl methacrylate (MMA). The polymer MMA was chosen as it is a widely used, commercially available polymer with FDA approval making it ideal for potential use in humans. The electrodes can also be easily sterilised, which is of necessity in a clinical environment. The polymer is used as a protective membrane due to the susceptibility of metal-based electrodes to surface poisoning. This enables the sensor to function and ensures biocompatibility, a necessity for safety reasons which have previously been examined for several biomaterials (Wilkins & Radford, 1990).

The *in vitro* characterisation of an electrode allows for the determination of the sensitivity, selectivity and stability of the sensor. The sensor's sensitivity was tested after exposure to proteins, lipids and brain tissue. The effects of various temperatures, pH, ions, convection and interferents were also examined along with the stability of the sensors in relation to time.

The brain's tissue immunological mechanisms (Wisniewski *et al.*, 2000) as well as its range of endogenous species can have an effect on the performance of the sensor (Lyne & O'Neill, 1990; Garguilo & Michael, 1994; Gifford *et al.*, 2006). Once the sensor is implanted the surface can change dramatically as observed with CPEs (Ormonde & O'Neill, 1989, 1990). The placement of sensors in tissue can also effect the sensor's surface morphology (O'Neill, 1993) and in terms of mass transport, there is a restriction due to the

tissue matrix (Cheng *et al.*, 1979; Dayton *et al.*, 1983; Nicholson & Syková, 1998) which can have an effect in terms of sensitivity, stability and selectivity of the sensors. The *in vitro* characterisation allows for an indication of the consequences of implantation of the sensor into tissue and how the response of the sensor may differ.

4.2 Experimental *In Vitro*

The instrumentation and software used are detailed in Section 3.2 and all chemicals and solutions are detailed in Section 3.3.

Pt disk electrodes (125 µm bare diameter) were constructed as described in Section 3.4.5 and modified using MMA as detailed in Section 3.5.2.1. CPEs (200 µm bare diameter) were constructed as described in Section 3.4.1.

Electrochemical experiments are detailed in Section 3.6 and electrode treatments in Section 3.5.4.

Data is represented as the mean ± SEM where n = number of electrodes used, unless otherwise stated. The slope, nA/µM was obtained from calibration plots using linear regression analysis and is used to represent the sensitivity. Goodness of fit is denoted by the R^2 value. Sensitivities were compared using unpaired *t*-tests and ANOVA. To compare the different electrodes due to varying physical dimensions current values were converted to current densities (Section 2.8.3).

4.3 Results and Discussion *In Vitro*

4.3.1 *Characterisation of CPEs*

The optimal reduction potential of O_2 at the surface of CPEs has previously been determined using cyclic voltammetry (Lowry *et al.*, 1996). The chosen reduction potential was -650 mV and subsequent constant potential amperometry (CPA) experiments were carried out at this potential.

4.3.1.1 Oxygen calibrations

O_2 calibrations were performed on CPEs as described in Section 3.6.1.4. A typical O_2 calibration trace can be seen in Figure 4.1

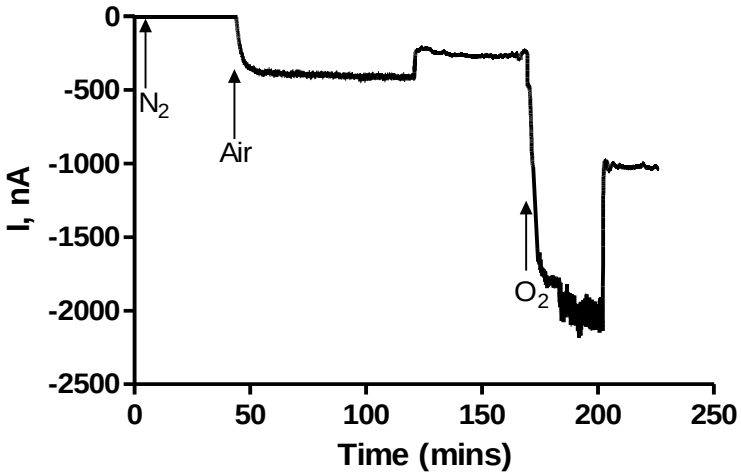

Figure 4.1: An example of typical raw data for an O_2 calibration in PBS using a CPE. CPA performed at -650 mV *vs.* SCE in PBS (pH 7.4) at 21˚C.

Average results obtained for high concentration O_2 calibrations performed in PBS on CPEs (*n*=24) are presented below in Table 4.1 and plotted in Figure 4.2. The mean background current of -3.00 ± 1.82 nA was subtracted.

$[O_2]$, µM	Mean I, nA	SEM
0	0	0
240	-285.9	10.0
1200	-1255.1	44.5

Table 4.1: Table of results for O_2 calibrations (0-1200 µM) for CPEs (*n*=24). CPA performed at -650 mV *vs.* SCE in PBS (pH 7.4) at 21˚C. Mean background subtracted.

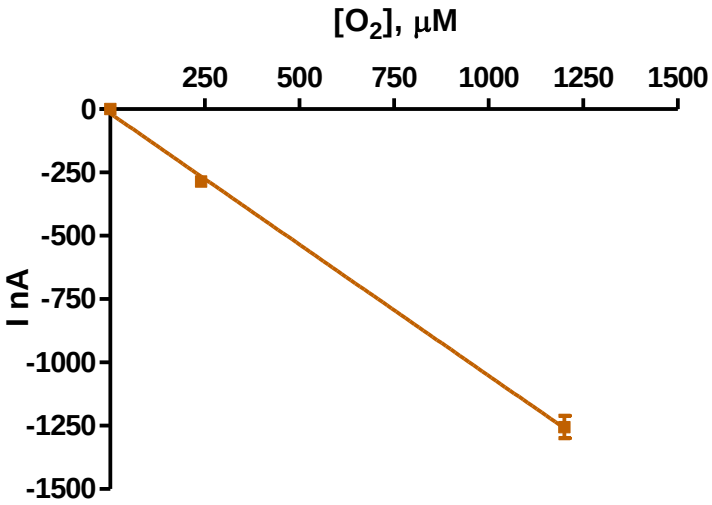

Figure 4.2: O_2 calibration data (0-1200 µM) for CPEs (*n*=24). CPA performed at -650 mV *vs.* SCE in PBS (pH 7.4) at 21˚C.

Linear regression analysis shows that the electrodes have a sensitivity (slope value) of -1.036 ± 0.030 nA/µM (*n* = 24). The response was linear over the range with an R^2 value of 0.9992 (*n* = 24). The average current value at the physiological O_2 level of 50 µM was -51.80 ± 1.50 nA (*n* = 24).

To allow for an accurate comparison between the CPEs and Pt-MMA electrodes (Section 4.3.2) due to the different dimensions of the electrodes the mean current values were converted to current densities presented in Table 4.2 and plotted in Figure 4.3.

	Current		Current Density	
$[O_2]$, µM	**Mean I, nA**	**SEM**	**J, µAmm^{-2}**	**SEM**
0	0	0	0	0
240	-285.9	10.0	-9.1	0.3
1200	-1255.1	44.5	-40.0	1.4

Table 4.2: Table of results for O_2 calibrations (0-1200 µM) for CPEs (*n*=24) converted to current density. CPA performed at -650 mV *vs.* SCE in PBS (pH 7.4) at 21˚C. Mean background subtracted.

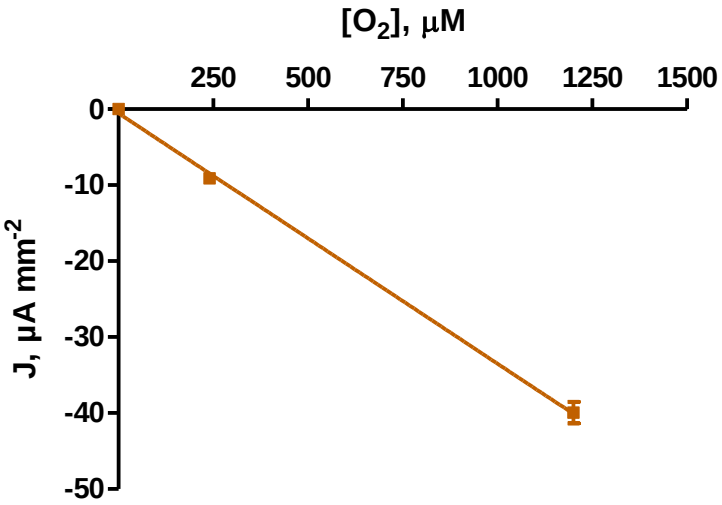

Figure 4.3: O_2 calibration data (0-1200 µM) in terms of current density for CPEs (*n*=24). CPA performed at -650 mV *vs.* SCE in PBS (pH 7.4) at 21˚C.

The average sensitivity for CPEs in terms of current density for high concentration O_2 calibrations was -0.033 ± 0.001 $\mu Amm^{-2}\mu M^{-1}$ (*n*=24). The average current density value at the physiological O_2 level of 50 µM was -1.65 ± 0.05 μAmm^{-2} (*n* = 24).

4.3.1.2 Effect of temperature

Membrane covered O_2 sensors tend to have significant temperature dependence primarily due to the effects of temperature on the diffusion coefficient and the solubility of the gas in the membrane with temperature. The signal typically increasing by 1-6% for a rise of 1˚C (Hitchman, 1978; Jeroschewski & Zur Linden, 1997). *In vitro* experiments are routinely performed at a room temperature of *ca.* 21˚C. The effect of an increase in the temperature of the PBS on the CPEs O_2 sensitivity at the physiological temperate of 37˚C was investigated. O_2 calibrations performed in PBS at 21°C and 37°C on CPEs are presented below in Table 4.3 and plotted in Figure 4.4. The concentration of dissolved O_2 was calculated to be 214 µM for air saturated PBS and 1020 µM for O_2 saturated PBS at 37°C detailed in Section 2.8.4.

	PBS 37˚C	
[O_2], µM	**Mean I, nA**	**SEM**
0	0	0
214	-467.54	37.80
1020	-1525.45	121.72

	PBS 21˚C	
[O_2], µM	**Mean I, nA**	**SEM**
0	0	0
240	-285.87	9.99
1200	-1255.08	44.47

Table 4.3: Tables of results for O_2 calibrations for CPEs. CPA performed at -650 mV *vs.* SCE in PBS (pH 7.4) at 37˚C (0-1020 µM) (*n*=8) and 21˚C (0-1200 µM) (*n*=24). Mean background subtracted.

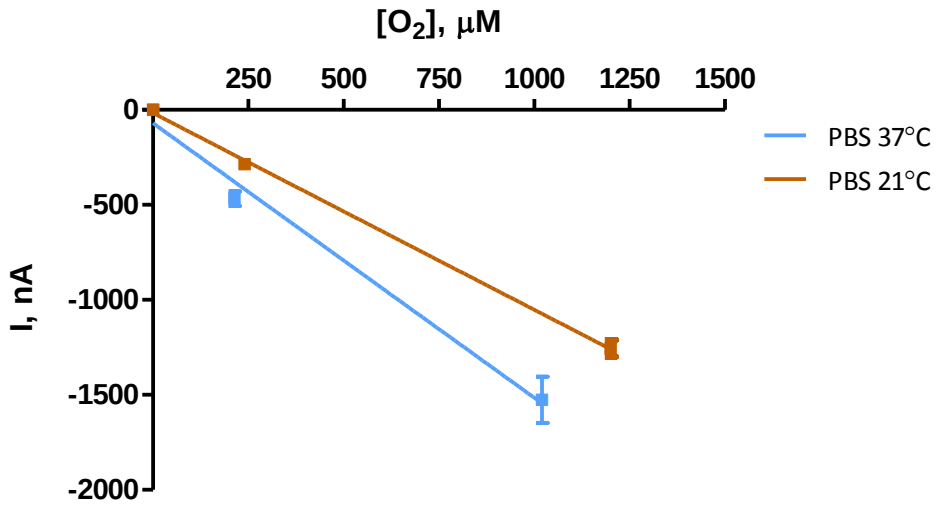

Figure 4.4: O_2 calibration data for CPEs. CPA performed at -650 mV *vs.* SCE in PBS (pH 7.4) at 37˚C (0-1020 µM) & 21˚C (0-1200 µM).

Linear regression analysis was performed on electrodes to compare sensitivities of CPEs calibrated in PBS solutions at the physiological temperature of 37˚C and room temperature, 21˚C, presented in Table 4.4 and plotted in Figure 4.5.

	Sensitivity (nA/µM)	R^2	*n*
PBS 37˚C	-1.445 ± 0.1501	0.9893	8
PBS 21˚C	-1.036 ± 0.02995	0.9992	24

Table 4.4: Comparison of calculated sensitivity values of O_2 calibrations for CPEs calibrated in PBS solutions of 37˚and 21˚C.

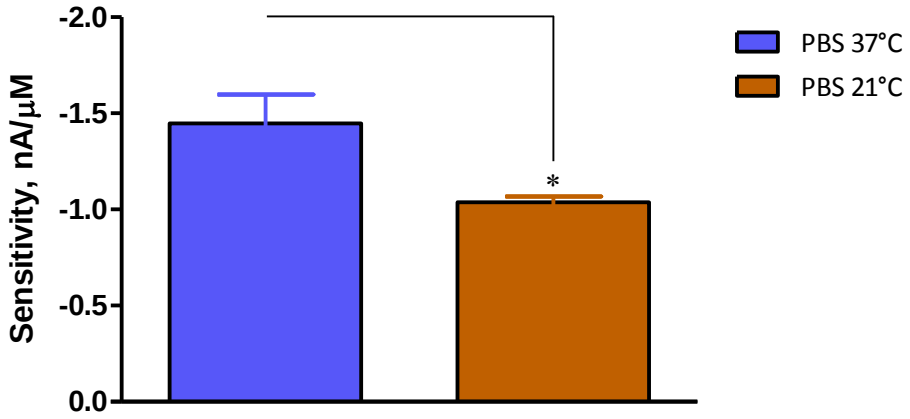

Figure 4.5: Comparison graph of calculated sensitivity values for O_2 calibrations for CPEs calibrated in PBS at 37˚C (*n*=8) & 21˚C (*n*=24).

Unpaired *t*-test statistical analysis was performed and it can be seen there is a significant difference in the sensitivities of CPEs calibrated at 37˚C and 21˚C with a *P* value of 0.0319. From the results obtained for CPEs it can be seen that the sensitivity increases by 39.48 ± 22.14 % corresponding to a 2.47 ± 1.22 % for every 1˚C increase determining that CPEs exhibit significant temperature dependence at the physiological temperature.

4.3.1.3 Effect of pH

Changes in pH may occur during physiological experiments *in vivo* (Zimmerman & Wightman, 1991) these changes in pH could also affect the cathodic reduction of O_2 at the electrode surface involving proton transfer. Previous reports for carbon-based electrodes found that for pH 12-14 the reduction of O_2 seems to be independent of pH, but as pH decreases the reduction becomes pH dependent (Taylor & Humffray, 1975; Yang & McCreery, 2000). The effect of varying pH on the sensitivities of CPEs was investigated.

O_2 calibrations performed in PBS (pH 6.5, 7 and 8) on CPEs are presented below in Table 4.5 and plotted in Figure 4.6.

	PBS pH 6.5		PBS pH 7.4		PBS pH 8	
$[O_2]$, µM	**Mean I, nA**	**SEM**	**Mean I, nA**	**SEM**	**Mean I, nA**	**SEM**
0	0	0	0	0	0	0
240	-323.2	36.5	-344.6	23.4	-306.0	59.5
1200	-1264.2	165.2	-1319.4	108.9	-965.8	153.7

Table 4.5: Table of results for O_2 calibrations (0-1200 µM) for CPEs. CPA performed at -650 mV *vs.* SCE in PBS pH 6.5 (*n*=4), pH 7.4 (*n*=8) and pH 8 (n=4) at 21˚C. Mean background subtracted.

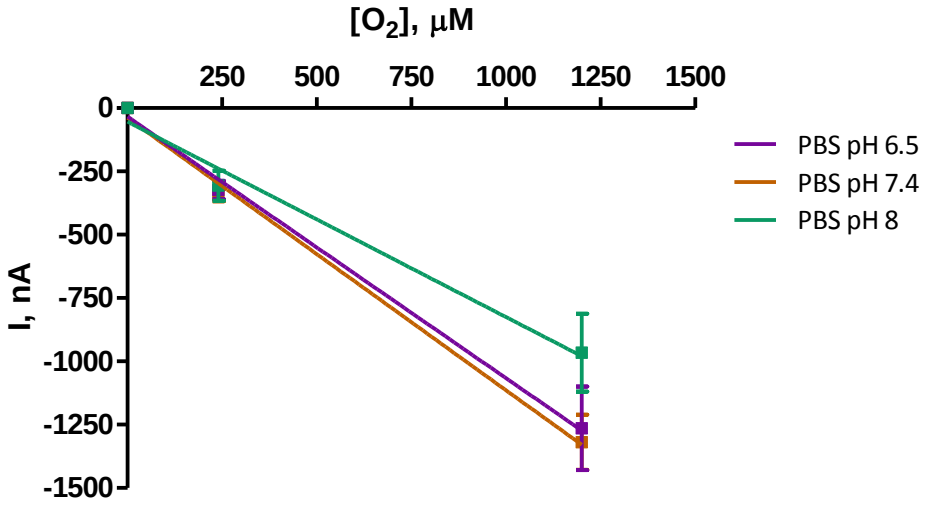

Figure 4.6: O_2 calibration data (0-1200 µM) for CPEs. CPA performed at -650 mV *vs.* SCE in PBS (pH 6.5, 7.4 & 8) at 21˚C.

Linear regression analysis was performed on electrodes to compare sensitivities of CPEs calibrated in PBS solutions with a pH of 6.5, 7.4 and 8, presented in Table 4.6 and plotted in Figure 4.7.

	Sensitivity (nA/µM)	R^2	*n*
PBS pH 6.5	-1.076 ± 0.069	0.9962	4
PBS pH 7.4	-1.033 ± 0.060	0.9991	8
PBS pH 8	-0.771 ± 0.097	0.9934	4

Table 4.6: Comparison of calculated sensitivity values of O_2 calibrations (0-1200 µM) CPEs calibrated in PBS 6.5, 7.4 & 8.

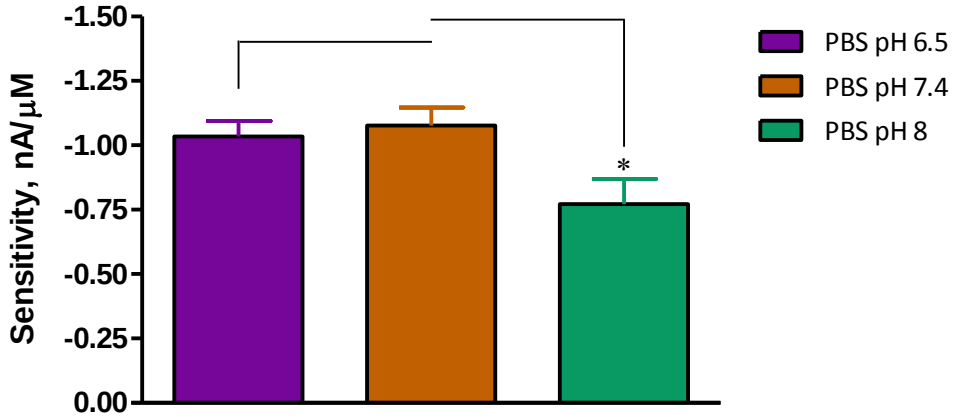

Figure 4.7: Comparison graph of calculated sensitivity values for O_2 calibrations (0-1200 µM) CPEs calibrated in PBS pH 6.5 (*n*=4), 7.4 (*n*=8) and 8 (*n*=4).

Unpaired *t*-test statistical analysis was performed and it can be seen there is no significant difference in the sensitivities of CPEs calibrated in PBS pH 6.5 and 7.4 with a *P* value of 0.6514. There is a significant difference in the sensitivities between electrodes calibrated in PBS pH 8 and 7.4 with a *P* value of 0.0431.

4.3.1.4 aCSF Cyclic Voltammetry

The technique cyclic voltammetry (CV) was performed on the CPEs to confirm the diffusion limited reduction potential of O_2 at the surface of these electrodes in aCSF. This was performed as described in Section 3.6.1.2. The results obtained are presented graphically in Figure 4.8 below.

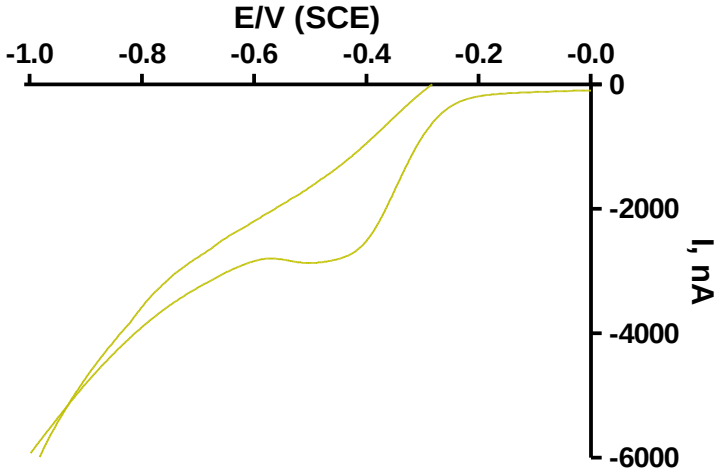

Figure 4.8: Cyclic voltammograms from -1 to 0 V *vs.* SCE at 100 mVs^{-1} performed in O_2 saturated aCSF (21˚C) buffer solution, illustrating the reduction of O_2 at a CPE.

As with PBS - 650 mV *vs.* SCE is within the mass-transport limited region after the peak potential of O_2 reduction at CPEs. All experiments performed in aCSF were carried out at this potential. This compares well with previous data shown by Lowry *et al.* (1996) who performed CV on Triton-X modified electrodes and found that the optimum reduction potential for O_2 at the surface of these electrodes was -650 mV (Figure 4.9).

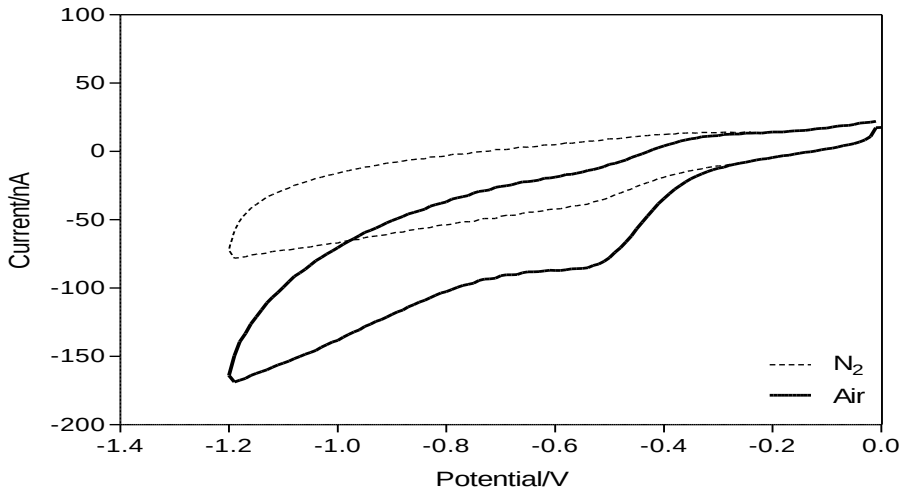

Figure 4.9: Typical cyclic staircase voltammograms recorded at 50 mVs^{-1} with a surfactant (0.2% Triton-X 100)-treated carbon paste electrode in N_2-saturated (dashed line) and air-saturated (solid line) PBS (pH 7.4) (Lowry *et al.*, 1996).

4.3.1.5 Effect of ion changes

The media-dependence of redox reactions for several physiologically vital electroactive species (dopamine (DA), 3,4-dihydroxyphenylacetic acid (DOPAC), serotonin (5-HT) and 5-hydroxyindoleacetic acid (5-HIAA)) have previously been investigated (Rice & Nicholson, 1995; Kume-Kick & Rice, 1998; Chen & Rice, 1999). Fast cyclic voltammetry (FCV) sensitivities to DA and 5-HT at carbon fibre electrodes have been reported to be 2-3-fold higher in non-physiological phosphate or HEPES-buffered saline compared to artificial cerebrospinal fluid (aCSF) which more accurately reflects the ionic composition of the brain and the reverse was observed for the acid metabolites DOPAC and 5-HIAA (Kume-Kick & Rice, 1998; Chen & Rice, 1999). Shifts in oxidation peaks and higher sensitivities using differential pulse voltammetry for aCSF that contained Ca^{2+} but not Mg^{2+}, than in PBS that contained Mg^{2+} but not Ca^{2+} have been reported (Crespi, 1996). It has also been reported that Ca^{2+} concentrations can fall under conditions of electrical stimulation and intense tissue depolarisation (Rice & Nicholson, 1995). Changes in ion concentrations are of interest as in *vivo* extracellular concentrations are in a continuous state of flux and can change significantly with disturbances to normal physiology also; electrode surface interactions differ for anions and cations, consistent with adsorption or repulsion effects at the modified electrode surfaces. The effect of ion changes on the sensitivities of CPEs was investigated. O_2 calibrations performed in aCSF, aCSF no Ca^{2+} and aCSF no Mg^{2+} on CPEs are presented below in

	aCSF		aCSF no Ca^{2+}		aCSF no Mg^{2+}		aCSF no $Ca^{2+}$and Mg^{2+}	
[O_2], µM	**Mean I, nA**	**SEM**	**Mean I, nA**	**SEM**	**Mean I, nA**	**SEM**	**Mean I, nA**	**SEM**
0	0	0	0	0	0	0	0	0
240	-389.45	25.41	-403.73	33.02	-359.96	26.92	-403.86	63.35
1200	-1947.23	127.05	-2018.66	165.08	-1799.81	134.59	-2210.20	309.99

Table 4.7 and plotted in Figure 4.10.

	aCSF		aCSF no Ca^{2+}		aCSF no Mg^{2+}		aCSF no $Ca^{2+}$and Mg^{2+}	
[O_2], µM	**Mean I, nA**	**SEM**	**Mean I, nA**	**SEM**	**Mean I, nA**	**SEM**	**Mean I, nA**	**SEM**
0	0	0	0	0	0	0	0	0
240	-389.45	25.41	-403.73	33.02	-359.96	26.92	-403.86	63.35
1200	-1947.23	127.05	-2018.66	165.08	-1799.81	134.59	-2210.20	309.99

Table 4.7: Table of results for O_2 calibrations (0-1200 µM) for CPEs. CPA performed at -650 mV *vs.* SCE in aCSF (*n*=16), aCSF no Ca^{2+} (*n*=16), aCSF no Mg^{2+} (*n*=16) at 21˚C. Mean background subtracted.

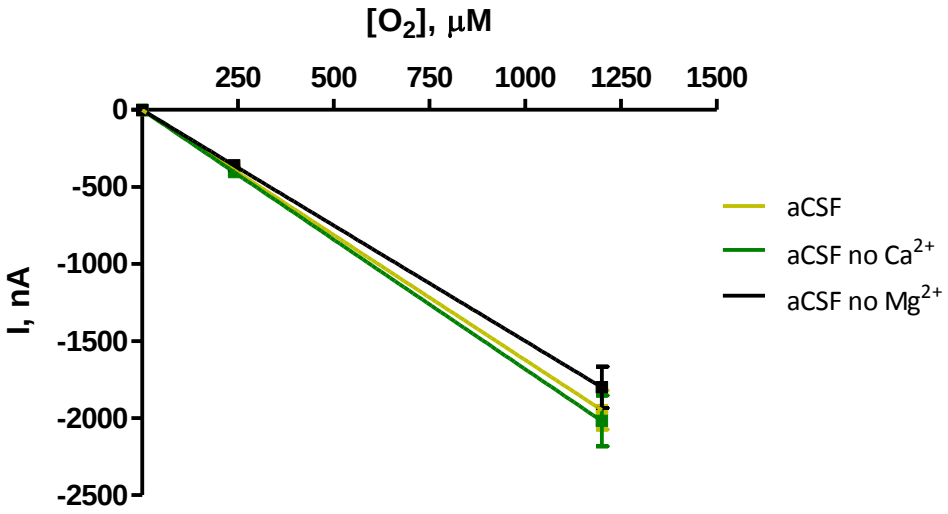

Figure 4.10: O_2 calibration data (0-1200 µM) for CPEs. CPA performed at -650 mV *vs.* SCE in aCSF, aCSF no Ca^{2+}, aCSF no Mg^{2+} at 21˚C.

Linear regression analysis was performed on electrodes to compare sensitivities of CPEs calibrated in aCSF solutions in the presence and absence of ions, presented in Table 4.8 and plotted in Figure 4.11.

CPE	Sensitivity (nA/µM)	R^2	*n*
aCSF	-1.623 ± 0.106	0.9970	16
aCSF no Ca^{2+}	-1.682 ± 0.138	0.9989	16
aCSF no Mg^{2+}	-1.500 ± 0.112	0.9945	16

Table 4.8: Comparison of calculated sensitivity values of O_2 calibrations (0-1200 µM) CPEs calibrated in aCSF, aCSF no Ca^{2+}, aCSF no Mg^{2+},at 21˚C.

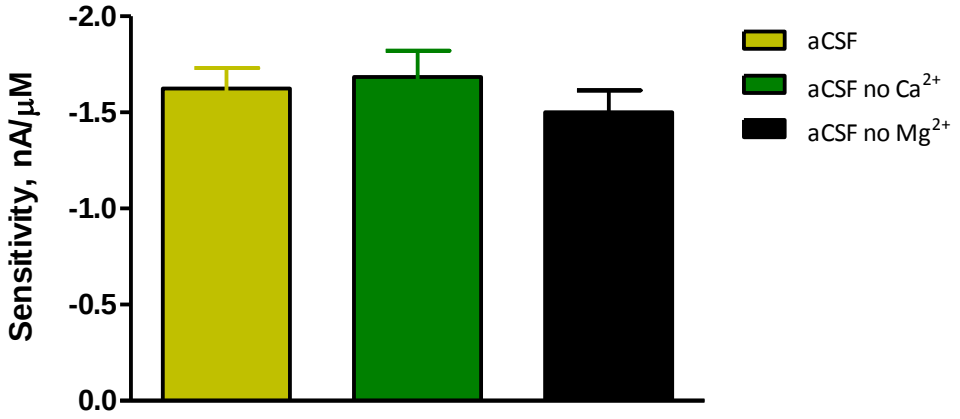

Figure 4.11: Comparison graph of calculated sensitivity values for O_2 calibrations (0-1200 µM) CPEs calibrated in aCSF(*n*=16), aCSF no Ca^{2+} (*n*=16), aCSF no Mg^{2+} (*n*=16).

Unpaired *t*-test statistical analysis was performed and it can be seen there is no significant difference in the sensitivities of CPEs calibrated in aCSF with *P* values of 0.7343, (aCSF no Ca^{2+}) and 0.4324 (aCSF no Mg^{2+}). There is an increase in the sensitivity CPEs calibrated in aCSF (-1.623 ± 0.106 nA/µM) compared to PBS (-1.036 ± 0.030 nA/µM) with a significant difference $P < 0.0001$.

4.3.1.6 Effect of stirring

The dependence of the O_2 electrode's signal on flow is commonly investigated by evaluating the signal sensitivity to fluid convection (Gotoh *et al.*, 1961; Schneiderman & Goldstick, 1978). Convection results in a reduced diffusion layer thickness at the sensor surface (Bard & Faulkner, 1980; Amatore *et al.*, 2000) which causes an increase in current. However, in *vivo* we expect to see small changes in current, as it has been reported that O_2 electrodes in brain tissue do not show a dependence upon flow. This is thought to be due to the movement of blood through the tissue which causes the diffusion layer effect to be negligible *in vivo* (Cooper, 1963). It was found that the O_2 concentration varies in accordance with the acceleration and not the velocity of the blood.

The reduction of O_2 at the CPEs surface was examined in quiescent and stirred solutions with convection produced using a magnetic stirrer (Sharan *et al.*, 2008). Results are presented below in Table 4.9 and plotted in Figure 4.12.

	Control: PBS Bubbling		PBS Quiescent		Stirring @ *c.a* 1 Hz		Stirring @ *c.a* 10 Hz	
[O_2], µM	**Mean I, nA**	**SEM**	**Mean I, nA**	**SEM**	**Mean I, nA**	**SEM**	**Mean I, nA**	**SEM**
240	-1101.0	86.2	-617.4	56.7	-643.0	61.9	-708.3	60.8
1200	-3018.1	262.1	-3387.7	344.7	-2341.3	269.6	-2398.3	259.4

Table 4.9: Table of results for O_2 calibrations (240-1200 µM) for CPEs (*n*=4). CPA performed at -650 mV *vs.* SCE in PBS (pH 7.4) at 21˚C. Mean background subtracted

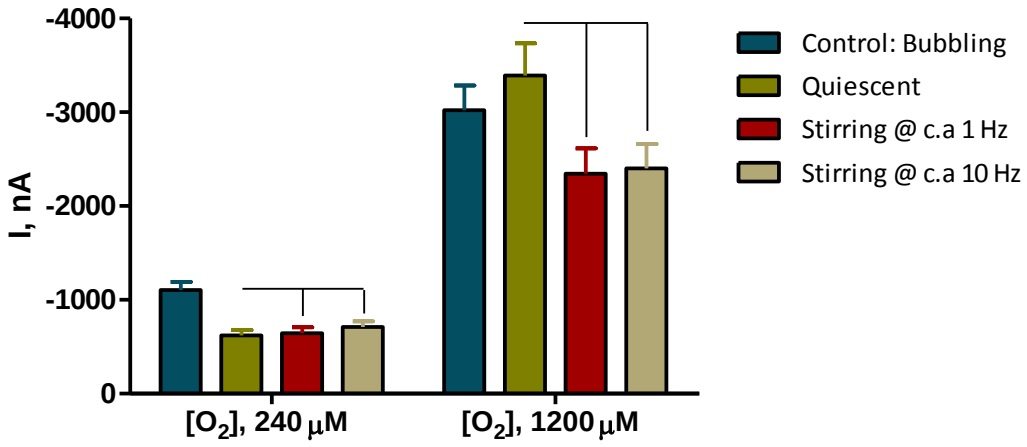

Figure 4.12: O_2 calibration data (240-1200 µM) for CPEs (n=4). CPA performed at -650 mV *vs.* SCE in PBS (pH 7.4) quiescent and in the presence of forced convection at 21˚C.

Unpaired *t*-test statistical analysis was performed and it can be seen there is no significant difference in the sensitivities between CPEs calibrated in quiescent PBS and agitated PBS stirred at approximately 1 Hz in the presence of 240 µM O_2 with a *P* value of 0.7632. There was also no significant difference found between CPEs calibrated in quiescent PBS and agitated PBS stirred at approximately 10 Hz in the presence of 240 µM O_2 with a *P* value of 0.2865.

There is no significant difference in the sensitivities between CPEs calibrated in quiescent PBS and agitated PBS stirred at approximately 1 Hz in the presence of 1200 µM O_2 with a *P* value of 0.0623. There was also no significant difference found between CPEs calibrated in quiescent PBS and agitated PBS stirred at approximately 10 Hz in the presence of 1200

µM O_2 with a *P* value of 0.0703. From the results presented in Figure 4.12 it can be seen there is no significant increase on the current monitored using CPEs at 1 Hz in the presence 240 µM O_2 compared to quiescent conditions, concluding that there is no dependence on flow *in vitro.*

4.3.1.7 Post- implantation calibrations

The effect of the living brain on electrodes was investigated. The effects of proteins and lipids on the electrooxidation of AA at CPEs was investigated (Kane & O'Neill, 1998) showing no evidence of fowling at CPEs unlike carbon fibre electrodes. This resilience appears to be due to the silicone oil present in the paste mixture. Post-implantation O_2 calibrations were performed when possible on CPEs upon removal from the brain (implanted for 6 ± 1 days), presented below in Table 4.10 and plotted in Figure 4.13.

	CPE (pre-implantation)		CPE (post-implantation)	
[O_2], µM	**Mean I, nA**	**SEM**	**Mean I, nA**	**SEM**
0	0	0	0	0
240	-273.7	15.2	-377.9	86.1
1200	-1237.9	53.4	-1206.9	106.2

Table 4.10: Table of results for O_2 calibrations (0-1200 µM) for CPEs pre-implantation and post-implantation (*n*=13) for a standard O_2 calibration. CPA performed at -650 mV *vs.* SCE in PBS (pH 7.4) at 21˚C. Mean background subtracted.

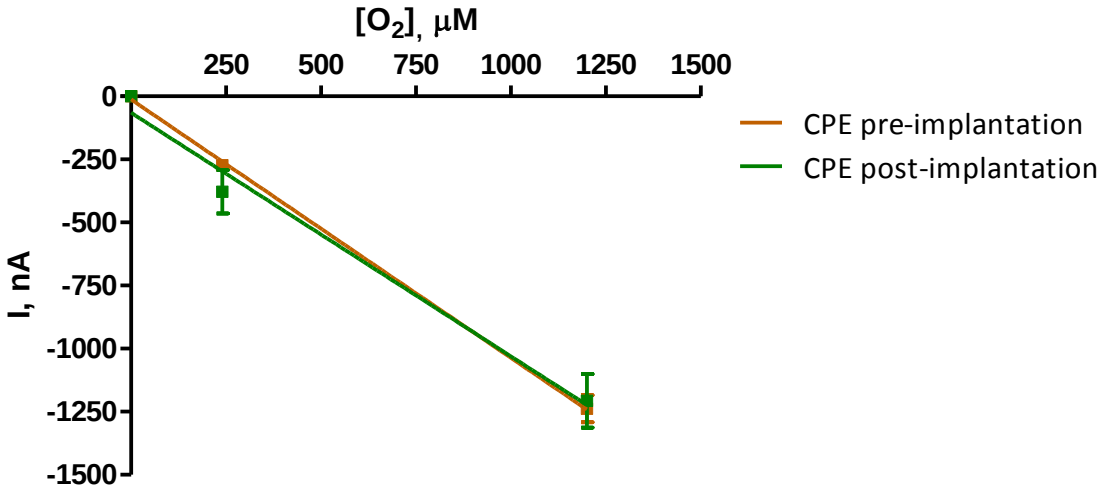

Figure 4.13: O_2 calibration data (0-1200 µM) for CPEs pre-implantation and post-implantation (*n*=13) for a standard O_2 calibration. CPA performed at -650 mV *vs.* SCE in PBS (pH 7.4) at 21˚C.

Linear regression analysis was performed on electrodes to compare sensitivities of CPEs calibrated before and after implantation, presented in Table 4.1and plotted in Figure 4.15.

	Sensitivity (nA/µM)	R^2	*n*
Pre-implantation	-1.024 ± 0.022	0.9995	13
Post-implantation	-0.965 ± 0.117	0.9855	13

Figure 4.14: Table of calculated sensitivity values of O_2 calibrations (0-1200 µM) for CPEs pre-implantation and post-implantation.

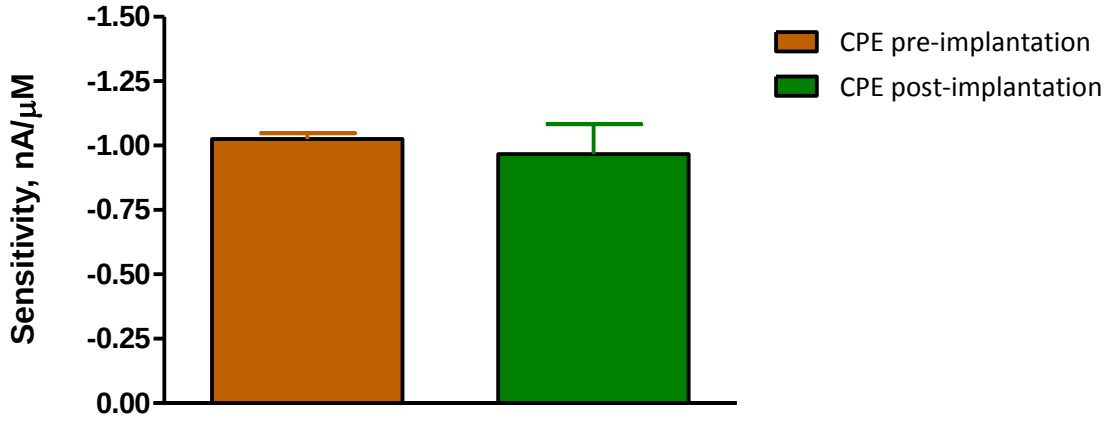

Figure 4.15: Graph of calculated sensitivity values for O_2 calibrations (0-1200 µM) for CPEs pre-implantation and post-implantation (*n*=13).

Unpaired *t*-test statistical analysis was performed and it can be seen there is no significant difference in the sensitivities between CPEs calibrated pre and post-implantation with a *P* value of 0.6308. There is no significant difference in the sensitivities of the electrodes post-implantation compared to pre-implantation. There is a trend towards a lower sensitivity post-implantation which can be attributed to endogenous proteins and lipids present in the brain interacting with the CPEs active surface, causing a leaching of silicone oil from the carbon paste and changing the morphology of the surface to a carbon powder (Ormonde & O'Neill, 1989, 1990).

Results above are verified by results presented by Bolger *et al.* (2011b) confirm that CPEs are stable *in vivo*. Analysis of baseline levels show although there was a gradual decrease in the first three weeks (Week 1, −167.0 ± 1.5 nA; Week 2, −151.9 ± 2.3 nA; Week 3, −141.7 ± 0.9 nA), no significant variation was observed over the 21-day period (*P* = 0.89,

one-way ANOVA; n = 17–26, 12 animals). Pooled data from 12 animals over a 12 week period are shown in Figure 4.16.

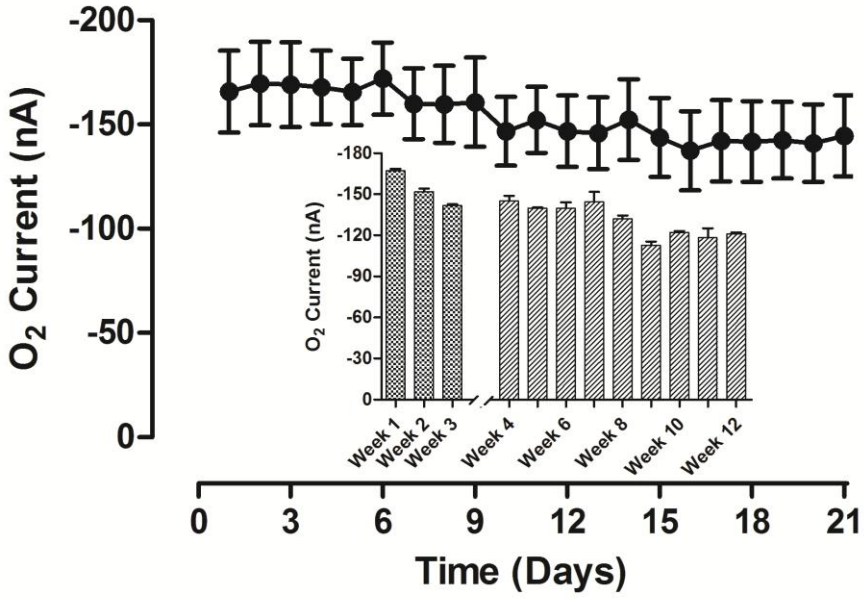

Figure 4.16: Figure from (Bolger *et al.*, 2011b) showing: Average (±SEM) baseline *in vivo* data (pooled from 12 animals-striatum, hippocampus, prefrontal cortex and nucleus accumbens) for CPEs (n = 17-26) recorded using CPA at −650mV over 21 days. Inset: average weekly baseline data recorded over the 3 week period and extended to 3 months using data from 3 animals (n = 12). All data taken from a six-hour period covering morning/afternoon (10am–4pm).

4.3.2 *Characterisation of Pt-MMA electrodes In Vitro*

4.3.2.1 Cyclic Voltammetry

CV was initially performed on the Pt-MMA electrodes to determine the diffusion limited reduction potential of O_2 at the surface of these electrodes. This was performed as described in Section 3.6.1.2. The results obtained are presented graphically in Figure 4.17 below.

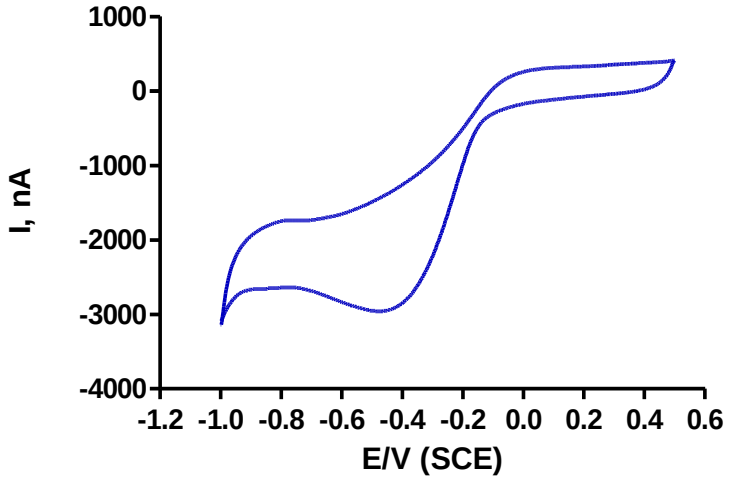

Figure 4.17: Cyclic voltammogram from -1 to +0.5 V *vs.* SCE at 100 mVs^{-1} performed in O_2 saturated PBS (pH 7.4, 21˚C) buffer solution, illustrating the reduction of O_2 at a Pt-MMA electrode.

For the Pt-MMA electrodes an O_2 reduction peak was observed at *ca*. -600 mV with the foot of the wave occurring at *ca*. -200 mV. The chosen reduction potential was -650 mV and subsequent constant potential amperometry (CPA) experiments were carried out at this potential.

4.3.2.2 Oxygen calibrations

4.3.2.2.1 High concentration O_2 calibrations (0-1200 µM)

High concentration O_2 calibrations were performed on Pt-MMA electrodes as described in Section 3.6.1.4. A typical O_2 calibration trace can be seen in Figure 4.18.

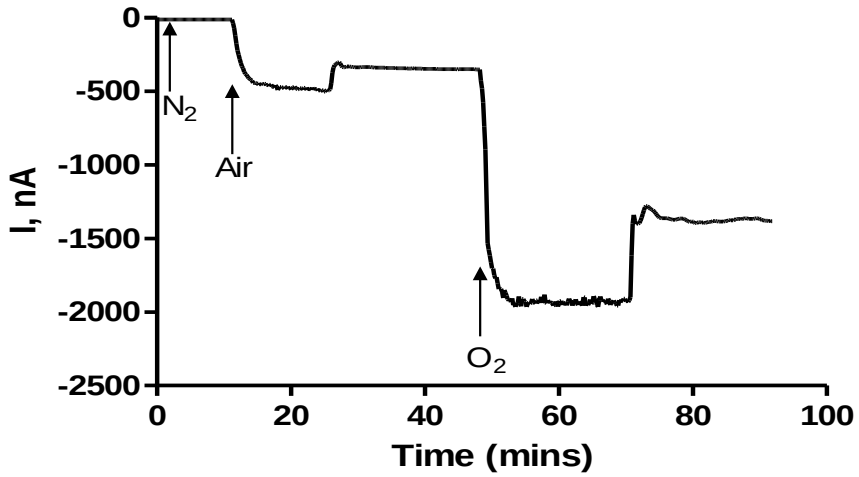

Figure 4.18: An example of typical raw data for an O_2 calibration in PBS using a Pt-MMA electrode. CPA performed at -650 mV *vs.* SCE in PBS (pH 7.4) at 21˚C.

Average results obtained for high concentration O_2 calibrations performed in PBS on Pt-MMA electrodes (n=64) are presented below in Table 4.11 and plotted in Figure 4.19. The mean background current -0.41 ± 1.19 nA was subtracted.

$[O_2]$, µM	Mean I, nA	SEM
0	0	0
240	-322.5	16.3
1200	-1388.9	66.7

Table 4.11: Table of results for O_2 calibrations (0-1200 µM) for Pt-MMA electrodes (n=64). CPA performed at -650 mV *vs.* SCE in PBS (pH 7.4) at 21˚C. Mean background subtracted

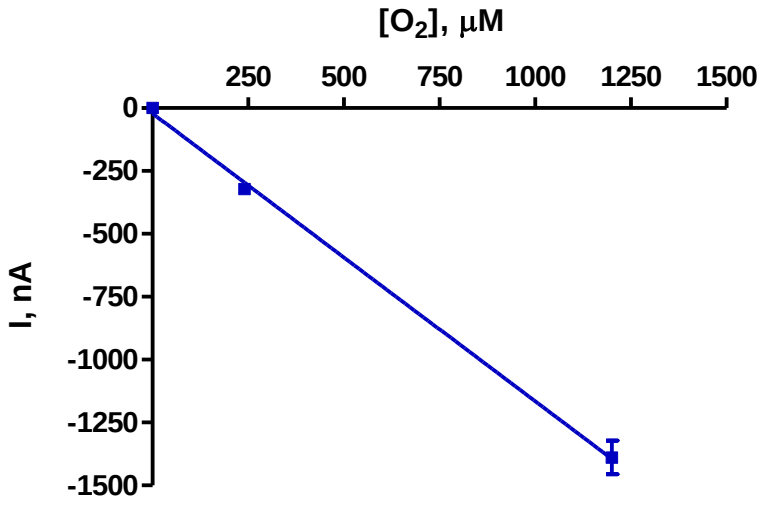

Figure 4.19: O_2 calibration data (0-1200 µM) for Pt-MMA electrodes (*n*=64). CPA performed at -650 mV *vs.* SCE in PBS (pH 7.4) at 21˚C.

Linear regression analysis shows that the electrodes have a sensitivity (slope value) of -1.14 ± 0.01 nA/µM (*n* = 64). The response was linear over the range with an R^2 value of 0.9989 (*n* = 64). The average current value at the physiological O_2 level of 50 µM was -57.20 ± 0.19 nA (*n* = 64).

The sensitivity for Pt-MMA compares favourably to O_2 calibration data (0-1200 µM) for bare Pt electrodes (Bolger *et al.*, 2011a) which gave a sensitivity of -1.12 ± 0.08 nA/µM (*n*=18), *P* = 0.8058 showing no significant difference between the bare metal and the MMA coated electrodes.

To allow for an accurate comparison between the Pt-MMA electrodes and CPEs (Section 4.3.1) due to the different dimensions of the electrodes the mean current values were converted to current densities, presented in Table 4.12 and plotted in Figure 4.20.

	Current		Current Density	
$[O_2]$, µM	**Mean I, nA**	**SEM**	**J, µAmm^{-2}**	**SEM**
0	0	0	0	0
240	-322.5	16.3	-26.3	1.3
1200	-1388.9	66.7	-113.2	5.5

Table 4.12: Table of results for O_2 calibrations (0-1200 µM) for Pt-MMA electrodes (*n*=64) converted to current density. CPA performed at -650 mV *vs.* SCE in PBS (pH 7.4) at 21˚C. Mean background subtracted.

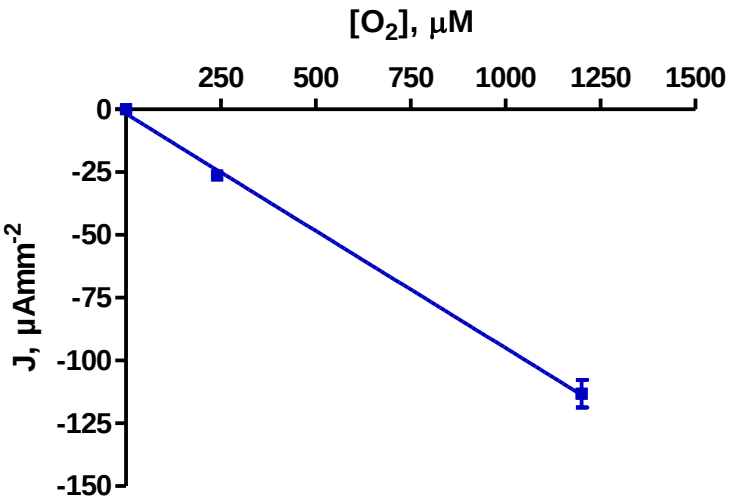

Figure 4.20: O_2 calibration data (0-1200 µM) in terms of current density for Pt-MMA electrodes (*n*= 64). CPA performed at -650 mV *vs.* SCE in PBS (pH 7.4) at 21˚C.

The average sensitivity for Pt-MMA electrodes in terms of current density for high concentration O_2 calibrations was -0.093 ± 0.003 µAmm^{-2}µM^{-1} (*n*=64). The average current density value at the physiological O_2 level of 50 µM was -4.66 ± 0.02 µAmm^{-2} (*n* = 64).

4.3.2.2.2 Low concentration O_2 calibrations (0-125 µM)

Low concentration O_2 saturated PBS calibrations were performed on Pt-MMA electrodes as described in Section 3.6.1.5, to determine sensitivity at low concentrations of O_2 similar to that of the *in vivo* environment.

Average results obtained for low concentration O_2 calibrations performed in PBS on Pt-MMA electrodes (n=15) are presented below in Table 4.13 and plotted in Figure 4.21. The mean background current -10.86 ± 2.65 nA was subtracted.

[O_2], µM	Mean I, nA	SEM
0	0	0
25	-32.0	6.9
50	-80.3	11.1
75	-128.2	15.3
100	-161.5	18.9
125	-207.7	20.6

Table 4.13: Table of results for O_2 calibrations (0-125 µM) for Pt-MMA electrodes (n=15). CPA performed at -650 mV *vs.* SCE in PBS (pH 7.4) at 21˚C. Mean background subtracted.

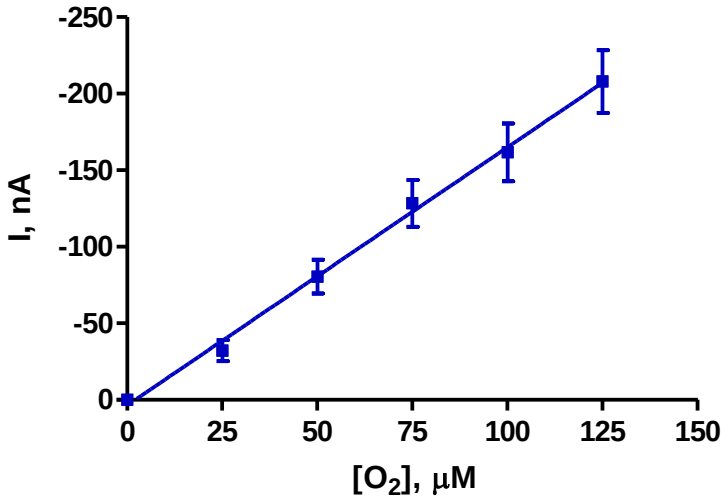

Figure 4.21: Low concentration O_2 calibration data (0-125 µM) for Pt-MMA electrodes (n=15). CPA performed at -650 mV *vs.* SCE in PBS (pH 7.4) at 21˚C.

Linear regression analysis shows that the electrodes have a sensitivity of -1.69 ± 0.005 nA/µM (n = 15). The response was linear over the range with an R^2 value of 0.9969 (n = 15). The average current value at the physiological O_2 level of 50 µM was -84.30 ± 2.36 nA (n = 15).

The mean current values for low concentration O_2 calibrations were converted to current density values, presented in Table 4.14 and plotted in Figure 4.22.

	Current		Current Density	
$[O_2]$, µM	**Mean I, nA**	**SEM**	**J, µAmm^{-2}**	**SEM**
0	0	0	0	0
25	-31.95	6.87	-2.60	0.56
50	-80.30	11.05	-6.54	0.90
75	-128.18	15.26	-10.45	1.24
100	-161.47	18.87	-13.16	1.54
125	-207.72	20.61	-16.93	1.68

Table 4.14: Table of results for O_2 calibrations (0-125 µM) for Pt-MMA electrodes (*n*=15) converted to current density. CPA performed at -650 mV *vs.* SCE in PBS (pH 7.4) at 21˚C. Mean background subtracted.

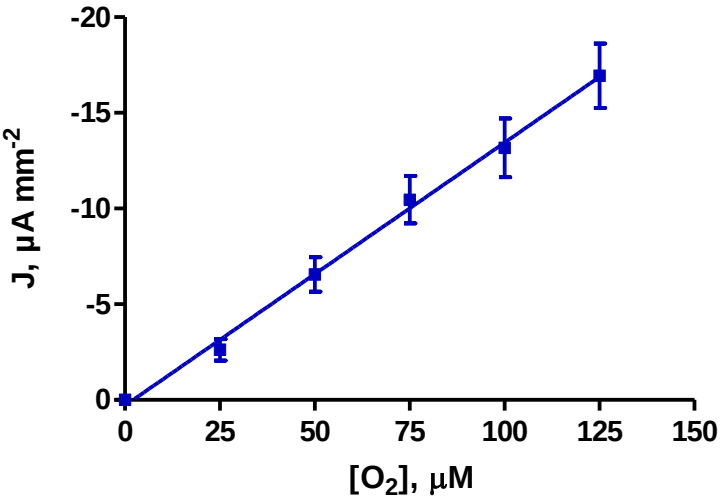

Figure 4.22: Low concentration O_2 calibration data (0-125 µM) in terms of current density for Pt-MMA electrodes (*n*=15). CPA performed at -650 mV *vs.* SCE in PBS (pH 7.4) at 21˚C.

The average sensitivity for Pt-MMA electrodes in terms of current density for low concentration O_2 calibrations was -0.137 ± 0.004 µAmm^{-2}µM^{-1} (*n*=15). The average current density value at the physiological O_2 level of 50 µM was -6.87 ± 0.194 µAmm^{-2} (*n* = 15). From the calibration data on Pt-MMA electrodes it can be seen that these electrodes can reliably detect O_2 *in vitro* over a range of 0-125 µM.

Now that the electrodes sensitivity to O_2 has been confirmed the selectivity, stability and biocompatibility of the Pt-MMA electrodes was investigated.

4.3.2.3 Biocompatibility

As previously discussed metal-based electrodes are more susceptible to surface poisoning than CPEs. The presence of the polymer MMA serves to act as protective membrane to minimise fouling at the Pt electrode surface. In this section the effects of proteins, lipids and brain tissue on the sensitivity of Pt-MMA electrodes was investigated, based on previous work (Ormonde & O'Neill, 1989, 1990) to determine if there is a significant reduction in the electrodes ability to remain sensitive to O_2 *in vivo*.

4.3.2.3.1 Protein (BSA) treated Pt-MMA electrodes

The effect of exposure to the protein BSA (Section 3.5.4.1) on Pt-MMA electrodes with respect to time was investigated. Untreated Pt-MMA electrodes (0 days) were calibrated and subsequently exposed to BSA for 24 hours, 3 days, 7 days and 14 days. The results obtained for O_2 calibrations on these treated electrodes are presented below in Table 4.15 and plotted in Figure 4.23.

	BSA (0 days) *n*=20		**BSA (24 hrs) *n*=6**		**BSA (3 days) *n*=8**		**BSA (7 days) *n*=8**		**BSA (14 days) *n*=8**	
[O_2], µM	**Mean I, nA**	**SEM**	**Mean I, nA**	**SEM**	**Mean I, nA**	**SEM**	**Mean I, nA**	**SEM**	**Mean I, nA**	**SEM**
0	0	0	0	0	0	0	0	0	0	0
240	-280.8	36.8	-345.2	31.8	-296.6	21.0	-308.4	20.8	-287.9	20.5
1200	-1250.7	100.9	-1145.5	104.4	-929.6	57.4	-966.0	46.6	-892.2	51.1

Table 4.15: Table of results for O_2 calibrations (0-1200 µM) for Pt-MMA electrodes exposed to BSA. CPA performed at -650 mV *vs.* SCE in PBS (pH 7.4) at 21˚C. Mean background subtracted.

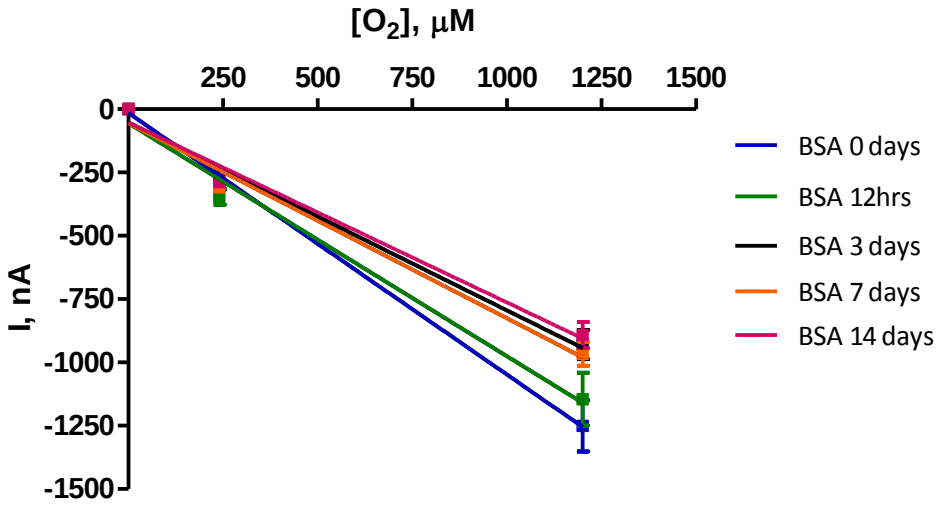

Figure 4.23: O_2 calibration data (0-1200 µM) for Pt-MMA electrodes untreated (0 days) and treated with BSA (12 hrs, 3 days, 7 days and 14 days). CPA performed at -650 mV *vs.* SCE in PBS (pH 7.4) at 21˚C.

Linear regression analysis was performed on electrodes to compare sensitivities of Pt-MMA electrodes before and after exposure to BSA, presented in Table 4.16 and plotted in Figure 4.24.

BSA treatment	Sensitivity (nA/µM)	R^2	*n*
0 days	-1.033 ± 0.026	0.9994	20
24 hrs	-0.920 ± 0.100	0.9884	6
3 days	-0.742 ± 0.095	0.9838	8
7 days	-0.771 ± 0.099	0.9838	8
14 days	-0.711 ± 0.094	0.9828	8

Table 4.16: Table of calculated sensitivity values of O_2 calibrations (0-1200 µM) for Pt-MMA electrodes exposed to BSA.

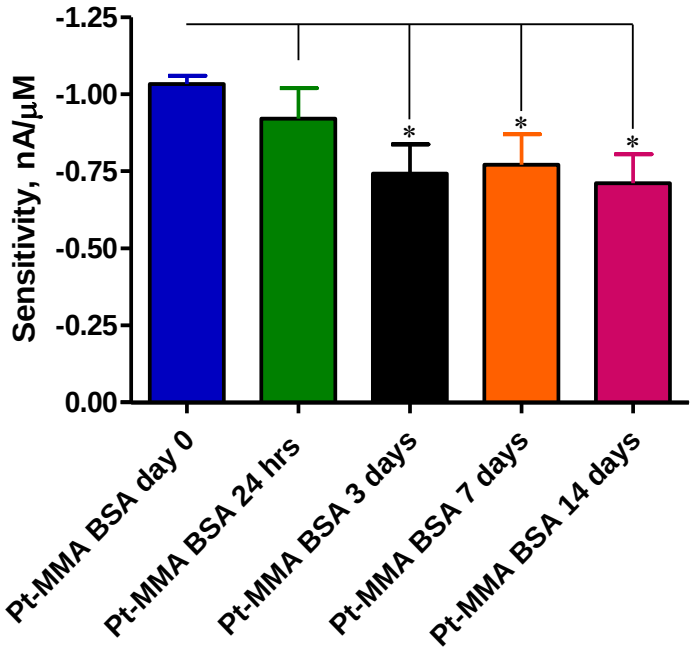

Figure 4.24: Comparison graph of calculated sensitivity values for O_2 calibrations (0-1200 µM) at Pt-MMA electrodes exposed to BSA.

Unpaired *t*-test statistical analysis was performed and it can be seen there is no significant difference in the sensitivities with a *P* value greater than 0.05 between untreated (0 days exposure) and electrodes exposed to BSA for 24 hrs (*P* = 0.3231). There is a significant difference in the sensitivities between untreated (0 days exposure) and 3 days (*P* = 0.0184), 7 days (*P* = 0.0335) and 14 days (*P* = 0.0109).

One-way Analysis of Variance (ANOVA) was performed on Pt-MMA electrodes only exposed to BSA with a *P* value of 0.5118 showing no significant difference in the sensitivities between the electrodes once exposed to BSA over a period of 14 days. From these results it can be seen that there is a significant initial reduction in the sensitivity of Pt-MMA electrodes following exposure to BSA for a 24 hr period. However, it can be concluded following initial exposure that there is no further significant reduction in the sensitivity over a 14 day period.

4.3.2.3.2 Lipid (PEA) treated Pt-MMA electrodes

The effect of exposure to the protein PEA (Section 3.5.4.2) on Pt-MMA electrodes with respect to time was investigated. Untreated Pt-MMA electrodes (0 days) were calibrated and subsequently exposed to PEA for 24 hours, 3 days and 14 days. The results obtained for O_2 calibrations on these treated electrodes are presented below in Table 4.17 and plotted in Figure 4.25.

	PEA (0 days) *n*=15		PEA (24 hrs) *n*=4		PEA (3 days) *n*=7		PEA (14 days) *n*=6	
[O_2], µM	**Mean I, nA**	**SEM**	**Mean I, nA**	**SEM**	**Mean I, nA**	**SEM**	**Mean I, nA**	**SEM**
0	0	0	0	0	0	0	0	0
240	-360.2	15.4	-342.7	11.7	-315.9	14.9	-327.5	14.1
1200	-1305.7	57.8	-1197.5	53.9	-1006.0	40.8	-1197.6	70.2

Table 4.17: Table of results for O_2 calibrations (0-1200 µM) for Pt-MMA electrodes exposed to PEA. CPA performed at -650 mV *vs.* SCE in PBS (pH 7.4) at 21˚C. Mean background subtracted.

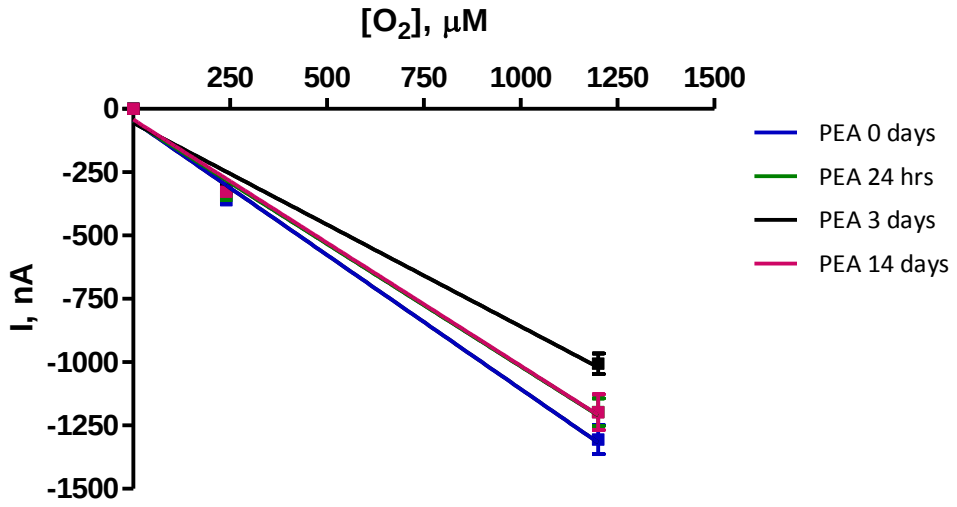

Figure 4.25: O_2 calibration data (0-1200 µM) for Pt-MMA electrodes untreated (0 days) and treated with PEA (24 hrs, 3 days and 14 days). CPA performed at -650 mV *vs.* SCE in PBS (pH 7.4) at 21˚C.

Linear regression analysis was performed on electrodes to compare sensitivities of Pt-MMA electrodes before and after exposure to PEA, presented in Table 4.18 and plotted in Figure 4.26.

PEA treatment	Sensitivity (nA/µM)	R^2	*n*
0 days	-1.059 ± 0.085	0.9936	15
24 hrs	-0.967 ± 0.089	0.9917	4
3 days	-0.804 ± 0.099	0.9852	7
14 days	-0.972 ± 0.076	0.9940	6

Table 4.18: Table of calculated sensitivity values of O_2 calibrations (0-1200 µM) for Pt-MMA electrodes exposed to PEA.

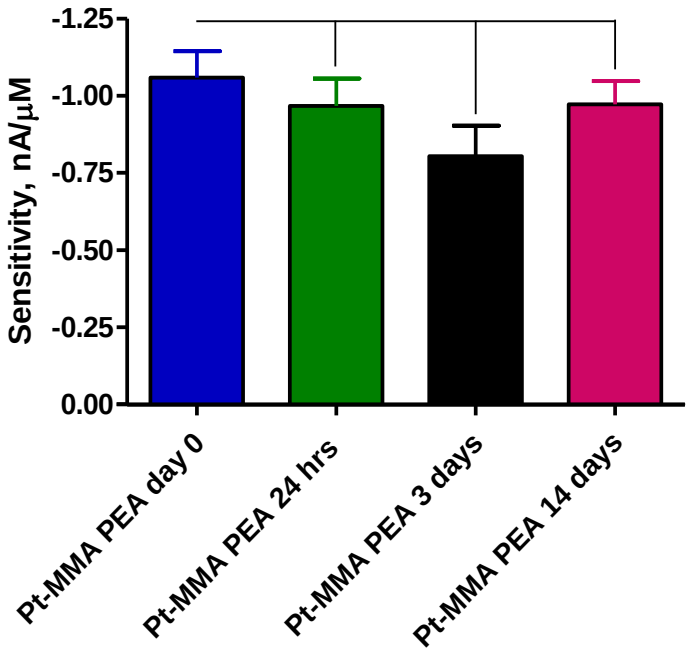

Figure 4.26: Comparison graph of calculated sensitivity values for O_2 calibrations (0-1200 µM) Pt-MMA electrodes exposed to PEA.

Unpaired *t*-test statistical analysis was performed and it can be seen there is no significant different in the sensitivities with *P* values greater than 0.05 between untreated (0 days exposure) and PEA treated electrodes with *P* values of 0.4742 (24 hrs), 0.0707 (3 days) and 0.4552 (14 days).

One-way Analysis of Variance (ANOVA) was performed on Pt-MMA electrodes only exposed to PEA with a *P* value of 0.3370 showing no significant difference in the sensitivities between the electrodes once exposed to PEA over a period of 14 days. From these results it can be seen that there is small but non-significant reduction in the sensitivity of Pt-MMA electrodes following exposure to PEA over a period of 14 days.

4.3.2.3.3 Brain tissue (BT) treated Pt-MMA electrodes

The effect of exposure to a sample of *ex-vivo* BT (Section 3.5.4.3) on Pt-MMA electrodes with respect to time was investigated. Untreated Pt-MMA electrodes (0 days) were calibrated and subsequently exposed to BT for 24 hours, 3 days and 14 days. The results obtained for O_2 calibrations on these treated electrodes are presented below in Table 4.19 and plotted in Figure 4.27.

	BT (0 days) *n*=17		BT (24 hrs) *n*=4		BT (3 days) *n*=4		BT (14 days) *n*=4	
[O_2], µM	**Mean I, nA**	**SEM**	**Mean I, nA**	**SEM**	**Mean I, nA**	**SEM**	**Mean I, nA**	**SEM**
0	0	0	0	0	0	0	0	0
240	-335.2	19.5	-331.9	18.3	-339.1	28.9	-380.1	42.5
1200	-1266.0	54.6	-1107.4	56.3	-1088.4	85.1	-1141.7	110.5

Table 4.19: Table of results for O_2 calibrations (0-1200 µM) for Pt-MMA electrodes exposed to BT. CPA performed at -650 mV *vs.* SCE in PBS (pH 7.4) at 21˚C. Mean background subtracted.

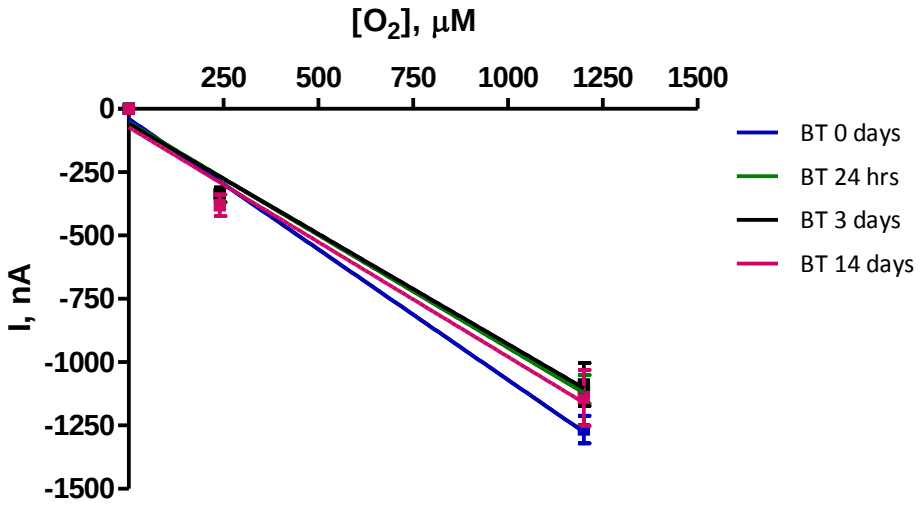

Figure 4.27: O_2 calibration data (0-1200 µM) for Pt-MMA electrodes untreated (0 days) and treated with BT (24 hrs, 3 days and 14 days). CPA performed at -650 mV *vs.* SCE in PBS (pH 7.4) at 21˚C.

Linear regression analysis was performed on electrodes to compare sensitivities of Pt-MMA electrodes before and after exposure to BT, presented in Table 4.20 and plotted in Figure 4.28.

BT treatment	Sensitivity (nA/µM)	R^2	*n*
0 days	-1.031 ± 0.070	0.9953	17
24 hrs	-0.890 ± 0.095	0.9888	4
3 days	-0.871 ± 0.104	0.9859	4
14 days	-0.906 ± 0.130	0.9797	4

Table 4.20: Table of calculated sensitivity values of O_2 calibrations (0-1200 µM) for Pt-MMA electrodes exposed to BT.

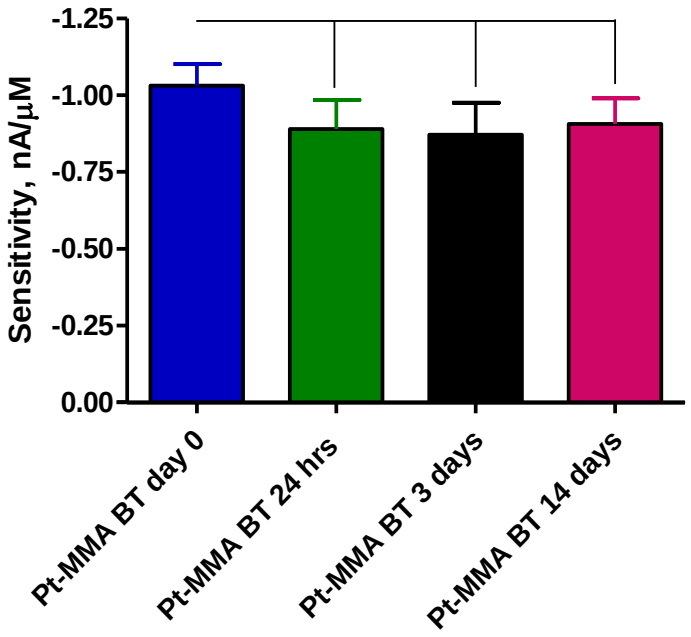

Figure 4.28: Comparison graph of calculated sensitivity values for O_2 calibrations (0-1200 µM) for Pt-MMA electrodes exposed to BT.

Unpaired *t*-test statistical analysis was performed and it can be seen there is no significant difference in the sensitivities with *P* values greater than 0.05 between untreated (0 days exposure) and BT treated electrodes with *P* values of 0.1163 (24 hrs), 0.0877 (3 days) and 0.2201 (14 days).

One-way Analysis of Variance (ANOVA) was performed on Pt-MMA electrodes only exposed to BT with a *P* value of 0.9044 showing no significant difference in the sensitivities between the electrodes once exposed to BT over a period of 14 days. From

these results it can be seen that there is a small but non-significant reduction in the sensitivity of Pt-MMA electrodes following exposure to BT over a period of 14 days.

4.3.2.4 Stability

The stability of Pt-MMA electrodes with respect to time was investigated. Pt-MMA electrodes (0 days) were calibrated, refrigerated and re-calibrated after 7 days, 21 days, 28 days, 35 days, 48 days and 56 days. The results obtained for O_2 calibrations on these electrodes are presented below in Table 4.21 and Figure 4.29.

	0 days *n*=4		7 days *n*=4		21 days *n*=4		28 days *n*=4		35 days *n*=4		48 days *n*=4		56 days *n*=4	
[O_2], µM	Mean I, nA	SE M	Mean I, nA	SE M	Mean I, nA	SE M	Mean I, nA	SE M	Mean I, nA	SE M	Mean I, nA	SE M	Mean I, nA	SE M
0	0	0	0	0	0	0	0	0	0	0	0	0	0	0
240	-290.6	25.7	-284.3	19.3	-310.0	6.0	-338.2	14.4	-270.3	14.8	-256.9	14.1	-272.8	13.7
1200	-1130.2	75.4	-1219.2	65.7	-1147.4	45.2	-1283.8	38.7	-1004.7	56.5	-963.9	50.9	-992.7	37.5

Table 4.21: Table of results for O_2 calibrations (0-1200 µM) for Pt-MMA electrodes stored in the refrigerator at 4˚C and re-calibrated on given days. CPA performed at -650 mV *vs.* SCE in PBS (pH 7.4) at 21˚C. Mean background subtracted.

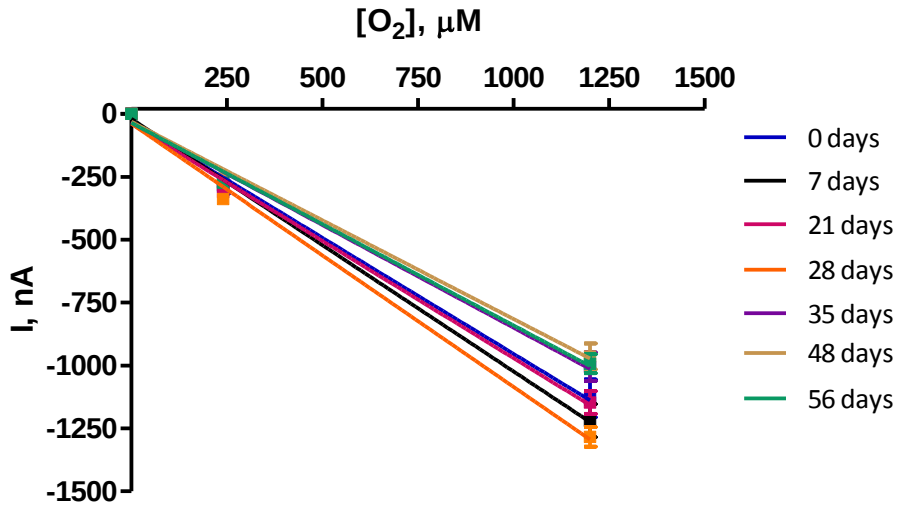

Figure 4.29: O_2 calibration data (0-1200 µM) for Pt-MMA electrodes (0 days) stored in the refrigerator (4˚C) and re-calibrated after (7 days, 21 days, 28 days, 35 days, 48 days and 56 days). CPA performed at -650 mV *vs.* SCE in PBS (pH 7.4) at 21˚C.

Linear regression analysis was performed on electrodes to compare sensitivities of Pt-MMA electrodes stored at 4˚C and re-calibrated over 56 days, presented in Table 4.22 and plotted in Figure 4.30.

	Sensitivity (nA/µM)	R^2	*n*
0 days	-0.923 ± 0.055	0.9964	4
7 days	-1.004 ± 0.035	0.9988	4
21 days	-0.932 ± 0.069	0.9945	4
28 days	-1.046 ± 0.070	0.9955	4
35 days	-0.817 ± 0.060	0.9947	4
48 days	-0.784 ± 0.055	0.9951	4
56 days	-0.805 ± 0.064	0.9938	4

Table 4.22: Table of calculated sensitivity values of O_2 calibrations (0-1200 µM) Pt-MMA electrodes calibrated over 56 days.

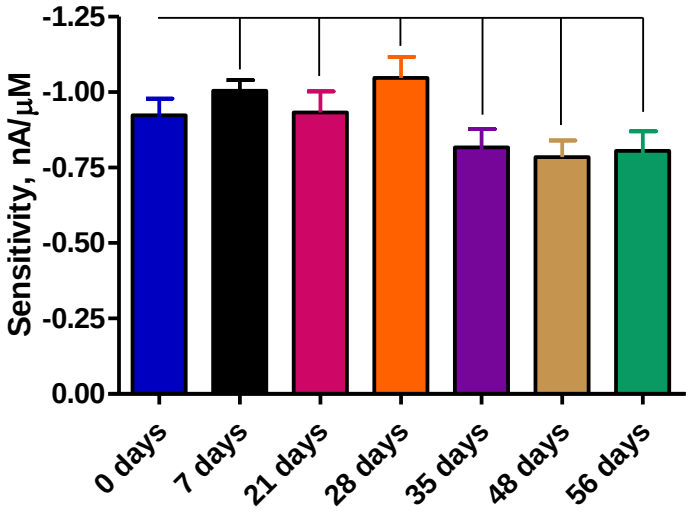

Figure 4.30: Comparison graph of calculated sensitivity values for O_2 calibrations (0-1200 µM) Pt-MMA (0 days), stored at 4˚C and re-calibrated after (7 days, 21 days, 28 days, 35 days, 48 days and 56 days).

Unpaired *t*-test statistical analysis was performed and it can be seen there is no significant difference in the sensitivities with *P* values of 0.2686 (7 days), 0.9180 (21 days), 0.2254 (28 days), 0.2497 (35 days), 0.1367 (48 days) and 0.2233 (56 days), all less than 0.05 between electrodes calibrated on day 0 and electrodes re-calibrated 6 times over a period of

56 days. From these results it can be concluded that Pt-MMA electrodes are stable with respect to time displaying a shelf-life of at least of 56 days (current study) when stored at 4˚C.

4.3.2.5 Effect of temperature

The effect of temperature on membrane covered O_2 sensors has been previously discussed in Section 4.3.1.2. The effect of an increase in the temperature of the PBS on the Pt-MMA electrodes O_2 sensitivity at the physiological temperate of 37˚C was investigated. O_2 calibrations performed in PBS at 21°C and 37°C on Pt-MMA electrodes are presented below in Table 4.23 and plotted in Figure 4.31. The concentration of dissolved O_2 was calculated to be 214 µM for air saturated PBS and 1020 µM for O_2 saturated PBS at 37°C detailed in Section 2.8.4.

	PBS 37˚C	
[O_2], µM	**Mean I, nA**	**SEM**
0	0	0
214	-467.55	28.61
1020	-1706.64	83.28

	PBS 21˚C	
[O_2], µM	**Mean I, nA**	**SEM**
0	0	0
240	-311.06	14.94
1200	-1365.89	51.54

Table 4.23: Tables of results for O_2 calibrations (0-1200 µM) for Pt-MMA electrodes. CPA performed at -650 mV *vs.* SCE in PBS (pH 7.4) at 37˚C (0-1020 µM) (*n*=5) and 21˚C (0-1200 µM) (*n*=10). Mean background subtracted.

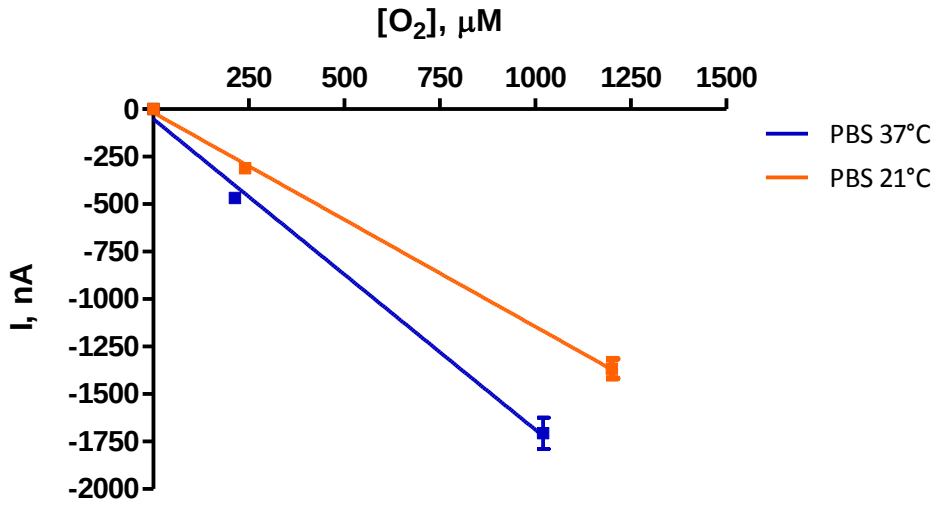

Figure 4.31: O_2 calibration data for Pt-MMA electrodes. CPA performed at -650 mV *vs.* SCE in PBS (7.4) at 37˚C (0-1020 µM) & 21˚C (0-1200 µM).

Linear regression analysis was performed on electrodes to compare sensitivities of Pt-MMA electrodes calibrated in PBS solutions at the physiological temperature of 37˚C and room temperature, 21˚C, presented in Table 4.24 and plotted in Table 4.32.

	Sensitivity (nA/µM)	R^2	*n*
PBS 37˚C	-1.636 ± 0.1114	0.9954	5
PBS 21˚C	-1.127 ± 0.03255	0.9992	10

Table 4.24: Comparison of calculated sensitivity values of O_2 calibrations for Pt-MMA electrodes calibrated in PBS solutions of 37˚and 21˚C.

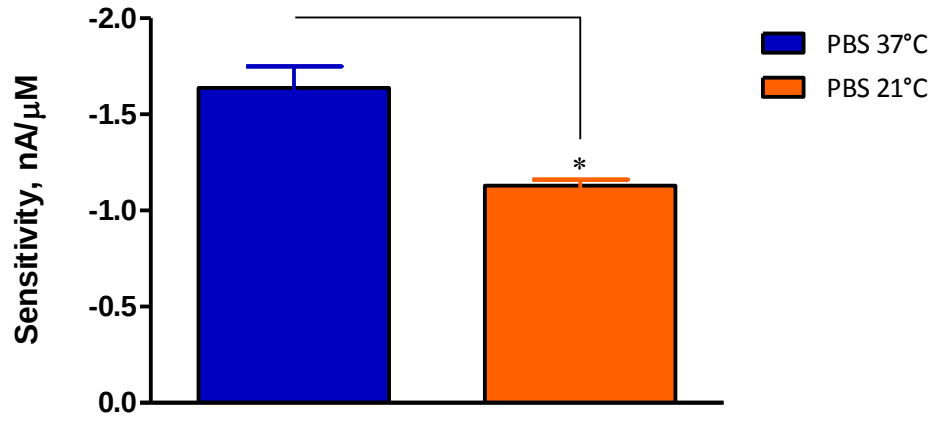

Figure 4.32: Comparison graph of calculated sensitivity values for O_2 calibrations for Pt-MMA electrodes calibrated in PBS at 37˚C (*n*=5) & 21˚C (*n*=10).

Unpaired *t*-test statistical analysis was performed and it can be seen there is no significant difference in the sensitivities of Pt-MMA electrodes calibrated at 37˚C and 21˚C with a *P* value of 0.0118.

For O_2 calibrations on bare Pt electrodes there was found to be a significant difference in the sensitivity of the electrodes calibrated at 22˚C and 37˚C with sensitivities of -1.12 ± 0.08 nA/µM, R^2 = 0.995 (*n* = 18) and -1.57 ± 0.06 nA/µM, R^2 = 0.9963 (*n* = 12), *P* = 0.0002) (Bolger *et al.*, 2011a). From the results obtained for Pt-MMA it can be concluded that in the presence of the polymer MMA, the sensitivity increases by 45.16 ± 9.88 % corresponding to a 2.82 ± 0.44 % for every 1˚C increase.

4.3.2.6 Effect of pH

Changes in pH may occur during physiological experiments *in vivo* as discussed in Section 4.3.1.3. The effect of varying pH on the sensitivities of Pt-MMA electrodes was investigated. O_2 calibrations performed in PBS (pH 6.5, 7 and 8) on Pt-MMA electrodes are presented below in Table 4.25 and plotted in Figure 4.33.

	PBS pH 6.5		**PBS pH 7.4**		**PBS pH 8**	
[O_2], µM	**Mean I, nA**	**SEM**	**Mean I, nA**	**SEM**	**Mean I, nA**	**SEM**
0	0	0	0	0	0	0
240	-289.8	12.2	-299.1	15.1	-328.2	10.8
1200	-1119.4	22.6	-1307.9	43.2	-1185.8	41.8

Table 4.25: Table of results for O_2 calibrations (0-1200 µM) for Pt-MMA electrodes. CPA performed at -650 mV *vs.* SCE in PBS: pH 6.5 (*n*=4), 7.4 (*n*=8) & 8 (*n*=4) at 21˚C. Mean background subtracted.

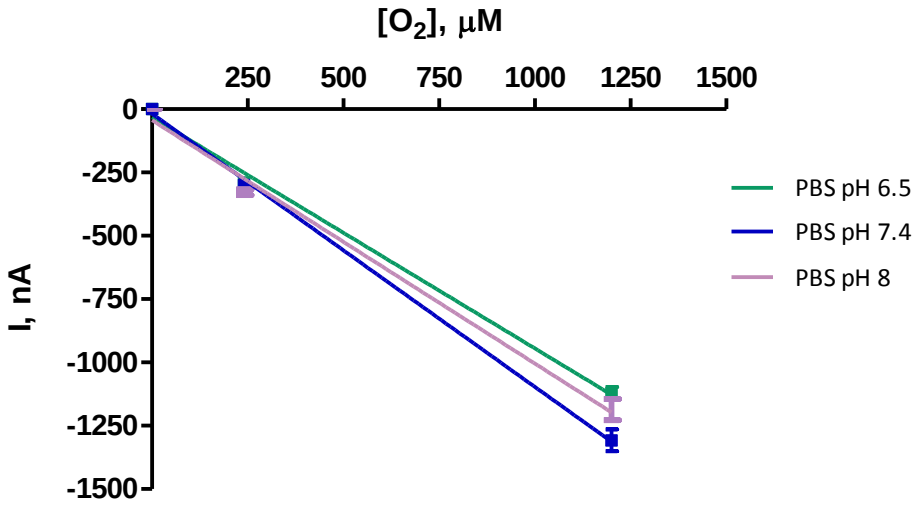

Figure 4.33: O_2 calibration data (0-1200 µM) for Pt-MMA electrodes. CPA performed at -650 mV *vs.* SCE in PBS (pH 6.5, 7.4 & 8) at 21˚C.

Linear regression analysis was performed on electrodes to compare sensitivities of Pt-MMA electrodes calibrated in PBS solutions with a pH of 6.5, 7.4 and 8, presented in Table 4.26 and plotted in Figure 4.34.

	Sensitivity (nA/µM)	R^2	*n*
PBS pH 6.5	-0.913 ± 0.057	0.9962	4
PBS pH 7.4	-1.079 ± 0.032	0.9991	8
PBS pH 8	-0.961 ± 0.078	0.9934	4

Table 4.26: Comparison of calculated sensitivity values of O_2 calibrations (0-1200 µM) for Pt-MMA electrodes calibrated in PBS 6.5, 7.4 & 8.

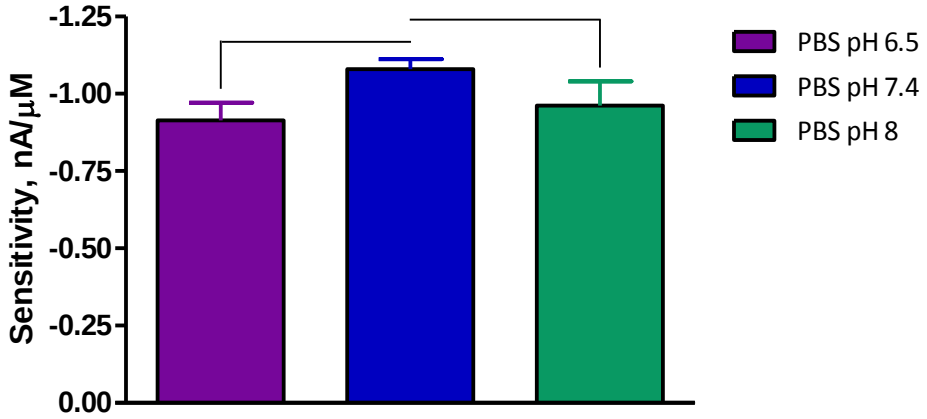

Figure 4.34: Comparison graph of calculated sensitivity values for O_2 calibrations (0-1200 µM) for Pt-MMA electrodes calibrated in PBS pH 6.5 (*n*=4), 7.4 (*n*=8) and 8 (*n*=4).

Unpaired *t*-test statistical analysis was performed and it can be seen there is no significant difference in the sensitivities of Pt-MMA electrodes calibrated in PBS pH 6.5 and 7.4 with a *P* value of 0.0516 and there is no significant difference in the sensitivities between electrodes calibrated in PBS pH 8 and 7.4 with a *P* value of 0.2355.

These results are similar to data observed with O_2 calibrations on bare Pt electrodes calibrated in PBS pH 7.4 (-1.12 ± 0.08 nA/µM, R^2 = 0.995, *n* = 18), pH 6.5 (-1.06 ± 0.04 nA/µM, R^2 = 0.9987, *n* = 8) and pH 8 (-1.07 ± 0.04 nA/µM, R^2 = 0.9951, *n* = 8), where a small decrease in the sensitivity was observed with pH 6.5 and 8 compared to 7.4. (Bolger *et al.*, 2011a).

4.3.2.7 aCSF CV

CV was performed on the Pt-MMA electrodes to confirm the diffusion limited reduction potential of O_2 at the surface of these electrodes in aCSF. This was performed as described in Section 3.6.1.2. The results obtained are presented graphically in Figure 4.35 below.

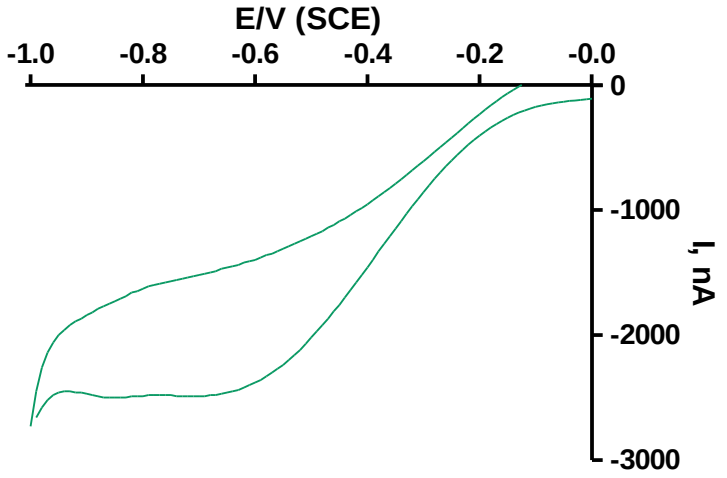

Figure 4.35: Cyclic voltammograms from -1 to 0 V *vs.* SCE at 100 mVs^{-1} performed in O_2 saturated aCSF (21˚C) buffer solution, illustrating the reduction of O2 at a Pt-MMA electrode.

As with PBS - 650 mV *vs.* SCE (see Figure 4.17) is in the mass-transport limited region after the peak potential of O_2 reduction at Pt-MMA electrodes. All experiments performed in aCSF were carried out at this potential.

4.3.2.8 Effect of ion changes

Changes in ion concentrations are of interest in *vivo* as previously discussed in Section 0. The effect of ion changes on the sensitivities of Pt-MMA electrodes was investigated. O_2 calibrations performed in aCSF, aCSF no Ca^{2+} and aCSF no Mg^{2+} on Pt-MMA electrodes are presented below in Table 4.27 and plotted in Figure 4.36 .

	aCSF (*n*=7)		aCSF no Ca^{2+} (*n*=4)		aCSF no Mg^{2+}(*n*=4)	
[O_2], µM	**Mean I, nA**	**SEM**	**Mean I, nA**	**SEM**	**Mean I, nA**	**SEM**
0	0	0	0	0	0	0
240	-626.7	106.8	-352.5	22.6	-158.8	3.1
1200	-1866.3	173.7	-1102.9	84.2	-890.9	24.9

Table 4.27: Table of results for O_2 calibrations (0-1200 µM) for Pt-MMA electrodes. CPA performed at -650 mV *vs.* SCE in aCSF (*n*=7), aCSF no Ca^{2+} (*n*=4), aCSF no Mg^{2+} (*n*=4) at 21˚C. Mean background subtracted.

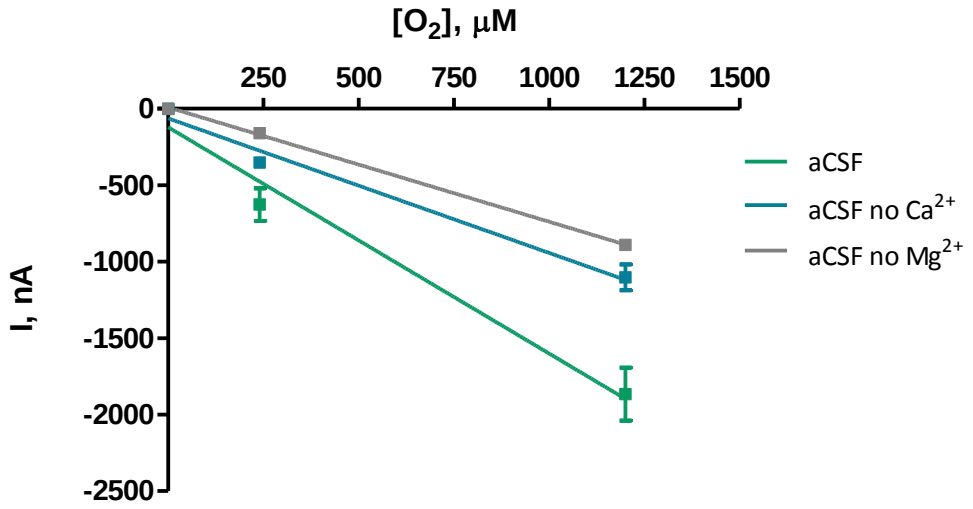

Figure 4.36: O_2 calibration data (0-1200 µM) for Pt-MMA electrodes. CPA performed at -650 mV *vs.* SCE in aCSF, aCSF no Ca^{2+} and aCSF no Mg^{2} at 21˚C.

Linear regression analysis was performed on electrodes to compare sensitivities of Pt-MMA electrodes calibrated in aCSF solutions in the presence and absence of ions, presented in Table 4.28 and plotted in Figure 4.37.

	Sensitivity (nA/µM)	R^2	***n***
aCSF	-1.480 ± 0.218	0.9788	7
aCSF no Ca^{2+}	-0.880 ± 0.113	0.9837	4
aCSF no Mg^{2+}	-0.748 ± 0.017	0.9995	4

Table 4.28: Comparison of calculated sensitivity values of O_2 calibrations (0-1200 µM) for Pt-MMA electrodes calibrated in aCSF, aCSF no Ca^{2+}, aCSF no Mg^{2+} at 21˚C.

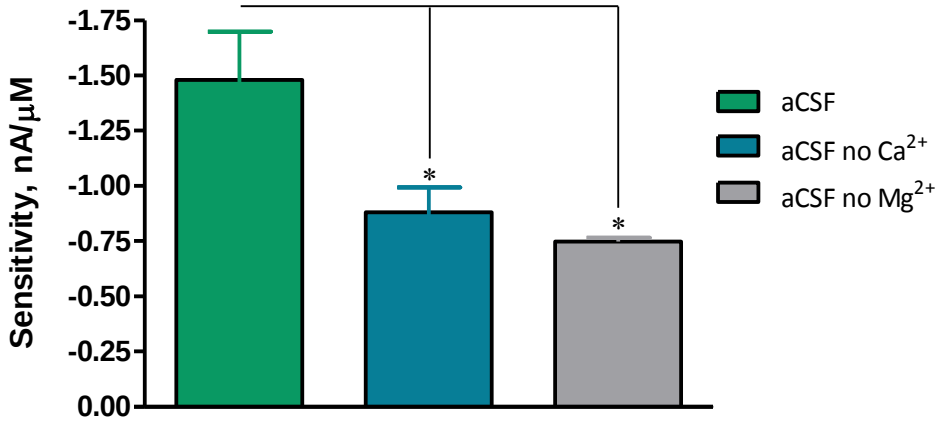

Figure 4.37: Comparison graph of calculated sensitivity values for O_2 calibrations (0-1200 µM) for Pt-MMA electrodes calibrated in aCSF (*n*=7), aCSF no Ca^{2+} (*n*=4), aCSF no Mg^{2}+ (*n*=4).

Unpaired *t*-test statistical analysis was performed and it can be seen there is a significant difference in the sensitivities of Pt-MMA electrodes calibrated in aCSF and aCSF with no Ca^{2+}or Mg^{2+} with *P* values of 0.0402 (aCSF no Ca^{2+}) and 0.0154 (aCSF no Mg^{2+}).

There is an increase in the sensitivity for Pt-MMA electrodes calibrated in aCSF (-1.480 ± 0.218 nA/µM) compared to PBS (-1.140 ± 0.004 nA/µM) although the difference is not significant P = 0.1699. The significant differences observed in the sensitivities of Pt-MMA electrodes plotted in Figure 4.37, with and without the presence of ions are unexpected as there were no significant differences seen with bare Pt electrodes (Bolger *et al.*, 2011a).

4.3.2.9 Effect of stirring

The reduction of O_2 at the Pt-MMA electrode was examined in quiescent and stirred solutions as discussed previously in Section 4.3.1.6. Results are presented below in Table 4.29 and plotted in Figure 4.38.

	Control: PBS Bubbling		PBS Quiescent		Stirring @ *c.a* 1 Hz		Stirring @ *c.a* 10 Hz	
$[O_2]$, µM	**Mean I, nA**	**SEM**	**Mean I, nA**	**SEM**	**Mean I, nA**	**SEM**	**Mean I, nA**	**SEM**
240	-651.9	93.6	-447.6	97.4	-561.6	153.7	-680.7	193.6
1200	-2452.2	99.4	-1517.6	43.2	-1688.0	55.8	-1774.1	62.3

Table 4.29: Table of results for O_2 calibrations (240-1200 µM) for Pt-MMA electrodes (*n*=4). CPA performed at -650 mV *vs.* SCE in PBS (pH 7.4) at 21˚C. Mean background subtracted.

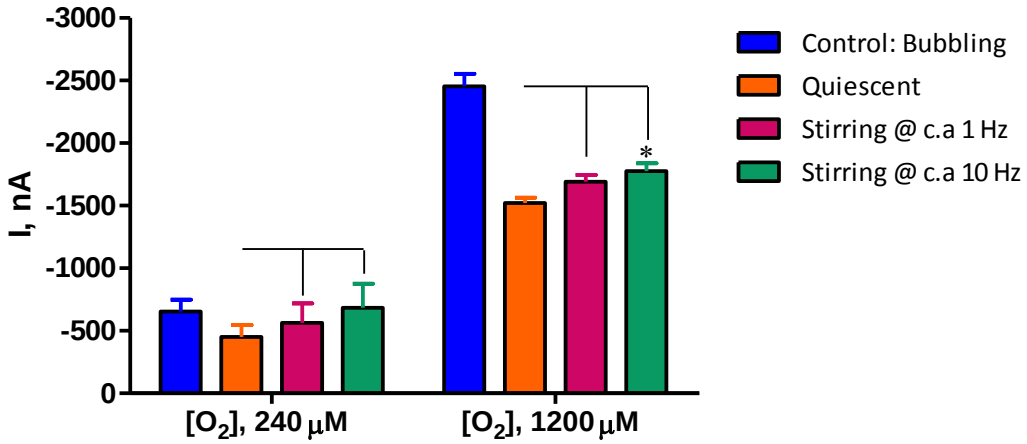

Figure 4.38: O_2 calibration data (240-1200 µM) for Pt-MMA electrodes (*n*=4). CPA performed at -650 mV *vs.* SCE in PBS (pH 7.4) quiescent and in the presence of forced convection at 21˚C.

Unpaired *t*-test statistical analysis was performed and it can be seen there is no significant difference in the sensitivities between Pt-MMA electrodes calibrated in quiescent PBS and agitated PBS stirred at approximately 1 Hz in the presence of 240 µM O_2 with a *P* value of 0.5585. There was also no significant difference found between Pt-MMA electrodes calibrated in quiescent PBS and agitated PBS stirred at approximately 10 Hz in the presence of 240 µM O_2 with a *P* value of 0.3426.

There is no significant difference in the sensitivities between Pt-MMA electrodes calibrated in quiescent PBS and agitated PBS stirred at approximately 1 Hz in the presence of 1200 µM O_2 with a *P* value of 0.0605. There was a significant difference found between Pt-MMA electrodes calibrated in quiescent PBS and agitated PBS stirred at approximately 10 Hz in the presence of 1200 µM O_2 with a *P* value of 0.0196. From the results presented in Figure 4.38 it can be seen that there is no significant increase in the current monitored using

Pt-MMA electrodes at 1 Hz in the presence 240 µM O_2 compared to quiescent conditions, concluding that there is no dependence on flow *in vitro.*

4.3.2.10 Selectivity

4.3.2.10.1 Ascorbic Acid (AA) calibrations

The effect of the most abundant interferent in the brain ascorbic acid (AA) was investigated (Miele & Fillenz, 1996). Calibrations were performed as described in Section 3.6.1.7. The addition of a 500 µM aliquot of AA prior to a high concentration (0-1200 µM) O_2 calibration allows for the determination of the effect of AA on the O_2 signal. O_2 calibrations performed in PBS with and without 500 µM AA present on Pt-MMA electrodes are presented below in Table 4.30 and plotted in Figure 4.39.

	Pt-MMA (*n*=4)		**Pt-MMA: 500 µM AA (*n*=4)**	
[O_2], µM	**Mean I, nA**	**SEM**	**Mean I, nA**	**SEM**
0	0	0	0	0
240	-342.9	39.7	-224.1	12.2
1200	-1425.8	150.0	-959.2	67.1

Table 4.30: Table of results for O_2 calibrations (0-1200 µM) for Pt-MMA electrodes (*n*=4) for a standard O_2 calibration and re-calibration in the presence of 500 µM AA. CPA performed at -650 mV *vs.* SCE in PBS (pH 7.4) at 21˚C. Mean background subtracted.

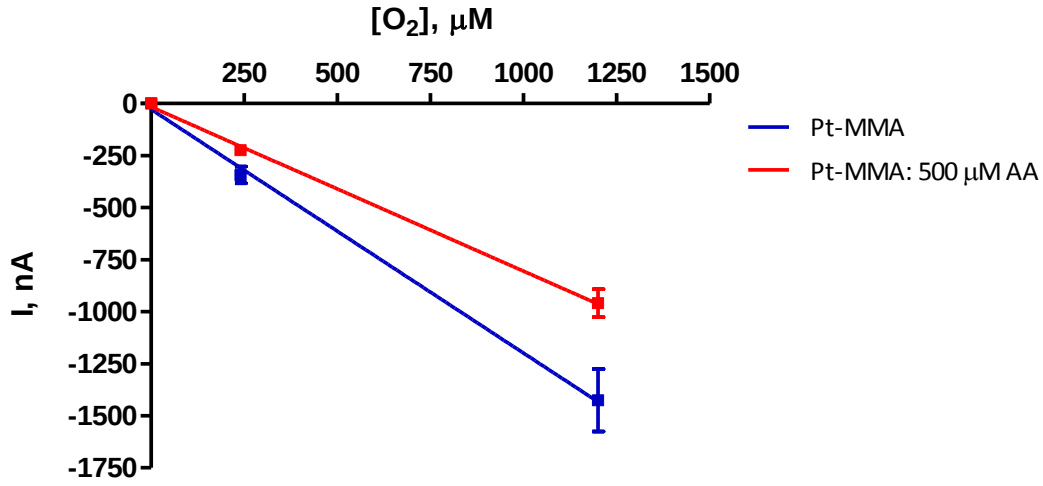

Figure 4.39: O_2 calibration data (0-1200 µM) for Pt-MMA electrodes (*n*=4) for a standard O_2 calibration and re-calibration in the presence of 500 µM AA. CPA performed at -650 mV *vs.* SCE in PBS (pH 7.4) at 21˚C.

Linear regression analysis was performed on electrodes to compare sensitivities of Pt-MMA electrodes calibrated with and without 500 µM of AA present, presented in Table 4.13 and plotted in Figure 4.40.

	Sensitivity (nA/µM)	R^2	*n*
Pt-MMA	-1.171 ± 0.050	0.9982	4
Pt-MMA: 500 µM AA	-0.790 ± 0.028	0.9988	4

Table 4.31: Table of calculated sensitivity values of O_2 calibrations (0-1200 µM) for Pt-MMA electrodes with and without 500 µM of AA present.

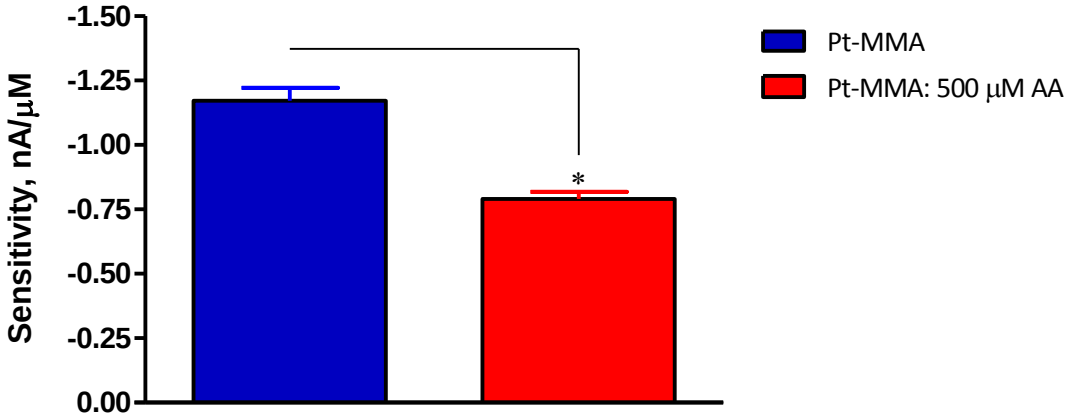

Figure 4.40: Comparison graph of calculated sensitivity values for O_2 calibrations (0-1200 µM) Pt-MMA electrodes with and without 500 µM of AA present (*n=4*).

Unpaired *t*-test statistical analysis was performed and it can be seen there is a significant difference in the sensitivities of Pt-MMA electrodes calibrated with and without the presence of 500 µM AA with a *P* value of 0.0026.

The significant difference in the sensitivities between Pt-MMA electrodes and Pt-MMA electrodes calibrated in the presence of 500 µM AA is thought to be due to the AA accumulating at the electrode surface and decreasing the surface area resulting in a reduction in sensitivity to O_2. Results for a 500 µM AA injection looked at the current response (Bolger *et al.*, 2011a). This experiment showed that the signal recorded in a N_2 atmosphere did not deviate from the typical baseline current.

4.3.2.11 Post- implantation calibrations

The effects of proteins, lipids and brain tissue on the sensitivity of Pt-MMA electrodes *in vitro* was investigated (Section 4.3.2.3). Although this gives an indication as to the effect that proteins, lipids and *ex-vivo* brain tissue has on the sensitivity of the electrodes the effect of the living brain with endogenous species present was investigated by performing post implantation calibrations where possible on the Pt-MMA electrodes (implanted for 19 ± 3 days) once removed from the brain, presented in Table 4.32 and plotted in Figure 4.41. These calibrations are described in Section 3.6.1.8.

	Pt-MMA (pre-implantation)		**Pt-MMA (post-implantation)**	
[O_2], µM	**Mean I, nA**	**SEM**	**Mean I, nA**	**SEM**
0	0	0	0	0
240	-312.0	13.9	-247.6	72.2
1200	-1403.4	74.0	-1038.2	121.3

Table 4.32: Table of results for O_2 calibrations (0-1200 µM) for Pt-MMA electrodes pre-implantation and post-implantation (*n*=4) for a standard O_2 calibration. CPA performed at -650 mV *vs.* SCE in PBS (pH 7.4) at 21˚C. Mean background subtracted.

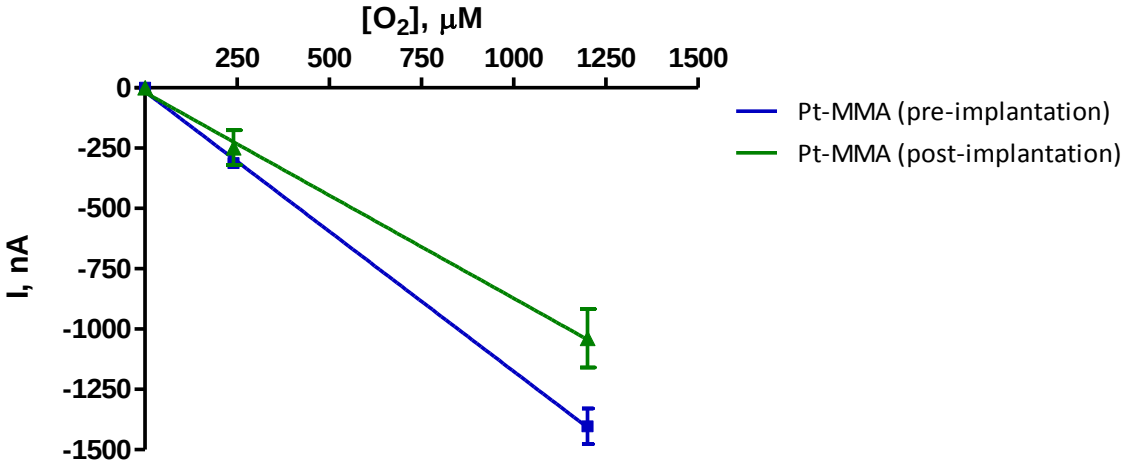

Figure 4.41: O_2 calibration data (0-1200 µM) for Pt-MMA electrodes pre-implantation and post-implantation (*n*=4) for a standard O_2 calibration). CPA performed at -650 mV *vs.* SCE in PBS (pH 7.4) at 21˚C.

Linear regression analysis was performed on electrodes to compare sensitivities of Pt-MMA electrodes calibrated before and after implantation, presented in Table 4.33 and plotted in Figure 4.42.

	Sensitivity (nA/µM)	R^2	*n*
Pre-implantation	-1.160 ± 0.027	0.9995	4
Post-implantation	-0.853 ± 0.034	0.9984	4

Table 4.33: Table of calculated sensitivity values of O_2 calibrations (0-1200 µM) for Pt-MMA electrodes pre-implantation and post-implantation.

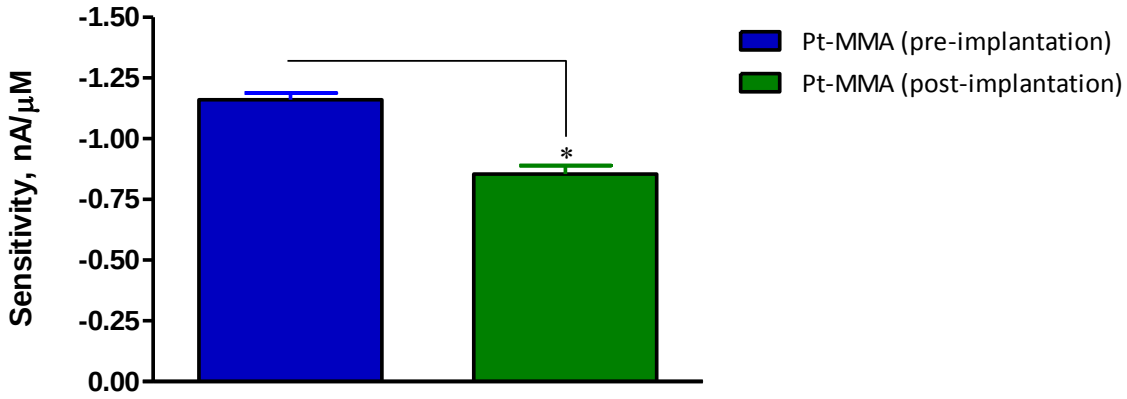

Figure 4.42: Graph of calculated sensitivity values for O_2 calibrations (0-1200 µM) for Pt-MMA electrodes pre-implantation and post-implantation (*n*=4).

Unpaired *t*-test statistical analysis was performed and it can be seen there is a significant difference in the sensitivities between Pt-MMA electrodes calibrated pre and post-implantation with a *P* value of 0.0009. From the results presented in **Error! Reference source not found.** it can be seen that the brain has a detrimental effect on the sensitivity of the Pt-MMA electrodes to O_2. This represents a decrease in sensitivity of 26.44 ± 2.96 % for the electrodes post-implantation compared to pre-implantation. This decrease is thought to be due to fouling and even an accumulation of tissue at the electrode surface preventing O_2 from reaching the active surface of the electrode.

4.3.3 *CPE and Pt-MMA Electrode Comparisons*

To allow for an accurate comparison between the CPEs and Pt-MMA electrodes due to the different dimensions of the electrodes the mean sensitivity values were converted to current densities.

4.3.3.1 Oxygen calibrations

The average sensitivity for CPEs in terms of current density for high concentration O_2 calibrations was -0.033 ± 0.001 $\mu Amm^{-2}\mu M^{-1}$ (n=24). The average current density value at the physiological O_2 level of 50 µM was -1.65 ± 0.05 μAmm^{-2} (n = 24).

The average sensitivity for Pt-MMA electrodes in terms of current density for high concentration O_2 calibrations was -0.093 ± 0.003 $\mu Amm^{-2}\mu M^{-1}$ (n=64). The average current density value at the physiological O_2 level of 50 µM was -4.66 ± 0.02 μAmm^{-2} (n = 64). Current density comparisons were made between CPEs and Pt-MMA electrodes for O_2 calibrations, plotted in Figure 4.43.

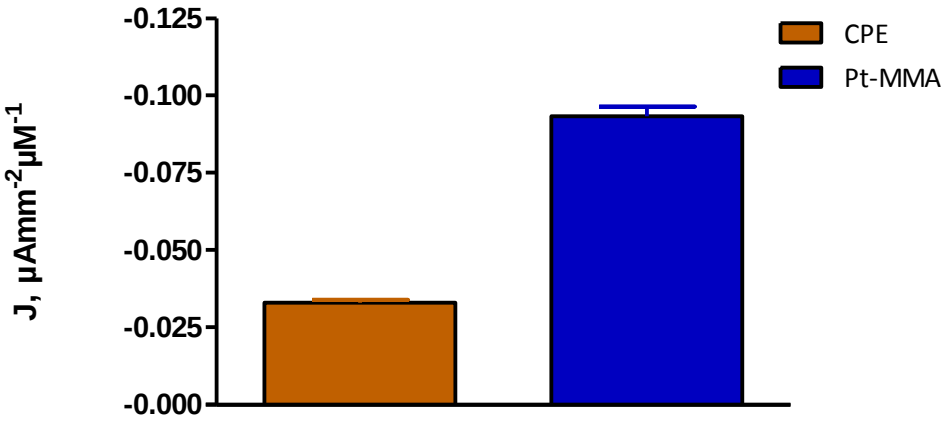

Figure 4.43: Comparison graph of calculated current density sensitivity values for O_2 calibrations (0-1200 µM) CPEs and Pt-MMA electrodes calibrated in PBS (pH 7.4) at 21˚C.

From these results it can be seen that the Pt-MMA electrodes exhibit a higher sensitivity to O_2 at the physiological concentration of 50 µM O_2 than CPEs.

4.3.3.2 Temperature dependence comparisons

The average sensitivity for CPEs in terms of current density for high concentration O_2 calibrations at 37°C was -0.046 ± 0.005 µAmm^{-2}µM^{-1} (*n*=8) and at 21°C was -0.033 ± 0.001 µAmm^{-2}µM^{-1} (*n*=24).

The average sensitivity for Pt-MMA electrodes in terms of current density for high concentration O_2 calibrations at 37°C was -0.133 ± 0.009 µAmm^{-2}µM^{-1} (*n*=5) and at 21°C was -0.092 ± 0.003 µAmm^{-2}µM^{-1} (*n*=10). Current density comparisons were made between CPEs and Pt-MMA electrodes for O_2 calibrations in PBS at 21°C and 37°C, plotted in Figure 4.44.

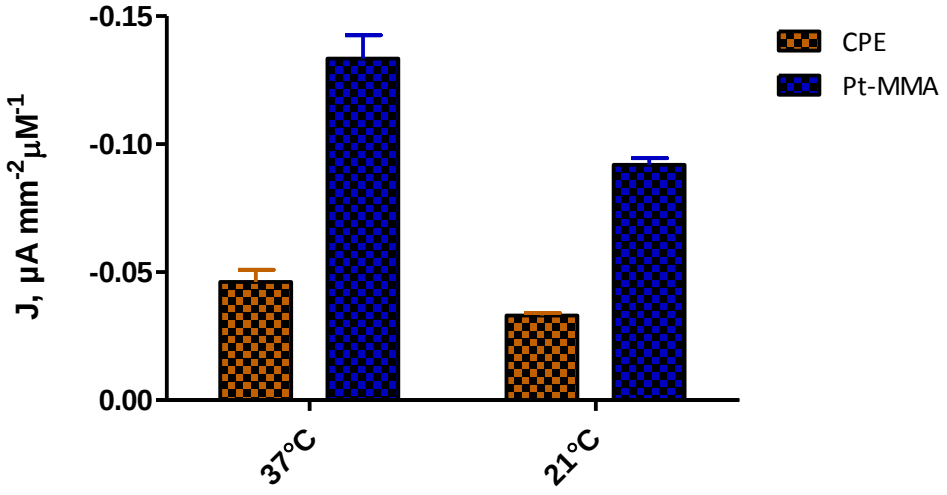

Figure 4.44: Comparison graph of calculated current density sensitivity values for O_2 calibrations (0-1200 µM) CPEs and Pt-MMA electrodes calibrated in PBS (pH 7.4) at 21˚C and 37 ˚C.

The Pt-MMA electrodes give a higher sensitivity in terms of current density at the physiological temperature of 37°C at 50 µM (-6.665 ± 0.454 µAmm^{-2}) than CPEs (-2.300 ± 0.239 µAmm^{-2}). However there is an increase of 2.47 ± 1.22 % for every 1˚C increase for CPEs and a 2.82 ± 0.44 % for every 1˚C increase for Pt-MMA electrodes showing that the electrodes behave similarly in terms of temperature dependence.

4.3.3.3 Convection comparisons

The average sensitivity for CPEs in terms of current density for O_2 calibrations at stirred (*ca.)* 1 Hz was -0.060 ± 0.005 µAmm^{-2}µM^{-1} (*n*=12 (240 µM) *n*=4 (1200 µM)) and at *ca.* 10 Hz was -0.061 ± 0.006 µAmm^{-2}µM^{-1} (*n*=12 (240 µM) *n*=4 (1200 µM)). There is a 33.15 ± 5.28 % decrease in the sensitivity of CPEs stirred at *ca.* 1 Hz compared to no stirring (-0.090 ± 0.002 µAmm^{-2}µM^{-1} (*n*=12 (240 µM) *n*=4 (1200 µM)) and a decrease of 32.10 ± 6.91 % for CPEs stirred at *ca.* 10 Hz.

The average sensitivity for Pt-MMA electrodes in terms of current density for O_2 calibrations at stirred at *ca.* 1 Hz was -0.109 ± 0.016 µAmm^{-2}µM^{-1} (*n*=4) and at *ca.* 10 Hz was -0.113 ± 0.023 µAmm^{-2}µM^{-1} (*n*=4). There is a 9.68 ± 15.75 % increase in the sensitivity of Pt-MMA electrodes stirred at *ca.* 1 Hz compared to no stirring (-0.100 ± 0.010 µAmm^{-2}µM^{-1} (*n*=4)) and an increase of 13.10 ± 22.92 % for Pt-MMA electrodes

stirred at *ca.* 10 Hz. Current density comparisons were made between CPEs and Pt-MMA electrodes for O_2 calibrations in quiescent and agitated solutions of PBS, plotted in Figure 4.45.

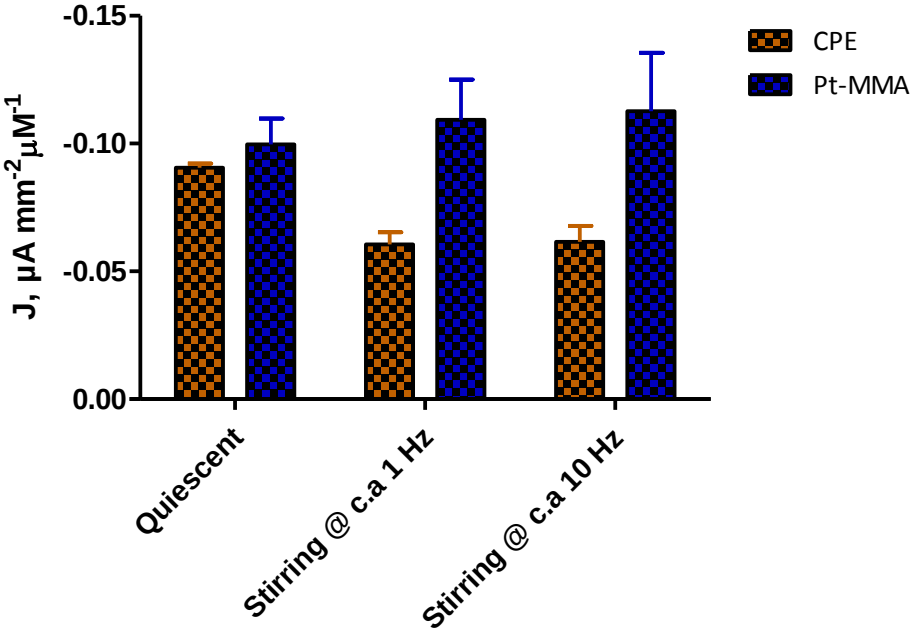

Figure 4.45: Comparison graph of calculated current density sensitivity values for O_2 calibrations on CPEs and Pt-MMA electrodes calibrated in PBS (pH 7.4) quiescent and in the presence of forced convection at 21˚C.

From the results it can be seen that convection has less of an effect on the sensitivity of Pt-MMA electrodes than CPEs. These results have little bearing on *in vivo* experiments but would be more relevant to brain slice or tissue culture experiments as discussed previously in Section 4.3.1.6.

4.3.3.4 Post implantation comparisons

The average sensitivity for CPEs in terms of current density for O_2 calibrations (0-1200 µM) post-implantation was -0.031 ± 0.004 $\mu Amm^{-2}\mu M^{-1}$ (n=13) corresponding to a 5.75 ± 11.46 % decrease when compared to pre-implantation calibrations (-0.033 ± 0.001 $\mu Amm^{-2}\mu M^{-1}$ (n=13)).

The average sensitivity for Pt-MMA electrodes in terms of current density for O_2 calibrations (0-1200 µM) post-implantation was -0.070 ± 0.003 $\mu Amm^{-2}\mu M^{-1}$ (n=4) corresponding to a 26.44 ± 2.96 % decrease when compared to pre-implantation calibrations (-0.095 ± 0.002 $\mu Amm^{-2}\mu M^{-1}$ (n=4)). Current density comparisons were made between CPEs and Pt-MMA electrodes pre and post-implantation, plotted in Figure 4.46.

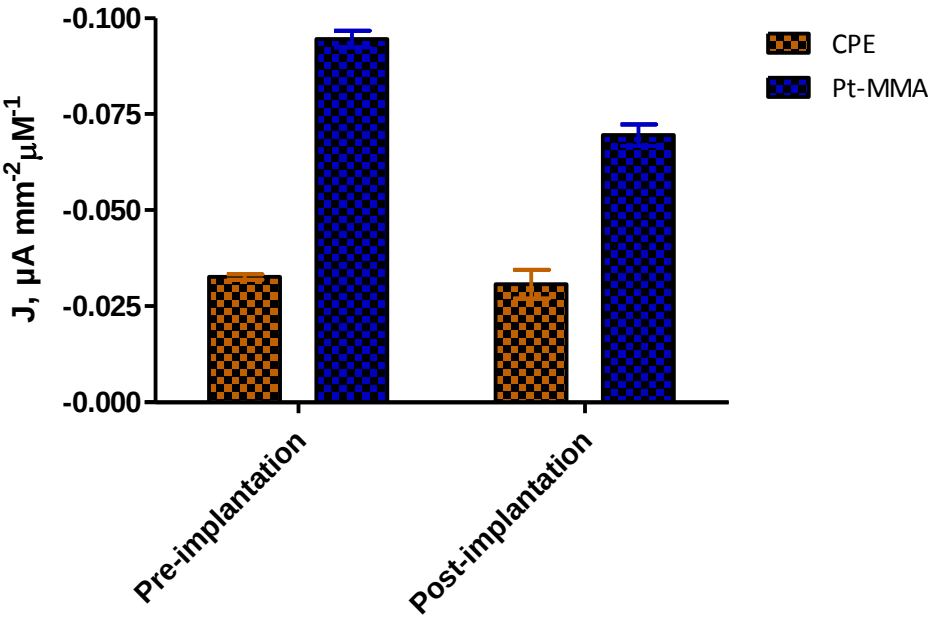

Figure 4.46: Comparison graph of calculated current density sensitivity values for O_2 calibrations on CPEs and Pt-MMA electrodes calibrated before and after implantation in PBS (pH 7.4) at 21°C.

From the results it can be seen that implantation has less of an effect on the sensitivity of CPEs than Pt-MMA electrodes when compared to pre-implantation calibrations. This is thought to be due to fowling of the Pt-MMA electrodes, characteristic of noble metal electrodes. However the CPEs were only implanted for a period of 6 ± 1 days compared to Pt-MMA electrodes which were implanted for a period of 19 ± 3 days. There is an approximate 2 week difference in the length of implantation which could account for the vast difference in sensitivities. The stability of CPEs have been investigated *in vivo* indicating a stable baseline signal over 12 weeks (Bolger *et al.*, 2011b), showing that CPEs are suitable for long-term recording of brain tissue O_2 compared to Pt-MMA electrodes which exhibit a significant drop in sensitivity of 26.44 ± 2.96 % after 19 ± 3 days.

4.4 Conclusions

The *in vitro* characterisation of an electrode allows for the determination of the sensitivity, selectivity and stability of the sensor. This chapter examines the effect of changes in temperature, pH, ions, convection and implantation on the sensitivity of CPEs to O_2 (Section 4.3.1). Pt-MMA electrodes were fully characterised *in vitro* by determining the sensitivity of the sensor to O_2 and the effects on the sensitivity following exposure to proteins, lipids and brain tissue. The effects of temperatures, pH, ions, convection, interferents and implantation were also examined along with the stability of the sensors in relation to time (Section 4.3.2.4).

From the results observed in this chapter it can be concluded that Pt-MMA electrodes have a higher sensitivity to O_2 than CPEs (Section 4.3.3.1). The physiological temperature (37°C) affects the sensitivity of CPEs and Pt-MMA electrodes similarly (Section 4.3.3.2) and although convection experiments show that Pt-MMA electrodes are less affected by stirring than CPEs (Section 4.3.3.3) these results only prove to be relevant for *in vitro* experiments. The effect of implantation of the sensors into the living brain showed that implantation has less of an effect on CPEs than Pt-MMA electrodes although there was a difference of the period implanted of approximately 2 weeks (Section 4.3.3.4). Our previously published data shows that CPEs have a stable baseline over 12 (Bolger *et al.*, 2011b). These results indicate that Pt-MMA electrodes are an ideal choice for detection of brain tissue O_2 *in vivo* over short periods of time but CPEs would be the sensor of choice for long-term monitoring of brain tissue O_2.

References

Amatore C, Szunerits S, Thouin L & Warkocz J-S. (2000). Mapping concentration profiles within the diffusion layer of an electrode: Part III. Steady-state and time-dependent profiles via amperometric measurements with an ultramicroelectrode probe. *Electrochemistry Communications* **2,** 353-358.

Bard AJ & Faulkner LR. (1980). *Electrochemical Methods: Fundamentals and Applications*. John Wiley & Sons.

Bolger F & Lowry J. (2005). Brain Tissue Oxygen: *In Vivo* Monitoring with Carbon Paste Electrodes. *Sensors* **5,** 473-487.

Bolger FB, Bennett R & Lowry JP. (2011a). An *in vitro* characterisation comparing carbon paste and Pt microelectrodes for real-time detection of brain tissue oxygen. *The Analyst* **136,** 4028-4035.

Bolger FB, McHugh SB, Bennett R, Li J, Ishiwari K, Francois J, Conway MW, Gilmour G, Bannerman DM, Fillenz M, Tricklebank M & Lowry JP. (2011b). Characterisation of carbon paste electrodes for real-time amperometric monitoring of brain tissue oxygen. *Journal of neuroscience methods* **195,** 135-142.

Chen BT & Rice ME. (1999). Calibration Factors for Cationic and Anionic Neurochemicals at Carbon-Fiber Microelectrodes are Oppositely Affected by the Presence of $Ca^{2+}$and Mg^{2+}. *Electroanalysis* **11,** 344-348.

Cheng HY, Schenk J, Huff R & Adams RN. (1979). *In vivo* electrochemistry: behavior of micro electrodes in brain tissue. *Journal of Electroanalytical Chemistry and Interfacial Electrochemistry* **100,** 23-31.

Cooper R. (1963). Local changes of intra-cerebral blood flow and oxygen in humans. *Medical and Biological Engineering and Computing* **1,** 529-536.

Crespi F. (1996). Carbon fibre micro-electrode and *in vitro* or in brain slices voltammetric measurement of ascorbate, catechol and indole oxidation signals: influence of temperature and physiological media. *Biosensors and Bioelectronics* **11,** 743-749.

Dayton MA, Ewing AG & Wightman RM. (1983). Diffusion processes measured at microvoltammetric electrodes in brain tissue. *Journal of Electroanalytical Chemistry and Interfacial Electrochemistry* **146,** 189-200.

Garguilo MG & Michael AC. (1994). Quantitation of Choline in the Extracellular Fluid of Brain Tissue with Amperometric Microsensors. *Analytical chemistry* **66,** 2621-2629.

Gifford R, Kehoe JJ, Barnes SL, Kornilayev BA, Alterman MA & Wilson GS. (2006). Protein interactions with subcutaneously implanted biosensors. *Biomaterials* **27,** 2587-2598.

Gotoh F, Tazaki Y & Meyer JS. (1961). Transport of gases through brain and their extravascular vasomotor action. *Experimental Neurology* **4,** 48-58.

Hitchman ML. (1978). Measurement of dissolved oxygen. *John Wiley and Sons, New York N Y 1978 255*.

Jeroschewski P & Zur Linden D. (1997). A flow system for calibration of dissolved oxygen sensors. *Fresenius' Journal of Analytical Chemistry* **358,** 677-682.

Kane DA & O'Neill RD. (1998). Major differences in the behaviour of carbon paste and carbon fibre electrodes in a protein–lipid matrix: implications for voltammetry *in vivo*. *The Analyst* **123,** 2899-2903.

Kume-Kick J & Rice ME. (1998). Dependence of dopamine calibration factors on media Ca^{2+} and Mg^{2+} at carbon-fiber microelectrodes used with fast-scan cyclic voltammetry. *Journal of neuroscience methods* **84,** 55-62.

Lowry JP, Boutelle MG & Fillenz M. (1997). Measurement of brain tissue oxygen at a carbon paste electrode can serve as an index of increases in regional cerebral blood flow. *Journal of neuroscience methods* **71,** 177-182.

Lowry JP, Boutelle MG, O'Neill RD & Fillenz M. (1996). Characterization of carbon paste electrodes *in vitro* for simultaneous amperometric measurement of changes in oxygen and ascorbic acid concentrations *in vivo*. *The Analyst* **121,** 761-766.

Lyne PD & O'Neill RD. (1990). Stearate-modified carbon paste electrodes for detecting dopamine *in vivo*: decrease in selectivity caused by lipids and other surface-active agents. *Analytical Chemsitry* **62,** 2347-2351.

Miele M & Fillenz M. (1996). *In vivo* determination of extracellular brain ascorbate. *Journal of neuroscience methods* **70,** 15-19.

Nicholson C & Syková E. (1998). Extracellular space structure revealed by diffusion analysis. *Trends Neuroscience* **21,** 207-215.

O'Neill RD. (1993). Sensor-tissue interactions in neurochemical analysis with carbon paste electrodes *in vivo*. *The Analyst* **118,** 433-438.

Ormonde DE & O'Neill RD. (1989). Altered response of carbon paste electrodes after contact with brain tissue: Implications for modified electrode use *in vivo*. *Journal of Electroanalytical Chemistry and Interfacial Electrochemistry* **261,** 463-469.

Ormonde DE & O'Neill RD. (1990). The oxidation of ascorbic acid at carbon paste electrodes: Modified response following contact with surfactant, lipid and brain tissue. *Journal of Electroanalytical Chemistry and Interfacial Electrochemistry* **279,** 109-121.

Rice ME & Nicholson C. (1995). Diffusion and ion shifts in the brain extracellular microenvironment and their relevance for voltammetric measurements. *Voltammetric Methods in Brain Systems Neuromethods* **27,** 27-79.

Schneiderman G & Goldstick T. (1978). Oxygen electrode design criteria and performance characteristics: recessed cathode. *Journal of Applied Physiology: Respiratory, Environmental and Exercise Physiology* **45,** 145.

Sharan M, Vovenko EP, Vadapalli A, Popel AS & Pittman RN. (2008). Experimental and theoretical studies of oxygen gradients in rat pial microvessels. *Journal of Cerebral Blood Flow & Metabolism* **28,** 1597-1604.

Taylor R & Humffray A. (1975). Electrochemical studies on glassy carbon electrodes:: III. Oxygen reduction in solutions of low pH (pH< 10). *Journal of Electroanalytical Chemistry and Interfacial Electrochemistry* **64,** 85-94.

Wilkins E & Radford W. (1990). Biomaterials for implanted closed loop insulin delivery system: A review. *Biosensors and Bioelectronics* **5,** 167-213.

Wisniewski N, Moussy F & Reichert WM. (2000). Characterization of implantable biosensor membrane biofouling. *Fresenius' Journal of Analytical Chemistry* **366,** 611-621.

Yang HH & McCreery RL. (2000). Elucidation of the mechanism of dioxygen reduction on metal-free carbon electrodes. *Journal of The Electrochemical Society* **147,** 3420-3428.

Zimmerman JB & Wightman RM. (1991). Simultaneous electrochemical measurements of oxygen and dopamine *in vivo*. *Analytical Chemsitry* **63,** 24-28.

5. RESULTS: CHARACTERISATION OF A PT-BASED SENSOR FOR THE DETECTION OF BRAIN TISSUE OXYGEN *IN VIVO*

5.1 Introduction

Brain tissue oxygen (O_2) is one of the most important energy substrates for brain energy metabolism. Molecular O_2 was one of the first substances to be detected voltammetrically *in vivo* in the brain (Clark *et al.*, 1958; Clark Jr & Lyons, 1965) and in peripheral tissue (Clark Jr & Clark, 1964). O_2 is delivered by the blood and the tissue concentration is determined by the balance of supply and utilisation. In different brain regions the O_2 turnover rate varies and it has been established that the cerebral cortex has a higher turnover rate than others (Nair *et al.*, 1987). The concentration of O_2 in the brain varies as supply is altered in different layers of the brain tissue (Baumgärtl *et al.*, 1989) and depends on the tissue heterogeneity (Murr *et al.*, 1994; Lubbers & Baumgärtl, 1997). O_2 tissue concentrations have been reported to range from 40 µM (Murr *et al.*, 1994), 50 µM (Zimmerman & Wightman, 1991), 60 µM (Zauner *et al.*, 1995) to 80 µM (McCreery *et al.*, 1990).

Carbon-based electrodes such as glassy carbon (Clark Jr & Clark, 1964), carbon fiber electrodes (Zimmerman & Wightman, 1991; Zimmerman *et al.*, 1992; Venton *et al.*, 2003), carbon epoxy (Bazzu *et al.*, 2009) and carbon paste electrodes (Lowry *et al.*, 1996; Lowry *et al.*, 1997; Bolger & Lowry, 2005; Bolger *et al.*, 2011b) are commonly used for detecting changes in tissue O_2. Carbon electrodes have their advantages and disadvantages over noble metal electrodes. The main advantage of carbon fibre electrodes (CFEs) and carbon paste electrodes (CPEs) for use *in vivo* are that they are less susceptible to surface poisoning than noble metal electrodes, which usually require the addition of a protective membrane (Wisniewski *et al.*, 2000; Zhao *et al.*, 2001; Gifford *et al.*, 2006). CFEs (Zimmerman & Wightman, 1991) are advantageous due to their small diameter (5-50 µm), however if placed closely to blood vessels or metabolically active sites the O_2 concentration can vary (Lowry *et al.*, 1997). CPEs are advantageous as *in vivo* they are stable over long periods (O'Neill, 1993; O'Neill & Lowry, 1995; O'Neill, 2005; Bolger *et al.*, 2011b). CPEs have a diameter of 200 µm greater than the scale of the capillary zone (<100 µm) (Silver, 1965) which allows detection of average tissue O_2 levels. However due to their size they do cause greater tissue damage than noble metal electrodes.

Platinum(Pt)-based electrodes have been shown to be a potential alternative to CPEs to monitor brain tissue O_2 (Bolger *et al.*, 2011a). Pt electrodes are easier to manufacture than CPEs and have a smaller diameter (125 µm) resulting in less tissue damage.

This chapter investigates and characterises the use of Pt-coated in methyl methacrylate (MMA) for the detection of brain tissue O_2 in the striatum following on from the previous chapter (Chapter 4) where the Pt-MMA electrodes were fully characterised *in vitro*. As previously discussed in Section 4.1 the *in vitro* characterisation allows for an indication of the potential consequences of implantation of the sensor into tissue but does not allow us to know the full extent of the effect of the brain on the sensitivity, selectivity and stability of the sensor.

5.2 Experimental *In Vivo*

The instrumentation and software used are detailed in Section 3.2 and all chemicals and solutions are detailed in Section 3.3.

Pt disk electrodes (125 µm bare diameter) were constructed as described in Section 3.4.5 and modified using MMA as detailed in Section 3.5.2.1. A potential of -650 mV *vs.* SCE was applied to the working electrodes and all experiments were performed on freely-moving Wistar rats.

In vivo procedures are detailed in Section 3.7. Pt-MMA electrodes were implanted in the striatum.

Data is represented via the mean ± SEM where n = number of administrations, unless otherwise stated. Significant differences were calculated using two-tailed unpaired *t*-tests unless otherwise stated.

5.3 Results and Discussion *In Vivo*

5.3.1 *Characterisation of Pt-MMA electrodes In Vivo*

5.3.2 *Gaseous Administrations*

5.3.2.1 Hyperoxia

Mild hyperoxia was achieved by administration of O_2 gas to the snout of the animal. The flow was maintained at a slow steady rate similar to the method used previously (Lowry *et al.*, 1998) and as described in Section 3.7.4. The inhalation of the O_2 gas for 3 minutes resulted in a change from baseline levels for the O_2 signals, monitored using Pt-MMA electrodes as can be seen in Figure 5.1 below.

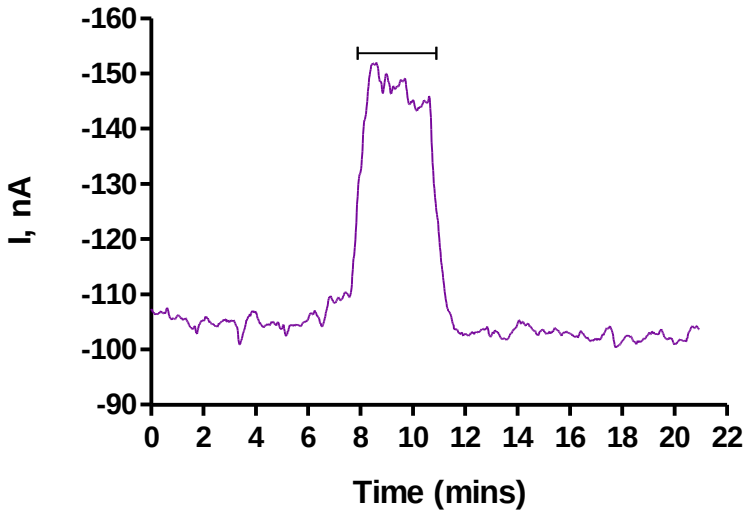

Figure 5.1 : A typical example of a 3-min period of mild hyperoxia (administration of O_2 gas) monitored *in vivo* using a Pt-MMA electrode implanted in the striatum of a freely-moving rat. The bar indicates the period of gaseous administration.

A 3-min period of mild hyperoxia shows an average immediate increase in current from the baseline level of -93.70 ± 3.57 nA (n=51, 4 animals) to -133.51 ± 6.14 nA (n=51, 4 animals). This increase was found to be significant ($P < 0.0001$). The percentage increase

was found to be 43.25 ± 4.01 % (*n*=51, 4 animals). Changes were immediate and on cessation of inhalation the signals quickly returned to baseline levels of -94.86 ± 3.55 nA after 4.51 ± 0.63 min (*n*=41, 4 animals) (*P*=0.8183), indicating a rapid return to normoxic conditions. A summary of these results can be seen in Table 5.1.

Hyperoxia	
Baseline (nA)	-93.70 ± 3.57
Max Increase (nA)	-133.51 ± 6.14
% Increase	43.25 ± 4.01
Post-baseline (nA)	-94.86 ± 3.55
***t* to post-baseline (min)**	4.51 ± 0.63

Table 5.1 : Summary of results for a 3-min period of mild hyperoxia monitored *in vivo* using Pt-MMA electrodes (*n* = 41, 4 animals), implanted in the striatum of freely-moving rats.

From these results it can be seen that there is a significant increase in striatal tissue O_2 upon administration of O_2 gas to the animal's snout and this change can be reliably monitored using Pt-MMA electrodes.

5.3.2.2 Hypoxia

Mild hypoxia was achieved by administration of N_2 gas to the snout of the animal. The flow was maintained at a slow steady rate similar to the method used previously (Lowry *et al.*, 1998) and as described in Section 3.7.4. The inhalation of the N_2 gas for 3 minutes resulted in a change from baseline levels for the O_2 signals, monitored using Pt-MMA electrodes as can be seen in Figure 5.2 below.

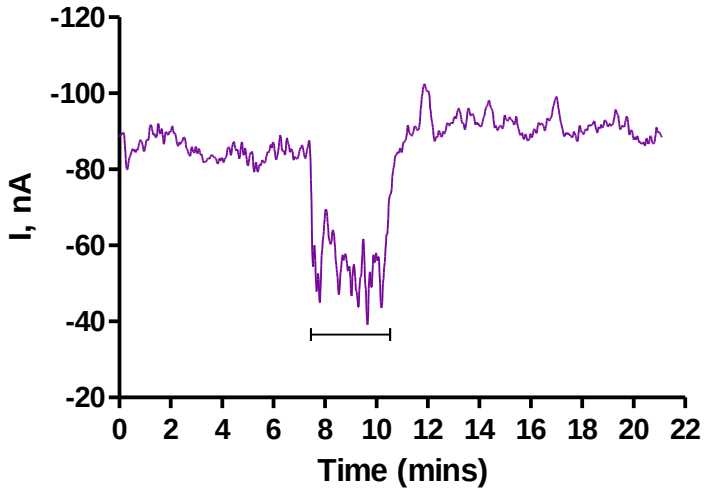

Figure 5.2 : A typical example of a 3-min period of mild hypoxia (administration of N_2 gas) monitored *in vivo* using a Pt-MMA electrode implanted in the striatum of a freely-moving rat. The bar indicates the period of gaseous administration.

A 3-min period of mild hypoxia shows an average immediate decrease in current from the baseline level of -89.62 ± 3.89 nA (*n*=42, 4 animals) to -63.87 ± 3.91 nA (*n*=42, 4 animals). This decrease was found to be significant ($P < 0.0001$). The percentage decrease was found to be 28.13 ± 2.05 % (*n*=42, 4 animals). Changes were immediate and on cessation of inhalation the signals quickly returned to baseline levels of -90.16 ± 6.37 nA after 2.95 ± 0.11 min (*n*=34, 4 animals) (P= 0.9426), indicating a rapid return to normoxic conditions. A summary of these results can be seen in Table 5.2.

Hypoxia	
Baseline (nA)	-89.62 ± 3.89
Max Decrease (nA)	-63.87 ± 3.91
% Decrease	28.13 ± 2.05
Post-baseline (nA)	-90.16 ± 6.37
***t* to post-baseline (min)**	2.95 ± 0.11

Table 5.2: Summary of results for a 3-min period of mild hypoxia monitored *in vivo* using Pt-MMA electrodes (*n* = 42, 4 animals), implanted in the striatum of freely-moving rats.

From these results it can be seen that there is a significant decrease in striatal tissue O_2 upon administration of N_2 gas to the animal's snout and this change can be reliably monitored using Pt-MMA electrodes.

5.3.3 *Neuronal Activation*

5.3.3.1 Tail Pinch

Neuronal activation was stimulated physiologically by means of a tail pinch. A tail pinch induces a well characterised behaviour pattern consisting of gnawing, licking, eating and a general increase in the level of motor activity (Antelman *et al.*, 1975). The tail pinch was performed for a duration of 5 minutes similar to methods used previously (Bolger & Lowry, 2005) and as described in Section 3.7.5.1. Induced neuronal activation for 5 minutes resulted in a change from baseline levels for the O_2 signals, monitored using Pt-MMA electrodes as can be seen in Figure 5.3.

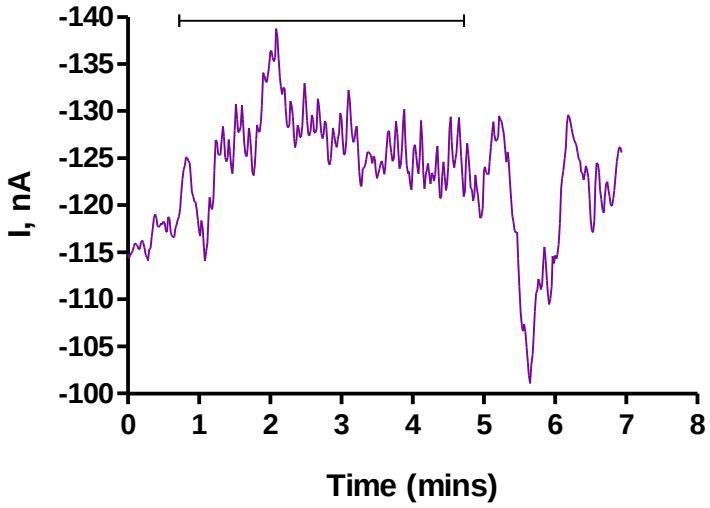

Figure 5.3: A typical example of a 5-min tail pinch (neuronal activation) monitored *in vivo* using a Pt-MMA electrode implanted in the striatum of a freely-moving rat. . The bar indicates the duration of the tail pinch.

A 5-min period of neuronal activation shows an average increase in current from baseline level of -106.22 ± 5.36 nA (n=14, 3 animals) to -121.26 ± 6.66 nA (n=14, 3 animals) after

2.04 ± 0.41 min, representing a significant increase of 15.33 ± 1.96 % (n=14, 3 animals) compared to baseline levels (P< 0.0001 (paired t-test)). Upon cessation of the tail pinch, the current increased to -117.71 ± 5.86 nA (n=14, 3 animals) corresponding to a mean percentage increase of 11.16 ± 1.77 % (n=14, 3 animals) from baseline levels. The post-tail pinch current returned to baseline levels of -103.03 ± 8.47 nA (n=14, 3 animals) (P=0.7534) after 10.91 ± 4.16 min. A summary of these results can be seen in Table 5.3.

Tail pinch	
Baseline (nA)	-106.22 ± 5.36
Max Increase (nA)	-121.26 ± 6.66
% Increase	15.33 ± 1.96
Post-baseline (nA)	-103.03 ± 8.47
***t* to post-baseline (min)**	10.91 ± 4.16

Table 5.3: Summary of results for a 5-min tail pinch monitored *in vivo* using Pt-MMA electrodes (*n* = 14, 3 animals), implanted in the striatum of freely-moving rats.

From these results it can be seen that there is an increase in striatal tissue O_2 upon neuronal activation and this change can be reliably monitored using Pt-MMA electrodes. The percentage increase however is low which is thought to be due to variations in the stress score between experiments and habituation of the animal to the tail pinch.

5.3.4 *Control Administrations*

5.3.4.1 Saline

The effect of i.p. injections of saline (0.9% NaCl) on the O_2 signal was investigated. Saline serves as a vehicle for drug administration so the effects of saline and the i.p. injection on the O_2 signal, monitored using Pt-MMA electrodes can be seen in Figure 5.4 below.

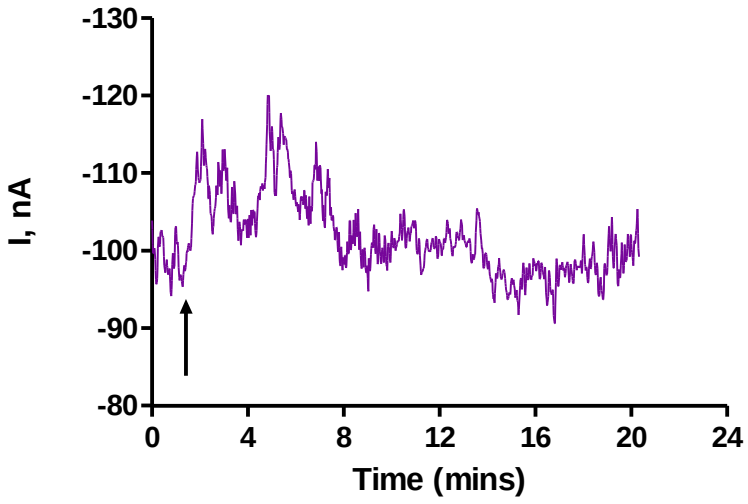

Figure 5.4: A typical example of an i.p. administration of saline (0.9% NaCl) monitored *in vivo* using a Pt-MMA electrode implanted in the striatum of a freely-moving rat. The arrow indicates the point of injection.

An i.p. injection of saline shows an average immediate increase in the O_2 signal from baseline levels of -93.51 ± 5.89 nA (*n*=14, 3 animals) to -105.63 ± 7.05 nA after 25.80 ± 3.34 seconds (*n*=14, 3 animals) this sharp increase in current of 13.35 ± 2.42 % can be attributed to injection stress. A maximum increase of -109.58 ± 7.68 nA (*n*=14, 3 animals) was observed after 3.57 ± 0.77 min representing a non-significant increase of 19.84 ± 3.30% (*n*=14, 3 animals) compared to baseline levels (*P*= 0.1118). The current returned to post-injection baseline levels of -95.43 ± 5.92 nA (*n*=14, 3 animals) (*P*= 0.8214) after 5.21 ± 1.09 min. A summary of these results can be seen in Table 5.4.

Saline i.p.	
Baseline (nA)	-93.51 ± 5.89
Max Increase (nA)	-109.58 ± 7.68
t to max increase (min)	3.57 ± 0.77
% Increase	19.84 ± 3.30
Post-baseline (nA)	-95.43 ± 5.92
***t* to post-baseline (min)**	5.21 ± 1.09

Table 5.4: Summary of results for i.p. administrations of saline (0.9% NaCl) monitored *in vivo* using Pt-MMA electrodes (*n* = 14, 3 animals), implanted in the striatum of freely-moving rats.

From these results it can be seen that there is no significant effect on striatal tissue O_2 levels upon administration of a saline (0.9%) i.p. injection monitored using Pt-MMA electrodes. The increase observed can be attributed to injection stress. It can therefore be concluded that any increase seen using saline as a vehicle for drug administrations is a drug effect.

5.3.4.2 Dimethyl sulfoxide (DMSO)

The effect of i.p. injections of DMSO (2%) on the O_2 signal was investigated. DMSO serves as a vehicle for drug administration so the effects of DMSO and the i.p. injection on the O_2 signal, monitored using Pt-MMA electrodes can be seen in Figure 5.5 below.

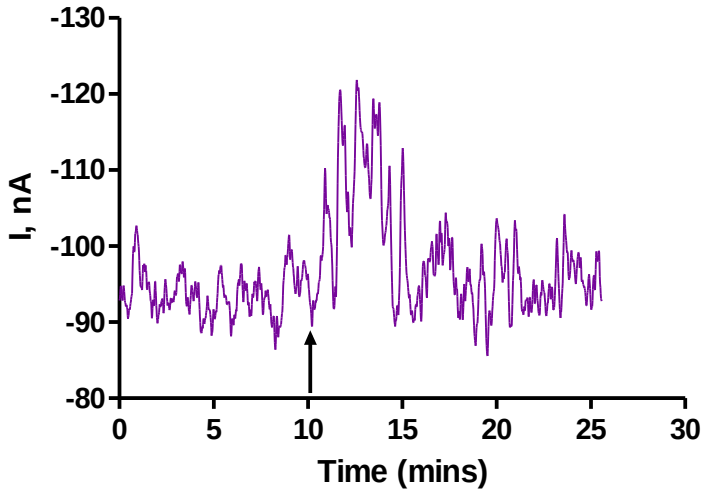

Figure 5.5: A typical example of an i.p. administration of DMSO (2%) monitored *in vivo* using a Pt-MMA electrode implanted in the striatum of a freely-moving rat. The arrow indicates the point of injection.

An i.p. injection of DMSO shows an average immediate increase in the O_2 signal from baseline levels of -85.30 ± 10.03 nA (*n*=6, 3 animals) to -97.31 ± 11.78 nA after 32.63 ± 6.42 seconds (*n*=6, 3 animals) this sharp increase in current of 13.28 ± 2.80 % can be attributed to injection stress. A maximum increase of -92.94 ± 8.92 nA (*n*=6, 3 animals) was observed after 13.64 ± 4.79 min representing a non-significant increase of 6.98 ± 1.83 % (*n*= 6, 3 animals) compared to baseline levels (*P*= 0.5832). The current returned to post-

injection baseline levels of -87.10 ± 10.24 nA (*n*=6, 3 animals) (*P*= 0.9028) after 11.44 ± 4.24 min. A summary of these results can be seen in Table 5.5.

DMSO i.p.	
Baseline (nA)	-85.30 ± 10.03
Max Increase (nA)	-92.94 ± 8.92
t to max increase (min)	13.64 ± 4.79
% Increase	6.98 ± 1.83
Post-baseline (nA)	-87.10 ± 10.24
***t* to post-baseline (min)**	11.44 ± 4.24

Table 5.5: Summary of results for i.p. administrations of DMSO (2%) monitored *in vivo* using Pt-MMA electrodes (*n* = 6, 3 animals), implanted in the striatum of freely-moving rats.

From these results it can be seen that there is no significant effect on striatal tissue O_2 levels upon administration of a DMSO (2 %) i.p. injection monitored using Pt-MMA electrodes. It can therefore be concluded that any increase seen using DMSO as a vehicle for drug administrations is a drug effect.

5.3.5 *Drug Administration*

5.3.5.1 The Effect of Acetazolamide

Acetazolamide (Diamox) is a carbonic anhydrase inhibitor and when administered systematically has been shown to increase brain tissue oxygen concentrations (Clark Jr & Lyons, 1965; Dixon *et al.*, 2002; Bolger & Lowry, 2005). Acetazolamide acts by inhibiting the carbonic anhydrase enzymes whose function is to catalyse the conversion of CO_2 and H_2O_2 to bicarbonate (HCO_3^-). This increase in CO_2 and a subsequent decrease in pH results in vasodilatation and an increase in tissue O_2. The effect of acetazolamide on the O_2 signal, monitored with Pt-MMA electrodes can be seen in Figure 5.6 below.

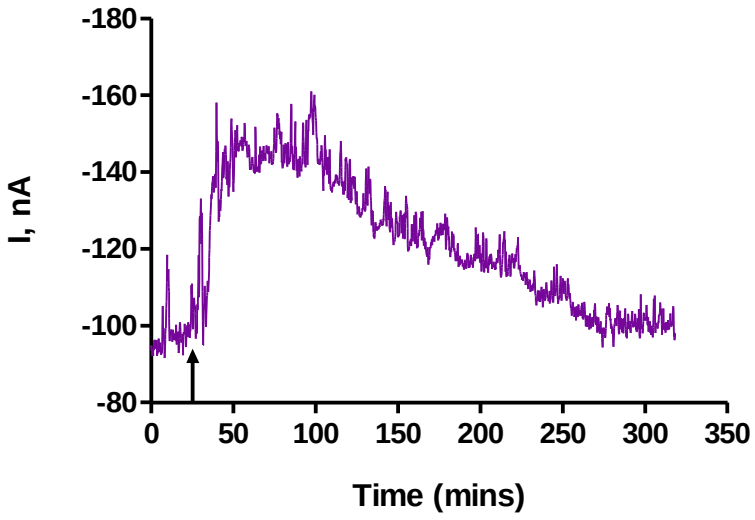

Figure 5.6: A typical example of an i.p. administration of Diamox (50 mg/kg) monitored *in vivo* using a Pt-MMA electrode implanted in the striatum of a freely-moving rat. The arrow indicates the point of injection.

An i.p. injection of Diamox shows an immediate sharp increase in the O_2 signal from average baseline levels of -85.93 ± 9.11 nA (*n*=8, 3 animals) to -109.18 ± 11.34 nA (*n*=8, 3 animals) after 1.06 ± 0.12 min this sharp increase in current of 29.32 ± 6.19 % can be attributed to injection stress. The subsequent rapid decrease was followed by a sustained maximum increase in the O_2 signal to -120.03 ± 11.65 nA (*n*=8, 3 animals) after 47.85 ± 5.15 min, representing a significant increase of 37.57 ± 5.40 % (*n*=8, 3 animals) compared to baseline levels (*P*= 0.0382). The current returned to post-injection baseline levels of -94.10 ± 10.01 nA (*n*=8, 3 animals) (*P*= 0.5565) after 2.62 ± 0.40 hrs. A summary of these results can be seen in Table 5.6.

Diamox i.p.	
Baseline (nA)	-85.93 ± 9.11
Max Increase (nA)	-120.03 ± 11.65
t to max increase (min)	47.85 ± 5.15
% Increase	37.57 ± 5.40
Post-baseline (nA)	-94.10 ± 10.01
***t* to post-baseline (hrs)**	2.62 ± 0.40

Table 5.6: Summary of results for i.p. administrations of Diamox (50mg/kg)) monitored *in vivo* using Pt-MMA electrodes (*n* = 8, 3 animals), implanted in the striatum of freely-moving rats.

From these results it can be seen that there is a significant increase in striatal tissue O_2 upon administration of Diamox (50 mg/kg) and this change can be reliably monitored using Pt-MMA electrodes.

5.3.6 *Effect of Anesthesia*

5.3.6.1 Chloral Hydrate

Chloral hydrate was amongst one of the first CNS depressants used in veterinary medicine. Chloral hydrate is metabolised by alcohol dehydrogenase to trichloroethanol and trichloroacetic acid (Butler, 1948). Although the precise mechanism is unknown (Sourkes, 1992), trichloroethanol is the active metabolite (Tao & Auerbach, 1994; Gauillard *et al.*, 2002) and it's thought its binding site is at the exogenous γ-aminobutyric acid (GABA) receptor resulting in an influx of chloride ions causing it to potentiate the function of GABA in a way similar to that of barbitutes (Lovinger *et al.*, 1993).

Chloral hydrate has been previously used to increase brain tissue O_2 (Lowry & Fillenz, 2001; Bolger & Lowry, 2005). This increase in O_2 is thought to be due to an increase in rCBF. The effect of chloral hydrate on the O_2 signal, monitored with Pt-MMA electrodes can be seen in Figure 5.7 below.

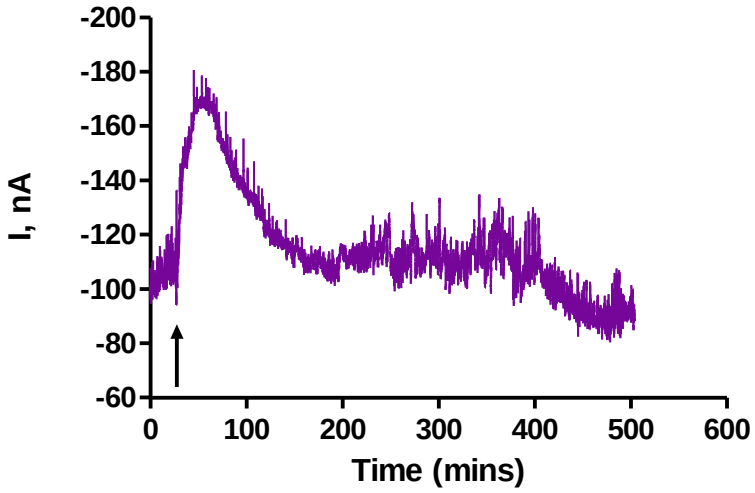

Figure 5.7: A typical example of an i.p. administration of chloral hydrate (350 mg/kg), monitored *in vivo* using a Pt-MMA electrode implanted in the striatum of a freely-moving rat. The arrow indicates the point of injection.

An i.p. injection of chloral hydrate shows an immediate sharp increase in the O_2 signal from average baseline levels of -97.80 ± 7.83 nA (*n*=12, 4 animals) to -107.94 ± 6.42 nA (*n*=12, 4 animals) after 47.25 ± 12.60 seconds this sharp increase in current of 38.90 ± 4.78 % can be attributed to injection stress. This initial increase rapidly decreases and there is a sustained maximum increase in the O_2 signal to -137.19 ± 12.91 nA (*n*=12, 4 animals) after 24.60 ± 5.11 min, representing a significant increase of 38.90 ± 4.78 % (*n*=12, 4 animals) compared to baseline levels (*P*=0.0178). The current returned to post- injection baseline levels of -100.30 ± 7.94 nA (*n*=12, 4 animals) (*P*= 0.8248) after 3.43 ± 0.35 hrs. A summary of these results can be seen in Table 5.7.

Chloral Hydrate i.p.	
Baseline (nA)	-97.80 ± 7.83
Max Increase (nA)	-137.19 ± 12.91
t to max increase (min)	24.60 ± 5.11
% Increase	38.90 ± 4.78
Post-baseline (nA)	-100.30 ± 7.94
***t* to post-baseline (hrs)**	3.43 ± 0.35

Table 5.7: Summary of results for i.p. administrations of chloral hydrate (350mg/kg) monitored *in vivo* using Pt-MMA electrodes (*n* = 12, 4 animals), implanted in the striatum of freely-moving rats.

From these results it can be seen that there is a significant increase in striatal tissue O_2 upon administration of chloral hydrate (350 mg/kg) and this change can be reliably monitored using Pt-MMA electrodes.

5.3.7 *Comparisons*

To allow for an accurate comparison between Pt-MMA electrodes and the CPEs due to the different dimensions of the electrodes, ΔI, nA values were converted to current densities (ΔJ, μA mm^{-2}) for both types of electrodes.

Carbon paste electrodes have been previously characterised *in vivo* by our group (Bolger & Lowry, 2005). The results from this publication were used to make comparisons.

5.3.7.1 Gaseous administrations

The ΔJ, μA mm^{-2} for 3-min periods of hyperoxia and hypoxia are 3.43 ± 0.35 ΔJ, μA mm^{-2} (*n*=51, 4 animals) and 2.32 ± 0.13 ΔJ, μA mm^{-2} (*n*=42, 4 animals) respectively for Pt-MMA electrodes. The ΔJ, μA mm^{-2} for a 3 min period of hyperoxia and hypoxia are 0.87 ± 0.13 ΔJ, μA mm^{-2} (*n*=4) and 0.88 ± 0.09 ΔJ, μA mm^{-2} (*n*=4) respectively for CPEs (Bolger & Lowry, 2005). The current change (ΔI) in terms of current densities (ΔJ, μA mm^{-2}) for Pt-MMA electrodes and CPEs for mild hyperoxia and hypoxia are plotted in Figure 5.8.

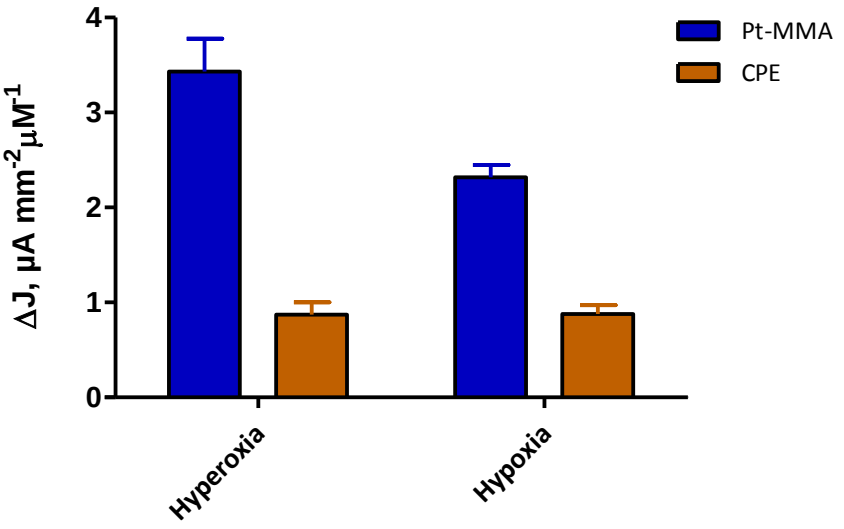

Figure 5.8: Comparison graph of calculated current density ΔJ, μA mm^{-2} values for hyperoxia and hypoxia administrations, monitored using Pt-MMA and CPEs implanted in the striatum of freely-moving rats.

From these results it can be seen that the Pt-MMA electrodes exhibit a greater change in O_2 current in terms of current density compared to CPEs when monitoring 3-min periods of hyperoxia and hypoxia in the striatum of freely-moving rats.

5.3.7.2 Neuronal Activation

The ΔJ, μA mm^{-2} for a 5-min tail pinch are 1.53 ± 0.33 ΔJ, μA mm^{-2} (n=14, 3 animals) for Pt-MMA electrodes and 0.34 ± 0.06 ΔJ, μA mm^{-2} (n=8, 2 animals) for CPEs (Bolger & Lowry, 2005). The current changes (ΔI) in terms of current densities (ΔJ, μA mm^{-2}) for Pt-MMA electrodes and CPEs for neuronal activation in the form of a tail pinch are plotted in Figure 5.9.

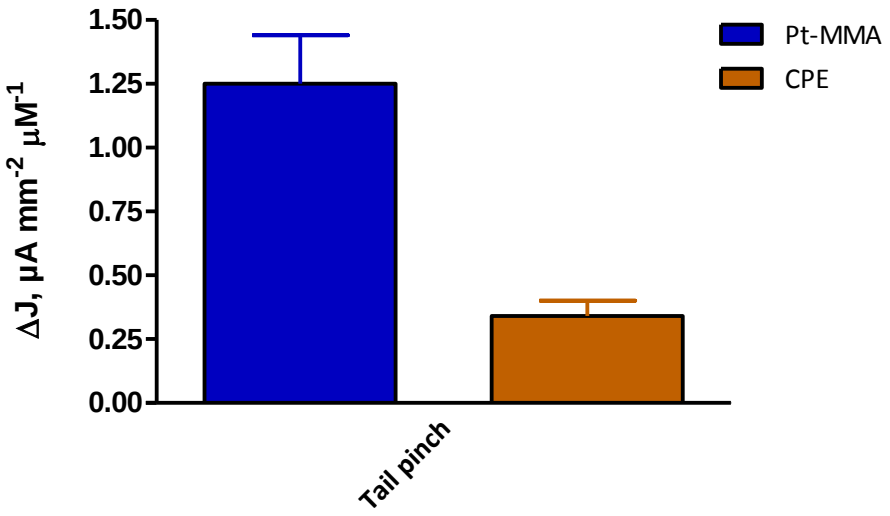

Figure 5.9: Comparison graph of calculated current density ΔJ, μA mm^{-2} values for a 5-min tail pinch, monitored using Pt-MMA and CPEs implanted in the striatum of freely-moving rats.

From these results it can be seen that the Pt-MMA electrodes exhibit a greater change in O_2 current in terms of current density compared to CPEs when monitoring a 5-min tail pinch in the striatum of freely-moving rats. This difference is thought to be due to variations in the stress score of the animals and habituation to the tail pinch.

5.3.7.3 Saline administrations

The ΔJ, μA mm^{-2} for saline (0.9%) i.p. administrations are 1.53 ± 0.33 ΔJ, μA mm^{-2} (*n*=14, 3 animals) for Pt-MMA electrodes and 0.43 ± 0.12 ΔJ, μA mm^{-2} (*n*=4) for CPEs (Bolger & Lowry, 2005). The current changes (ΔI) in terms of current densities (ΔJ, μA mm^{-2}) for Pt-MMA electrodes and CPEs for an i.p saline (0.9%) injection are plotted in Figure 5.10.

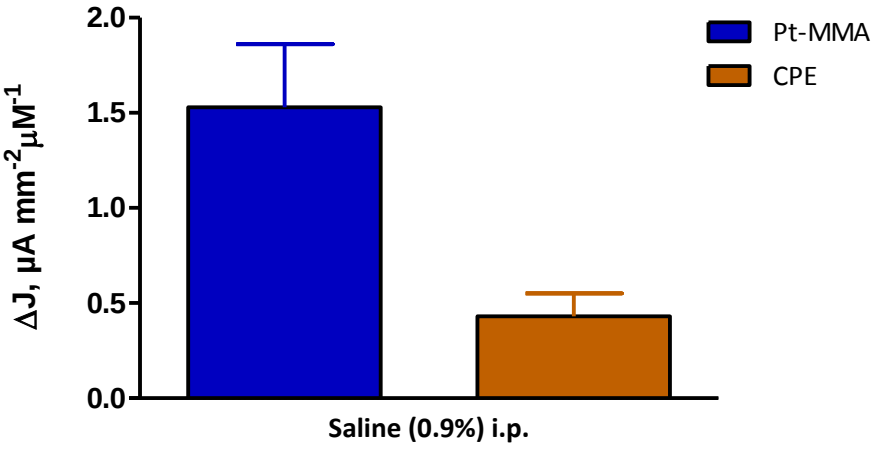

Figure 5.10: Comparison graph of calculated current density ΔJ, μA mm^{-2} values for an i.p. administration of saline (0.9% NaCl), monitored using Pt-MMA and CPEs implanted in the striatum of freely-moving rats.

From these results it can be seen that the Pt-MMA electrodes exhibit a greater change in O_2 current in terms of current density compared to CPEs when monitoring an i.p. administration of saline (0.9% NaCl) in the striatum of freely-moving rats. In terms of the time course of these increases Pt-MMA electrodes and CPEs are similar. For Pt-MMA electrodes the max increase was observed after 3.57 ± 0.77 min (*n*=14, 3 animals) with a return to baseline after 5.21 ± 1.09 min (*n*=14, 3 animals) and for CPEs the max increase was observed after 2.5 ± 0.4 min (*n*=4) with a return to baseline after 4.1 ± 3.7 min (*n*=4).

5.3.7.4 Acetazolamide (Diamox)

The ΔJ, μA mm^{-2} for Diamox (50 mg/kg) i.p. administrations are 2.78 ± 0.37 ΔJ, μA mm^{-2} (*n*= 8, 3 animals) for Pt-MMA electrodes and 1.37 ± 0.32 ΔJ, μA mm^{-2} (*n*=5) for CPEs (Bolger & Lowry, 2005). The current changes (ΔI) in terms of current densities (ΔJ, μA mm^{-2}) for Pt-MMA electrodes and CPEs for an i.p Diamox (50 mg/kg) injection are plotted in Figure 5.11.

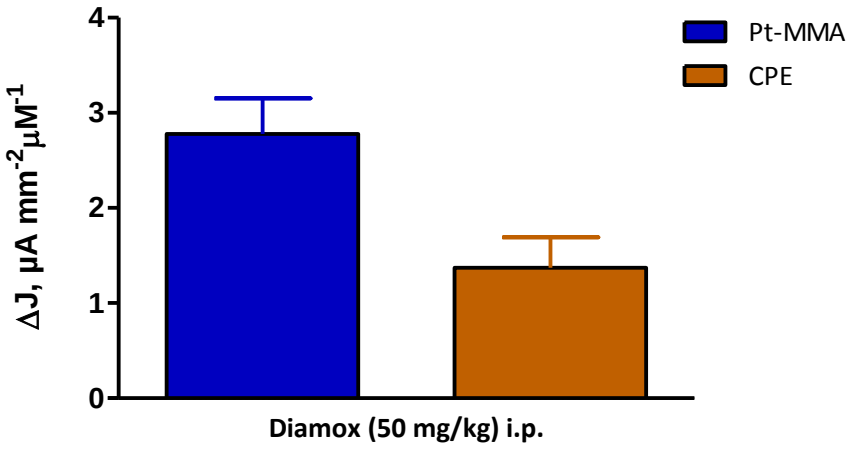

Figure 5.11: Comparison graph of calculated current density ΔJ, μA mm^{-2} values for an i.p. administration of Diamox (50 mg/kg), monitored using Pt-MMA and CPEs implanted in the striatum of freely-moving rats.

From these results it can be seen that the Pt-MMA electrodes exhibit a greater change in O_2 current in terms of current density compared to CPEs when monitoring an i.p. administration of Diamox (50 mg/kg) in the striatum of freely-moving rats.

5.3.7.5 Chloral Hydrate

The ΔJ, μA mm^{-2} for chloral hydrate (350 mg/kg) i.p. administrations are 3.21 ± 0.50 ΔJ, μA mm^{-2} (*n*= 12, 4 animals) for Pt-MMA electrodes and 0.60 ± 0.10 ΔJ, μA mm^{-2} (*n*=10) for CPEs (Bolger & Lowry, 2005). The current changes (ΔI) in terms of current densities (ΔJ, μA mm^{-2}) for Pt-MMA electrodes and CPEs for an i.p. chloral hydrate (350 mg/kg) injection are plotted in Figure 5.12.

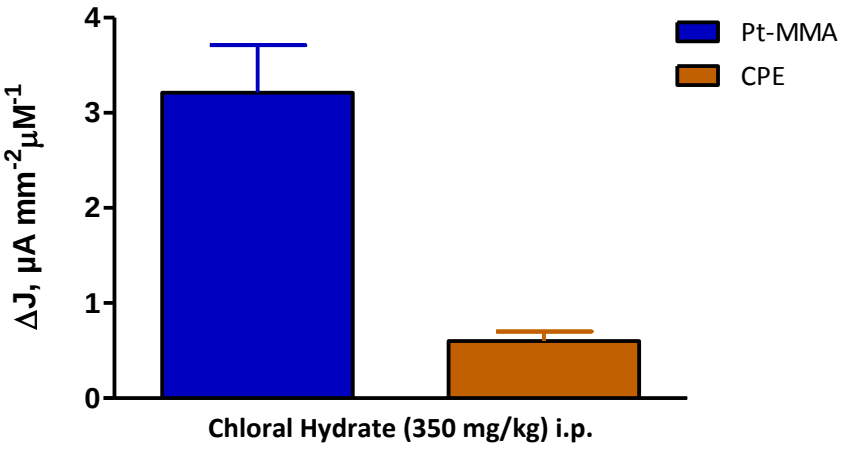

Figure 5.12: Comparison graph of calculated current density ΔJ, μA mm^{-2} values for an i.p. administration of chloral hydrate (350 mg/kg), monitored using Pt-MMA and CPEs implanted in the striatum of freely-moving rats.

From these results it can be seen that the Pt-MMA electrodes exhibit a greater change in O_2 current in terms of current density compared to CPEs when monitoring an i.p. administration of chloral hydrate (350 mg/kg) in the striatum of freely-moving rats.

5.4 Conclusions

Pt-based electrodes have been shown by characterisation *in vitro* to be a potential alternative to CPEs to monitor brain tissue O_2 (Bolger *et al.*, 2011a). Carbon paste electrodes have been previously characterised *in vivo* by our group (Bolger & Lowry, 2005). In this chapter the *in vivo* characterisation of Pt-MMA electrodes was investigated using similar protocols to that of the CPE characterisation (Bolger & Lowry, 2005).

Results presented in this chapter demonstrate that Pt-MMA electrodes have the ability to monitor changes in striatal O_2, evidenced by response of the sensors to the administration of O_2 and N_2 gases to the snout of the animals. The changes in tissue O_2 following neuronal activation in the form of a tail pinch and the administrations of saline, DMSO, acetazolamide and chloral hydrate have also been demonstrated. The Pt-MMA electrodes were directly compared to CPEs (Section 5.3.7) using previously published data (Bolger &

Lowry, 2005) and from these results it can be said that Pt-MMA electrodes exhibit a greater change in O_2 current in terms of current density compared to CPEs when implanted in the striatum of freely-moving rats. It can therefore be concluded that Pt-MMA electrodes provide a viable alternative to CPEs to monitor tissue O_2 in the brain. This is advantageous due to the smaller probe size of Pt-MMA electrodes (125 µm) less than 160 µm the maximum recommended diameter for brain tissue damage, resulting in uric acid production (Duff & O'Neill, 1994). However Pt-MMA electrodes are only suitable for short-term monitoring, established in Chapter 4 (Section 4.3.3.4) as there is a large reduction in sensitivity after 19 ± 3 days. The degradation of the signal over a period of time is apparent upon examination of the raw data trace. Even though CPEs are above the threshold for tissue damage they are stable over a 12 week period (Bolger *et al.*, 2011b) making them the sensor of choice for long-term chronic monitoring of brain tissue O_2.

References

Antelman SM, Szechtman H, Chin P & Fisher AE. (1975). Tail pinch-induced eating, gnawing and licking behavior in rats: Dependence on the nigrostriatal dopamine system. *Brain Research* **99,** 319-337.

Baumgärtl H, Heinrich U & Lübbers D. (1989). Oxygen supply of the blood-free perfused guinea-pig brain in normo-and hypothermia measured by the local distribution of oxygen pressure. *Pflügers Archiv European Journal of Physiology* **414,** 228-234.

Bazzu G, Puggioni GGM, Dedola S, Calia G, Rocchitta G, Migheli R, Desole MS, Lowry JP, O'Neill RD & Serra PA. (2009). Real-Time Monitoring of Brain Tissue Oxygen Using a Miniaturized Biotelemetric Device Implanted in Freely Moving Rats. *Analytical chemistry* **81,** 2235-2241.

Bolger F & Lowry J. (2005). Brain Tissue Oxygen: *In Vivo* Monitoring with Carbon Paste Electrodes. *Sensors* **5,** 473-487.

Bolger FB, Bennett R & Lowry JP. (2011a). An *in vitro* characterisation comparing carbon paste and Pt microelectrodes for real-time detection of brain tissue oxygen. *The Analyst* **136,** 4028-4035.

Bolger FB, McHugh SB, Bennett R, Li J, Ishiwari K, Francois J, Conway MW, Gilmour G, Bannerman DM, Fillenz M, Tricklebank M & Lowry JP. (2011b). Characterisation of carbon paste electrodes for real-time amperometric monitoring of brain tissue oxygen. *Journal of neuroscience methods* **195,** 135-142.

Butler TC. (1948). The metabolic fate of chloral hydrate. *The Journal of Pharmacology and Experimental Therapeutics* **92,** 49-58.

Clark Jr L & Clark E. (1964). Epicardial oxygen measured with a pyrolytic graphite electrode *The Alabama Journal of Medical Sciences* **1,** 142.

Clark Jr L & Lyons C. (1965). Studies of a glassy carbon electrode for brain polarography with observations on the effect of carbonic anhydrase inhibition. *The Alabama Journal of Medical Sciences* **2,** 353.

Clark LC, Misrahy G & Fox RP. (1958). Chronically implanted polarographic electrodes. *Journal of Applied Physiology* **13,** 85-91.

Dixon BM, Lowry JP & O'Neill RD. (2002). Characterization *in vitro* and *in vivo* of the oxygen dependence of an enzyme/polymer biosensor for monitoring brain glucose. *Journal of neuroscience methods* **119,** 135-142.

Duff A & O'Neill RD. (1994). Effect of probe size on the concentration of brain extracellular uric acid monitored with carbon paste electrodes. *Journal of Neurochemistry* **62,** 1496-1502.

Gauillard J, Cheref S, Vacherontrystram MN & Martin JC. (2002). Chloral hydrate: a hypnotic best forgotten? *L'Encephale* **28,** 200-204.

Gifford R, Kehoe JJ, Barnes SL, Kornilayev BA, Alterman MA & Wilson GS. (2006). Protein interactions with subcutaneously implanted biosensors. *Biomaterials* **27,** 2587-2598.

Lovinger DM, Zimmerman SA, Levitin M, Jones MV & Harrison NL. (1993). Trichloroethanol potentiates synaptic transmission mediated by gamma-aminobutyric acidA receptors in hippocampal neurons. *Journal of Pharmacology and Experimental Therapeutics* **264,** 1097-1103.

Lowry JP, Boutelle MG & Fillenz M. (1997). Measurement of brain tissue oxygen at a carbon paste electrode can serve as an index of increases in regional cerebral blood flow. *Journal of neuroscience methods* **71,** 177-182.

Lowry JP, Boutelle MG, O'Neill RD & Fillenz M. (1996). Characterization of carbon paste electrodes *in vitro* for simultaneous amperometric measurement of changes in oxygen and ascorbic acid concentrations *in vivo*. *The Analyst* **121,** 761-766.

Lowry JP, Demestre M & Fillenz M. (1998). Relation between Cerebral Blood Flow and Extracellular Glucose in Rat Striatum during Mild Hypoxia and Hyperoxia. *Developmental Neuroscience* **20,** 52-58.

Lowry JP & Fillenz M. (2001). Real-time monitoring of brain energy metabolism in vivo using microelectrochemical sensors: the effects of anesthesia. *Bioelectrochemistry* **54,** 39-47.

Lubbers DW & Baumgärtl H. (1997). Heterogeneities and profiles of oxygen pressure in brain and kidney as examples of the pO_2 distribution in the living tissue: Oxygen sensing on the cellular and molecular level. *Kidney International* **51,** 372-380.

McCreery D, Agnew W, Bullara L & Yuen T. (1990). Partial pressure of oxygen in brain and peripheral nerve during damaging electrical stimulation. *Journal of Biomedical Engineering* **12,** 309-315.

Murr R, Berger S, Schuerer L, Peter K & Baethmann A. (1994). A novel, remote-controlled suspension device for brain tissue PO_2 measurements with multiwire surface electrodes. *Pflügers Archiv European Journal of Physiology* **426,** 348-350.

Nair PK, Buerk DG & Halsey J. (1987). Comparisons of oxygen metabolism and tissue PO_2 in cortex and hippocampus of gerbil brain. *Stroke* **18,** 616-622.

O'Neill RD. (1993). Sensor-tissue interactions in neurochemical analysis with carbon paste electrodes *in vivo*. *The Analyst* **118,** 433-438.

O'Neill RD & Lowry JP. (1995). On the significance of brain extracellular uric acid detected with *in-vivo* monitoring techniques: a review. *Behavioural brain research* **71,** 33-49.

O'Neill RD. (2005). Long-term monitoring of brain dopamine metabolism *in vivo* with carbon paste electrodes. *Sensors* **5,** 317-342.

Silver I. (1965). Some observations on the cerebral cortex with an ultramicro, membrane-covered, oxygen electrode. *Medical and Biological Engineering and Computing* **3,** 377-387.

Sourkes T. (1992). Early clinical neurochemistry of CNS-active drugs. *Molecular and Chemical Neuropathology* **17,** 21-30.

Tao R & Auerbach SB. (1994). Anesthetics block morphine-induced increases in serotonin release in rat CNS. *Synapse* **18,** 307-314.

Venton BJ, Michael DJ & Wightman RM. (2003). Correlation of local changes in extracellular oxygen and pH that accompany dopaminergic terminal activity in the rat caudate–putamen. *Journal of Neurochemistry* **84,** 373-381.

Wisniewski N, Moussy F & Reichert WM. (2000). Characterization of implantable biosensor membrane biofouling. *Fresenius' Journal of Analytical Chemistry* **366,** 611-621.

Zauner A, Bullock R, Di X & Young HF. (1995). Brain oxygen, CO_2, pH, and temperature monitoring: evaluation in the feline brain. *Neurosurgery* **37,** 1168.

Zhao H, Zhang Y & Yuan Z. (2001). Electrochemical Behaviour of Norepinephrine at Poly(2,4,6-trimethylpyridine) Modified Glassy Carbon Electrode. *Journal of Electroanalytical Chemistry* **14,** 445-448.

Zimmerman JB, Kennedy RT & Wightman RM. (1992). Evoked Neuronal Activity Accompanied by Transmitter Release Increases Oxygen Concentration in Rat Striatum *In Vivo* But Not *In Vitro*. *Welcome to Journal of Cerebral Blood Flow & Metabolism* **12,** 629-637.

Zimmerman JB & Wightman RM. (1991). Simultaneous electrochemical measurements of oxygen and dopamine *in vivo*. *Analytical Chemsitry* **63,** 24-28.

6. RESULTS: CARBON-BASED COMPOSITE ELECTRODE FOR THE DETECTION OF TISSUE O_2, SUITABLE FOR USE IN fMRI IMAGING STUDIES

6.1 Introduction

The hemodynamic response refers to changes in cerebral blood flow, blood volume and blood oxygenation, a result of increases in neuronal activity. The imaging technique blood oxygenation dependent (BOLD) functional magnetic imaging (fMRI) is founded on this hemodynamic response (Ogawa *et al.*, 1990; Bandettini *et al.*, 1992; Ogawa *et al.*, 1992). The MRI signal intensity is sensitive to the amount of oxygen (O_2) carried by hemoglobin in the blood as this changes the degree to which hemoglobin disturbs the magnetic field. An increase in the O_2 hemoglobin oxygenation results in an increase in the BOLD signal and vice versa. BOLD fMRI is a valuable, non-invasive way of mapping the regional activity of the brain during sensory, motor and cognitive tasks. fMRI imaging has been employed to map rodent brains (Houston *et al.*, 2001; Preece *et al.*, 2001). Both these and the majority of such studies use anesthetics to prevent motion of the animals which is common practice in most experiments; however the use of these anesthetics can alter brain metabolism.

Metal-free electrodes based on a carbon transducer have been utilised in conjunction with fMRI imaging studies, simultaneously obtaining BOLD fMRI and amperometric tissue O_2 data from a rat cerebral cortex (Lowry *et al.*, 2010). This study verifies that real-time metabolic information can be acquired during fMRI investigations and that the changes in the magnitude of the BOLD response can be directly correlated to changes in tissue O_2 concentrations. This technique provides an alternative to fMRI experiments as these O_2 sensors can be used in freely-moving animals eliminating the disadvantages of anaesthesia. The sensors used in this study were carbon fibre bundle electrodes. Carbon fibre was selected as it has very weak paramagnetic properties compared to metal electrodes which can produce artifacts. Previously carbon fibre electrodes (CFEs) were manufactured as a method for direct cortical stimulation in the rat (Austin *et al.*, 2003). In this study the electrodes were used to stimulate neuronal firing, therefore the CFEs were not standardised in terms of manufacture. There were variations in both the amount of carbon fibre strands that were used in each electrode and also the length of the carbon fibres. Due to the

varying dimensions of the carbon fibre bundle, reproducibility was difficult to obtain therefore hindering the characterisation of these sensors.

The aim of this chapter was to fabricate a stable and reproducible sensor that can be characterised *in vitro* and *in vivo*.

The first part of this chapter (Section 6.3.1) explores the standardisation of the CFEs whilst the latter sections explore the use of a carbon (graphite) based composite electrode.

6.2 Experimental

The instrumentation and software used are detailed in Section 3.2 and all chemicals and solutions are detailed in Section 3.3.

Silver based carbon composite electrodes were constructed as described in Section 3.4.2, Carbon Rhoplex® composite electrodes - fMRI design (CRCEs) are described in Section 3.4.3, Carbon Rhoplex® composite electrodes - *in vivo* freely-moving design (CRCEs) are described in Section 3.4.4.

Electrochemical experiments are detailed in Section 3.6 and electrode treatments in Section 3.5.4.

Data is represented as the mean ± SEM where n = number of electrodes used, unless otherwise stated. The slope, nA/µM was obtained from calibration plots using linear regression analysis and is used to represent the sensitivity. Goodness of fit is denoted by the R^2 value. Sensitivities were compared using unpaired t-tests and ANOVA. To compare the different electrodes due to varying physical dimensions current values were converted to current densities (Section 2.8.3).

6.3 Results and discussion

6.3.1 *Carbon fibre electrodes*

CFEs to monitor O_2 for use in an MRI scanner have been recently described by (Lowry *et al.*, 2010). This electrode, based on the design by Austin (2003) and co-workers, can reliably measure tissue O_2 but the reproducibility of the sensor is an issue due to variations in both the amount of carbon fibre strands that were used in each electrode and also the length of the carbon fibres. Therefore the standardisation of the CFEs in terms of manufacture was investigated.

6.3.1.1 Preliminary investigations: Carbon fibre wire (30 µm)

The optimal reduction potential of O_2 at the surface of CFEs has previously been determined using cyclic voltammetry (Lowry *et al.*, 2010). The chosen reduction potential was -900 mV and subsequent constant potential amperometry (CPA) experiments were carried out at this potential.

CF wire with a diameter of 30 µm was used for the preliminary experiments in this section. Varying CF lengths were used to give an estimation of the currents expected with the different lengths with the view to standardising the electrodes.

O_2 calibrations were performed on CFEs as described in Section 3.6.1.4.

Results obtained for O_2 calibrations performed in PBS on CFEs (30 µm x 4) are presented below in Table 6.1 and plotted in Figure 6.1. The mean background current of -1937.6 ± 315.6 nA (n=3) was subtracted. Current in nA was converted to current densities (J, µA $mm^{-2)}$ to allow for the comparison of the electrodes due to their varying geometries.

	CF 30µm x 4 (*n*=3)	
$[O_2]$, µM	**Mean J, µA mm^{-2}**	**SEM**
0	0	0
240	-760.8	88.3
1200	-2950.9	441.1

Table 6.1: Table of results for O_2 calibrations (0-1200 µM) for CFEs. CPA performed at -900 mV *vs.* SCE in PBS (pH 7.4) at 21˚C. Mean background subtracted.

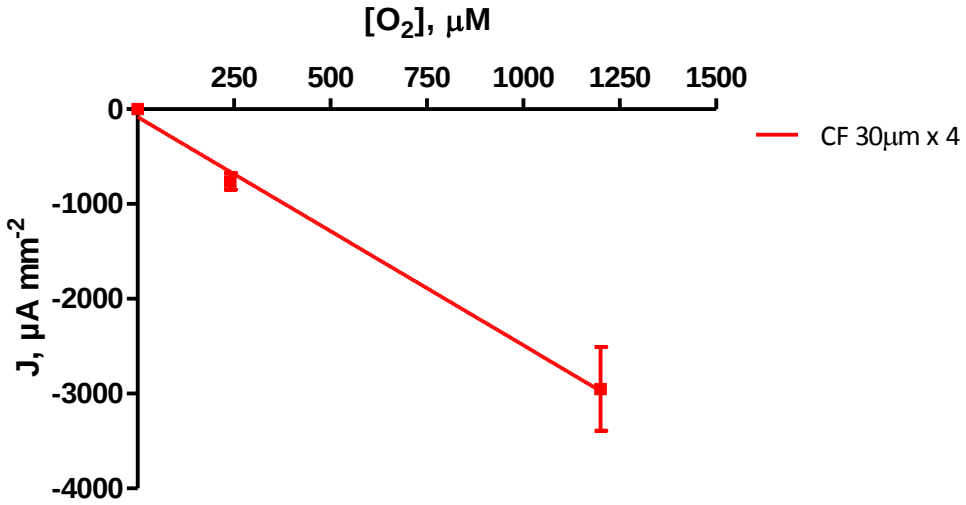

Figure 6.1: O_2 calibration data (0-1200 µM) for CFEs (*n*=3). CPA performed at -900 mV *vs.* SCE in PBS (pH 7.4) at 21˚C.

Results obtained for O_2 calibrations performed in PBS on CFEs (30µm x 4, 2mm cylinders) and (30µm x 4, 3mm cylinders) are presented below in Table 6.2 and plotted in Figure 6.2.

	CF 30µm x 4, 2mm cylinders (*n*=1)	CF 30µm x 4 3mm cylinders (*n*=1)
$[O_2]$, µM	**J, µA mm^{-2}**	**J, µA mm^{-2}**
0	0	0
240	-1.4	-3.8
1200	-5.3	-10.6

Table 6.2: Table of results for O_2 calibrations (0-1200 µM) for CFEs. CPA performed at -900 mV *vs.* SCE in PBS (pH 7.4) at 21˚C. Mean background subtracted.

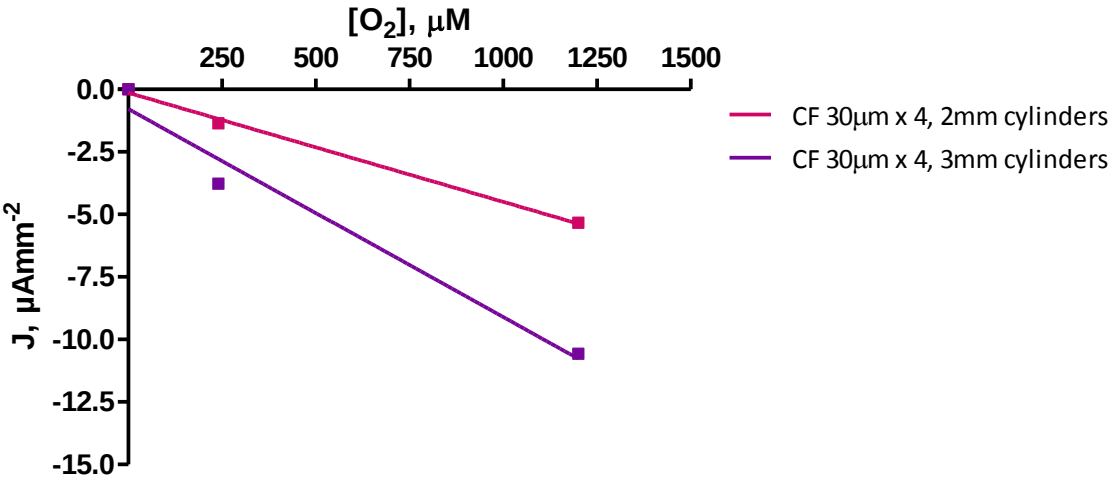

Figure 6.2: O_2 calibration data (0-1200 µM) for CF 30µm x 4, 2mm cylinders (*n*=1) and CF 30µm x 4 3mm cylinders (*n*=1). CPA performed at -900 mV *vs.* SCE in PBS (pH 7.4) at 21˚C.

Linear regression analysis was performed on electrodes to compare sensitivities in terms of current density of CFEs calibrated in PBS solutions, presented in Table 6.3 and plotted in Figure 6.3. All further data will be presented in a similar format: O_2 calibrations data presented via a table and graph, followed by linear regression analysis comparing electrode sensitivities presented via a table and graph.

	Sensitivity (µAmm^{-2}µM^{-1})	R^2	*n*
CF 30 µm x 4	-2.4080 ± 0.1465	0.9963	3
CF 30 µm x 4, 2mm cylinders	-0.0044 ± 0.0002	0.9969	1
CF 30 µm x 4, 3mm cylinders	-0.0083 ± 0.0014	0.9718	1

Table 6.3: Calculated sensitivity values of O_2 calibrations (0-1200 µM) for CFEs.

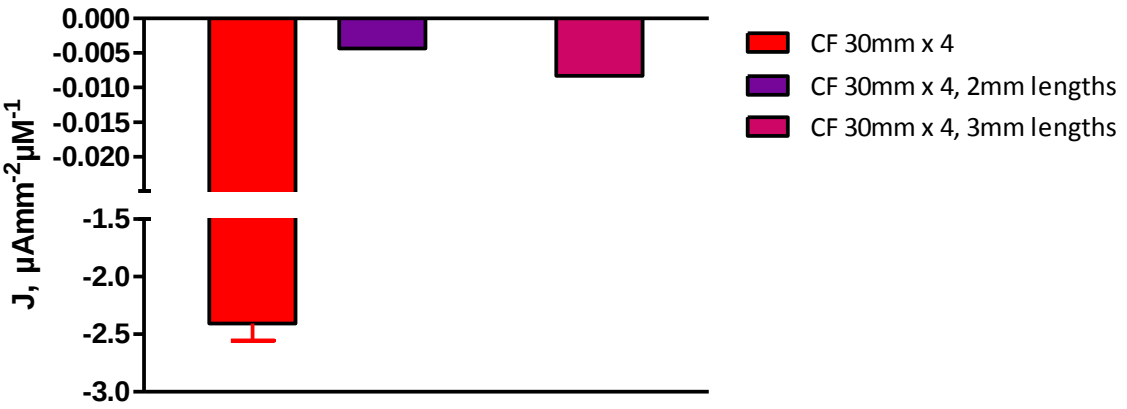

Figure 6.3: Comparison graph of calculated sensitivity values for O_2 calibrations (0-1200 µM) for CF 30µm x 4 (*n*=3), CF 30µm x 4, 2mm cylinders (*n*=1) and CF 30µm x 4 3mm cylinders (*n*=1).

From the results presented it can be seen from the preliminary investigations that the sensitivity values are variable. The CF 30 µm x 4 CFE has a much higher sensitivity although it was a disk shape. This is thought to be due to the electrode design. The space between the carbon fibres and the silica tubing are easily sealed with epoxy with the cylindrical geometries however this was not possible for the disk electrodes. It is thought that the active surface was not just the disk shape and that the electrolyte (PBS) was able to migrate past the silica tubing causing a much larger surface area to be present. The standardisation of the electrodes was the main focus of this section. Four cylindrical electrodes combined as one electrode could not be standardised easily therefore it was decided to move away from single carbon fibres and to investigate a carbon fibre coated bundle with a known diameter.

6.3.1.2 Polyamide coated CF (1mm)

6.3.1.2.1 Cyclic Voltammetry

CV was initially performed on the polyamide coated CF (1mm) to determine the diffusion limited reduction potential of O_2 at the surface of these electrodes. This was performed as

described in Section 3.6.1.2. The results obtained are presented graphically below in Figure 6.4.

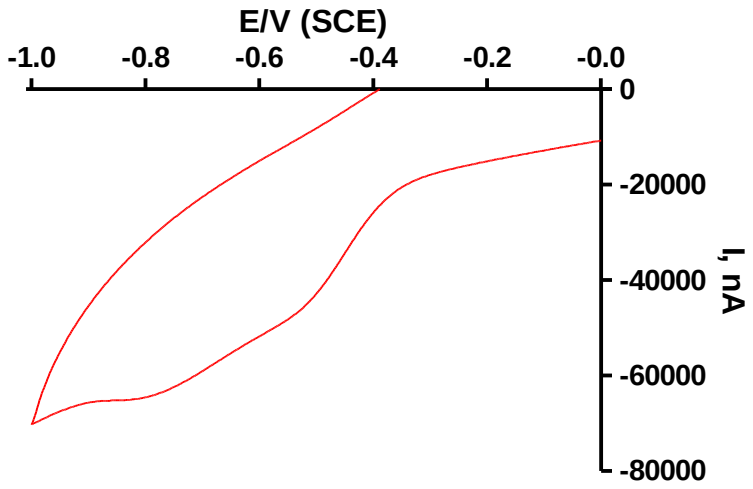

Figure 6.4: Cyclic voltammogram from -1 to 0 V *vs.* SCE at 100 mVs^{-1} performed in O_2 saturated PBS (pH 7.4, 21˚C) buffer solution, illustrating the reduction of O_2 at a polyamide coated CFE.

For the polyamide coated CFEs an O_2 reduction peak was observed at *ca*. -500 mV with the foot of the wave occurring at *ca*. -350 mV. The chosen reduction potential was -650 mV which allows for comparisons with CPEs and subsequent constant potential amperometry (CPA) experiments were carried out at this potential.

6.3.2 *Silver based carbon composite electrodes*

Carbon composite electrodes have been previously utilised to detect brain tissue O_2 (Bazzu *et al.*, 2009). The use of Carbon Polyvinyl Acetate (PVA) and Rhoplex® combined with varying amounts of carbon (graphite) powder was preliminarily investigated as a means of standardising the surface area of the sensors. The PVA or Rhoplex® and carbon were uniformly mixed and then packed into the cavity of a silver wire (200 µm) as described in Section 3.4.2, in a similar way to the construction of carbon paste electrodes (CPE). This method was employed as a simpler way of determining the viability of the mixture for use in conjunction with the carbon fibres.

6.3.2.1 PVA silver composite electrodes

The results obtained for O_2 calibrations (0-1200 µM) on PVA silver composite electrodes containing:

- PVA (0.05g)/ Carbon (0.01g)
- PVA (0.05g)/ Carbon (0.02g)
- PVA (0.05g)/ Carbon (0.03g)

are presented below in Table 6.4 and plotted in Figure 6.5.

	PVA (0.05g)/ Carbon (0.01g) (*n*=4)		**PVA (0.05g)/ Carbon (0.02g) (*n*=5)**		**PVA (0.05g)/ Carbon (0.03g) (*n*=4)**	
[O_2], µM	**Mean I, nA**	**SEM**	**Mean I, nA**	**SEM**	**Mean I, nA**	**SEM**
0	0	0	0	0	0	0
240	-1010.1	125.7	-1055.1	107.2	-571.1	175.2
1200	-2965.2	283.8	-3195.1	318.1	-1837.2	479.2

Table 6.4: Table of results for O_2 calibrations (0-1200 µM) for PVA silver composite electrodes. CPA performed at -650 mV *vs.* SCE in PBS (pH 7.4) at 21°C. Mean background subtracted.

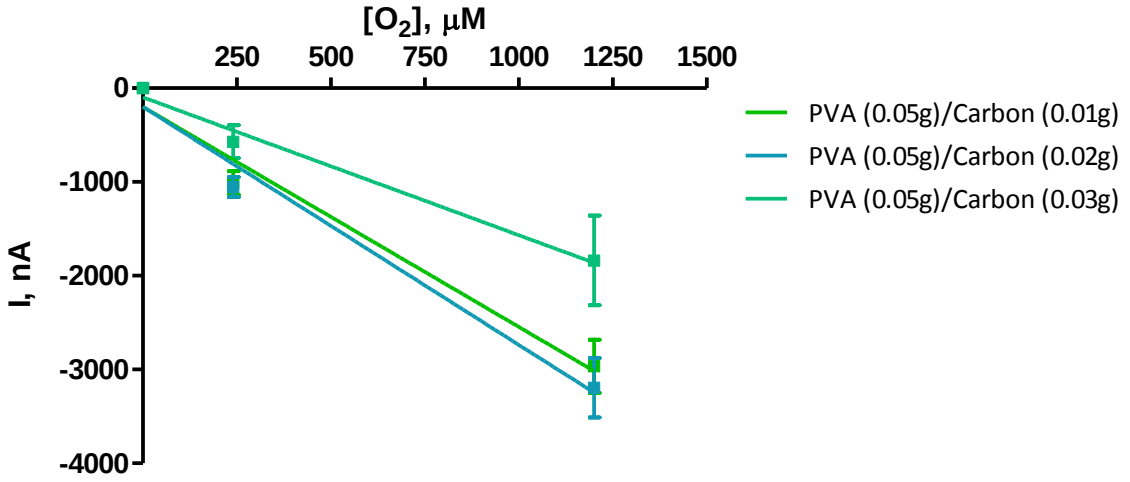

Figure 6.5: O_2 calibration data (0-1200 µM) for PVA silver composite electrodes. CPA performed at -650 mV *vs.* SCE in PBS (7.4) at 21˚C.

	Sensitivity (nA/µM)	R^2	*n*
PVA (0.05g)/ Carbon (0.01g)	-2.347 ± 0.358	0.9772	4
PVA (0.05g)/ Carbon (0.02g)	-2.539 ± 0.358	0.9806	5
PVA (0.05g)/ Carbon (0.03g)	-1.470 ± 0.175	0.9860	4

Table 6.5: Table of calculated sensitivity values of O_2 calibrations (0-1200 µM) for PVA silver composite electrodes.

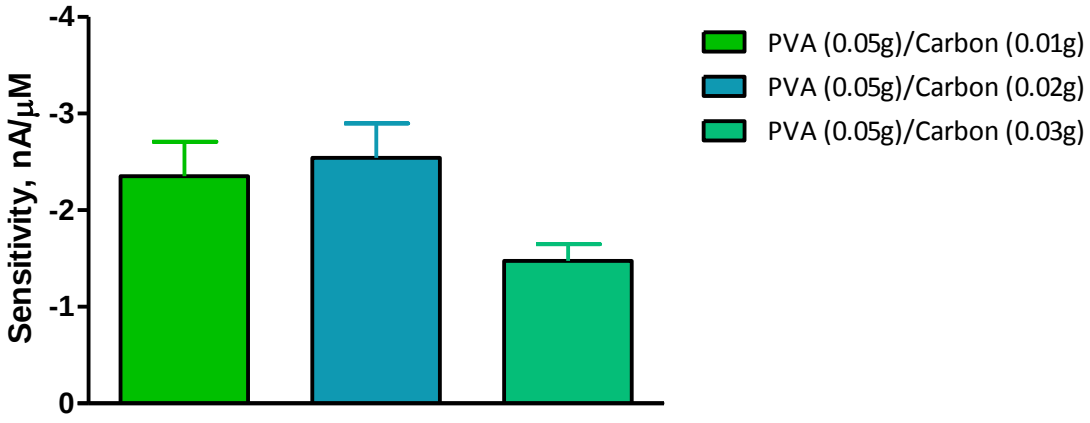

Figure 6.6: Comparison graph of calculated sensitivity values for O_2 calibrations (0-1200 µM) PVA silver composite electrodes. PVA (0.05g)/ Carbon (0.01g) (*n*=4), PVA (0.05g)/ Carbon (0.02g) (*n*=5) and PVA (0.05g)/ Carbon (0.03g) (*n*=4).

Although there was no statistically significant difference between PVA (0.05g)/Carbon (0.01g) and PVA (0.05g)/Carbon (0.02g) composites (*P*= 0.7176) the PVA (0.05g)/Carbon (0.02g) had the highest sensitivity of -2.539 ± 0.358 nA/µM.

6.3.2.2 Rhoplex® silver composite electrodes

The results obtained for O_2 calibrations (0-1200 µM) on Rhoplex® silver composite electrodes containing:

- Rhoplex® (0.05g)/ Carbon (0.01g)
- Rhoplex® (0.05g)/ Carbon (0.02g)
- Rhoplex® (0.05g)/ Carbon (0.03g)

are presented below in Table 6.6 and plotted in Figure 6.7.

	Rhoplex® (0.05g)/ Carbon (0.01g) (*n*=3)		Rhoplex® (0.05g)/ Carbon (0.02g) (*n*=4)		Rhoplex® (0.05g)/ Carbon (0.03g) (*n*=4)	
$[O_2]$, µM	**Mean I, nA**	**SEM**	**Mean I, nA**	**SEM**	**Mean I, nA**	**SEM**
0	0	0	0	0	0	0
240	-150.4	61.3	-733.7	85.8	-529.2	111.0
1200	-676.0	115.4	-2015.6	328.0	-1454.2	245.3

Table 6.6: Table of results for O_2 calibrations (0-1200 µM) for Rhoplex® silver composite electrodes. CPA performed at -650 mV *vs.* SCE in PBS (pH 7.4) at 21°C. Mean background subtracted.

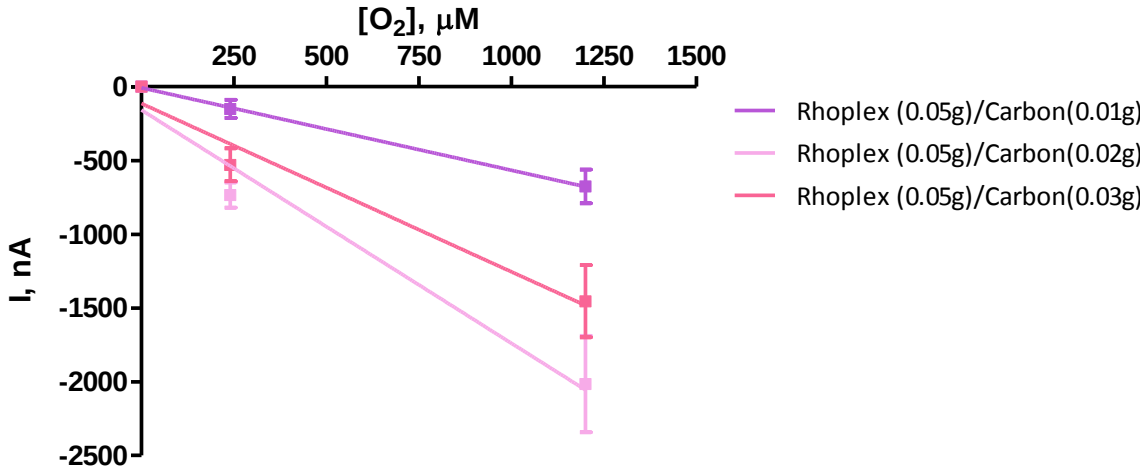

Figure 6.7: O_2 calibration data (0-1200 µM) for Rhoplex® silver composite electrodes. CPA performed at -650 mV *vs.* SCE in PBS (7.4) at 21˚C.

	Sensitivity (nA/µM)	R^2	*n*
Rhoplex® (0.05g)/ Carbon (0.01g)	-0.559 ± 0.013	0.9995	3
Rhoplex® (0.05g)/ Carbon (0.02g)	-1.581 ± 0.284	0.9687	4
Rhoplex® (0.05g)/ Carbon (0.03g)	-1.141 ± 0.205	0.9688	4

Table 6.7: Table of calculated sensitivity values of O_2 calibrations (0-1200 µM) for Rhoplex® silver composite electrodes.

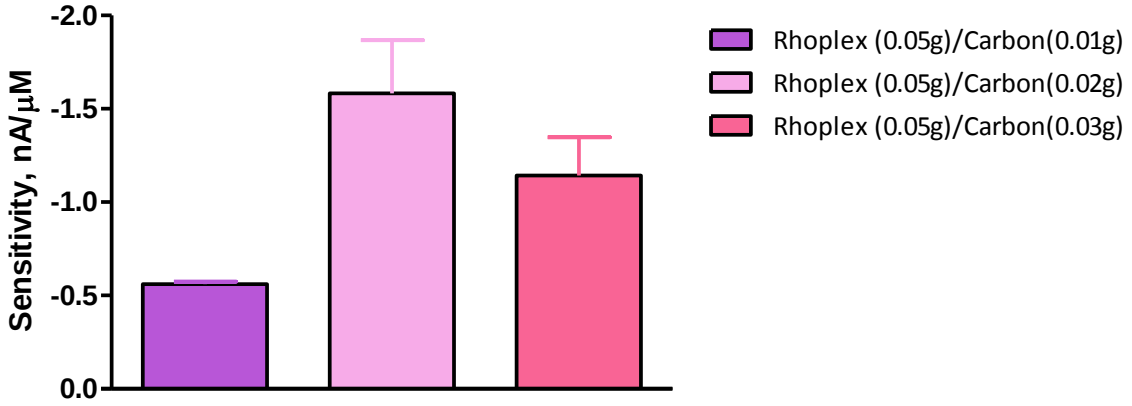

Figure 6.8: Comparison graph of calculated sensitivity values for O_2 calibrations (0-1200 µM) for Rhoplex® silver composite electrodes. Rhoplex® (0.05g)/ Carbon (0.01g) (*n*=3), Rhoplex® (0.05g)/ Carbon (0.02g) (*n*=4) and Rhoplex® (0.05g)/ Carbon (0.03g) (*n*=4).

From these results it can be seen that the Rhoplex® (0.05g)/Carbon (0.02g) composite has the highest sensitivity of -1.581 ± 0.284 nA/µM.

6.3.3 *Carbon Fibre based composite electrodes*

From the results presented in Section 6.3.2 both silver PVA and Rhoplex® composite electrodes can detect O_2 *in vitro*. The sensitivity of the sensor, although important, is not the only determining factor as ease of construction plays an important role in sensor design and development. The ease at which the electrodes are packed is a crucial factor in the construction. The higher the carbon content of the composite the easier the sensor is to construct so the following composites were used to construct the carbon fibre based O_2 fMRI compatible sensor:

- PVA (0.05g)/Carbon (0.03g)
- Rhoplex® (0.05g)/Carbon (0.02g)
- Rhoplex® (0.05g)/Carbon (0.03g)

Although the PVA (0.05g)/Carbon (0.02g) silver composite electrodes had the highest sensitivity (Table 6.5), construction of the carbon fibre based sensors were attempted but due to the difficulty in packing the tip of the electrode the sensors were not suitable for calibration. The difficulty in the construction of these sensors arises from the inability to plunge the composite with bare silver wire like the CPEs. This method ensures good packing at the tip of the electrode producing good reproducibility.

6.3.3.1 CF PVA composite electrodes

6.3.3.1.1 CV

CV was initially performed on the CF PVA (0.05g)/Carbon (0.03g) composite electrodes to determine the diffusion limited reduction potential of O_2 at the surface of these electrodes. This was performed as described in Section 3.6.1.2. The results obtained are presented graphically below in Figure 6.9.

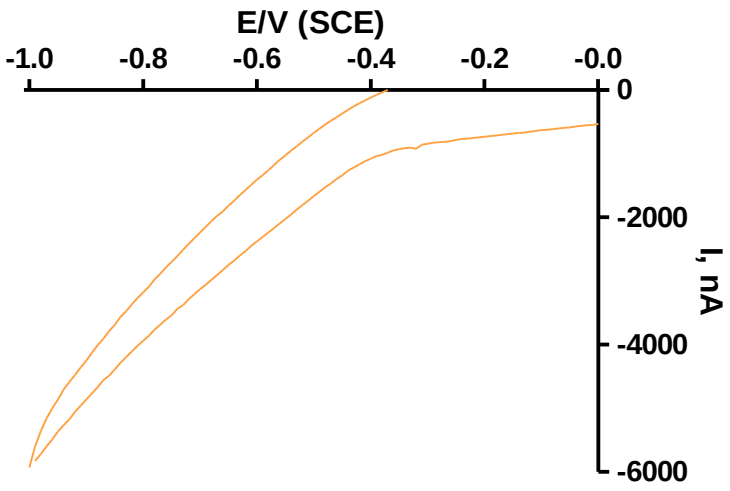

Figure 6.9: Cyclic voltammogram from -1 to 0 V *vs.* SCE at 100 mVs^{-1} performed in O_2 saturated PBS (pH 7.4, 21˚C) buffer solution, illustrating the reduction of O_2 at a CF PVA (0.05g)/Carbon (0.03g) composite electrodes.

For the CF PVA (0.05g)/Carbon (0.03g) composite electrodes there was no observable O_2 reduction peak. The chosen reduction potential was -650 mV for comparative purposes

with other O_2 electrodes and subsequent constant potential amperometry (CPA) experiments were carried out at this potential.

6.3.3.1.2 Oxygen calibrations

O_2 calibrations were performed on CF PVA (0.05g)/Carbon (0.03g) composite electrodes as described in Section 3.6.1.4.

	CF PVA (0.05g)/Carbon (0.03g) (*n*=11)	
[O_2], µM	**Mean I, nA**	**SEM**
0	0	0
240	-231.5	102.9
1200	-1544.2	244.0

Table 6.8: Table of results for O_2 calibrations (0-1200 µM) for CF PVA (0.05g)/Carbon (0.03g) composite electrodes (*n*=11). CPA performed at -650 mV *vs.* SCE in PBS (pH 7.4) at 21˚C. Mean background subtracted.

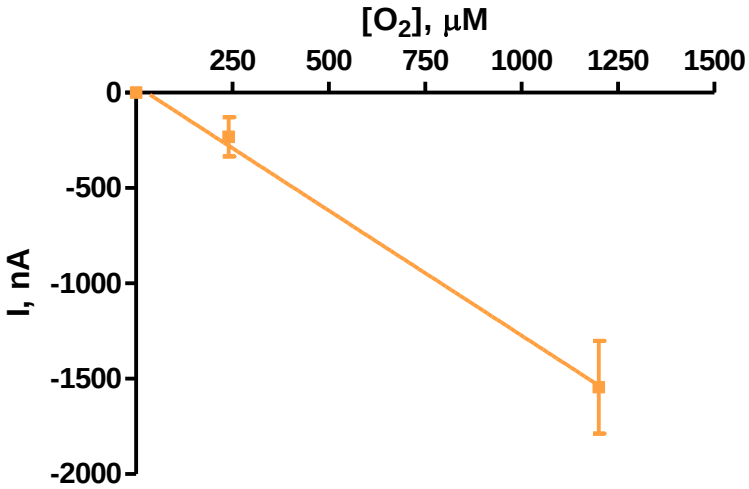

Figure 6.10: O_2 calibration data (0-1200 µM) for CF PVA (0.05g)/Carbon (0.03g) composite electrodes (*n*=11). CPA performed at -650 mV *vs.* SCE in PBS (pH 7.4) at 21˚C.

	Sensitivity (nA/µM)	R^2	*n*
CF PVA (0.05g)/Carbon (0.03g)	-1.310 ± 0.066	0.9974	11
Ag PVA (0.05g)/Carbon (0.03g)	-1.470 ± 0.175	0.9860	4

Table 6.9: Table of calculated sensitivity values of O_2 calibrations (0-1200 µM) for CF PVA (0.05g)/Carbon (0.03g) and Silver PVA (0.05g)/Carbon (0.03g) composite electrodes.

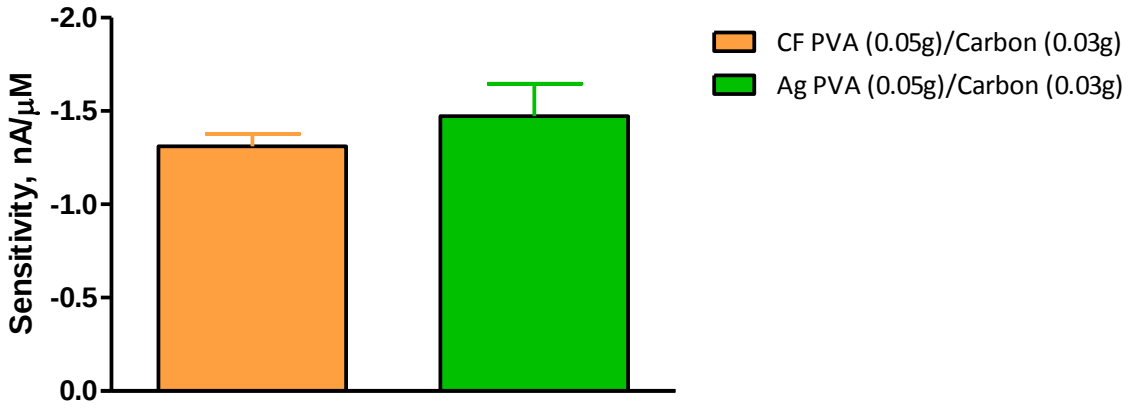

Figure 6.11: Comparison graph of calculated sensitivity values for O_2 calibrations (0-1200 µM) for CF PVA (0.05g)/Carbon (0.03g) composite electrodes (*n*=11) and Silver PVA (0.05g)/Carbon (0.03g) composite electrodes (*n*=4).

From the results presented in Table 6.9 it can be seen that the CF PVA (0.05g)/Carbon (0.03g) composite electrodes have a similar high sensitivities. However the packing of theses electrodes using the CF transducer proved to be taxing as the composite dried too quickly to pack more than one electrode at a time and a new composite had to be made for each electrode which was overly time consuming.

6.3.4 *CF Rhoplex® composite electrodes*

6.3.4.1 CV

CV was initially performed on the CF Rhoplex® (0.05g)/Carbon (0.03g) composite electrodes to determine the diffusion limited reduction potential of O_2 at the surface of these electrodes. This was performed as described in Section 3.6.1.2. The results obtained are presented graphically below in Figure 6.12.

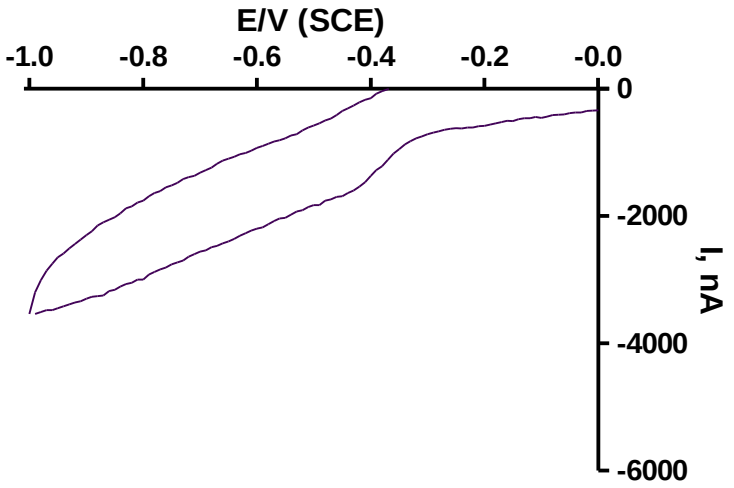

Figure 6.12: Cyclic voltammogram from -1 to 0 V *vs.* SCE at 100 mVs^{-1} performed in O_2 saturated PBS (pH 7.4, 21˚C) buffer solution, illustrating the reduction of O_2 at a CF Rhoplex® (0.05g)/Carbon (0.03g) composite electrodes.

For the CF Rhoplex® (0.05g)/Carbon (0.03g) electrodes an O_2 reduction peak was observed at *ca*. -450 mV. The chosen reduction potential was -650 mV and subsequent constant potential amperometry (CPA) experiments were carried out at this potential.

6.3.4.2 Oxygen calibrations

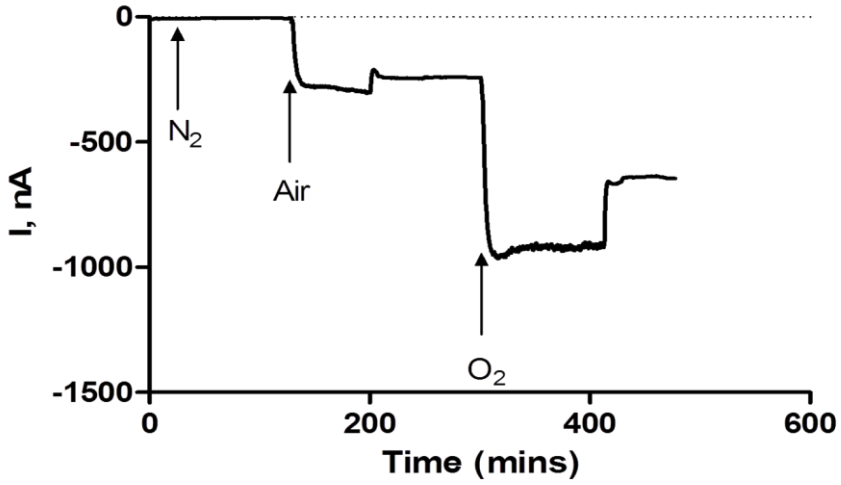

Figure 6.13: An example of typical raw data for an O_2 calibration in PBS using a CRCE (Rhoplex® (0.05g)/Carbon (0.03g). CPA performed at -650 mV *vs.* SCE in PBS (pH 7.4) at 21˚C.

O_2 calibrations were performed on CF Rhoplex® (0.05g)/Carbon (0.03g) and CF Rhoplex® (0.05g)/Carbon (0.02g) composite electrodes as described in Section 3.6.1.4.

	CF Rhoplex® (0.05g)/ Carbon (0.02g) (*n*=8)		Rhoplex® (0.05g)/ Carbon (0.03g) (*n*=4)	
[O_2], µM	**Mean I, nA**	**SEM**	**Mean I, nA**	**SEM**
0	0	0	0	0
240	-205.1	29.6	-323.1	30.1
1200	-849.9	102.0	-1175.3	94.3

Table 6.10: Table of results for O_2 calibrations (0-1200 µM) for CF Rhoplex® (0.05g)/Carbon (0.02g) and CF Rhoplex® (0.05g)/Carbon (0.03g) composite electrodes. CPA performed at -650 mV *vs.* SCE in PBS (pH 7.4) at 21˚C. Mean background subtracted.

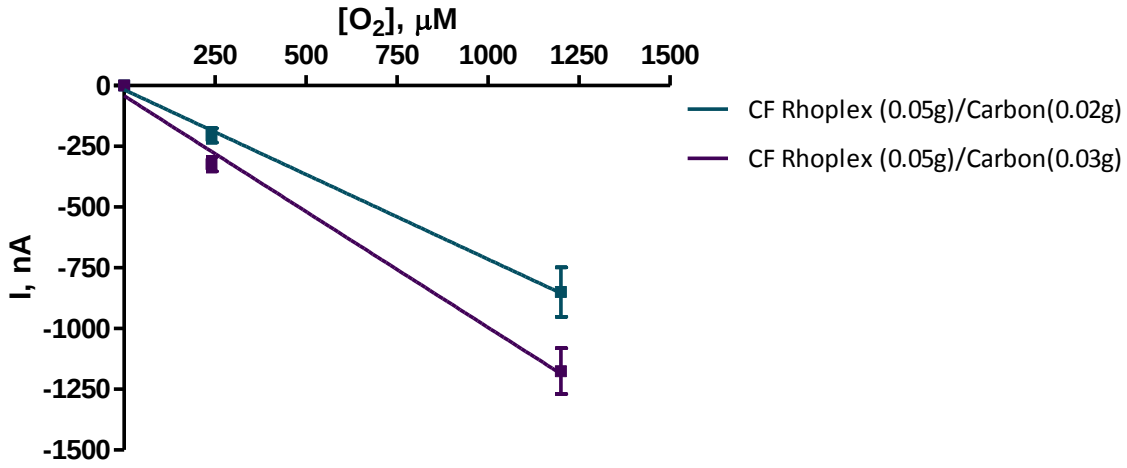

Figure 6.14: O_2 calibration data (0-1200 µM) for CF Rhoplex® (0.05g)/Carbon (0.02g) (*n*=8) and CF Rhoplex® (0.05g)/Carbon (0.03g) (*n*=4) composite electrodes (*n*=11). CPA performed at -650 mV *vs.* SCE in PBS (pH 7.4) at 21˚C.

	Sensitivity (nA/µM)	R^2	*n*
CF Rhoplex® (0.05g)/ Carbon (0.02g)	-0.698 ± 0.030	0.9981	8
Ag Rhoplex® (0.05g)/ Carbon (0.02g)	-1.581 ± 0.284	0.9687	4
CF Rhoplex® (0.05g)/ Carbon (0.03g)	-0.953 ± 0.076	0.9937	4
Ag Rhoplex® (0.05g)/ Carbon (0.03g)	-1.141 ± 0.205	0.9688	4

Table 6.11: Table of calculated sensitivity values of O_2 calibrations (0-1200 µM) for CF Rhoplex® (0.05g)/Carbon (0.02g), silver Rhoplex® (0.05g)/Carbon (0.02g), CF Rhoplex (0.05g)/Carbon (0.03g) and silver Rhoplex® (0.05g)/Carbon (0.03g) composite electrodes.

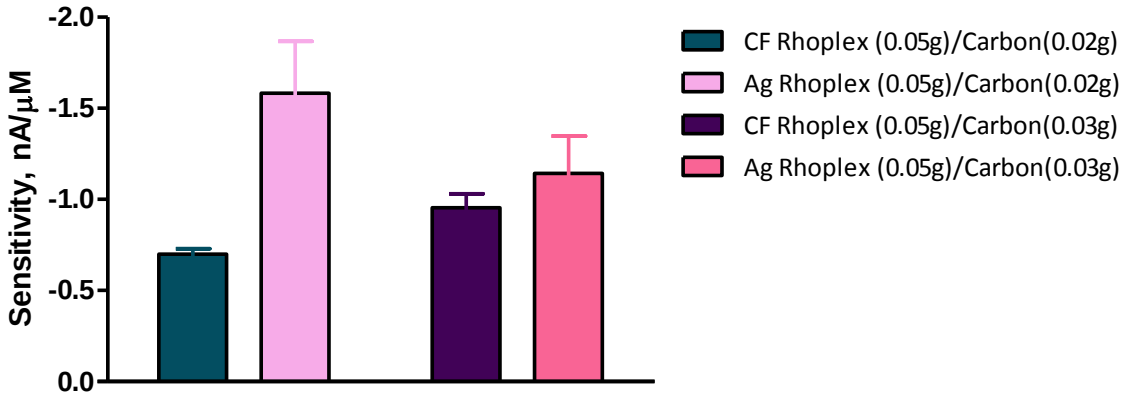

Figure 6.15: Comparison graph of calculated sensitivity values for O_2 calibrations (0-1200 µM) for CF Rhoplex® (0.05g)/Carbon (0.02g) (*n*=8), silver Rhoplex® (0.05g)/Carbon (0.02g) (*n*=4), CF Rhoplex® (0.05g)/Carbon (0.03g) (*n*=4) and silver Rhoplex® (0.05g)/Carbon (0.03g) (*n*=4) composite electrodes.

From these results presented in Table 6.11, it can be seen that the CF Rhoplex® (0.05g)/ Carbon (0.03g) composite electrode had the highest sensitivity of the two CF composite electrodes.

Unpaired *t*-test statistical analysis was performed and it can be seen there is no significant difference in the sensitivities of CF Rhoplex® (0.05g)/Carbon (0.03g) and silver Rhoplex® (0.05g)/Carbon (0.03g) composite electrodes with *P*= 0.4531.

The CF Rhoplex® (0.05g)/Carbon (0.03g) composite electrode (CRCE) was chosen as the final design due to it having the highest sensitivity for O_2 *in vitro* and was the easiest sensor to construct with good reproducibility.

6.3.4.3 CRCE Heat treatment

To attempt to reduce the construction time *ca.* 2 days and increase the sensitivity of the CRCEs the electrodes were dried in an oven at 50˚C for 1 hour. The active surface of the electrodes were very dry shortly after packing the tip of the electrodes but whether the composite was fully dry within the cavity was unclear.

	CRCE full MRI design, heated at 50°C for 1 hr (*n*=7)		CRCE full MRI design (*n*=4)	
[O_2], µM	**Mean I, nA**	**SEM**	**Mean I, nA**	**SEM**
0	0	0	0	0
240	-226.5	34.0	-323.1	30.1
1200	-1009.9	99.1	-1175.3	94.3

Table 6.12: Table of results for O_2 calibrations (0-1200 µM) for CRCE full MRI design, heated at 50°C for 1 hr and CRCE full MRI design. CPA performed at -650 mV *vs.* SCE in PBS (pH 7.4) at 21˚C. Mean background subtracted.

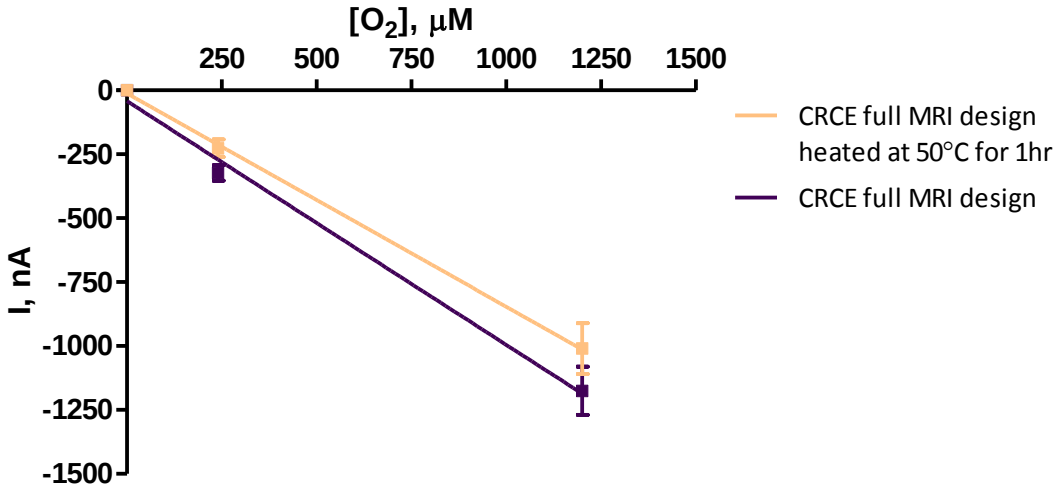

Figure 6.16: O_2 calibration data (0-1200 µM) for CRCE full MRI design, heated at 50°C for 1 hr (*n*=7) and CRCE full MRI design (*n*=4). CPA performed at -650 mV *vs.* SCE in PBS (pH 7.4) at 21˚C.

	Sensitivity (nA/µM)	R^2	*n*
CRCE full MRI design heated at 50°C for 1 hr	-0.834 ± 0.021	0.9994	7
CRCE full MRI design	-0.953 ± 0.076	0.9937	4

Table 6.13: Table of calculated sensitivity values of O_2 calibrations (0-1200 µM) for CRCE full MRI design, heated at 50°C for 1 hr and CRCE full MRI design.

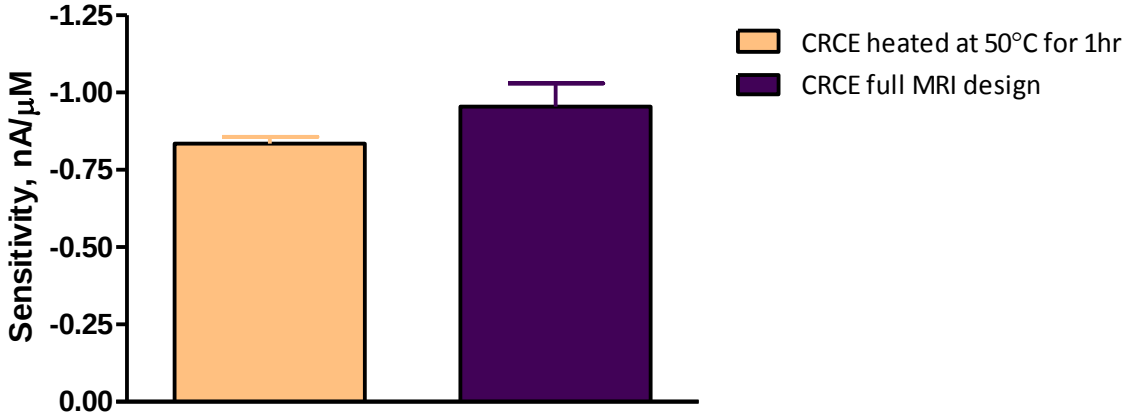

Figure 6.17: Comparison graph of calculated sensitivity values for O_2 calibrations (0-1200 µM) for CRCE full MRI design, heated at 50°C for 1 hr (*n*=7) and CRCE full MRI design (*n*=4).

Unpaired *t*-test statistical analysis was performed and it can be seen there is no significant difference in the sensitivities of air dried CRCEs and CRCEs dried at 50°C for 1 hr with a *P* value of 0.2284. As heat treating the electrodes gave no increase on the sensitivity of the CRCEs the original non-heat treated design was retained for further experiments.

6.3.4.4 CRCE *In Vivo* freely-moving design

As the construction of the CRCEs is very time consuming and for freely-moving *in vivo* experiments the length of the electrode (*ca.* 38 cm) is not feasible for implantation, the removal of the PVA coated carbon fibre bundle and shortening of the electrode length (*ca.* 7 cm) was investigated. The Teflon® coated carbon fibre was directly connected to the copper wire and the electrodes were calibrated to determine if there is a significant difference between the two designs.

	CRCE *in vivo* design (*n*=19)	
[O_2], µM	**Mean I, nA**	**SEM**
0	0	0
240	-326.3	47.9
1200	-1278.4	148.5

Table 6.14: Table of results for O_2 calibrations (0-1200 µM) for CRCE *in vivo* design (*n*=19). CPA performed at -650 mV *vs.* SCE in PBS (pH 7.4) at 21˚C. Mean background subtracted.

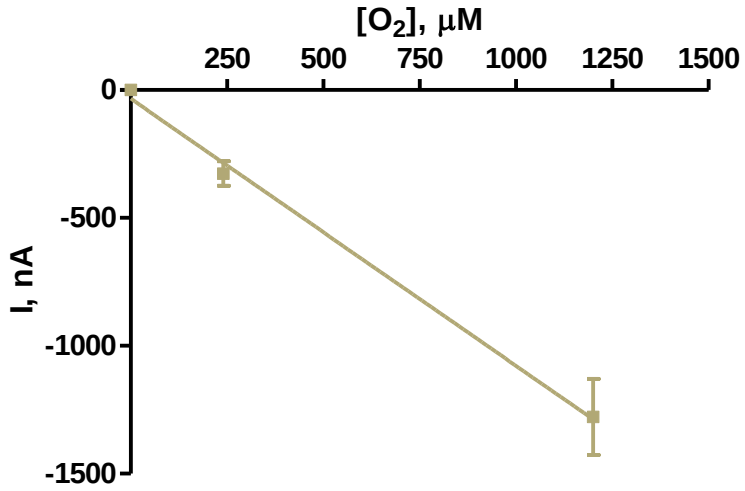

Figure 6.18: O_2 calibration data (0-1200 µM) for CRCE *in vivo* design (*n*=19). CPA performed at -650 mV *vs.* SCE in PBS (pH 7.4) at 21˚C.

	Sensitivity (nA/µM)	R^2	*n*
CRCE *in vivo* design	-1.044 ± 0.061	0.9966	19
CRCE full MRI design	-0.953 ± 0.076	0.9937	4

Table 6.15: Table of calculated sensitivity values of O_2 calibrations (0-1200 µM) for CRCE *in vivo* design and CRCE full MRI design.

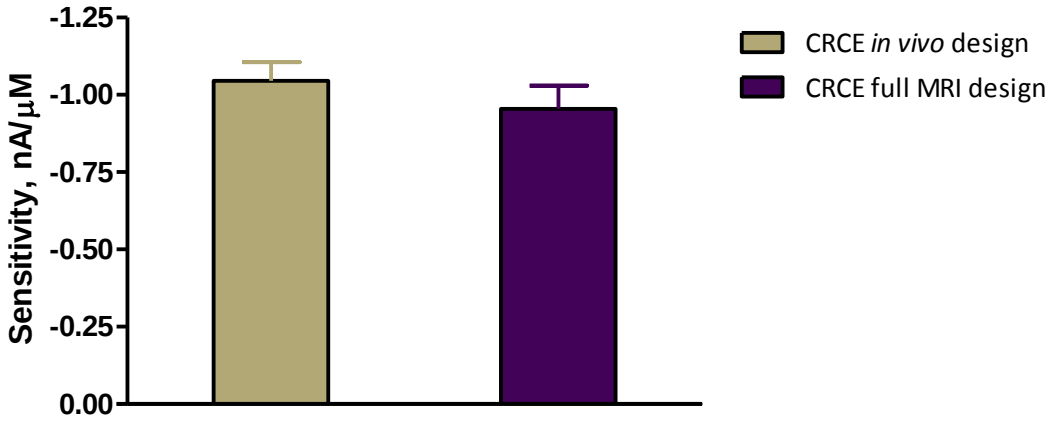

Figure 6.19: Comparison graph of calculated sensitivity values for O_2 calibrations (0-1200 µM) for CRCE *in vivo* design (*n*=19) and CRCE full MRI design (*n*=4).

Unpaired *t*-test statistical analysis was performed and it can be seen there is no significant difference in the sensitivities of CRCEs *in vivo* and full MRI designs with a *P* value of 0.3803.

6.3.4.5 Disk shaped active surface

It was observed that when the carbon Rhoplex® composite was left to dry that many of the electrodes had an active surface that was no longer disk shaped. The composite appeared to have expanded when drying causing the composite to push out so a cylindrical shape is observed at the active surface of the electrode. In order to eliminate the cylindrical shape the electrodes were left to dry overnight against a hard, flat surface.

	CRCE, dried on flat surface (*n*=4)	
$[O_2]$, µM	**Mean I, nA**	**SEM**
0	0	0
240	-293.7	17.4
1200	-1200.6	82.5

Table 6.16: Table of results for O_2 calibrations (0-1200 µM) for CRCE dried on a flat surface (*n*=4). CPA performed at -650 mV *vs.* SCE in PBS (pH 7.4) at 21˚C. Mean background subtracted.

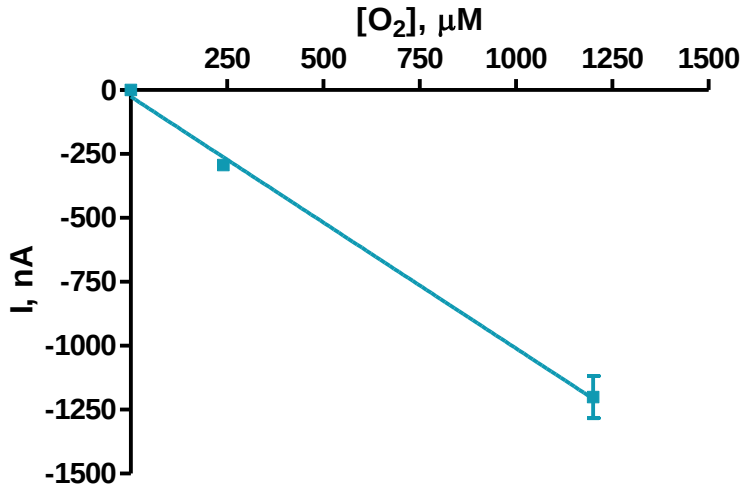

Figure 6.20: O_2 calibration data (0-1200 µM) for CRCE dried on a flat surface (*n*=4). CPA performed at -650 mV *vs.* SCE in PBS (pH 7.4) at 21˚C.

Linear regression analysis shows that the electrodes have a sensitivity of -0.985 ± 0.046 nA/µM (*n*=4). The response was linear over the range with an R^2 value of 0.9978 (*n*=4).

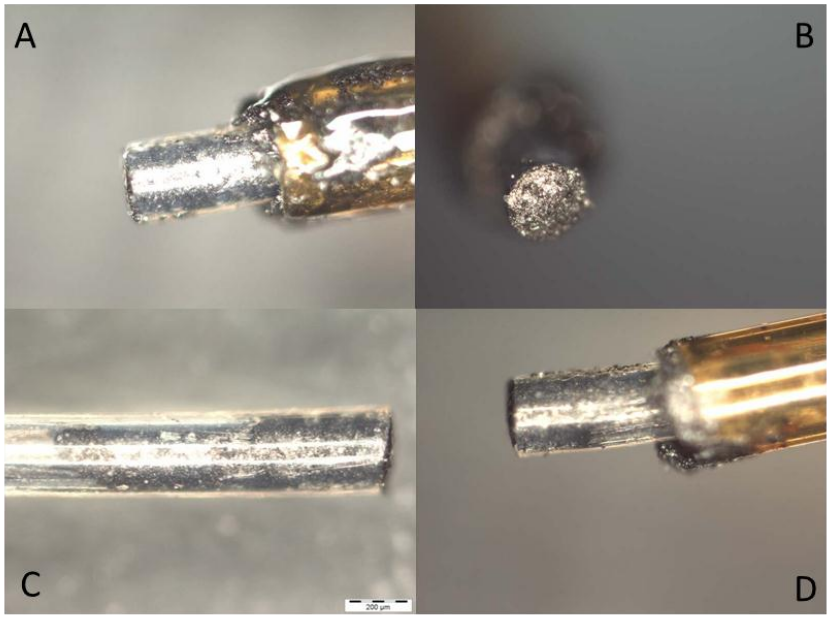

Figure 6.21: Images of the active surface of CRCEs (A,B,D) and (C) CRCE without silica tubing demonstrating packing at the active surface of the electrode.

6.3.4.6 Biocompatibility

In this section the effects of proteins, lipids and brain tissue on the sensitivity of CRCEs was investigated, based on previous work (Ormonde & O'Neill, 1989, 1990) to determine if there is a significant reduction in the electrodes ability to remain sensitive to O_2 *in vivo*.

6.3.4.6.1 Protein (BSA) treated CRCEs

The effect of exposure to the protein BSA (Section 3.5.4.1) on CRCEs with respect to time was investigated. Untreated CRCEs (0 days) were calibrated and subsequently exposed to BSA for 24 hours, 3 days, 7 days and 14 days.

	BSA (0 days) *n*=6		BSA (12 hrs) *n*=6		BSA (3 days) *n*=6		BSA (7 days) *n*=5		BSA (14 days) *n*=6	
[O_2], µM	**Mean I, nA**	**SEM**	**Mean I, nA**	**SEM**	**Mean I, nA**	**SEM**	**Mean I, nA**	**SEM**	**Mean I, nA**	**SEM**
0	0	0	0	0	0	0	0	0	0	0
240	-176.6	100.0	-229.5	58.8	-183.1	55.6	-173.5	30.2	-150.5	44.5
1200	-712.7	143.5	-742.9	110.5	-782.5	78.1	-724.1	104.5	-663.2	145.0

Table 6.17: Table of results for O_2 calibrations (0-1200 µM) for CRCEs exposed to BSA. CPA performed at -650 mV *vs.* SCE in PBS (pH 7.4) at 21˚C. Mean background subtracted.

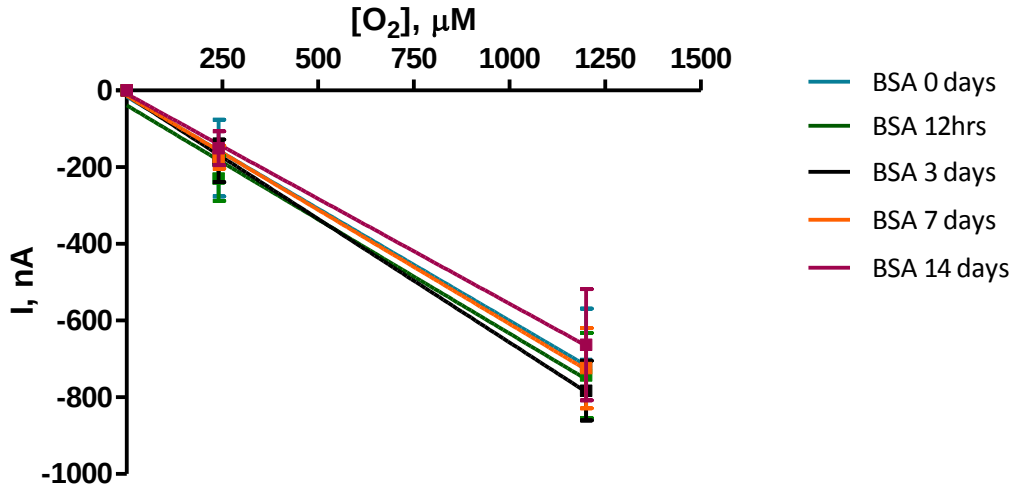

Figure 6.22: O_2 calibration data (0-1200 µM) for CRCEs untreated (0 days) and treated with BSA (12 hrs, 3 days, 7 days and 14 days). CPA performed at -650 mV *vs.* SCE in PBS (pH 7.4) at 21˚C.

BT treatment	Sensitivity (nA/µM)	R^2	*n*
0 days	-0.760 ± 0.165	0.9629	4
24 hrs	-0.683 ± 0.005	1.0000	3
3 days	-0.814 ± 0.094	0.9868	3
7 days	-0.733 ± 0.105	0.9799	3
14 days	-0.948 ± 0.060	0.9961	3

Table 6.18: Table of calculated sensitivity values of O_2 calibrations (0-1200 µM) for CRCEs exposed to BSA.

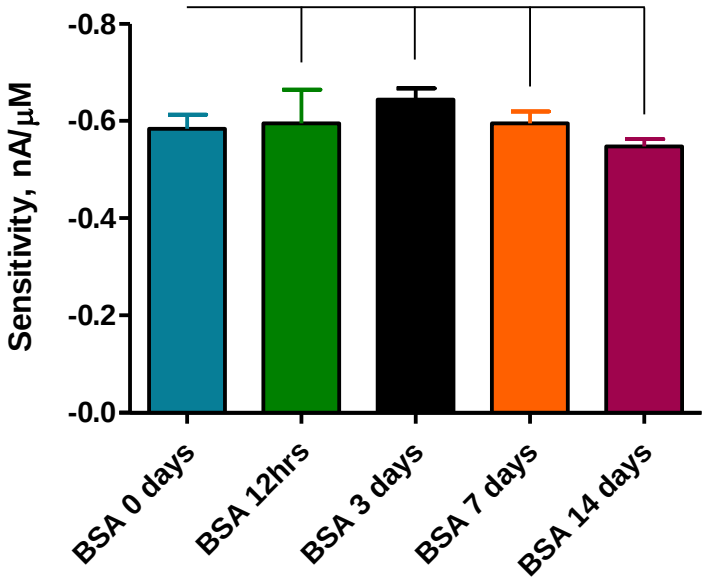

Figure 6.23: Comparison graph of calculated sensitivity values for O_2 calibrations (0-1200 µM) for CRCEs exposed to BSA.

Unpaired *t*-test statistical analysis was performed and it can be seen there is no significant different in the sensitivities with *P* values greater than 0.05 between untreated (0 days exposure) and BSA treated electrodes with *P* values of 0.8868 (12 hrs), 0.1382 (3 days), 0.7790 (7days) and 0.3056 (14 days).

One-way Analysis of Variance (ANOVA) was performed on CRCEs only exposed to BSA with a *P* value of 0.4179, showing no significant difference in the sensitivities between the electrodes once exposed to BSA over a period of 14 days. From these results it can be seen that there is a small but non-significant reduction in the sensitivity of CRCEs following exposure to BSA over a period of 14 days.

6.3.4.6.2 Lipid (PEA) treated CRCEs

The effect of exposure to the protein PEA (Section 3.5.4.2) on CRCEs with respect to time was investigated. Untreated CRCEs (0 days) were calibrated and subsequently exposed to PEA for 24 hours, 3 days and 14 days.

	PEA (0 days) *n*=8		PEA (12 hrs) *n*=8		PEA (3 days) *n*=7		PEA (7 days) *n*=6		PEA (14 days) *n*=7	
[O_2], µM	**Mean I, nA**	**SEM**	**Mean I, nA**	**SEM**	**Mean I, nA**	**SEM**	**Mean I, nA**	**SEM**	**Mean I, nA**	**SEM**
0	0	0	0	0	0	0	0	0	0	0
240	-282.8	56.6	-191.1	89.1	-281.7	122.7	-325.3	68.9	-307.7	82.0
1200	-948.5	134.0	-900.2	189.6	-942.7	204.8	-876.0	123.6	-904.1	197.9

Table 6.19: Table of results for O_2 calibrations (0-1200 µM) for CRCEs exposed to PEA. CPA performed at -650 mV *vs.* SCE in PBS (pH 7.4) at 21˚C. Mean background subtracted.

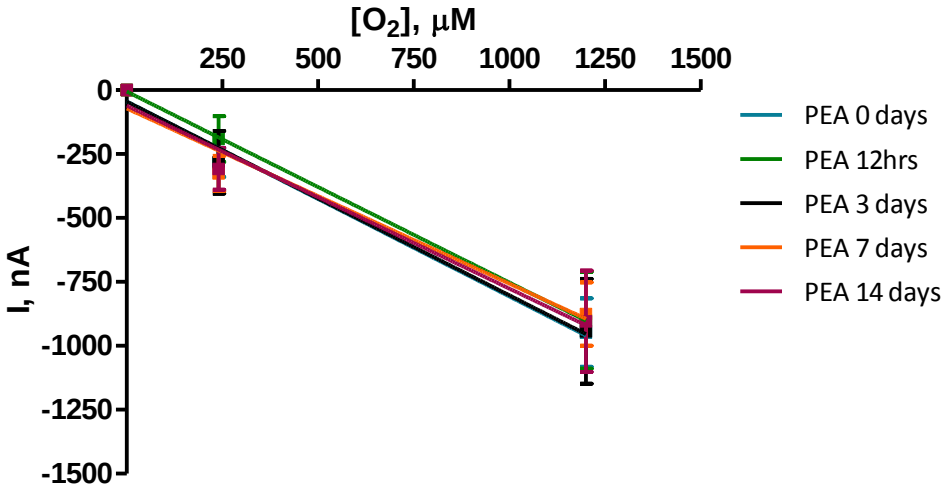

Figure 6.24: O_2 calibration data (0-1200 µM) for CRCEs untreated (0 days) and treated with PEA (12 hrs, 3 days, 7 days and 14 days). CPA performed at -650 mV *vs.* SCE in PBS (pH 7.4) at 21˚C.

PEA treatment	Sensitivity (nA/µM)	R^2	*n*
0 days	-0.763 ± 0.080	0.9891	8
24 hrs	-0.747 ± 0.009	0.9998	8
3 days	-0.758 ± 0.080	0.9890	7
7 days	-0.685 ± 0.129	0.9658	6
14 days	-0.716 ± 0.109	0.9773	7

Table 6.20: Table of calculated sensitivity values of O_2 calibrations (0-1200 µM) for CRCEs exposed to PEA.

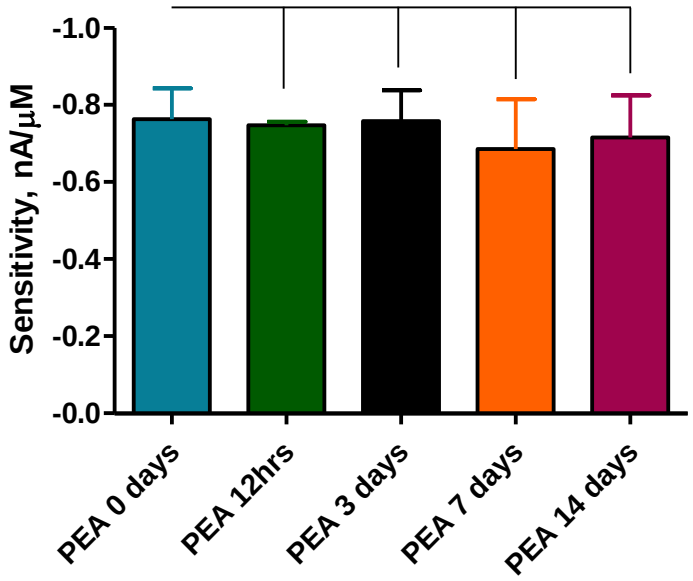

Figure 6.25: Comparison graph of calculated sensitivity values for O_2 calibrations (0-1200 µM) for CRCEs exposed to PEA.

Unpaired *t*-test statistical analysis was performed and it can be seen there is no significant different in the sensitivities with *P* values greater than 0.05 between untreated (0 days exposure) and PEA treated electrodes with *P* values of 0.8500 (12 hrs), 0.9669 (3 days), 0.6239 (7days) and 0.7347 (14 days).

One-way Analysis of Variance (ANOVA) was performed on CRCEs only exposed to PEA with a *P* value of 0.9396, showing no significant difference in the sensitivities between the electrodes once exposed to PEA over a period of 14 days. From these results it can be seen that there is small but non-significant reduction in the sensitivity of CRCEs following exposure to PEA over a period of 14 days.

6.3.4.6.3 Brain tissue (BT) treated CRCEs

The effect of exposure to a sample of *ex-vivo* BT (Section 3.5.4.3) on CRCEs with respect to time was investigated. Untreated CRCEs (0 days) were calibrated and subsequently exposed to BT for 24 hours, 3 days and 14 days.

	BT (0 days) *n*=4		BT (12 hrs) *n*=3		BT (3 days) *n*=3		BT (7 days) *n*=3		BT (14 days) *n*=3	
[O_2], µM	**Mean I, nA**	**SEM**	**Mean I, nA**	**SEM**	**Mean I, nA**	**SEM**	**Mean I, nA**	**SEM**	**Mean I, nA**	**SEM**
0	0	0	0	0	0	0	0	0	0	0
240	-395.3	68.0	-161.2	24.4	-312.8	94.3	-306.7	69.9	-301.8	54.7
1200	-1045.1	209.2	-815.3	93.6	-1016.4	191.0	-922.7	116.1	-1162.0	143.5

Table 6.21: Table of results for O_2 calibrations (0-1200 µM) for CRCEs exposed to BT. CPA performed at -650 mV *vs.* SCE in PBS (pH 7.4) at 21˚C. Mean background subtracted.

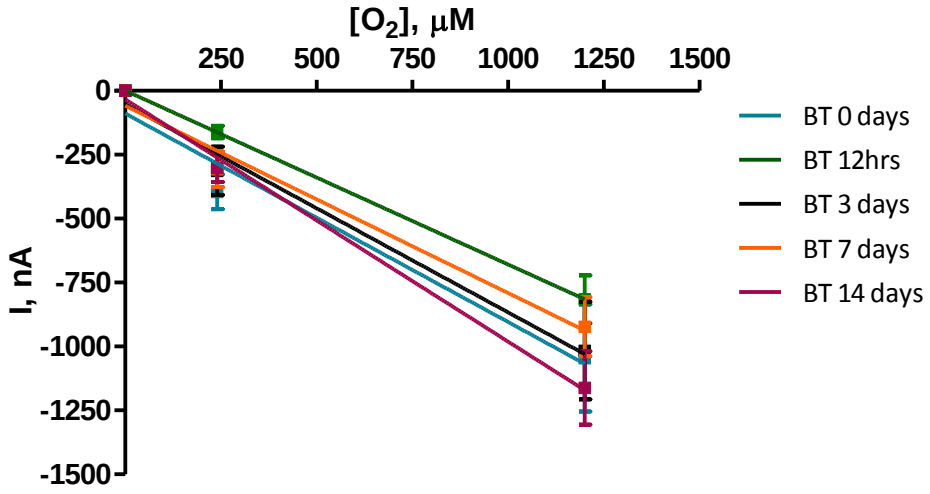

Figure 6.26: O_2 calibration data (0-1200 µM) for CRCEs untreated (0 days) and treated with BT (24 hrs, 3 days, 7 days and 14 days). CPA performed at -650 mV *vs.* SCE in PBS (pH 7.4) at 21˚C.

BT treatment	Sensitivity (nA/µM)	R^2	*n*
0 days	-0.760 ± 0.165	0.9629	4
24 hrs	-0.683 ± 0.005	1.0000	3
3 days	-0.814 ± 0.094	0.9868	3
7 days	-0.733 ± 0.105	0.9799	3
14 days	-0.948 ± 0.060	0.9961	3

Table 6.22: Table of calculated sensitivity values of O_2 calibrations (0-1200 µM) for CRCEs exposed to BT.

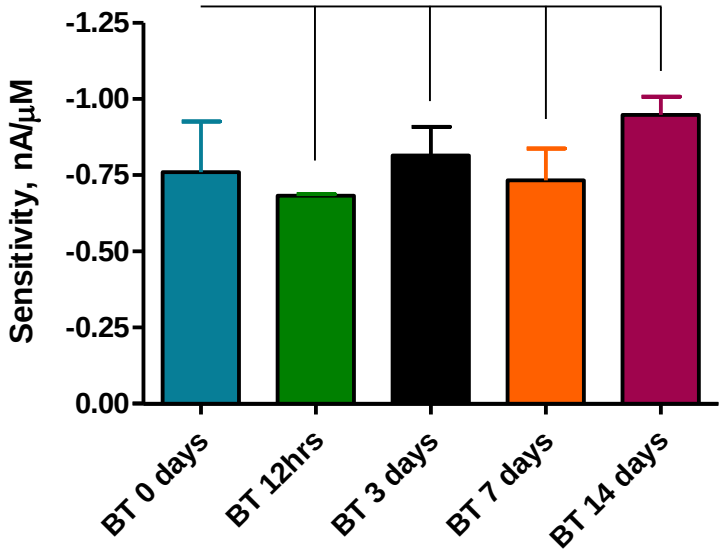

Figure 6.27: Comparison graph of calculated sensitivity values for O_2 calibrations (0-1200 µM) for CRCEs exposed to BT.

Unpaired *t*-test statistical analysis was performed and it can be seen there is no significant different in the sensitivities with *P* values greater than 0.05 between untreated (0 days exposure) and BT treated electrodes with *P* values of 0.6717 (12 hrs), 0.7895 (3 days) 0.8947 (7 days) and 0.3640 (14 days).

One-way Analysis of Variance (ANOVA) was performed on Pt-MMA electrodes only exposed to BT with a *P* value of 0.1555 showing no significant difference in the sensitivities between the electrodes once exposed to BT over a period of 14 days. From these results it can be seen that there is small but non-significant reduction in the sensitivity of CRCEs following exposure to BT over a period of 14 days.

6.3.4.7 CRCE heat damage

Construction of the CRCEs involves the use of a considerable amount of heat-shrink and therefore exposure to large amounts of heat. As can be seen in Section 6.3.4.5 it was observed for non-treated electrodes that there was a substantial reduction in the sensitivity ((BSA 0 days: -0.584 ± 0.029 nA/µM, *n*=6), (PEA 0 days: -0.763 ± 0.080 nA/µM, *n*=8),

(BT 0 days: -0.760 ± 0.165 nA/µM, *n*=4)) and also for CRCEs, full MRI design with a sensitivity of -0.672 ± 0.086 nA/µM, *n*=11.

This issue of reduced sensitivity was investigated. The following steps were taken to minimise that heat damage to the CRCEs:

• Heat-shrink use was minimised to use over the silver epoxy connections and the Teflon® containing the carbon fibres was protected with the PVA coating to ensure that the Teflon® did not come into contact with heat.

• The copper wire was soldered into a gold clip before sensor construction.

• The electrodes were packed at the final point instead of at the beginning of the sensor construction, as it was observed by eye that when the heat shrink was being heated the composite at the tip of the electrode would push out away from the Teflon® altering the active surface of the electrodes.

These precautions were taken for construction of the CRCEs full MRI and *in vivo* designs.

	CRCE full MRI design (*n*=11)		**CRCE full MRI design, no heat (*n*=2)**		**CRCE *in vivo* design, no heat (*n*=4)**	
[O_2], µM	**Mean I, nA**	**SEM**	**Mean I, nA**	**SEM**	**Mean I, nA**	**SEM**
0	0	0	0	0	0	0
240	-268.5	21.4	-428.2	19.4	-316.9	60.7
1200	-842.6	87.0	-1410.7	65.7	-1309.4	81.7

Table 6.23: Table of results for O_2 calibrations (0-1200 µM) for CRCE full MRI design, CRCE full MRI design, no heat and CRCE *in vivo* design, no heat. CPA performed at -650 mV *vs.* SCE in PBS (pH 7.4) at 21˚C. Mean background subtracted.

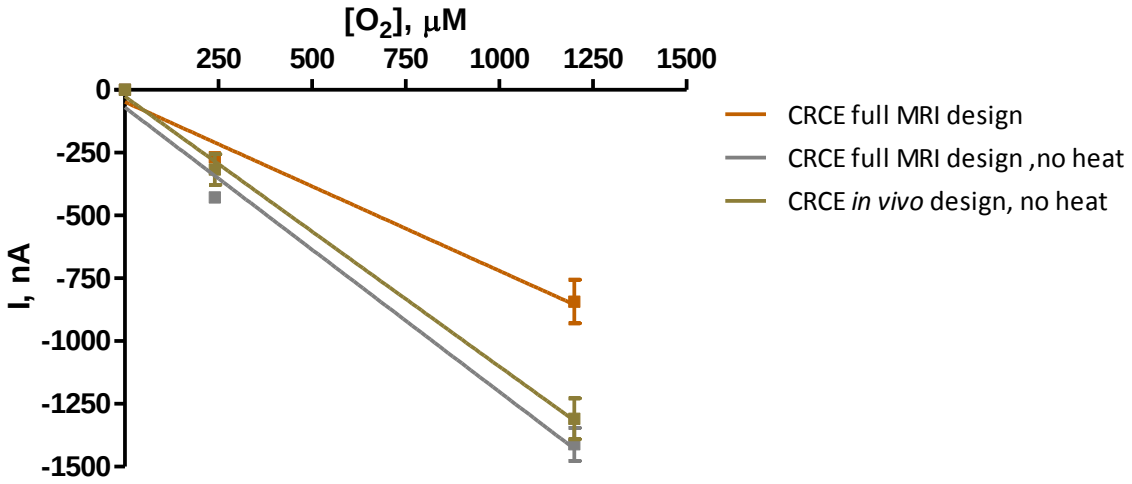

Figure 6.28: O_2 calibration data (0-1200 µM) for CRCE full MRI design (*n*=11), CRCE full MRI design, no heat (*n*=2) and CRCE *in vivo* design, no heat (*n*=4). CPA performed at -650 mV *vs.* SCE in PBS (pH 7.4) at 21˚C.

	Sensitivity (nA/µM)	R^2	*n*
CRCE full MRI design	-0.672 ± 0.086	0.9839	11
CRCE full MRI design, no heat	-1.132 ± 0.126	0.9879	2
CRCE *in vivo* design, no heat	-1.075 ± 0.047	0.9981	4

Table 6.24: Table of calculated sensitivity values of O_2 calibrations (0-1200 µM) for CRCE full MRI design, CRCE full MRI design, no heat and CRCE *in vivo* design, no heat.

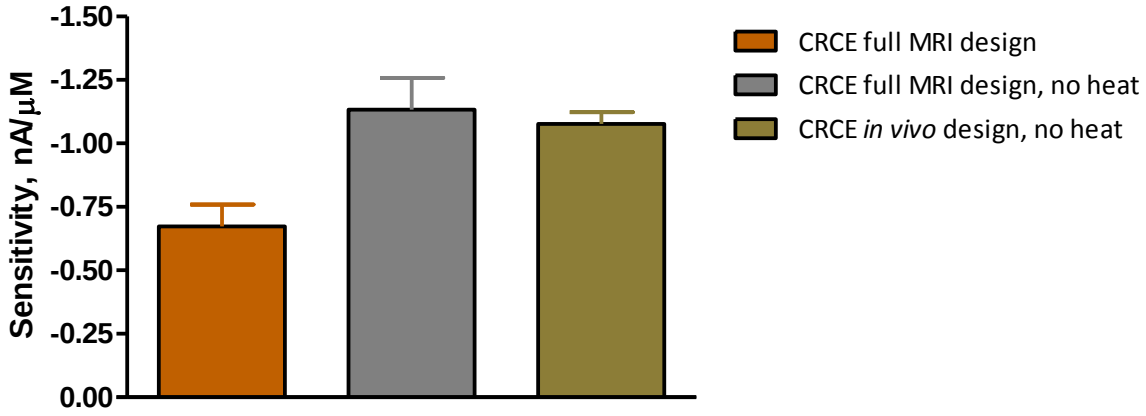

Figure 6.29: Comparison graph of calculated sensitivity values for O_2 calibrations (0-1200 µM) for CRCE full MRI design (*n*=11), CRCE full MRI design, no heat (*n*=2) and CRCE *in vivo* design, no heat (*n*=4).

It can be seen in Figure 6.29 that these modifications to the construction of the sensors were effective. The heat has an effect on the sensitivity so the no heat method was used following on from this. Experiments from this point onwards were performed using the CRCE *in vivo* no heat design unless otherwise stated.

6.3.4.8 Effect of temperature

Membrane covered O_2 sensors tend to have significant temperature dependence primarily due to the effects of temperature on the diffusion coefficient and the solubility of the gas in the membrane with temperature. The signal typically increasing by 1-6% for a rise of 1˚C (Hitchman, 1978; Jeroschewski & Zur Linden, 1997). *In vitro* experiments are routinely performed at a room temperature of *ca.* 21˚C. The effect of an increase in the temperature of the PBS on the CRCEs O_2 sensitivity at the physiological temperate of 37˚C was investigated. The concentration of dissolved O_2 was calculated to be 214 µM for air saturated PBS and 1020 µM for O_2 saturated PBS at 37°C detailed in Section 2.8.4.

	PBS 37°C	
$[O_2]$, µM	**Mean I, nA**	**SEM**
0	0	0
240	-798.4	138.3
1200	-2640.7	187.9

	PBS 21°C	
$[O_2]$, µM	**Mean I, nA**	**SEM**
0	0	0
240	-316.9	60.7
1200	-1309.4	81.7

Table 6.25: Tables of results for O_2 calibrations (0-1200 µM) for CRCEs. CPA performed at -650 mV *vs.* SCE in PBS (pH 7.4) at 37˚C (0-1020 µM) (*n*=4) and 21˚C (0-1200 µM) (*n*=4). Mean background subtracted.

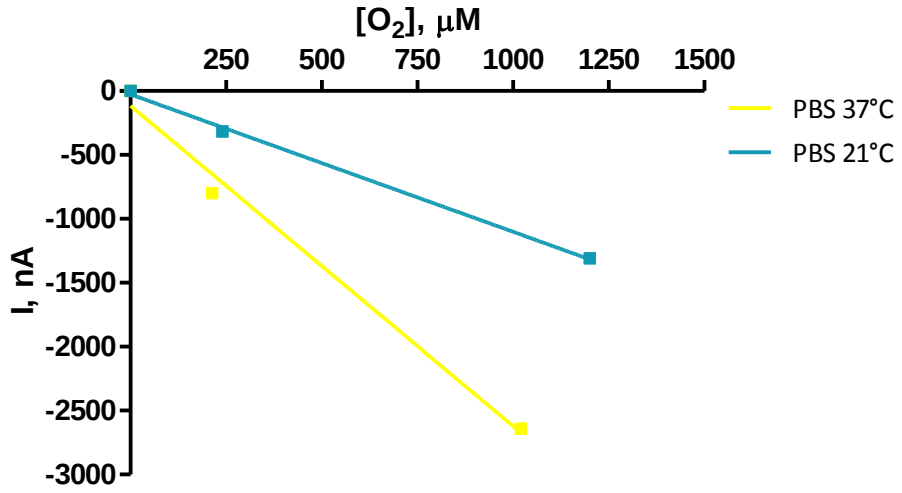

Figure 6.30: O_2 calibration data (0-1200 µM) for CRCEs. CPA performed at -650 mV *vs.* SCE in PBS (7.4) at 37˚C (0-1020 µM) & 21˚C (0-1200 µM).

	Sensitivity (nA/µM)	R^2	*n*
PBS 37°C	-2.506 ± 0.249	0.9902	4
PBS 21°C	-1.075 ± 0.047	0.9981	4

Table 6.26: Comparison of calculated sensitivity values of O_2 calibrations for CRCEs calibrated in PBS solutions of 37˚and 21˚C.

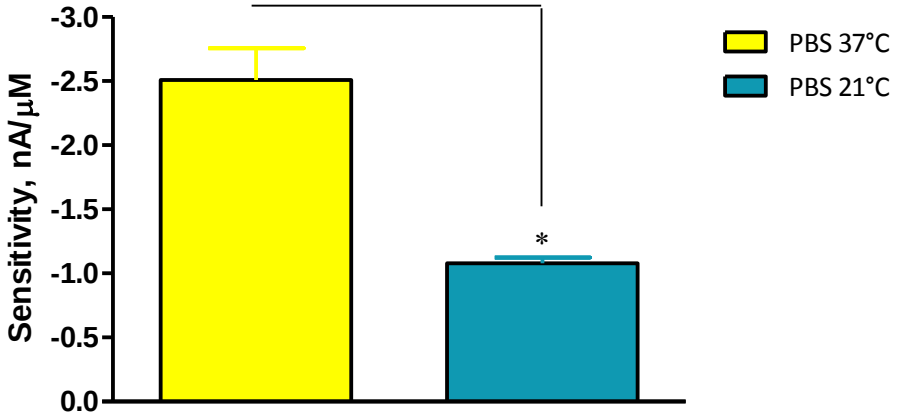

Figure 6.31: Comparison graph of calculated sensitivity values for O_2 calibrations for CRCEs calibrated in PBS at 37˚C (*n*=4) & 21˚C (*n*=4).

Unpaired *t*-test statistical analysis was performed and it can be seen there is a significant difference in the sensitivities of CRCEs calibrated at 37˚C and 21˚C with a *P* value of 0.0216. From the results obtained for CRCEs it can be seen that the sensitivity increases by 133.12 ± 23.14 % corresponding to a 3.60 ± 0.63 % for every 1˚C increase indicating that CRCEs do exhibit significant temperature dependence at the physiological temperature.

6.3.4.9 Effect of pH

Changes in pH may occur during physiological experiments *in vivo* (Zimmerman & Wightman, 1991) these changes in pH could also affect the cathodic reduction of O_2 at the electrode surface involving proton transfer. Previous reports for carbon-based electrodes found that for pH 12-14 the reduction of O_2 seems to be independent of pH, but as pH decreases the reduction becomes pH dependent (Taylor & Humffray, 1975; Yang & McCreery, 2000). The effect of changes in pH on CRCEs was investigated.

	PBS pH 6.5		PBS pH 7.4		PBS pH 8	
$[O_2]$, µM	**Mean I, nA**	**SEM**	**Mean I, nA**	**SEM**	**Mean I, nA**	**SEM**
0	0	0	0	0	0	0
240	-352.2	49.1	-316.9	60.7	-302.1	39.1
1200	-1616.7	145.6	-1309.4	81.7	-1636.9	78.6

Table 6.27: Table of results for O_2 calibrations (0-1200 µM) for CRCEs. CPA performed at -650 mV *vs.* SCE in PBS: pH 6.5 (*n*=4), 7.4 (*n*=4) & 8 (*n*=4) at 21˚C. Mean background subtracted.

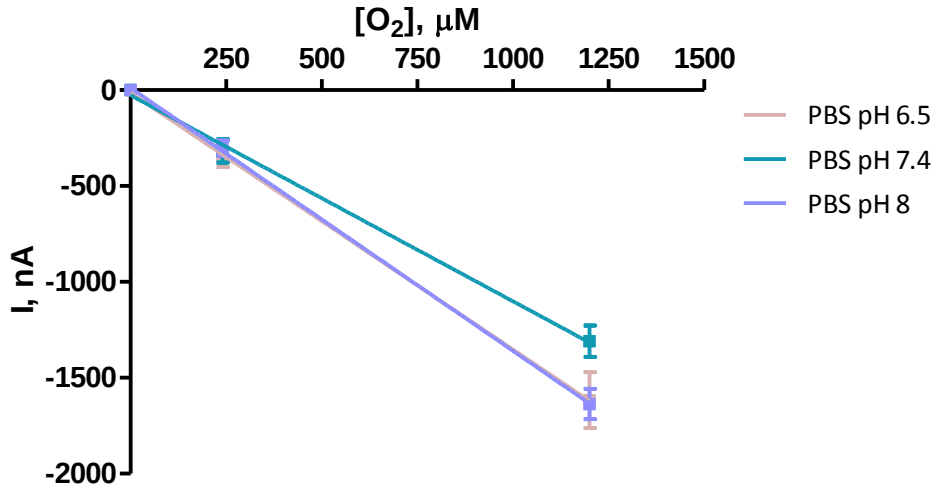

Figure 6.32: O_2 calibration data (0-1200 µM) for CRCEs. CPA performed at -650 mV *vs.* SCE in PBS (pH 6.5, 7.4 & 8) at 21˚C.

	Sensitivity (nA/µM)	R^2	*n*
PBS pH 6.5	-1.339 ± 0.025	0.9997	4
PBS pH 7.4	-1.075 ± 0.047	0.9981	4
PBS pH 8	-1.372 ± 0.022	0.9997	4

Table 6.28: Comparison of calculated sensitivity values of O_2 calibrations (0-1200 µM) for CRCEs calibrated in PBS 6.5, 7.4 & 8.

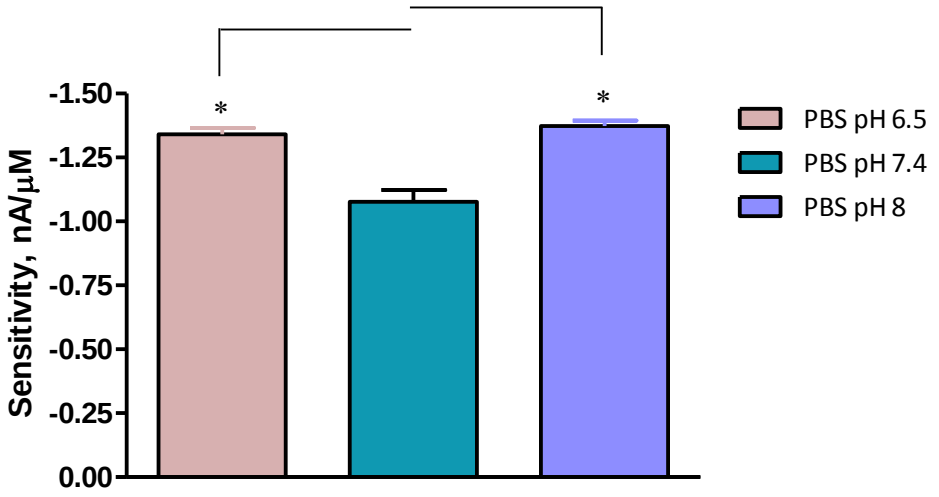

Figure 6.33: Comparison graph of calculated sensitivity values for O_2 calibrations (0-1200 µM) for CRCEs electrodes calibrated in PBS pH 6.5 (*n*=4), 7.4 (*n*=4) and 8 (*n*=4).

Unpaired *t*-test statistical analysis was performed and it can be seen there is a significant difference in the sensitivities of CRCEs calibrated in PBS pH 6.5 and 7.4 with a *P* value of 0.0078. There is a significant difference in the sensitivities between electrodes calibrated in PBS pH 8 and 7.4 with a *P* value of 0.0047.

6.3.4.10 Effect of ion changes

Changes in ion concentrations are of interest in *vivo* as previously discussed in Section 0. The effect of ion changes on the sensitivities of CRCEs was investigated.

	aCSF (*n*=7)		aCSF no Ca^{2+} (*n*=4)		aCSF no Mg^{2+} (*n*=8)		aCSF no Ca^{2+}or Mg^{2+}(*n*=8)	
[O_2], µM	**Mean I, nA**	**SEM**	**Mean I, nA**	**SEM**	**Mean I, nA**	**SEM**	**Mean I, nA**	**SEM**
0	0	0	0	0	0	0	0	0
240	-211.7	59.4	-358.9	77.2	-483.7	60.5	-536.8	57.3
1200	-1224.1	103.0	-1428.9	28.1	-1460.6	101.6	-1677.3	133.8

Table 6.29: Table of results for O_2 calibrations (0-1200 µM) for CRCEs. CPA performed at -650 mV *vs.* SCE in aCSF (*n*=7), aCSF no Ca^{2+} (*n*=4), aCSF no Mg^{2}+ (*n*=8) and aCSF no Ca^{2+} or Mg^{2+} (*n*=8) at 21˚C. Mean background subtracted.

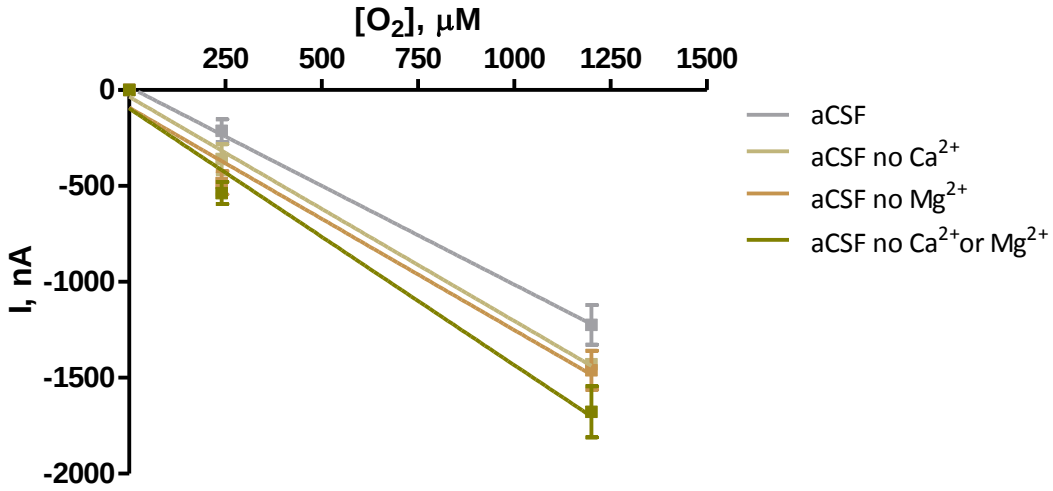

Figure 6.34: O_2 calibration data (0-1200 µM) for CRCEs. CPA performed at -650 mV *vs.* SCE in aCSF, aCSF no Ca^{2+}, aCSF no Mg^{2} and aCSF no Ca^{2+} or Mg^{2+} at 21˚C.

	Sensitivity (nA/µM)	R^2	*n*
aCSF	-1.030 ± 0.028	0.9992	7
aCSF no Ca^{2+}	-1.169 ± 0.063	0.9971	4
aCSF no Mg^{2+}	-1.160 ± 0.165	0.9803	8
aCSF no Ca^{2+}or Mg^{2+}	-1.338 ± 0.173	0.9835	8

Table 6.30: Comparison of calculated sensitivity values of O_2 calibrations (0-1200 µM) for CRCEs calibrated in aCSF, aCSF no Ca^{2+}, aCSF no Mg^{2+}, aCSF no Ca^{2+}or Mg^{2+} at 21˚C.

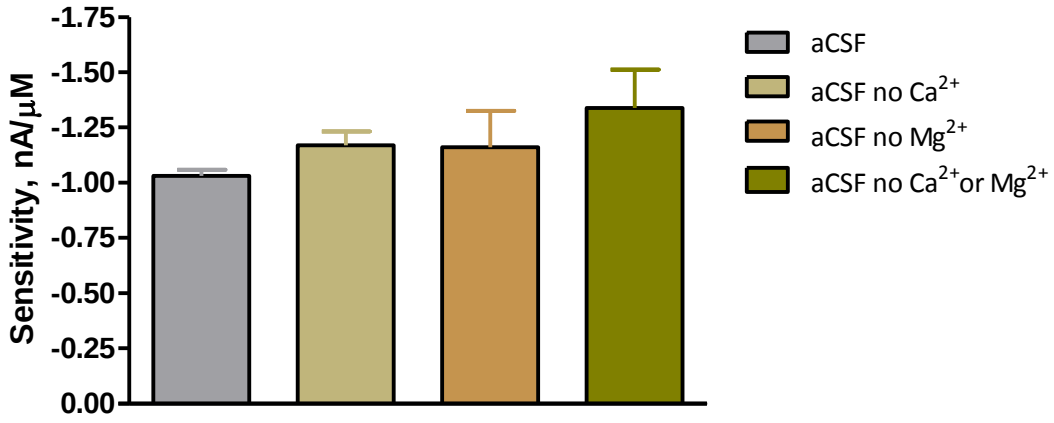

Figure 6.35: Comparison graph of calculated sensitivity values for O_2 calibrations (0-1200 µM) for Pt-MMA electrodes calibrated in aCSF (*n*=7), aCSF no Ca^{2+} (*n*=4), aCSF no Mg^{2+} (*n*=8) and aCSF no Ca^{2+}or Mg^{2+} (*n*=8).

Unpaired *t*-test statistical analysis was performed and it can be seen there is no significant difference in the sensitivities of CRCEs calibrated in aCSF and aCSF with no with Ca^{2+}, Mg^{2+} and Ca^{2+}or Mg^{2+} with *P* values of 0.1141 (aCSF no Ca^{2+}), 0.4619 (aCSF no Mg^{2+}) and 0.1224 (aCSF no Ca^{2+}or Mg^{2+}). There is a decrease in the sensitivity for CRCEs calibrated in aCSF (-1.030 ± 0.028 nA/µM) compared to PBS (-1.075 ± 0.047 nA/µM) although the difference is not significant *P* = 0.4482.

6.3.4.11 Post-implantation calibrations

The effect of proteins, lipids and brain tissue on the sensitivity of CRCEs *in vitro* was investigated (Section 6.3.4.5). Although this gives an indication as to the effect that proteins, lipids and *ex-vivo* brain tissue has on the sensitivity of the electrodes the effect of the living brain with endogenous species present was investigated by performing post implantation calibrations where possible on the CRCEs (implanted for 9 ± 2 days (*n*=3)) once removed from the brain. These calibrations are described in Section 3.6.1.8.

	CRCE (pre-implantation)		CRCE (post-implantation)	
$[O_2]$, µM	**Mean I, nA**	**SEM**	**Mean I, nA**	**SEM**
0	0	0	0	0
240	-432.0	58.5	-93.1	125.7
1200	-1727.4	137.4	-596.7	122.6

Table 6.31: Table of results for O_2 calibrations (0-1200 µM) for CRCEs pre-implantation and post-implantation (*n*=8) for a standard O_2 calibration. CPA performed at -650 mV *vs.* SCE in PBS (pH 7.4) at 21˚C. Mean background subtracted.

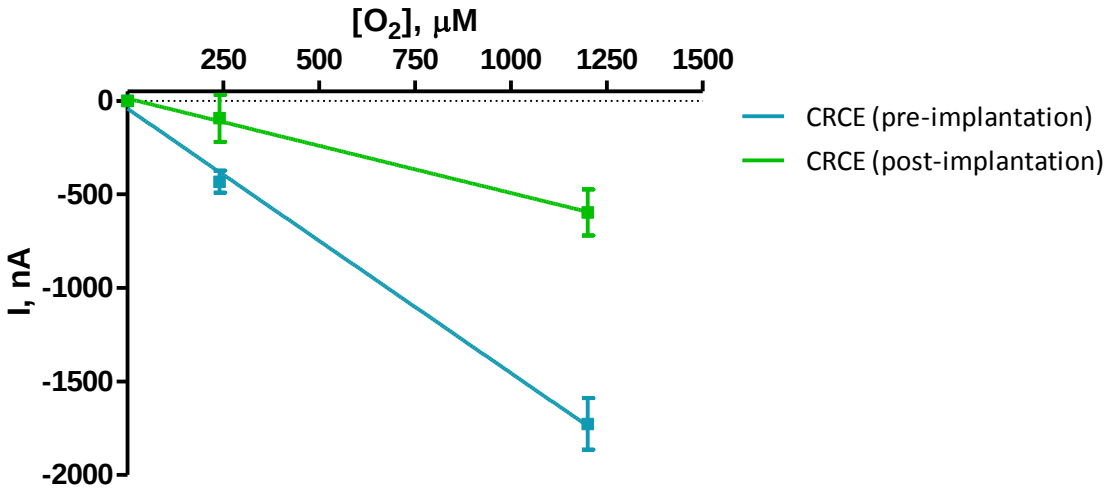

Figure 6.36: O_2 calibration data (0-1200 µM) for CRCEs pre-implantation and post-implantation (*n*=8). CPA performed at -650 mV *vs.* SCE in PBS (pH 7.4) at 21˚C.

	Sensitivity (nA/µM)	R^2	*n*
Pre-implantation	-1.414 ± 0.074	0.9972	8
Post-implantation	-0.505 ± 0.023	0.9989	8

Table 6.32: Table of calculated sensitivity values of O_2 calibrations (0-1200 µM) for CRCEs pre-implantation and post-implantation.

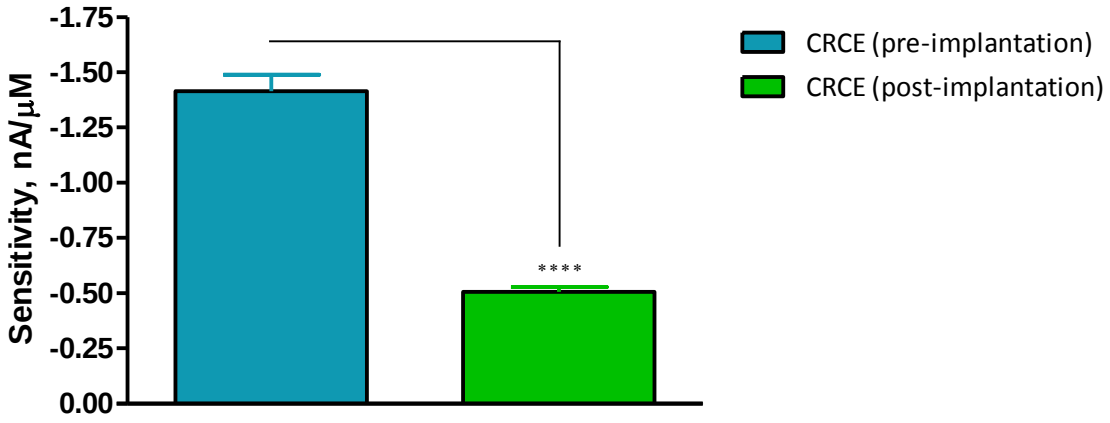

Figure 6.37: Graph of calculated sensitivity values for O_2 calibrations (0-1200 µM) for CRCEs pre-implantation and post-implantation (*n*=8).

Unpaired *t*-test statistical analysis was performed and it can be seen there is an extremely significant difference in the sensitivities between CRCEs calibrated pre and post-implantation with a *P* value < 0.0001.

From the results presented in it can be seen that the brain has detrimental effect on the sensitivity of the CRCEs to O_2. This decrease in sensitivity of 64.29 ± 1.60 % of the electrodes post-implantation compared to pre-implantation. This decrease is thought to be due to fouling at the electrode surface preventing O_2 from reaching the active surface of the electrode and example of which can be seen in Figure 6.38 .

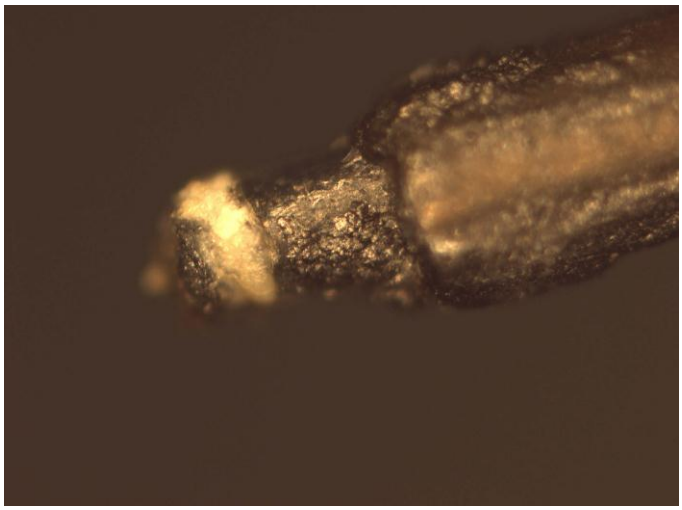

Figure 6.38: Image of a CRCE post-implantation demonstrating accumulation of tissue at active surface of the electrode.

6.3.4.12 Preliminary fMRI calibrations

Preliminary, acute *in vivo* experiments using the full fMRI CRCE were performed (see Section 7.3.6). During these experiments it was found that there was an issue with the background settling time. The permitted duration of these experiments were 2-3 hours and it was found that the background current was not sufficiently settled to accurately monitor changes in brain tissue O_2 (see Section 7.3.6). The settling time was not an issue for chronic *in vivo* experiments as the animals were allowed to recover overnight once connected to the recording equipment enabling the baseline to reach a steady-state. To allow for these acute *in vivo* experiments, alterations in the electrode's composition were investigated.

6.3.5 *fMRI compatible acute design*

To reduce the background current and minimise the settling time of the CRCEs, variations in the composite quantities were investigated. It was decided to increase the amount of carbon present and decrease the amount of Rhoplex® in the hope that a lesser amount of polymer present would increase the settling time and reduce any insulating effect that the polymer might have.

6.3.5.1 Silver based CRCEs acute designs

6.3.5.1.1 1:5 ratio of Rhoplex®:Carbon

Silver based CRCEs incorporating a 1:5 ratio of Rhoplex®:Carbon using 0.01g Rhoplex®/0.05g Carbon or 0.005g Rhoplex®/0.0125g Carbon were constructed as described in Section 3.4.2. The quantities were halved to ensure more accurate mixing of the composite. This method using silver wire was employed as discussed previously as a simpler way of determining the viability of the mixture for use in conjunction with the carbon fibre transducer. As there is a high carbon content and a small amount of binder, the use of a membrane in the form of nitrocellulose was investigated as a means of securing the composite in place. Nitrocellulose has been previously utilised with O_2 sensors (Dittmar *et al.*, 1997) as it is hydrophobic and allows for small charged ions and O_2 to permeate the membrane, acting as a barrier for larger organic molecules such as proteins. This barrier reduces the poisoning of the active surface of the electrode. O_2 calibrations on silver CRCEs were investigated. The mean background currents presented in Table 6.33 were subtracted.

	Mean Background I, nA (0 µM O_2)	**SEM**	***n***
Silver Rhoplex® (0.01g)/Carbon (0.05g)	-70.6	5.7	4
Silver Rhoplex® (0.005g)/Carbon (0.0125g)	-20.0	8.5	6
Silver Rhoplex® (0.005g)/Carbon (0.0125g), Nitrocellulose	-27.5	6.5	4
Silver Rhoplex® (0.005g)/Carbon (0.0125g), 10% Nitrocellulose	-19.7	4.1	4

Table 6.33: Table of results for mean background currents at 0 µM O_2 for Rhoplex®/Carbon silver composite electrodes with and without nitrocellulose. CPA performed at -650 mV *vs.* SCE in PBS (pH 7.4) at 21°C.

	Silver Rhoplex® (0.01g)/Carbon (0.05g) (*n*=4)		Silver Rhoplex® (0.005g)/Carbon (0.0125g) (*n*=6)		Silver Rhoplex® (0.005g)/Carbon (0.0125g), Nitrocellulose (*n*=4)		Silver Rhoplex® (0.005g)/Carbon (0.0125g), 10% Nitrocellulose (*n*=4)	
[O_2], µM	**Mean I, nA**	**SEM**	**Mean I, nA**	**SEM**	**Mean I, nA**	**SEM**	**Mean I, nA**	**SEM**
0	0	0	0	0	0	0	0	0
240	-910.7	38.0	-868.4	65.5	-582.0	48.3	-849.0	62.3
1200	-2962.0	119.6	-3193.0	180.1	-1885.8	150.8	-2955.6	179.5

Table 6.34: Table of results for O_2 calibrations (0-1200 µM) for Rhoplex®/Carbon silver composite electrodes with and without nitrocellulose. CPA performed at -650 mV *vs.* SCE in PBS (pH 7.4) at 21°C. Mean background subtracted.

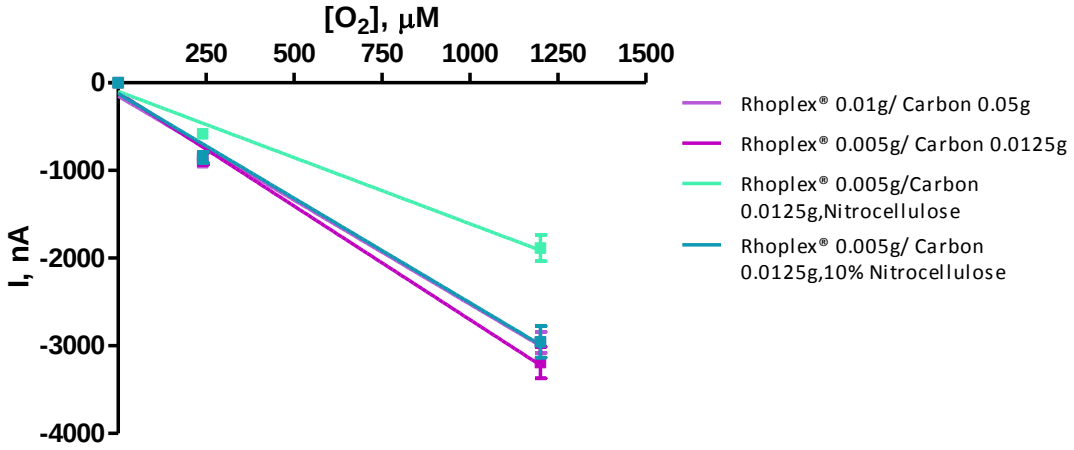

Figure 6.39: O_2 calibration data (0-1200 µM) for Silver Rhoplex® (0.01g)/Carbon (0.05g) (*n*=4), Silver Rhoplex® (0.005g)/Carbon (0.0125g) (*n*=6), Silver Rhoplex® (0.005g)/Carbon (0.0125g), Nitrocellulose (*n*=4), Silver Rhoplex® (0.005g)/Carbon (0.0125g), 10% Nitrocellulose (*n*=4). CPA performed at -650 mV *vs.* SCE in PBS (pH 7.4) at 21˚C.

	Sensitivity (nA/µM)	R^2	*n*
Silver Rhoplex® (0.01g)/Carbon (0.05g)	-2.374 ± 0.273	0.9869	4
Silver Rhoplex® (0.005g)/Carbon (0.0125g)	-2.592 ± 0.198	0.9942	6
Silver Rhoplex® (0.005g)/Carbon (0.0125g), Nitrocellulose	-1.511 ± 0.176	0.9866	4
Silver Rhoplex® (0.005g)/Carbon (0.0125g), 10% Nitrocellulose	-2.386 ± 0.222	0.9915	4

Table 6.35: Table of calculated sensitivity values of O_2 calibrations (0-1200 µM) for Rhoplex®/Carbon silver composite electrodes with and without nitrocellulose.

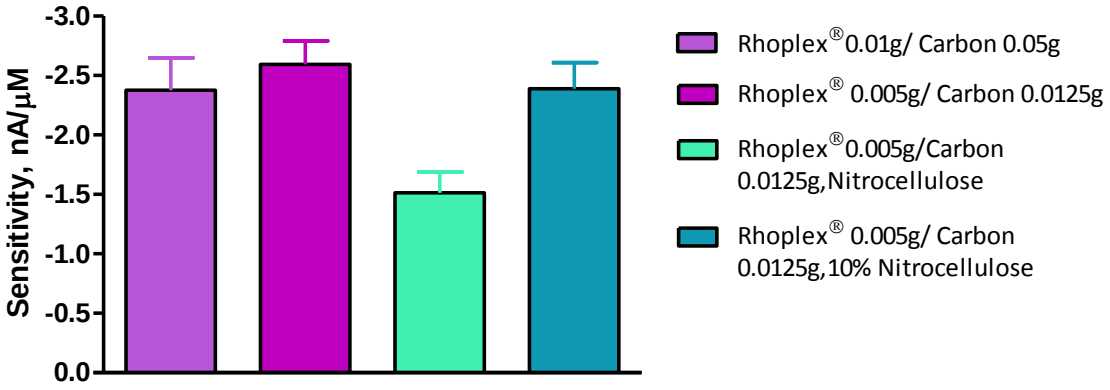

Figure 6.40: Graph of calculated sensitivity values for O_2 calibrations (0-1200 µM) for Silver Rhoplex® (0.01g)/Carbon (0.05g) (*n*=4), Silver Rhoplex® (0.005g)/Carbon (0.0125g) (*n*=6), Silver Rhoplex® (0.005g)/Carbon (0.0125g), Nitrocellulose (*n*=4), Silver Rhoplex® (0.005g)/Carbon (0.0125g), 10% Nitrocellulose (*n*=4).

It can be seen that there is improvement in sensitivity of the electrodes, presumably due to the higher carbon ratio of the composite. There is also a lower background current but this could be due to the silver wire as a transducer instead of carbon fibres. When the composites were constructed in combination with the fMRI design (CF transducer) the assembly of these electrodes was not achievable as the packing of the electrodes was not possible. The silver Rhoplex® (0.005g)/Carbon (0.0125g), nitrocellulose dipped electrodes had a lower sensitivity compared to the other designs (Table 6.35) this was due to the electrode being immersed in nitrocellulose which created a thick visible membrane on the electrode surface which had a negative effect on the sensitivity of the electrodes.

6.3.5.1.2 Rhoplex® (0.05g)/Carbon (0.03g) and Carbon paste composite electrodes (CRC/CPEs)

As the packing of the active surface of the electrode was an issue with a higher proportion of carbon, reported in Section 6.3.5.1.1, the original CRCE mixture (Rhoplex® (0.05g)/Carbon (0.03g)) was reassessed. The CF based electrode needs a glue-like mixture to ensure a good contact with the active surface as it cannot be packed with a silver wire traditionally used in CPEs. The composite was packed into the majority of the cavity of the

electrode and the end of the cavity (active surface) was packed using carbon paste. O_2 calibrations on silver CRC/CPEs were investigated. The mean background of -161.21 ± 98.12 nA (*n*=5) was subtracted.

	Silver CRC/CPEs (*n*=5)	
[O_2], µM	**Mean I, nA**	**SEM**
0	0	0
240	-343.8	38.8
1200	-1460.1	154.6

Table 6.36: Table of results for O_2 calibrations (0-1200 µM) for CRC/CP silver composite electrodes. CPA performed at -650 mV *vs.* SCE in PBS (pH 7.4) at 21°C. Mean background subtracted.

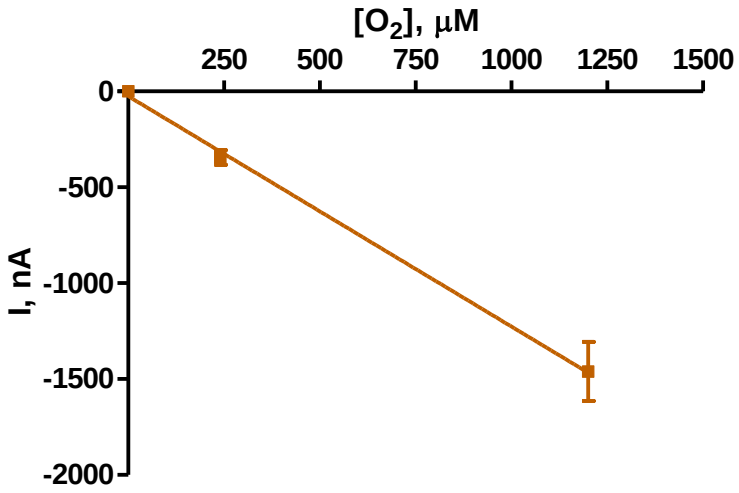

Figure 6.41: O_2 calibration data (0-1200 µM) for Silver CRC/CPEs (*n*=5). CPA performed at -650 mV *vs.* SCE in PBS (pH 7.4) at 21˚C.

Linear regression analysis shows that the electrodes have a sensitivity of -1.201 ± 0.045 nA/µM (*n*=5). The response was linear over the range with an R^2 value of 0.9986 (*n*=5).

As with the electrodes in Section 6.3.5.1.1 when the design was translated to the CF transducer the construction was not viable due to issues with the packing of the cavity of the electrode.

6.3.5.2 Liquid CPEs

As the attempts at constructing a reproducible fMRI compatible sensor with a rapid settling time were not successful using the composite mixtures previously employed in Section 6.3.4, a conductive, liquid carbon paste (SPI Supplies®) based electrode was investigated. The liquid carbon paste was utilised in conjunction with the full fMRI design to compare the sensitivities and background currents to the full fMRI CRCEs.

6.3.5.2.1 O_2 calibrations liquid CP full fMRI design

	Liquid carbon paste composite electrode (*n*=12)	
[O_2], µM	**Mean I, nA**	**SEM**
0	0	0
240	-402.5	29.8
1200	-1990.3	203.8

Table 6.37: Table of results for O_2 calibrations (0-1200 µM) for liquid CPEs full fMRI design. CPA performed at -650 mV *vs.* SCE in PBS (pH 7.4) at 21°C. Mean background subtracted.

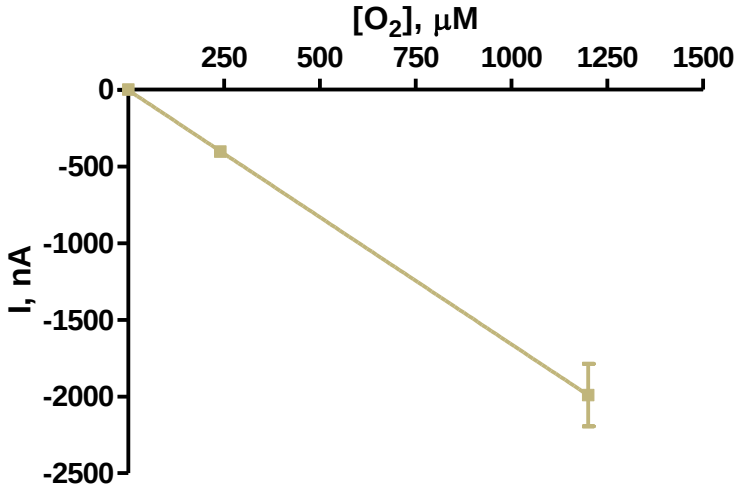

Figure 6.42: O_2 calibration data (0-1200 µM) for liquid CPEs full fMRI design (*n*=12). CPA performed at -650 mV *vs.* SCE in PBS (pH 7.4) at 21˚C.

Linear regression analysis shows that the electrodes have a sensitivity of -1.657 ± 0.004 nA/µM (*n*=12). The response was linear over the range with an R^2 value of 1.000 (*n*=12). From these results it can be concluded that the liquid CPEs can detect O_2 *in vitro* and that

the sensitivity was improved in comparison to the CRCEs full fMRI design (-0.953 ± 0.07 nA/µM (*n*=4)). The settling time for the background current was subsequently investigated.

6.3.5.2.2 CRCEs and liquid CPEs background settling time comparison

The background currents for CRCEs and liquid CPEs (full fMRI designs) were compared. The current (nA) was averaged for each electrode type settling in N_2 every 10 min for a duration of 50 min.

	CRCE full fMRI design (*n*=16)		**Liquid carbon paste full fMRI (*n*=12)**	
Time (mins)	**Mean I, nA**	**SEM**	**Mean I, nA**	**SEM**
0	-230.6	46.4	-327.1	59.2
10	-205.2	31.2	-285.6	43.7
20	-185.9	22.5	-933.4	80.1
30	-188.9	30.7	-688.1	55.8
40	-189.6	24.0	-2317.9	224.3
50	-199.5	23.7	-2426.2	203.5

Table 6.38: Table of results for mean background currents at 0 µM O_2 at 10 min intervals for 50 min for CRCEs full fMRI design and liquid CPEs full fMRI design. CPA performed at -650 mV *vs.* SCE in PBS (pH 7.4) at 21°C.

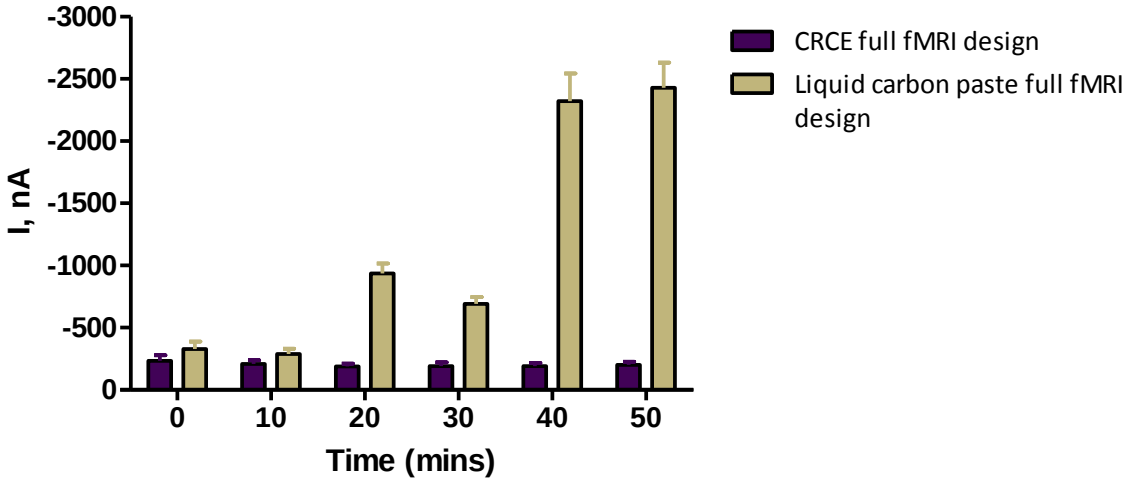

Figure 6.43: Mean background current data at 0 µM O_2 at 10 min intervals for a period of 50 min for CRCEs full fMRI design (*n*=16) and liquid CPEs full fMRI design (*n*=12).

It can be seen that the liquid CPEs background current increases instead of stabilising over 50 min. The CRCEs current decreases by -31.1 ± 22.7 nA over 50 min. From these results it was determined that the liquid CP was unsuitable for use in acute fMRI studies due to the background current being unstable.

6.4 Conclusions

This chapter examines the standardisation and use of metal free O_2 sensors based on a previous designs (Austin *et al.*, 2003; Lowry *et al.*, 2010) for use in conjunction with fMRI studies. The final design incorporating a carbon composite containing Rhoplex® (Section 6.3.4) was characterised *in vitro* to determine the sensitivity of the CRCEs to O_2 and the effects on the sensitivity following exposure to proteins, lipids and brain tissue (Section 6.3.4.5) The effects of temperature, pH, ions, and implantation were also examined. Due to issues with the background current settling times in preliminary acute experiments an alternative design for acute studies was investigated (Section 6.3.5).

From the results presented in this chapter it can be concluded that single carbon fibre bundles are not suitable for designing a reproducible sensor. With CRCEs it was found that the active surface requires drying against a flat surface and sensor construction with minimal heat exposure improved the sensitivity of the electrodes. It was found that the length of the electrode could be reduced approximately 5 times its original length and there was no significant reduction in the sensitivity. The CRCEs were found to be biocompatible with no significant reduction in the sensitivity following exposure to proteins, lipids and brain tissue. The physiological temperature (37°C) affects the CRCEs (Section 6.3.4.8) causing a large increase in sensitivity. Changes in pH did have an effect on the sensitivity, however changes in ions showed no significant effect. The effect of implantation of the sensors into the living brain indicated that implantation has a detrimental effect on the sensitivity of the CRCEs which is thought to be due to fouling of the active surface of the electrodes (Section 6.3.4.11). During preliminary acute *in vivo* experiments using the CRCE full fMRI design it was found that the electrodes background current did not reach a steady state quickly enough for experiments to take place. An fMRI compatible acute

design was explored with an attempt at minimising the settling time which was unsuccessful. The original CRCE design was found to be the superior design. It has previously been reported that the number of carbon fibre in a bundle has an effect on the resistance (Coeuret *et al.*, 2002) of the electrode. Future work for the acute fMRI sensor will involve elimination of the majority of the CF wire and pre-conditioning the sensors before the acute *in vivo* experiments by applying a potential to the electrodes overnight prior to the acute implantation. CRCEs can therefore be deemed suitable for use in chronic *in vivo* fMRI experiments for the detection of brain tissue O_2.

References

Austin V, Blamire A, Grieve S, O'Neill M, Styles P, Matthews P & Sibson N. (2003). Differences in the BOLD fMRI response to direct and indirect cortical stimulation in the rat. *Magnetic Resonance in Medicine* **49,** 838-847.

Bandettini PA, Wong EC, Hinks RS, Tikofsky RS & Hyde JS. (1992). Time course EPI of human brain function during task activation. *Magnetic Resonance in Medicine* **25,** 390-397.

Bazzu G, Puggioni GGM, Dedola S, Calia G, Rocchitta G, Migheli R, Desole MS, Lowry JP, O'Neill RD & Serra PA. (2009). Real-Time Monitoring of Brain Tissue Oxygen Using a Miniaturized Biotelemetric Device Implanted in Freely Moving Rats. *Analytical chemistry* **81,** 2235-2241.

Coeuret F, Vilar EO & Cavalcanti EB. (2002). Carbon fibre cloth as an electrode material: electrical conductivity and mass transfer. *Journal of Applied Electrochemistry* **32,** 1175-1182.

Dittmar A, Mangin S, Ruban C, Newman WH, Bowman HF, Dupuis V, Delhomme G, Shram NF, Cespuglio R, Jaffrezic-Renault N, Roussel P, Barbier D & Martelet C. (1997). *In vivo* and *in vitro* evaluation of specially designed gold and carbon fiber oxygen microelectrodes for living tissues. *Sensors and Actuators B: Chemical* **44,** 316-320.

Hitchman ML. (1978). Measurement of dissolved oxygen. *John Wiley and Sons, New York N Y 1978 255*.

Houston GC, Papadakis NG, Carpenter TA, Hall LD, Mukherjee B, James MF & Huang CLH. (2001). Mapping of brain activation in response to pharmacological agents using fMRI in the rat. *Magnetic Resonance Imaging* **19,** 905-919.

Jeroschewski P & Zur Linden D. (1997). A flow system for calibration of dissolved oxygen sensors. *Fresenius' Journal of Analytical Chemistry* **358,** 677-682.

Lowry JP, Griffin K, McHugh SB, Lowe AS, Tricklebank M & Sibson NR. (2010). Real-time electrochemical monitoring of brain tissue oxygen: a surrogate for functional magnetic resonance imaging in rodents. *NeuroImage* **52,** 549-555.

Ogawa S, Lee TM, Kay AR & Tank DW. (1990). Brain magnetic resonance imaging with contrast dependent on blood oxygenation. *Proceedings of the National Academy of Sciences* **87,** 9868-9872.

Ogawa S, Tank DW, Menon R, Ellermann JM, Kim SG, Merkle H & Ugurbil K. (1992). Intrinsic signal changes accompanying sensory stimulation: functional brain mapping with magnetic resonance imaging. *Proceedings of the National Academy of Sciences* **89,** 5951.

Ormonde DE & O'Neill RD. (1989). Altered response of carbon paste electrodes after contact with brain tissue: Implications for modified electrode use *in vivo*. *Journal of Electroanalytical Chemistry and Interfacial Electrochemistry* **261,** 463-469.

Ormonde DE & O'Neill RD. (1990). The oxidation of ascorbic acid at carbon paste electrodes: Modified response following contact with surfactant, lipid and brain tissue. *Journal of Electroanalytical Chemistry and Interfacial Electrochemistry* **279,** 109-121.

Preece M, Mukherjee B, Huang CLH, Hall LD, Leslie RA & James MF. (2001). Detection of pharmacologically mediated changes in cerebral activity by functional magnetic resonance imaging: the effects of sulpiride in the brain of the anaesthetised rat. *Brain Research* **916,** 107-114.

Taylor R & Humffray A. (1975). Electrochemical studies on glassy carbon electrodes:: III. Oxygen reduction in solutions of low pH (pH< 10). *Journal of Electroanalytical Chemistry and Interfacial Electrochemistry* **64,** 85-94.

Yang HH & McCreery RL. (2000). Elucidation of the mechanism of dioxygen reduction on metal-free carbon electrodes. *Journal of The Electrochemical Society* **147,** 3420-3428.

Zimmerman JB & Wightman RM. (1991). Simultaneous electrochemical measurements of oxygen and dopamine *in vivo*. *Analytical Chemsitry* **63,** 24-28.

7. RESULTS: AN *IN VIVO* CHARACTERISATION OF A CARBON-BASED COMPOSITE ELECTRODE FOR THE DETECTION OF BRAIN TISSUE O_2, SUITABLE FOR USE IN FMRI IMAGING STUDIES

7.1 Introduction

Carbon based composite electrodes have previously been used to detect brain tissue O_2 in freely-moving animals (Bazzu *et al.*, 2009). A metal free composite electrode containing Rhoplex® and graphite powder (CRCR) with a carbon fibre transducer, suitable for use in fMRI imaging studies was fabricated and characterised *in vitro* and presented in Chapter 6. It has been shown that BOLD fMRI and amperometric tissue O_2 data from rat cerebral cortex can be measured simultaneously using carbon fibre electrodes (Lowry *et al.*, 2010) verifying that real-time metabolic information can be acquired during fMRI investigations and that the changes in the magnitude of the BOLD response can be directly correlated to changes in tissue O_2 concentrations. This technique offers an alternative to fMRI experiments as the O_2 sensors can be used in freely-moving animals.

This chapter investigates and characterises the use of CRCEs for the detection of brain tissue O_2 in the striatum following on from the *in vitro* characterisation (Chapter 6) with the intention for use in conjunction with *in vivo* fMRI studies.

7.2 Experimental *In Vivo*

The instrumentation and software used are detailed in Section 3.2 and all chemicals and solutions are detailed in Section 3.3.

CRCEs (200 µm bare diameter) were constructed as described in Section 3.4.4. A potential of -650 mV *vs.* SCE was applied to the working electrodes and all experiments were performed on freely-moving Wistar rats. Full fMRI CRCEs were constructed as described in Section 3.4.3 and used for preliminary acute (non recoverable) experiments. A potential of -650 mV *vs.* SCE was applied to the working electrode implanted in the cortex and experiments were performed on an anesthetised Sprague Dawly rat.

In vivo procedures are detailed in Section 3.7. CRCEs were implanted in the striatum. The initial surgery contained bilateral CRCEs and a unilateral CPE in the left striatum for confirmation of the O_2 signal (results not presented).

Data is represented via the mean ± SEM where *n* = number of administrations, unless otherwise stated. Significant differences were calculated using two-tailed unpaired *t*-tests unless otherwise stated.

7.3 Results and Discussion

7.3.1 *Characterisation of CRCEs In Vivo*

7.3.2 *Gaseous Administrations*

7.3.2.1 Hyperoxia

Mild hyperoxia was achieved by administration of O_2 gas to the snout of the animal. The flow was maintained at a slow steady rate similar to the method used previously (Lowry *et al.*, 1998) and as described in Section 3.7.4. The inhalation of the O_2 gas for 3 minutes resulted in a change from baseline levels for the O_2 signals, monitored using CRCEs as can be seen in Figure 7.1 below.

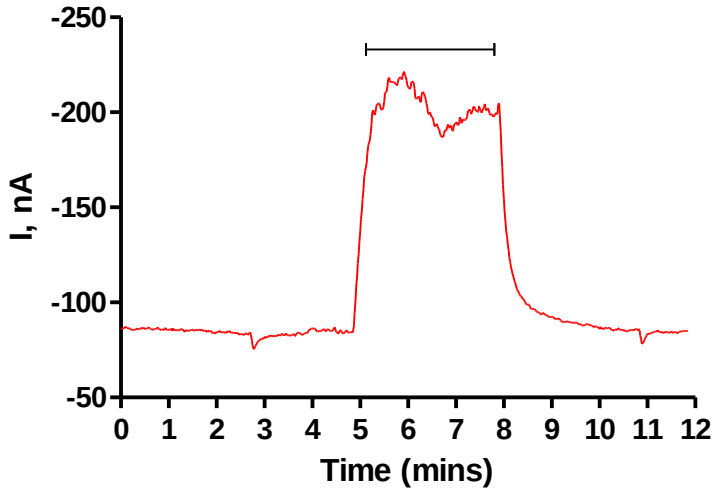

Figure 7.1: A typical example of a 3-min period of mild hyperoxia (administration of O_2 gas) monitored *in vivo* using a CRCE implanted in the striatum of a freely-moving rat. The bar indicates the period of gaseous administration.

A 3-min period of mild hyperoxia shows an average immediate increase in current from the baseline level of -72.20 ± 5.48 nA (*n*=23, 2 animals) to -107.96 ± 13.38 nA (*n*=23, 2

animals). This increase was found to be significant (P= 0.0195). The percentage increase was found to be 46.57 ± 11.88 % (n=23, 2 animals). Changes were immediate and on cessation of inhalation the signals quickly returned to baseline levels of -74.64 ± 5.83 nA after 8.13 ± 1.81 min (n =23, 2 animals) (P= 0.7619), indicating a rapid return to normoxic conditions. A summary of these results can be seen in Table 7.1.

Hyperoxia	
Baseline (nA)	-72.20 ± 5.48
Max Increase (nA)	-107.96 ± 13.38
% Increase	46.57 ± 11.88
Post-baseline (nA)	-74.64 ± 5.83
***t* to post-baseline (min)**	8.13 ± 1.81

Table 7.1: Summary of results for a 3-min period of mild hyperoxia monitored *in vivo* using CRCEs (*n* = 23, 2 animals), implanted in the striatum of freely-moving rats.

From these results it can be seen that there is a significant increase in striatal tissue O_2 upon administration of O_2 gas to the animal's snout and this change can be reliably monitored using CRCEs.

7.3.2.2 Hypoxia

Mild hypoxia was achieved by administration of N_2 gas to the snout of the animal. The flow was maintained at a slow steady rate similar to the method used previously (Lowry *et al.*, 1998) and as described in Section 3.7.4. The inhalation of the N_2 gas for 3 minutes resulted in a change from baseline levels for the O_2 signals, monitored using CRCEs as can be seen in Figure 7.2 below.

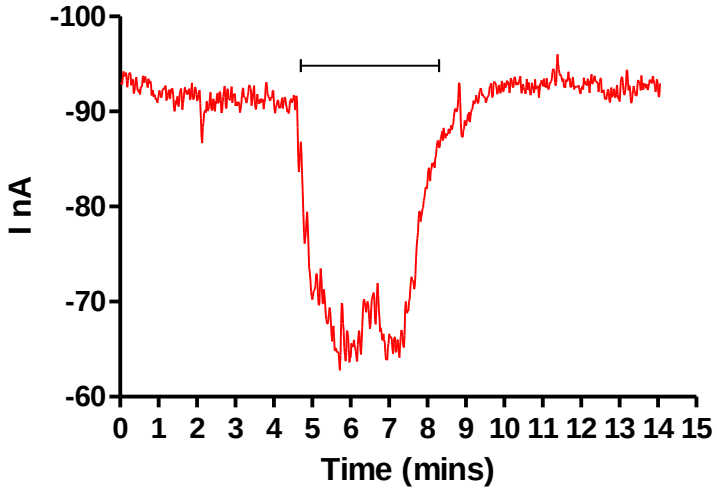

Figure 7.2: A typical example of a 3-min period of mild hypoxia (administration of N_2 gas) monitored *in vivo* using a CRCE implanted in the striatum of a freely-moving rat. The bar indicates the period of gaseous administration.

A 3-min period of mild hypoxia shows an average immediate decrease in current from the baseline level of -75.37 ± 6.22 nA (*n*=11, 2 animals) to -54.79 ± 4.98 nA (*n*=11, 2 animals). This decrease was found to be significant (*P* =0.0182). The percentage decrease was found to be 27.24 ± 3.19 % (*n*=11, 2 animals). Changes were immediate and on cessation of inhalation the signals quickly returned to baseline levels of -73.30 ± 5.88 nA after 4.86 ± 0.70 min (*n*=11, 2 animals) (*P*= 0.8115), indicating a rapid return to normoxic conditions. A summary of these results can be seen in Table 7.2.

Hypoxia	
Baseline (nA)	-75.37 ± 6.22
Max Decrease (nA)	-54.79 ± 4.98
% Decrease	27.24 ± 3.19
Post-baseline (nA)	-73.30 ± 5.88
***t* to post-baseline (min)**	4.86 ± 0.70

Table 7.2: Summary of results for a 3-min period of mild hypoxia monitored *in vivo* using CRCEs (*n* = 14, 2 animals), implanted in the striatum of freely-moving rats.

From these results it can be seen that there is a significant decrease in striatal tissue O_2 upon administration of N_2 gas to the animal's snout and this change can be reliably monitored using CRCEs.

7.3.3 *Neuronal Activation*

7.3.3.1 Tail pinch

Neuronal activation was stimulated physiologically by means of a tail pinch. A tail pinch induces a well characterised behaviour pattern consisting of gnawing, licking, eating and a general increase in the level of motor activity (Antelman *et al.*, 1975). The tail pinch was performed for a duration of 5 minutes similar to methods used previously (Bolger & Lowry, 2005) and as described in Section 3.7.5.1. Induced neuronal activation for 5 minutes resulted in a change from baseline levels for the O_2 signals, monitored using CRCEs as can be seen in Figure 7.3.

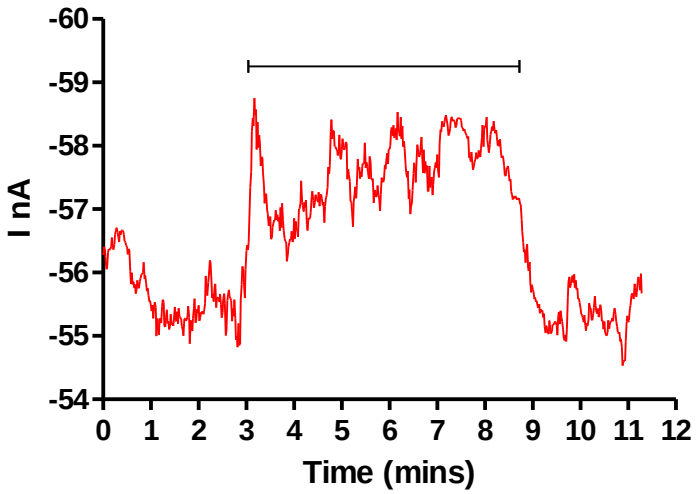

Figure 7.3: A typical example of a 5-min tail pinch (neuronal activation) monitored *in vivo* using a CRCE implanted in the striatum of a freely-moving rat. . The bar indicates the duration of the tail pinch.

A 5-min period of neuronal activation shows an average increase in current from a baseline level of -67.32 ± 10.80 nA (n=4, 2 animals) to -80.25 ± 10.38 nA (n=4, 2 animals) after

1.87 ± 0.93 min (P=0.4275). The percentage increase was found to be 21.79 ± 9.65 % (n=4, 2 animals). Upon cessation of the tail pinch, the current increased to -81.63 ± 10.01 nA (n=4, 2 animals) corresponding to a mean percentage increase of 24.62 ± 11.79 % (n=4, 2 animals) from baseline levels (P=0.3758). The post-tail pinch current returned to baseline levels of -77.87 ± 9.83 nA (n=4, 2 animals) after 15.59 ± 5.50 min. A summary of these results can be seen in Table 7.3.

Tail pinch	
Baseline (nA)	-67.32 ± 10.80
Max Increase (nA)	-80.25 ± 10.38
% Increase	21.79 ± 9.65
Post-baseline (nA)	-77.87 ± 9.83
***t* to post-baseline (min)**	15.59 ± 5.50

Table 7.3: Summary of results for a 5-min tail pinch monitored *in vivo* using CRCEs (n = 4, 2 animals), implanted in the striatum of freely-moving rats.

From these results it can be seen that there is a non significant increase in striatal tissue O2 with the tail pinch experiment. This is thought to be due to variations in the stress score between experiments and habituation of the animal to the tail pinch. Due to the lack of response from the tail pinch a restraint test was performed.

7.3.3.2 Restraint test

Neuronal activation was stimulated physiologically by means of a restraint test (Cloutier *et al.*, 2009). The animal was physically immobilised and the stress associated with freeing itself are associated with an increase in neuronal activation with an associated increase in blood flow. The restraint test was performed for a duration of 5 minutes as described in Section 3.7.5.2. Induced neuronal activation for 5 minutes resulted in a change from baseline levels for the O_2 signals, monitored using CRCEs as can be seen in Figure 7.4.

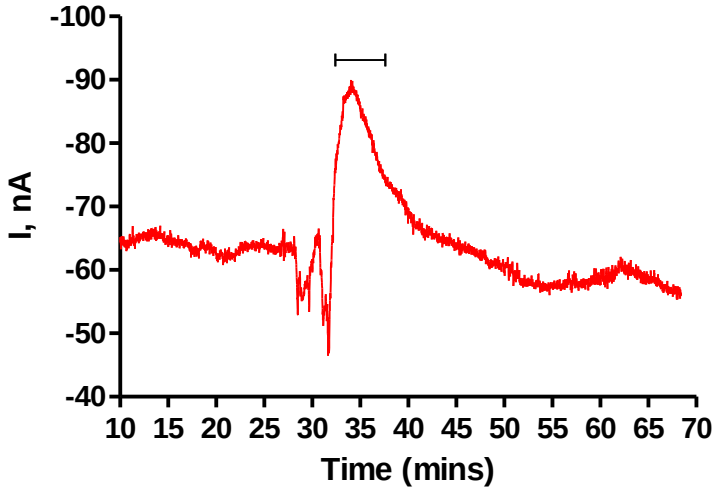

Figure 7.4: A typical example of a 5-min restraint test (neuronal activation) monitored *in vivo* using a CRCE implanted in the striatum of a freely-moving rat. The bar indicates the duration of the tail pinch.

A 5-min period of restraint shows an average increase in current from baseline level of -67.59 ± 7.48 nA (*n*=12, 2 animals) to -75.69 ± 8.35 nA (*n*=12, 2 animals) after 2.58 ± 0.49 min, representing a significant increase of 13.05 ± 4.63 % (*n*=12, 2 animals) compared to baseline levels (*P*=0.0015(paired *t*-test)). The current returned to baseline levels of -67.87 ± 7.44 nA (*n*=12, 2 animals) (*P*=0.9791) after 14.69 ± 3.60 min. The period following the cessation of the restraint shows a delay in returning to baseline levels. This sustained increase can be attributed to the animal grooming and to post-restraint stress/activation. A summary of these results can be seen in Table 7.4.

Restraint test	
Baseline (nA)	-67.59 ± 7.48
Max Increase (nA)	-75.69 ± 8.35
% Increase	13.05 ± 4.63
Post-baseline (nA)	-67.87 ± 7.44
***t* to post-baseline (min)**	14.69 ± 3.60

Table 7.4: : Summary of results for a 5-min restraint test monitored *in vivo* using CRCEs (*n* = 12, 2 animals), implanted in the striatum of freely-moving rats.

From these results it can be seen that there is a non significant increase in striatal tissue O_2 with the tail pinch experiment. This may be due to variations in the stress score between experiments (animals chewed for 2 mins on average) and habituation of the animal to the tail pinch. Due to the lack of response from the tail pinch a restraint test was performed.

7.3.4 *Drug Administration*

7.3.4.1 Effect of Acetazolamide

Acetazolamide (Diamox) is a carbonic anhydrase inhibitor and when administered systematically has been shown to increase brain tissue oxygen concentrations (Clark Jr & Lyons, 1965; Dixon *et al.*, 2002; Bolger & Lowry, 2005). Acetazolamide acts by inhibiting the carbonic anhydrase enzymes whose function is to catalyse the conversion of CO_2 and H_2O_2 to bicarbonate (HCO_3^-). This increase in CO_2 and a subsequent decrease in pH results in vasodilatation and an increase in tissue O_2. The vehicle used to administer Diamox intraperitoneally was DMSO which has been previously shown to have no long lasting effect on brain tissue O_2 (Section 5.3.4.2). The effect of acetazolamide on the O_2 signal, monitored with CRCEs can be seen in Figure 7.5 below.

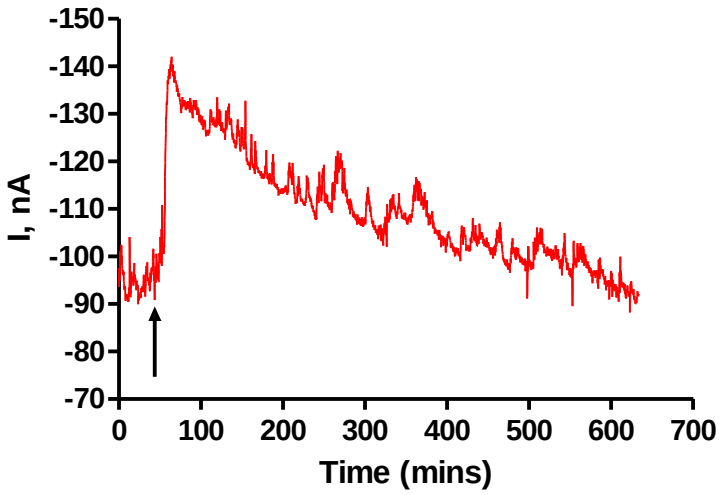

Figure 7.5: A typical example of an i.p. administration of Diamox (50 mg/kg) monitored *in vivo* using a CRCE implanted in the striatum of a freely-moving rat. The arrow indicates the point of injection.

An i.p. injection of Diamox shows an immediate sharp increase in the O_2 signal from average baseline levels of -75.36 ± 9.35 nA (*n*=6, 2 animals) to -90.04 ± 10.44 nA (*n*=5, 2 animals) after 48.60 ± 16.10 seconds, this sharp increase in current of 4.50 ± 1.35 % can be attributed to injection stress. The subsequent rapid decrease was followed by a sustained maximum increase in the O_2 signal to -120.87 ± 12.10 nA (*n*=5, 2 animals) after 28.98 ± 14.26 min, representing a significant increase of 41.62 ± 5.89 % (*n*=5, 2 animals) compared to baseline levels (*P*= 0.0206). The current returned to post-injection baseline levels of -78.20 ± 10.27 nA (*n*=5, 2 animals) (*P*= 0.8425) after 3.72 ± 0.87 hrs. A summary of these results can be seen in Table 7.5.

Diamox i.p.	
Baseline (nA)	-75.36 ± 9.35
Max Increase (nA)	-120.87 ± 12.10
***t* to max increase (min)**	28.98 ± 14.26
% Increase	41.62 ± 5.89
Post-baseline (nA)	-78.20 ± 10.27
***t* to post-baseline (hrs)**	3.72 ± 0.87

Table 7.5: Summary of results for i.p. administrations of Diamox (50mg/kg)) monitored *in vivo* using CRCEs (*n* = 5, 2 animals), implanted in the striatum of freely-moving rats.

From these results it can be seen that there is a significant increase in striatal tissue O_2 upon administration of Diamox (50 mg/kg) and this change can be reliably monitored using CRCEs.

7.3.5 *Effect of Anesthesia*

7.3.5.1 Chloral Hydrate

Chloral hydrate was amongst one of the first CNS depressants used in veterinary medicine. Chloral hydrate is metabolised by alcohol dehydrogenase to trichloroethanol and trichloroacetic acid (Butler, 1948). Although the precise mechanism is unknown (Sourkes, 1992), trichloroethanol is the active metabolite (Tao & Auerbach, 1994; Gauillard *et al.*, 2002) and it's thought its binding site is at the exogenous γ-aminobutyric acid (GABA)

receptor resulting in an influx of chloride ions causing it to potentiate the function of GABA in a way similar to that of barbitutes (Lovinger *et al.*, 1993).

Chloral hydrate has been previously used to increase brain tissue O_2 (Lowry & Fillenz, 2001; Bolger & Lowry, 2005). This increase in O_2 is thought to be due to an increase in rCBF. The vehicle used to administer chloral hydrate intraperitoneally was normal saline which has been previously shown to have no long lasting effect on brain tissue O_2 (Bolger & Lowry, 2005) and Section 5.3.4.1. The effect of chloral hydrate on the O_2 signal, monitored with CRCEs can be seen in Figure 7.6 below.

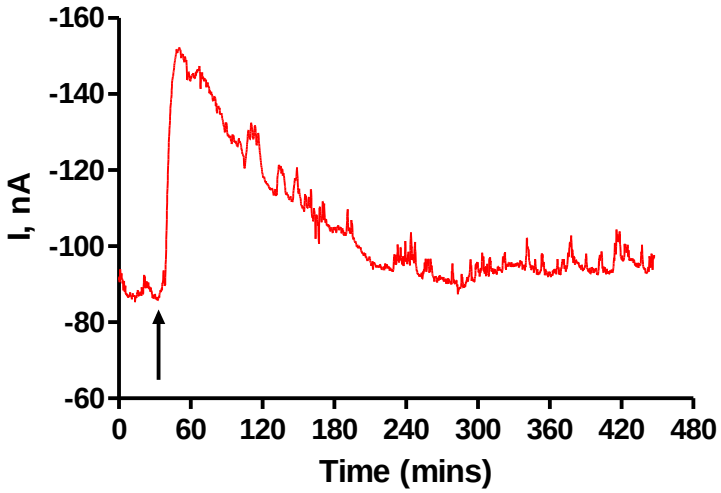

Figure 7.6: A typical example of an i.p. administration of chloral hydrate (350 mg/kg), monitored *in vivo* using a CRCE implanted in the striatum of a freely-moving rat. The arrow indicates the point of injection.

An i.p. injection of chloral hydrate shows an immediate increase in the O_2 signal from average baseline levels of -77.63 ± 11.27 nA (n=6, 2 animals) to -87.13 ± 8.70 nA (n=4, 2 animals) after 47.25 ± 12.60 seconds this increase in current of 6.34 ± 1.08 % can be attributed to injection stress. This initial increase rapidly decreases and there is a sustained maximum increase in the O_2 signal to -121.34 ± 10.68 nA (n=7, 2 animals) after 10.48 ± 1.01 min, representing a significant increase of 67.30 ± 15.16 % (n=7, 2 animals) compared to baseline levels (P=0.0183). The current returned to post- injection baseline levels of -77.13 ± 11.22 nA (n=6, 2 animals) (P= 0.9755) after 2.63 ± 0.32 hrs which corresponded to

when the animal was almost fully recovered from the anaesthetic. A summary of these results can be seen in Table 7.6.

Chloral Hydrate i.p.	
Baseline (nA)	-77.63 ± 11.27
Max Increase (nA)	-121.34 ± 10.68
***t* to max increase (min)**	10.48 ± 1.01
% Increase	67.30 ± 15.16
Post-baseline (nA)	-77.13 ± 11.22
***t* to post-baseline (hrs)**	2.63 ± 0.32

Table 7.6: Summary of results for i.p. administrations of chloral hydrate (350mg/kg) monitored *in vivo* using CRCEs, implanted in the striatum of freely-moving rats.

From these results it can be seen that there is a significant increase in striatal tissue O_2 upon administration of chloral hydrate (350 mg/kg) and this change can be reliably monitored using CRCEs.

7.3.6 *Preliminary acute in vivo experiment*

A preliminary, acute (non recovery) *in vivo* experiment using the full fMRI CRCE was performed in an anesthetised rat. It was found that there was an issue with the background settling time, presented in Table 7.7 and plotted in Figure 7.7.

	Time (min)	I, nA
Baseline	2.09	-579.7
Gains: potential reapplied		
20% O_2/ 80% N_2	6.16	-806.3
100% O_2	18.59	-1566.9
20% O_2/ 80% N_2	32.37	-1697.2
30% O_2/ 70% N_2	36.56	-1838.0
50% O_2/ 50% N_2	40.02	-1990.9
70% O_2/ 30% N_2	43.05	-2048.0
100% O_2	46.18	-2048.0
70% O_2/ 30% N_2	49.25	-2048.0
50% O_2/ 50% N_2	52.53	-2204.3
Gains: potential reapplied		
30% O_2/ 70% N_2	5.19	-2183.2
100% N_2	5.57	-2183.2
30% O_2/ 70% N_2	10.41	-2183.2
100% N_2	11.23	-2219.1
30% O_2/ 70% N_2	15.37	-2256.2
100% N_2	16.14	-2266.3
30% O_2/ 70% N_2	20.47	-2281.8
100% O_2	21.50	-2310.5
30% O_2/ 70% N_2	25.52	-2274.7
100% O_2	26.29	-2254.6
30% O_2/ 70% N_2	30.53	-2261.2
100% O_2	31.28	-2211.8
30% O_2/ 70% N_2	37.00	-2082.2
100% O_2	45.42	-2080.8
20% O_2/ 80% N_2	46.44	-2044.5

Table 7.7: Table of results for acute experiments for administration of varying O_2/N_2 %, monitored using CRCEs showing duration of experiment and I, nA.

The permitted duration of these experiments were 2 hours and it was found that the background current fluctuated during the experiment as the electrode was not sufficiently settled to accurately monitor changes in brain tissue O_2.

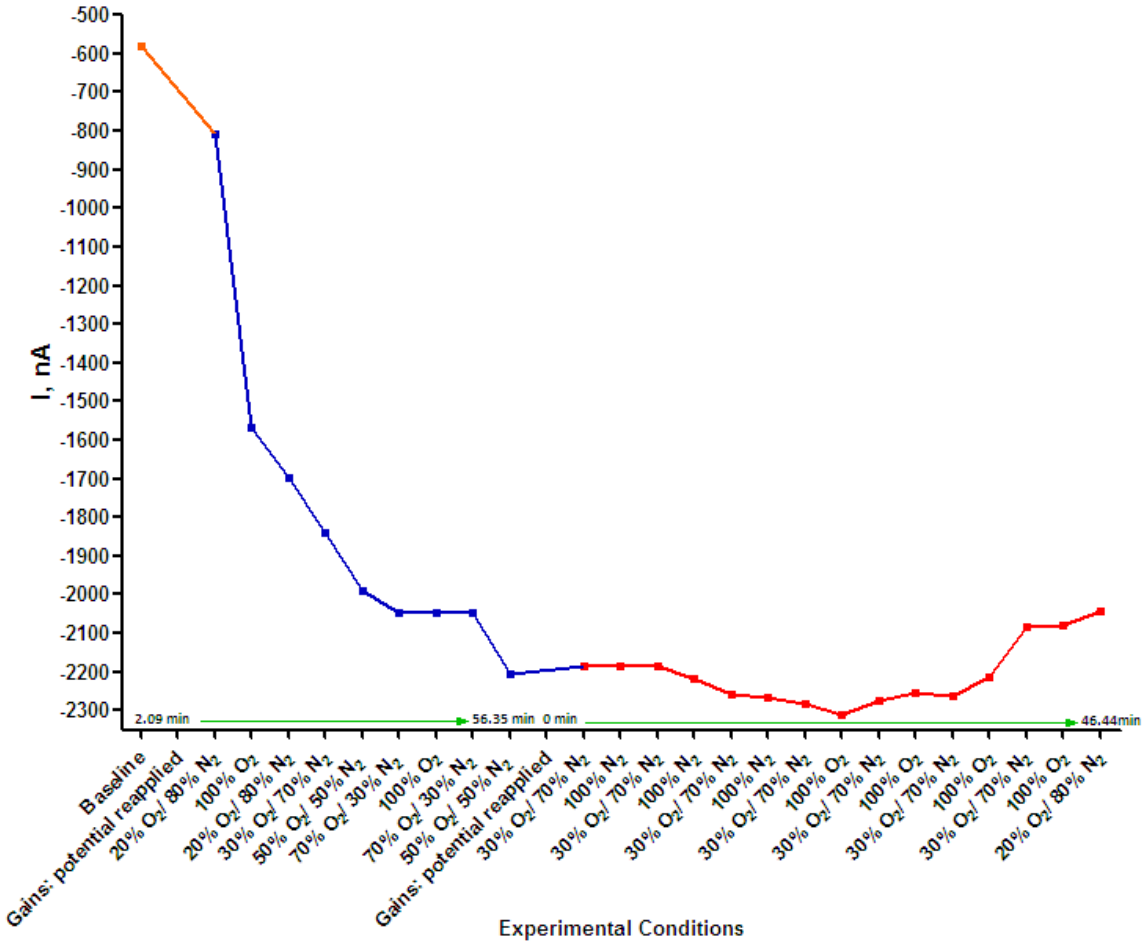

Figure 7.7: Data for an acute experiment performed with a CRCE implanted in the cortex of an anesthetised rat.

Future work for the acute application of the fMRI sensor will involve elimination of the majority of the CF wire and pre-conditioning the sensors before the acute *in vivo* experiments. By applying a potential to the electrodes overnight prior to the acute implantation it is hoped that the electrodes will settle far quicker. The experimental set-up for the acute experiments may also be an issue as the electrodes are not insulated from the experimental environment which may have a detrimental effect on the settling time.

7.4 Conclusions

A carbon-based composite electrode (CRCE) suitable for use in conjunction with fMRI studies has been characterised *in vitro* in the previous chapter (Chapter 6). A design intended for use in freely-moving animals (Section 6.3.4.4) was characterised *in vivo* using protocols employed previously by our group (Bolger & Lowry, 2005) and in this thesis (Chapter 5). A preliminary acute experiment using the CRCE full fMRI design was performed in an anesthetised animal.

Results presented in this chapter demonstrate that CRCEs (freely-moving design) have the ability to monitor changes in striatal $O_{2,}$ evidenced by response of the sensors to the administration of O_2 and N_2 gases to the snout of the animals. The changes in tissue O_2 following neuronal activation in the form of a restraint test as well as the administrations of acetazolamide and chloral hydrate have also been demonstrated. These results compare well to CPE data (Bolger & Lowry, 2005). It can therefore be concluded that CRCEs provide a viable alternative to metal electrodes to monitor brain tissue O_2 but do not offer any advantage in comparison to CPEs in terms of stability or biocompatibility. CRCEs are only suitable for short-term monitoring, established in Chapter 6 (Section 6.3.4.11) as there is a large reduction in sensitivity after 9 ± 2 days. The preliminary acute experiment using the CRCE full fMRI design performed in an anesthetised animal was not successful due to the background current not stabilising in time. An alternative design was investigated in Chapter 6, however the original CRCE proved to be the best design in terms of settling time (Section 6.3.5.2.2) therefore an elimination of the CF wire, pre-conditioning the electrodes and alterations to the acute experimental set-up are thought to be the remedy to this problem.

References

Antelman SM, Szechtman H, Chin P & Fisher AE. (1975). Tail pinch-induced eating, gnawing and licking behavior in rats: Dependence on the nigrostriatal dopamine system. *Brain Research* **99,** 319-337.

Bazzu G, Puggioni GGM, Dedola S, Calia G, Rocchitta G, Migheli R, Desole MS, Lowry JP, O'Neill RD & Serra PA. (2009). Real-Time Monitoring of Brain Tissue Oxygen Using a Miniaturized Biotelemetric Device Implanted in Freely Moving Rats. *Analytical chemistry* **81,** 2235-2241.

Bolger F & Lowry J. (2005). Brain Tissue Oxygen: *In Vivo* Monitoring with Carbon Paste Electrodes. *Sensors* **5,** 473-487.

Butler TC. (1948). The metabolic fate of chloral hydrate. *The Journal of Pharmacology and Experimental Therapeutics* **92,** 49-58.

Clark Jr L & Lyons C. (1965). Studies of a glassy carbon electrode for brain polarography with observations on the effect of carbonic anhydrase inhibition. *The Alabama Journal of Medical Sciences* **2,** 353.

Cloutier M, Bolger F, Lowry J & Wellstead P. (2009). An integrative dynamic model of brain energy metabolism using *in vivo* neurochemical measurements. *Journal of Computational Neuroscience* **27,** 391-414.

Dixon BM, Lowry JP & O'Neill RD. (2002). Characterization *in vitro* and *in vivo* of the oxygen dependence of an enzyme/polymer biosensor for monitoring brain glucose. *Journal of neuroscience methods* **119,** 135-142.

Gauillard J, Cheref S, Vacherontrystram MN & Martin JC. (2002). Chloral hydrate: a hypnotic best forgotten? *L'Encephale* **28,** 200-204.

Lovinger DM, Zimmerman SA, Levitin M, Jones MV & Harrison NL. (1993). Trichloroethanol potentiates synaptic transmission mediated by gamma-aminobutyric acidA receptors in hippocampal neurons. *Journal of Pharmacology and Experimental Therapeutics* **264,** 1097-1103.

Lowry JP, Demestre M & Fillenz M. (1998). Relation between Cerebral Blood Flow and Extracellular Glucose in Rat Striatum during Mild Hypoxia and Hyperoxia. *Developmental Neuroscience* **20,** 52-58.

Lowry JP & Fillenz M. (2001). Real-time monitoring of brain energy metabolism in vivo using microelectrochemical sensors: the effects of anesthesia. *Bioelectrochemistry* **54,** 39-47.

Lowry JP, Griffin K, McHugh SB, Lowe AS, Tricklebank M & Sibson NR. (2010). Real-time electrochemical monitoring of brain tissue oxygen: a surrogate for functional magnetic resonance imaging in rodents. *NeuroImage* **52,** 549-555.

Sourkes T. (1992). Early clinical neurochemistry of CNS-active drugs. *Molecular and Chemical Neuropathology* **17,** 21-30.

Tao R & Auerbach SB. (1994). Anesthetics block morphine-induced increases in serotonin release in rat CNS. *Synapse* **18,** 307-314.

8. RESULTS:
SIMULTANEOUS RECORDING OF HIPPOCAMPAL OXYGEN AND GLUCOSE IN FREELY-MOVING ANIMALS

8.1 Introduction

The hippocampus has been found to play essential roles in declarative memory (Scoville & Milner, 1957; Cohen *et al.*, 1999; Eacott & Easton, 2010), spatial navigation (O'Keefe & Nadel, 1978; Morris *et al.*, 1982; D'Hooge & De Deyn, 2001) and has been linked to various neurodegenerative/psychiatric disorders (Heckers & Konradi, 2010; Marlatt & Lucassen, 2010; Bast, 2011; Dhikav & Anand, 2011; Bonilha *et al.*, 2012).

Electrochemical sensors and biosensors have been previously utilised to detect brain tissue O_2 (Lowry *et al.*, 1996; Lowry *et al.*, 1997; Lowry & Fillenz, 2001; Bolger & Lowry, 2005; Bolger *et al.*, 2011) and glucose (Lowry *et al.*, 1994; Hu & Wilson, 1997; Fillenz & Lowry, 1998; Lowry *et al.*, 1998a; Lowry *et al.*, 1998b; Dixon *et al.*, 2002). Microelectrodes have been used to investigate O_2 and glucose in the hippocampus (Freund *et al.*, 1989; Hu & Wilson, 1997) whilst CPEs have been used to measure hippocampal O_2 during various behavioural tasks (McHugh *et al.*, 2011) but there have been few studies utilising sensors to measure hippocampal glucose as most research groups tend to employ microdialysis. There is a need for real-time sensor data to supplement the large amount of microdialysis data (McNay *et al.*, 2001; Gold, 2003; De Bundel *et al.*, 2009; López-Pérez *et al.*, 2012), electrophysiological data (Bliss & Lømo, 1973; Martin *et al.*, 2000; Morris *et al.*, 2003; Colgin & Moser, 2010) and molecular data from tissue samples (Gooney *et al.*, 2002; Minichiello, 2009; Barry & Commins, 2011) obtained from work in the hippocampus. There has been little work performed using sensors to measure basal levels of O_2 and glucose in the hippocampus or to determine how basic behavioural and pharmacological interventions can alter levels of these particular analytes. Therefore this chapter investigates and characterises the simultaneous measurements of tissue hippocampal O_2 and glucose in freely-moving rats using CPEs and Pt/PPD/GOx electrodes and how a maze task can alter the levels of this analytes.

8.2 Experimental

The instrumentation and software used are detailed in Section 3.2 and all chemicals and solutions are detailed in Section 3.3.

8.2.1 *In Vitro*

Pt/PPD/GOx disk electrodes (125 µm bare diameter) were constructed as described in Section 3.5.3.1. CPEs (200 µm bare diameter) were constructed as described in Section 3.4.1.

In vitro electrochemical experiments are detailed in Section 3.6.

Data is represented as the mean ± SEM where *n* = number of electrodes used, unless otherwise stated. The slope, nA/µM was obtained from O_2 calibration plots using linear regression analysis and is used to represent the sensitivity. Goodness of fit is denoted by the R^2 value. For enzymatic experiments calibration plots obeyed Michaelis-Menten Hill-type kinetics (Section 2.6.1). The kinetic parameter V_{max} was as an indication of sensitivity and the Hill coefficient (α) represents deviation from ideal Michaelis-Menten kinetics (α=1).

8.2.2 *In Vivo*

In vivo procedures are detailed in Section 3.7. Electrodes were implanted unilaterally in the dorsal hippocampus of Sprague Dawly rats. This strain of rat was also used for future behavioural experiments and to enable comparisons of basal concentrations to be directly compared to previous hippocampal data (McNay *et al.*, 2000).

Experimental data obtained was analysed in a different format to previous *in vivo* characterisation chapters with the focus here on time bins/points. This was to allow for comparisons with future microdialysis maze experiments. Data was either normalised to baseline levels for ease of comparison, or area under curve (AUC) analysis was performed to quantify any observed changes in the sensor signals for statistical analysis. For multiple

comparisons, repeated-measures and mixed-factorial analysis of variance tests (ANOVA) with Bonferroni *post-hoc* analysis were used as appropriate. Paired *t*-tests were also used when comparing results from two different time points. $P < 0.05$ was considered to be significant and all data is presented as the mean ± standard error of the mean (SEM).

8.3 Results

8.3.1 *In Vitro Pt/PPD/GOx*

A Pt-based glucose biosensor has been previously well characterised *in vitro* and *in vivo* (Lowry *et al.*, 1994; Fillenz & Lowry, 1998). The optimum enzyme batch and units of enzyme was investigated as over time, due to supplier availability, the batches of enzyme and units vary (Section 3.3.3). Below in Table 8.1 and plotted in Figure 8.1 is an example of a glucose calibration (0-100 µM) on Pt/PPD/GOx electrodes constructed using glucose oxidase obtained from Genzyme Chemical Co.

[Gluc], mM	Mean I, nA	SEM
0	0	0
1	0.25	0.02
5	1.12	0.07
10	1.98	0.12
15	2.59	0.16
20	3.18	0.21
30	4.27	0.33
50	5.32	0.49
80	5.95	0.60
100	5.93	0.60

Table 8.1: Table of results for glucose calibrations (0-100 mM) for Pt/PPD/GOx electrodes (*n*=4). CPA performed at +700 mV *vs.* SCE in PBS (pH 7.4) at 21˚C. Mean background (0.102 ± 0.002 nA (*n*=4)) subtracted.

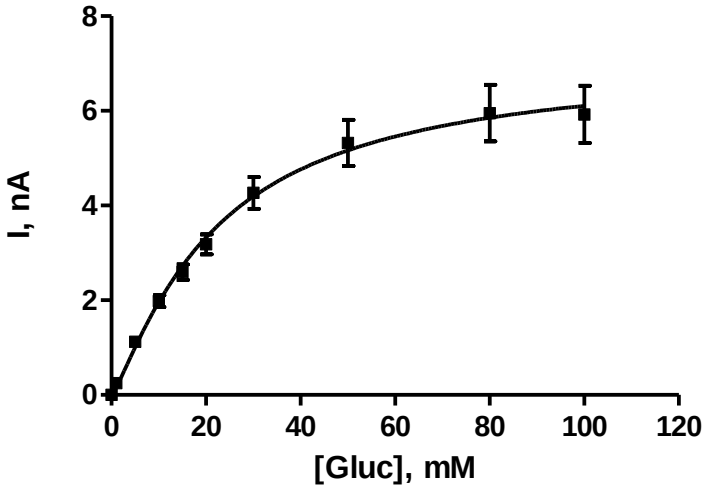

Figure 8.1: Glucose calibration data (0-100 mM) for Pt/PPD/GOx electrodes (*n*=4). CPA performed at +700 mV vs. SCE in PBS (pH 7.4) at 21˚C.

	Mean	SEM
V_{max}, nA	7.08	0.80
K_M, mM	22.13	5.35
α	1.21	0.24

Table 8.2: Michaelis Menten Hill-Type kinetic parameters for Pt/PPD/GOx electrodes.

It can be seen from the results presented above that the enzyme activity is very low as can be seen in the V_{max}. Similar results were observed for Glucose oxidase (Aspergillus Niger)-Sigma-Aldrich Co. and Glucose oxidase (G2133 50KU)-Sigma-Aldrich Co. However, Glucose oxidase (49180)-Sigma-Aldrich Co. proved to be successful in terms of exhibiting normal/expected sensitivity as can be seen from the results presented in Table 8.3.

[Gluc], mM	Mean I, nA	SEM
0	0	0
1	2.07	0.12
5	9.74	0.57
10	17.77	0.88
15	24.80	1.28
20	31.05	1.66
30	40.15	2.20
50	52.00	3.17
80	57.49	3.37
100	58.64	3.30

Table 8.3: Table of results for glucose calibrations (0-100 mM) for Pt/PPD/GOx electrodes (*n*=36). CPA performed at +700 mV *vs.* SCE in PBS (pH 7.4) at 21˚C. Mean background (0.232 ± 0.033 nA (*n*=36)) subtracted.

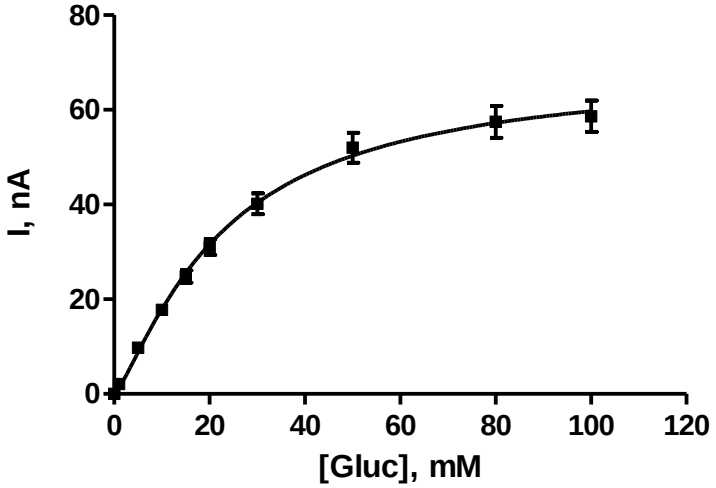

Figure 8.2: Glucose calibration data (0-100 mM) for Pt/PPD/GOx electrodes (*n*=36). CPA performed at +700 mV vs. SCE in PBS (pH 7.4) at 21˚C.

	Mean	SEM
$V_{max,}$ nA	68.80	5.05
$K_{M,}$ mM	22.76	3.46
α	1.27	0.16

Table 8.4: Michaelis Menten Hill-Type kinetic parameters for Pt/PPD/GOx electrodes.

It can be seen from the results presented above that the enzyme activity is high corresponding well with previously obtained results (Lowry *et al.*, 1994). The electrodes were also calibrated to verify that the PPD layer blocked out in interference caused by ascorbic acid (AA) (discussed in Section 2.7.4). Results for AA calibrations on Pt/PPD/GOx electrodes are presented below in Table 8.5 and plotted in Figure 8.3.

[AA], µM	Mean I, nA	SEM
0	0	0
200	0.32	0.02
400	0.46	0.03
600	0.54	0.03
800	0.50	0.05
1000	0.51	0.05

Table 8.5: Table of results for AA calibrations (0-1000 µM) for Pt/PPD/GOx electrodes (*n*=36). CPA performed at +700 mV *vs.* SCE in PBS (pH 7.4) at 21˚C. Mean background (0.329 ± 0.031 nA (*n*=36)) subtracted.

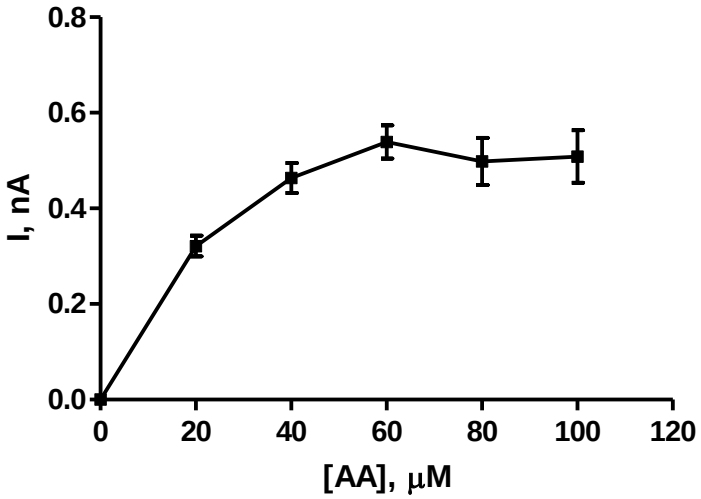

Figure 8.3: AA calibration data (0-1000 µM) for Pt/PPD/GOx electrodes (*n*=36). CPA performed at +700 mV *vs.* SCE in PBS (pH 7.4) at 21˚C.

From these results it can be determined that the PPD polymer layer on the electrode causes sufficient interference rejection of AA and that the enzyme is sensitive enough for the

detection of glucose *in vivo*. Therefore the Glucose oxidase (49180)-Sigma-Aldrich Co. batch of enzyme was used to construct the Pt/PPD/GOx electrodes used in this study.

8.3.2 *In Vitro CPE*

8.3.2.1 Pre-implantation calibrations

Average results obtained for O_2 calibrations (0-1200 µM) performed in PBS on CPEs (*n*=36) prior to implantation are presented below in Table 8.6 and plotted in Figure 8.4. The mean background current was subtracted.

$[O_2]$, µM	Mean I, nA	SEM
0	0	0
240	-287.1	8.1
1200	-1277.5	40.1

Table 8.6: Table of results for pre-implantation O_2 calibrations (0-1200 µM) for CPEs (*n*=35). CPA performed at -650 mV *vs.* SCE in PBS (pH 7.4) at 21˚C. Mean background (-7.65 ± 1.86 nA (*n*=35)) subtracted.

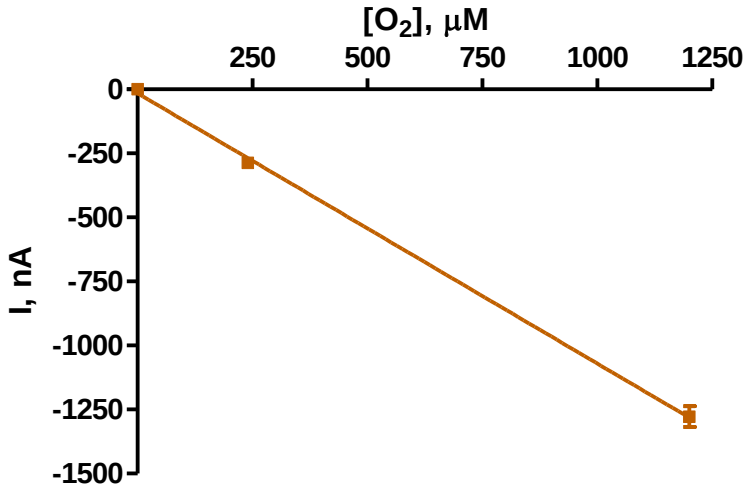

Figure 8.4: O_2 calibration data (0-1200 µM) for CPEs (*n*=35) pre-implantation. CPA performed at -650 mV *vs.* SCE in PBS (pH 7.4) at 21˚C.

Linear regression analysis shows that the electrodes have a sensitivity of -1.055 ± 0.027 nA/µM (*n*=35). The response was linear over the range with an R^2 value of 0.9993 (*n* =35).

8.3.2.2 Post-implantation calibrations

Average results obtained for O_2 calibrations (0-1200 µM) performed in PBS on CPEs (*n*=17) post-implantation are presented below in Table 8.7 and plotted in Figure 8.5. The mean background current was subtracted.

[O_2], µM	Mean I, nA	SEM
0	0	0
240	-311.4	13.5
1200	-1304.8	63.8

Table 8.7: Table of results for post-implantation O_2 calibrations (0-1200 µM) for CPEs (*n*=17). CPA performed at -650 mV *vs.* SCE in PBS (pH 7.4) at 21˚C. Mean background (-36.03 ± 13.85 (*n*=17)) subtracted.

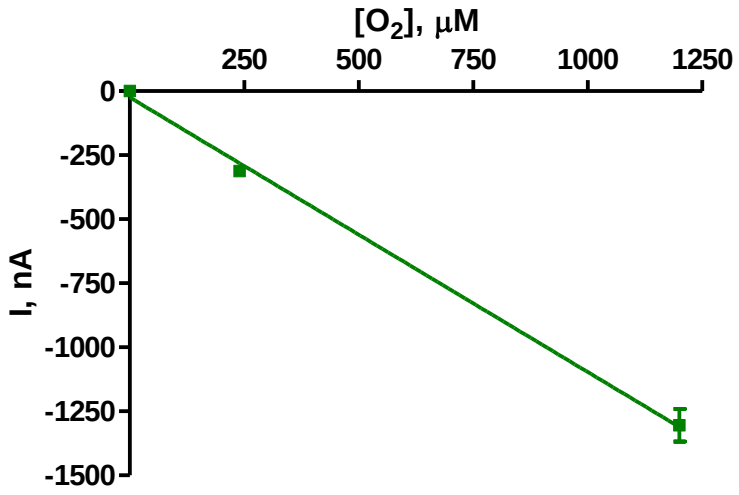

Figure 8.5: O_2 calibration data (0-1200 µM) for CPEs (*n*=17) post-implantation. CPA performed at -650 mV *vs.* SCE in PBS (pH 7.4) at 21˚C.

Linear regression analysis shows that the electrodes have a sensitivity of -1.072 ± 0.043 nA/µM (*n*=35). The response was linear over the range with an R^2 value of 0.9984 (*n*=17).

8.3.3 *In Vivo*

8.3.3.1 Gaseous Administrations

Mild hyperoxia and hypoxia were achieved by administration of O_2 and N_2 gas respectively to the snout of the animal. The flow was maintained at a slow steady rate similar to the method used previously (Lowry *et al.*, 1998a) (Bolger & Lowry, 2005) and as described in Section 3.7.4. The baseline period was taken as the 3 minutes prior to the beginning of the gas administration. The gaseous administration (O_2/N_2) was for a duration of 3 minutes and the post-baseline period was the 3 minutes following cessation of the gaseous administration. The data was split into 30 s time bins and all data were expressed as a percentage of baseline levels. AUC analysis was performed to determine the mean change from the baseline signal during each of the gaseous administrations, expressed as nA/min.

8.3.3.1.1 Hyperoxia

Administration of O_2 gas to the animals' snouts resulted in mild hyperoxia associated with an increase in hippocampal oxygen levels (n = 26, 9 animals) plotted below in Figure 8.6.

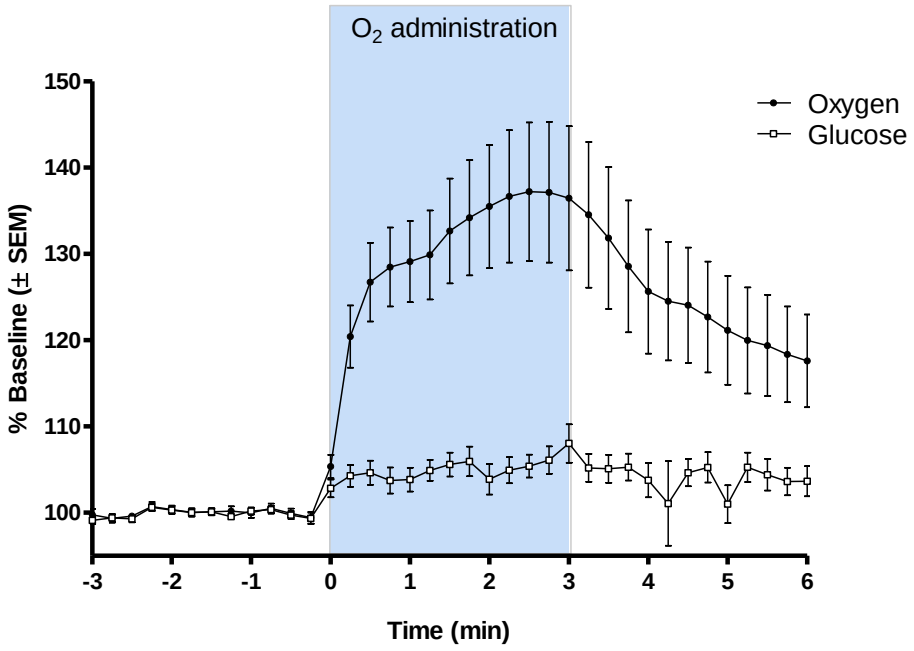

Figure 8.6: Effect of O_2 administration on hippocampal oxygen and glucose showing the mean changes in hippocampal oxygen (closed circles) and glucose (open squares) during a 3 min period of mild hyperoxia (blue box) with all data normalised to baseline levels.

Paired *t*-tests on the data analysed via AUC showed that hippocampal oxygen significantly increased by 67.37 nA.min (t = 4.353; df = 25; P < 0.001; Figure 8.7(A) and that hippocampal glucose also significantly increased at a rate of 0.0233 nA.min (t = 2.637; df = 25; P < 0.05; Figure 8.7(B) during the administration of O_2 gas compared to baseline levels.

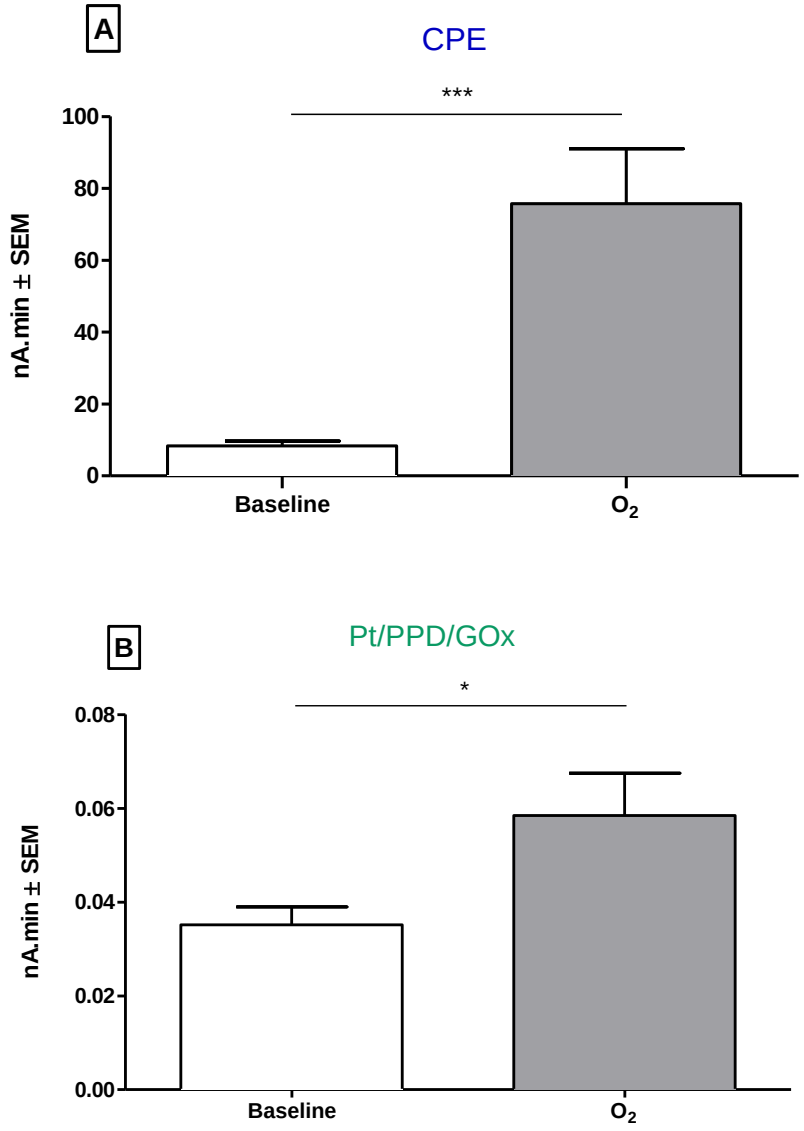

Figure 8.7: Effect of 3 min O_2 admin on hippocampal oxygen and glucose, showing the changes in area under the curve (AUC; nA.min) for (A) hippocampal oxygen (CPE) and (B) glucose (Pt/PPD/GOx).

Both analytes followed a similar time course after the end of the O_2 gas administration with hippocampal oxygen and glucose returning to baseline levels after 11.10 ± 1.35 min and 7.01 ± 1.25 min respectively.

8.3.3.1.2 Hypoxia

Administration of N_2 gas to the animals' snouts resulted in mild hypoxia associated with a decrease in hippocampal oxygen levels (*n*=23, 9 animals)) plotted below in Figure 8.8.

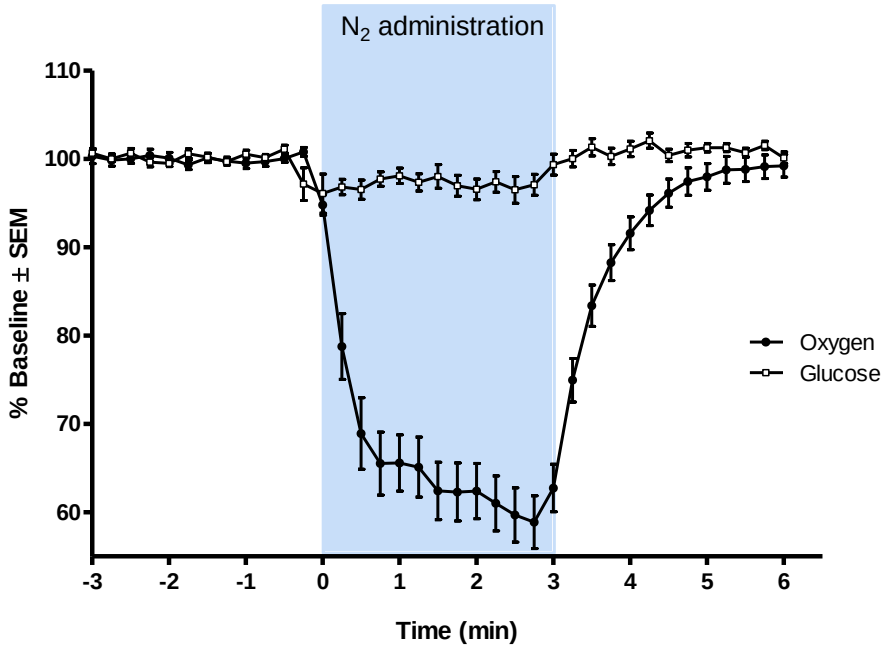

Figure 8.8: Effect of N_2 administration on hippocampal oxygen and glucose showing the mean changes in hippocampal oxygen (closed circles) and glucose (open squares) during a 3 min period of mild hypoxia (blue box) with all data normalised to baseline levels.

Paired *t*-tests on the data analysed via AUC showed that hippocampal oxygen significantly decreased by 77.20 nA.min (t = 9.628; df = 22; P < 0.001; Figure 8.9(A) but that there was no significant change in hippocampal glucose during the N_2 gas administration (t = 2.035; df = 22; P > 0.05; Figure 8.9(B) compared to baseline levels.

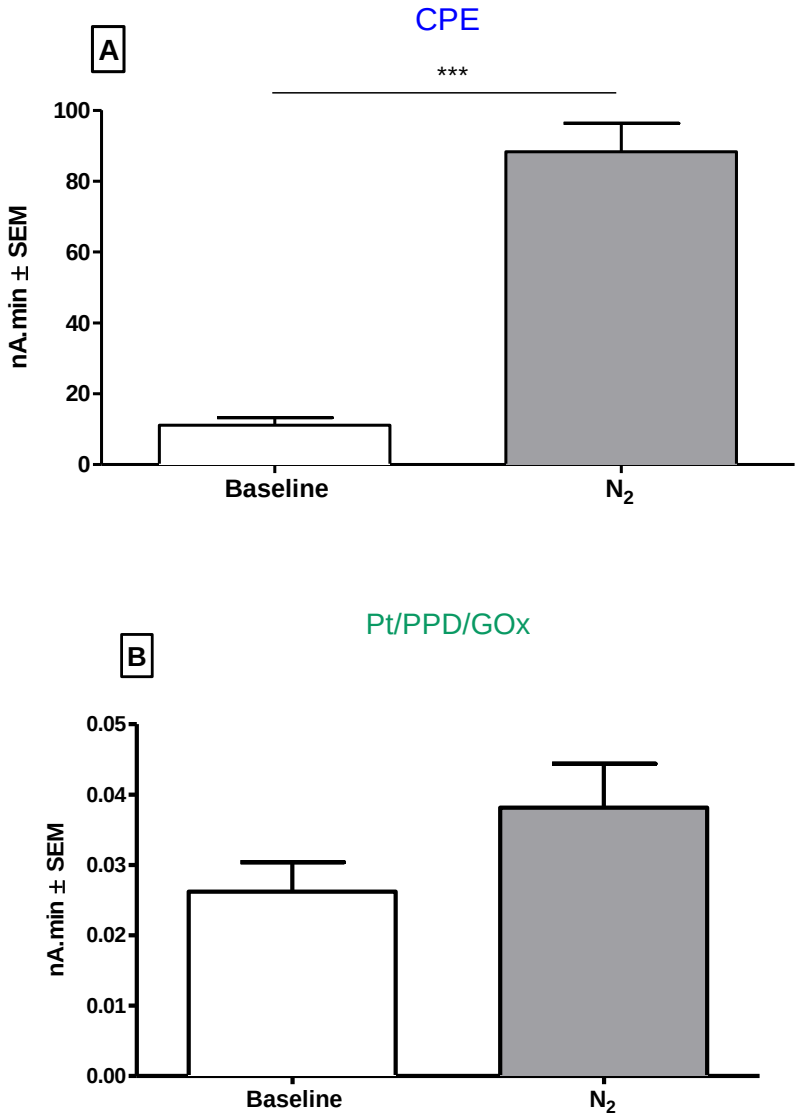

Figure 8.9: Effect of 3 min N_2 admin on hippocampal oxygen and glucose, showing the changes in area under the curve (AUC; nA.min) for (A) hippocampal oxygen (CPE) and (B) glucose (Pt/PPD/GOx).

Following the end of the N_2 gas administration, hippocampal oxygen levels returned to baseline levels after 8.09 ± 1.18 min. These results verify that CPEs respond rapidly to changes in hippocampal oxygen in response to different concentrations of inhaled oxygen.

8.3.3.2 Neuronal Activation

Neuronal activation was stimulated physiologically by means of a tail pinch (Section 3.7.5.1). A tail pinch induces a well characterised behaviour pattern consisting of gnawing, licking, eating and a general increase in the level of motor activity (Antelman *et al.*, 1975).

The tail pinch was performed for a duration of 5 minutes similar to methods used previously (Bolger & Lowry, 2005). As discussed in Section 7.3.3, the stress-score of the tail pinch and habituation to the experiment can have an effect on the response of the animal therefore neuronal activation was also stimulated physiologically by means of a restraint test (Section 3.7.5.2) (Cloutier *et al.*, 2009). The animal was physically immobilised and the stress associated with freeing itself are associated with an increase in neuronal activation with an associated increase in blood flow. The restraint test was performed for a duration of 5 minutes. Both paradigms were split into three time periods. The baseline period was taken as the 5 minutes prior to the beginning of the experiment, the neuronal activation period covered the 5 minutes of the actual experiment and post-baseline period covered the 5 minutes following the end of the experiment. The data was split into 30 s time bins and all data were expressed as a percentage of baseline levels for comparison. AUC analysis was performed on the raw data to determine the mean change from the baseline signal during each of the neuronal activation paradigms expressed as nA.min.

8.3.3.2.1 Tail pinch

Neuronal activation with an associated increase in rCBF from a tail pinch, resulted in an increase in hippocampal oxygen and glucose (n=14, 5 animals) plotted below in Figure 8.10.

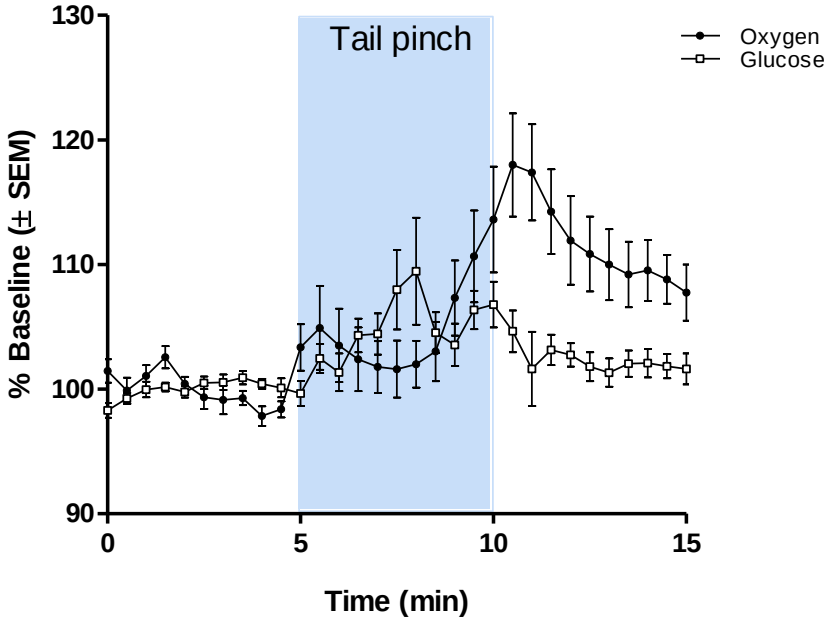

Figure 8.10: Effect of neuronal activation in the form of a tail pinch on hippocampal oxygen and glucose, showing the average changes in hippocampal oxygen (closed circles) and glucose (open squares) during a 5 min tail pinch (blue box) with all data normalised to baseline levels.

Paired *t*-tests on the data analysed via AUC showed that hippocampal oxygen significantly increased by 28.83 nA.min (t = 2.827; df = 13; P < 0.05;Figure 8.11(A)) and that hippocampal glucose also significantly increased at a rate of 0.1145 nA.min (t = 3.023; df = 13; P < 0.01; Figure 8.11(B)) during the tail pinch compared to baseline levels.

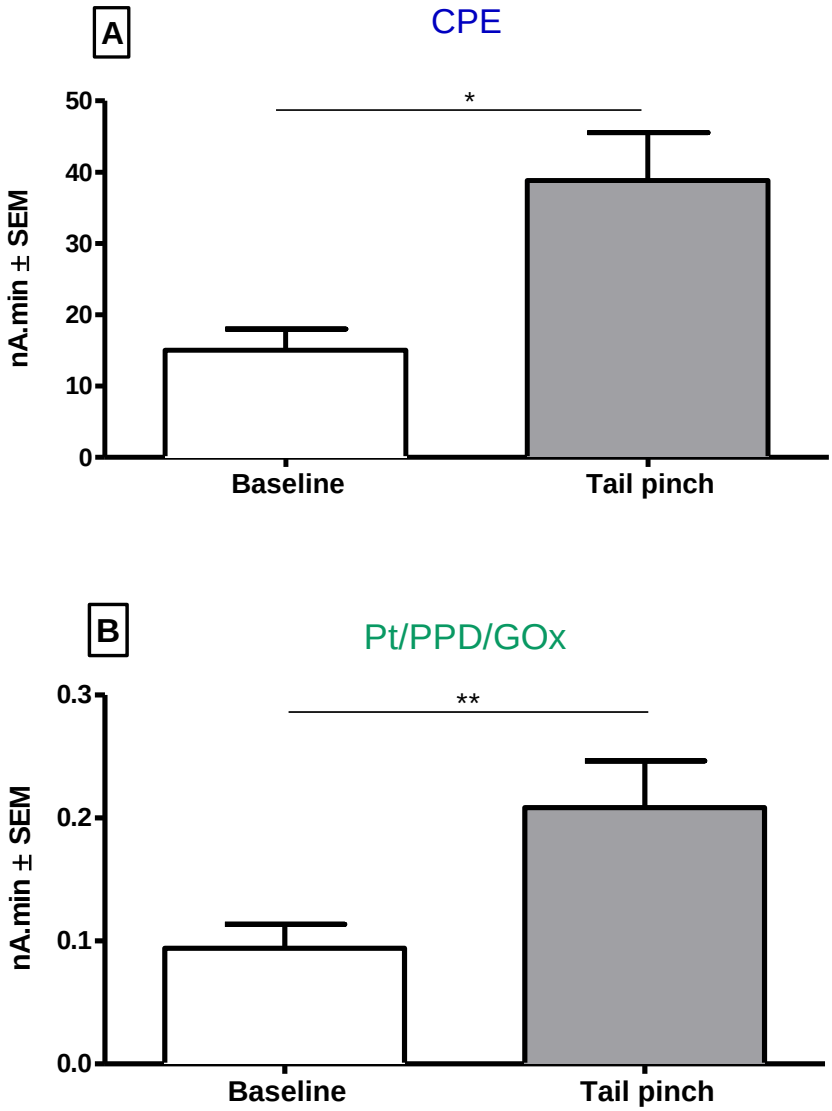

Figure 8.11: Effect of 5 min tail pinch on hippocampal oxygen and glucose, showing the changes in area under the curve (AUC; nA.min) for (A) hippocampal oxygen (CPE) and (B) glucose (Pt/PPD/GOx).

Both analytes followed a similar time course following the tail pinch with hippocampal oxygen and glucose returning to baseline levels after 17.20 ± 2.59 min and 17.98 ± 2.56 min respectively.

8.3.3.2.2 Restraint test

Neuronal activation with an associated increase in rCBF from a restraint test, resulted in an increase in hippocampal oxygen and glucose (n=13, 5 animals) plotted below in Figure 8.12.

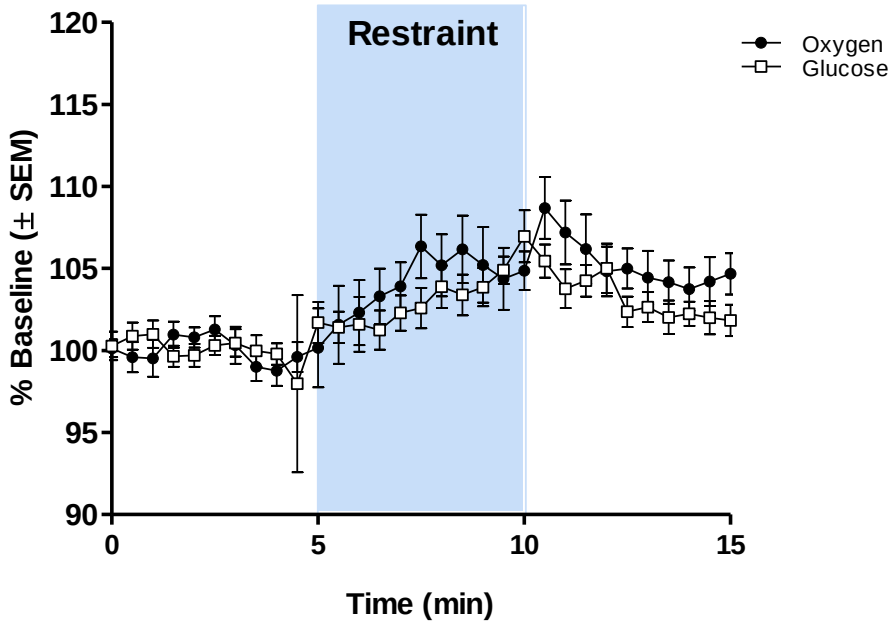

Figure 8.12: Effect of neuronal activation in the form of a restraint test on hippocampal oxygen and glucose, showing the average changes in hippocampal oxygen (closed circles) and glucose (open squares) during a 5 min restraint test (blue box) with all data normalised to baseline levels.

Paired *t*-tests on the data analysed via AUC showed that while hippocampal oxygen significantly increased at a rate of 32.13 nA.min (t = 2558; df = 12; P < 0.05; Figure 8.13(A)), the observed change in hippocampal glucose did not reach significance (t = 1.274; df = 12; P> 0.05; Figure 8.13(B)) during the restraint period compared to baseline levels.

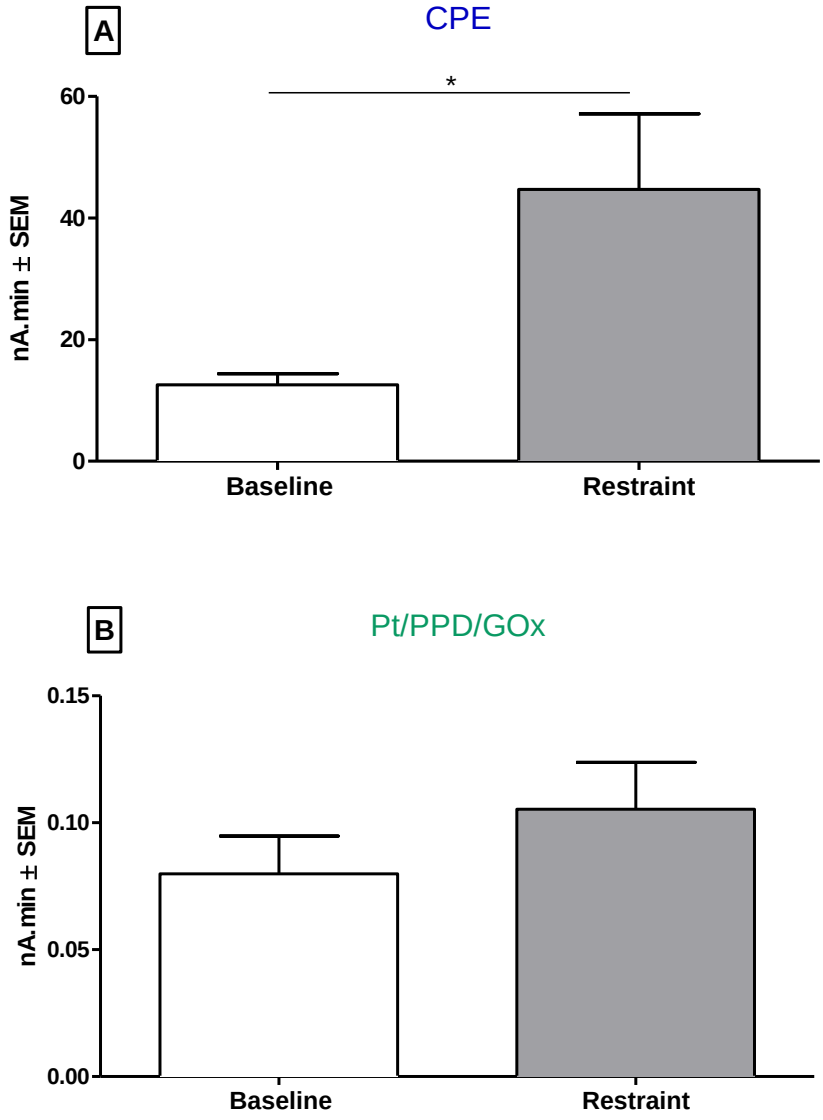

Figure 8.13: Effect of 5 min restraint test on hippocampal oxygen and glucose, showing the changes in area under the curve (AUC; nA.min) for (A) hippocampal oxygen (CPE) and (B) glucose (Pt/PPD/GOx).

Both analytes followed a similar time course after the period of restraint with hippocampal oxygen and glucose returning to baseline levels after 13.42 ± 1.97 min and 14.33 ± 2.43 min respectively.

8.3.3.3 Control Administrations

For control administrations (saline and DMSO) the baseline period was taken as the hour prior to the injection and data was collected for 10 hours following the injection. The data was split into 10 min time bins and all data were expressed as a percentage of baseline levels for visualisation and comparison.

8.3.3.3.1 Saline

Saline serves as a vehicle for drug administration so the effects of saline (0.9% NaCl) and the i.p. injection on hippocampal oxygen and glucose (*n*=6, 6 animals) are plotted below in Figure 8.14.

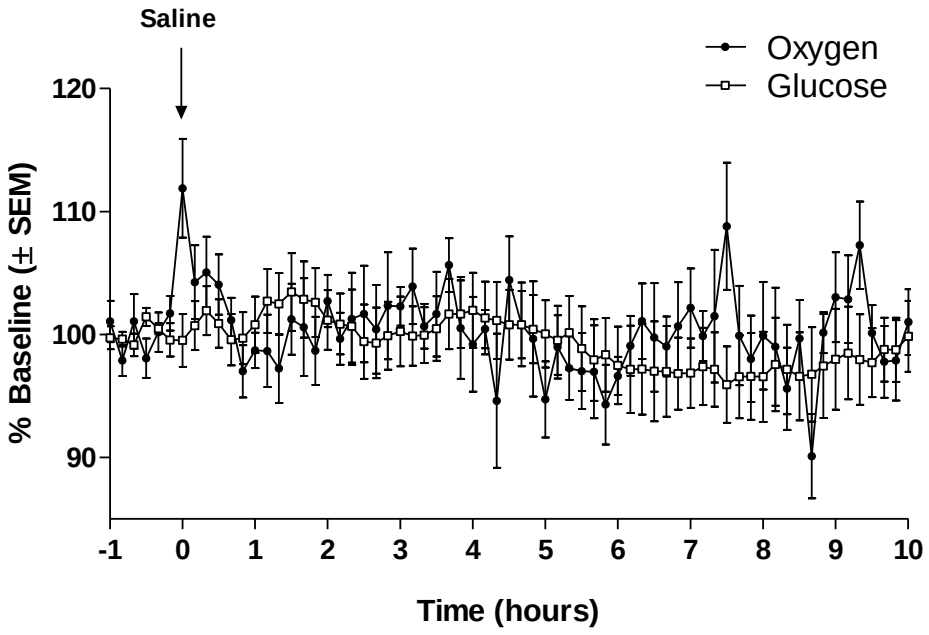

Figure 8.14: Effect of i.p. saline (0.9%) administrations on hippocampal oxygen (closed circles) and glucose (open squares). Injection is indicated by an arrow at time = 0 hours. All data expressed as a percentage of pre-injection baseline levels.

A repeated-measures ANOVA on the normalised data did not reveal any significant effect for saline treatment on hippocampal oxygen when compared to baseline (F = 1.153; df = 10; 50; $P > 0.05$). Similarly, there was no significant effect for saline treatment on

hippocampal glucose (F = 1.371; df = 10; 50; P > 0.05). However, there was a transient increase in hippocampal metabolism due to the injection stress. A paired t-test on the AUC-analysed data revealed a significant increase of 20.64 nA,min in hippocampal oxygen following the injection compared to baseline levels (t = 3.220; df = 5; P < 0.05) in the first 5 min post-injection. However, there was no such effect for injection stress on hippocampal glucose (t = 1.856; df = 5; P > 0.05). Saline treatment showed no significant long-term changes in hippocampal metabolism. It can therefore be concluded that any increase seen using saline as a vehicle for drug administrations is a drug effect.

8.3.3.3.2 DMSO

Acetazolamide (Diamox) does not dissolve easily in saline therefore a 33% solution of DMSO was used as a vehicle. Animals were treated with DMSO (33%) in order to act as a control for acetazolamide treatment. The effect of DMSO and the i.p. injection on hippocampal oxygen and glucose (n=6, 6 animals) are plotted below in Figure 8.15.

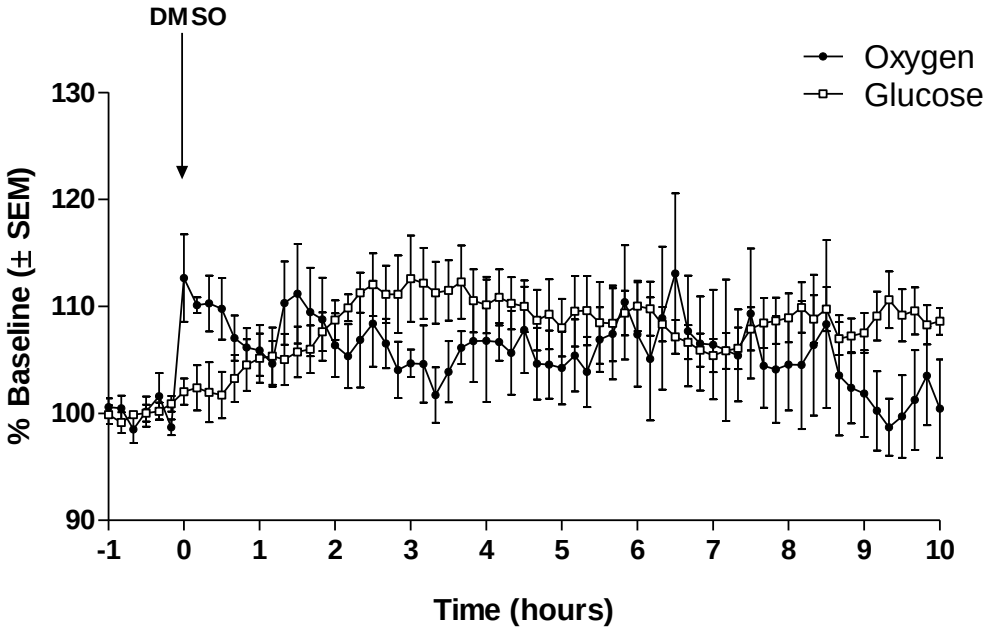

Figure 8.15: Effect of i.p. DMSO (33%) administrations on hippocampal oxygen (closed circles) and glucose (open squares). Injection is indicated by an arrow at time = 0 hours. All data expressed as a percentage of pre-injection baseline levels.

A repeated-measures ANOVA on the normalised data revealed that DMSO treatment had a significant effect on hippocampal oxygen (F = 2.124; df = 10; 50; P < 0.05) and on hippocampal glucose (F = 5.330; df = 10; 50; P < 0.001) when compared to baseline. Analysis on the normalised data suggests that DMSO treatment resulted in a significant increase in hippocampal metabolism. The increase in glucose levels began approximately 3 hours after the injection, the effects of this increase will be discussed in Section 8.3.3.4.

8.3.3.4 Drug Administration

8.3.3.4.1 Effect of Acetazolamide

Acetazolamide (Diamox) is a carbonic anhydrase inhibitor and when administered systematically has been shown to increase brain tissue oxygen concentrations (Clark Jr & Lyons, 1965; Dixon *et al.*, 2002; Bolger & Lowry, 2005). Acetazolamide acts by inhibiting the carbonic anhydrase enzymes whose function is to catalyse the conversion of CO_2 and H_2O_2 to bicarbonate (HCO_3^-). This increase in CO_2 and a subsequent decrease in pH results in vasodilatation and an increase in tissue O_2. It has been reported that acetazolamide has no effect on striatal glucose (Dixon *et al.*, 2002). The effect of acetazolamide on the hippocampal oxygen and glucose (n=6, 6 animals) are plotted below in Figure 8.16.

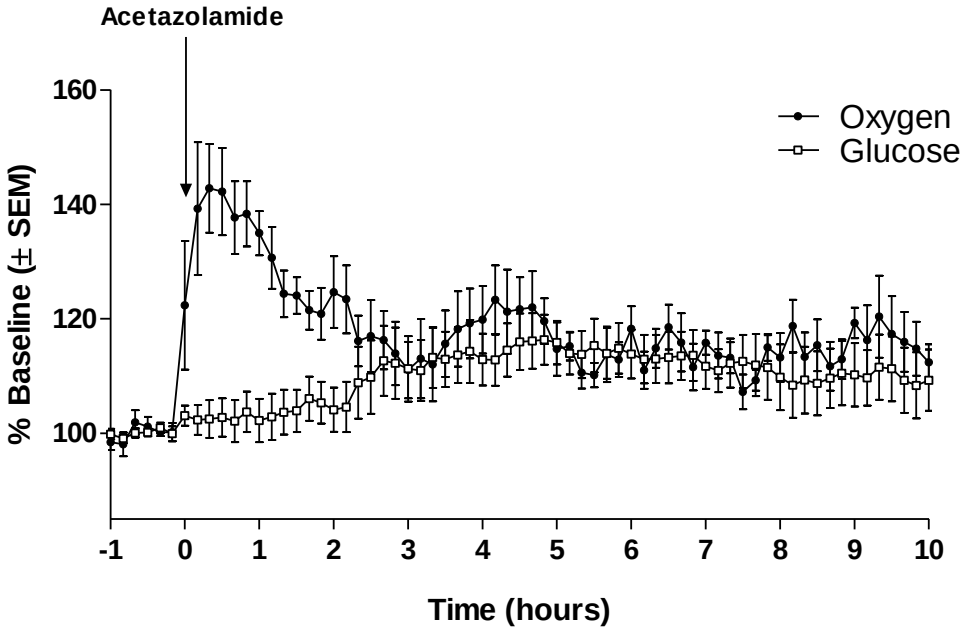

Figure 8.16: Effect of i.p. Diamox (50mg/kg) administrations on hippocampal oxygen (closed circles) and glucose (open squares). Injection is indicated by an arrow at time = 0 hours. All data expressed as a percentage of pre-injection baseline levels.

A repeated-measures ANOVA on the normalised data revealed that acetazolamide treatment had a significant effect on hippocampal oxygen (F = 7.626; df = 10; 50; P < 0.001) and on hippocampal glucose (F = 4.698; df = 10; 50; P < 0.001) when compared to baseline. We can thus conclude that acetazolamide administration had a significant effect on hippocampal metabolism.

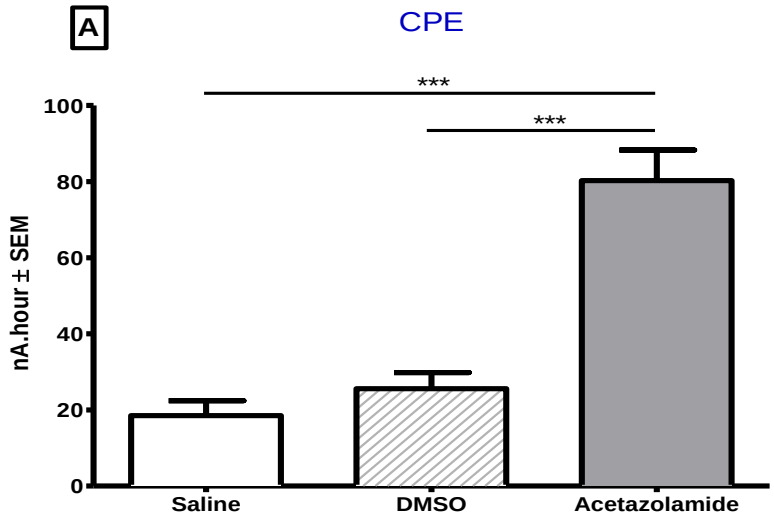

Figure 8.17: Effect of drug administrations on hippocampal oxygen (CPE), showing the changes in area under the curve (AUC; nA.hour) for hippocampal oxygen following DMSO and acetazolamide injections.

Comparing the effects of saline, DMSO and acetazolamide treatment on hippocampal oxygen, a 3 x 11 mixed factorial ANOVA with treatment (saline; DMSO; acetazolamide) as a between subject variable and time (baseline and hours 1-10 post-injection) as a within subject variable on the normalised data showed that there was a significant effect for treatment ($F = 11.82$; $df = 2, 15$; $P < 0.001$), time ($F = 7.90$; $df = 10, 150$; $p < 0.001$) as well as an interaction effect ($F = 3.69$; $df = 20, 150$; $P < 0.001$).

Compared to saline injections at the same time points (i.e. 0-3 hours post-injection), a one-way ANOVA on the AUC-analysed data showed that there was a significant effect for drug treatment on hippocampal oxygen ($F = 36.46$; $df = 2, 16$; $P < 0.001$;Figure 8.17). Bonferroni *post-hoc* analysis revealed that while there was no significant difference between saline- and DMSO-treated animals ($P > 0.05$), acetazolamide did have a significant effect on hippocampal oxygen. Acetazolamide treatment significantly increased hippocampal oxygen by 61.80 nA.hour compared to saline-treated animals ($P < 0.001$) and by 54.71 nA.hour compared to DMSO-treated animals ($P < 0.001$). It was found that administration of acetazolamide causes a rapid increase in hippocampal oxygen lasting for several hours.

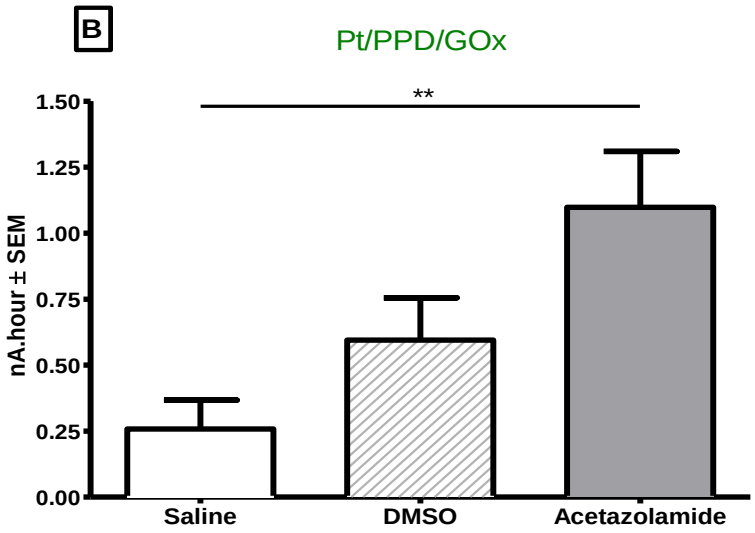

Figure 8.18: Effect of drug administrations on hippocampal glucose (Pt/PPD/GOx), showing the changes in area under the curve (AUC; nA.hour) for hippocampal glucose following DMSO and acetazolamide injections.

Comparing the effects of saline, DMSO and acetazolamide treatment on hippocampal glucose, a 3 x 11 mixed factorial ANOVA on the normalised data showed that there was a significant effect for treatment ($F = 3.75$; $df = 2, 15$; $P < 0.05$), time ($F = 6.05$; $df = 10, 150$; $P < 0.001$) as well as an interaction effect ($F = 3.00$; $df = 20, 150$; $P < 0.001$).

Compared to saline injections, a one-way ANOVA on the AUC-analysed data showed that there was a significant effect for drug treatment on hippocampal glucose ($F = 6.679$; $df = 2; 14$; $P < 0.01$;Figure 8.18). Bonferroni *post-hoc* analysis revealed that while there was no significant difference between saline- and DMSO-treated animals ($P > 0.05$), acetazolamide did have a significant effect on hippocampal glucose. Acetazolamide treatment significantly increases hippocampal glucose by 0.84 nA.hour compared to saline-treated animals ($P < 0.001$) but there was no significant difference between acetazolamide- and DMSO-treated animals ($P > 0.05$).

Analysis on the normalised data suggests that DMSO treatment resulted in a significant increase in hippocampal glucose levels beginning approximately 3 hours after the injection and this result was also found following acetazolamide treatment. As acetazolamide treatment in the absence of DMSO is not associated with any changes in striatal glucose

(Dixon *et al.*, 2002), this suggests that acetazolamide treatment itself has no effect on hippocampal glucose but the DMSO used as the vehicle does. There may be an interaction between the DMSO and acetazolamide as the AUC analysis showed that acetazolamide treatment significantly increased hippocampal glucose levels.

8.3.3.5 Effect of Anesthesia

Chloral hydrate has been previously used to increase brain tissue O_2 (Lowry & Fillenz, 2001; Bolger & Lowry, 2005). This increase in O_2 is thought to be due to an increase in rCBF. The effect of chloral hydrate on the hippocampal oxygen and glucose (*n*=6, 6 animals) is plotted below in Figure 8.19.

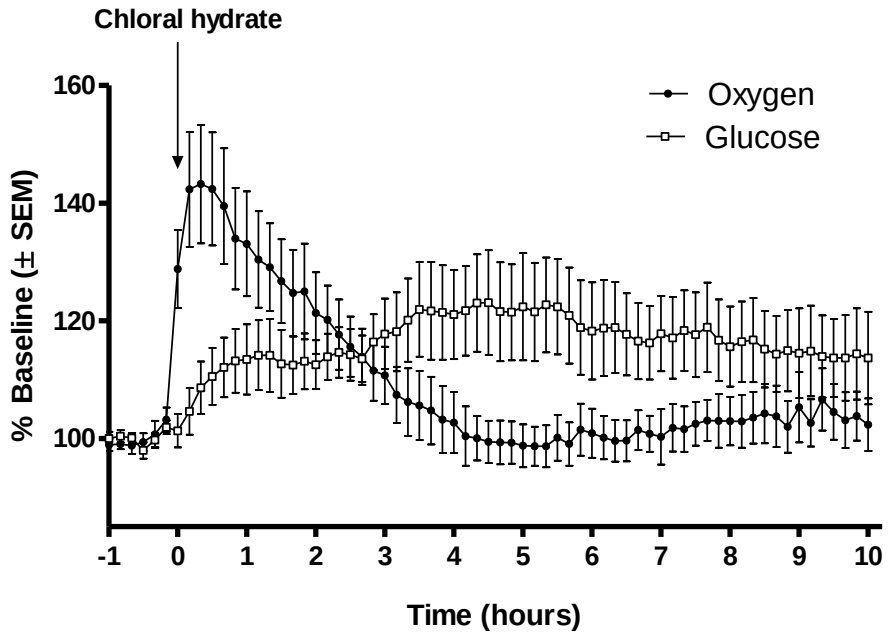

Figure 8.19: Effect of i.p. Chloral Hydrate (350mg/kg) administrations on hippocampal oxygen (closed circles) and glucose (open squares). Injection is indicated by an arrow at time = 0 hours. All data expressed as a percentage of pre-injection baseline levels.

A repeated-measures ANOVA on the normalised data revealed that chloral hydrate treatment had a significant effect on hippocampal oxygen when compared to baseline (F = 12.98; df = 10; 70; $P < 0.001$) and on hippocampal glucose when compared to baseline (F = 4.696; df = 10; 70; $P < 0.001$).

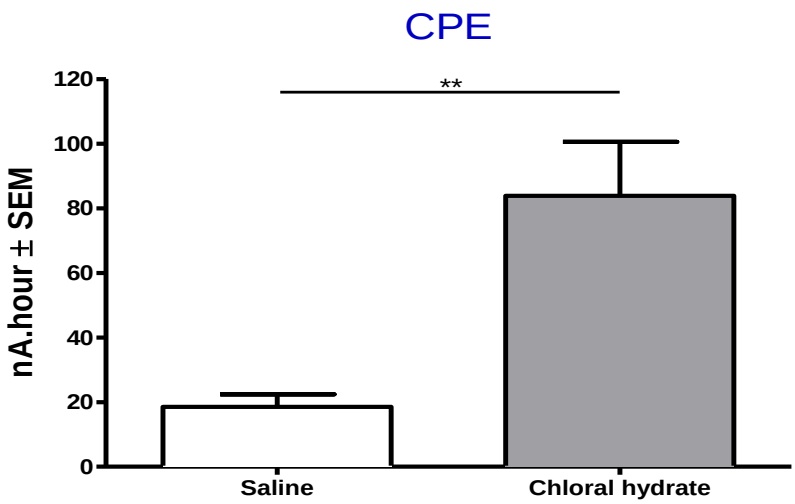

Figure 8.20: Effect of control and anaesthetic administrations on hippocampal oxygen (CPE), showing the changes in area under the curve (AUC; nA.hour) for hippocampal oxygen following saline and chloral hydrate injections.

Comparing the effects of saline and chloral hydrate treatment on hippocampal oxygen, a 2 x 11 mixed factorial ANOVA with treatment (saline; chloral hydrate) as a between subject variable, and time (baseline and hours 1-10 post-injection) as a within subject variable on the normalised data showed that there was no overall significant effect for treatment when compared to the saline-treated group ($F = 3.539$; $df = 1, 120$; $P > 0.05$). However, there was a significant effect for time ($F = 9.661$; $df = 10, 120$; $p < 0.001$) and a significant interaction effect ($F = 7.121$; $df = 10, 120$; $P < 0.001$).

Compared to saline injections at the same time points (0-3 hours post-injection), an unpaired *t*-test on the AUC-analysed data revealed that there was a significant increase in hippocampal oxygen of 65.36 ± 18.33 nA.min compared to baseline ($t = 3.565$; $df = 13$; $P < 0.01$; Figure 8.20).

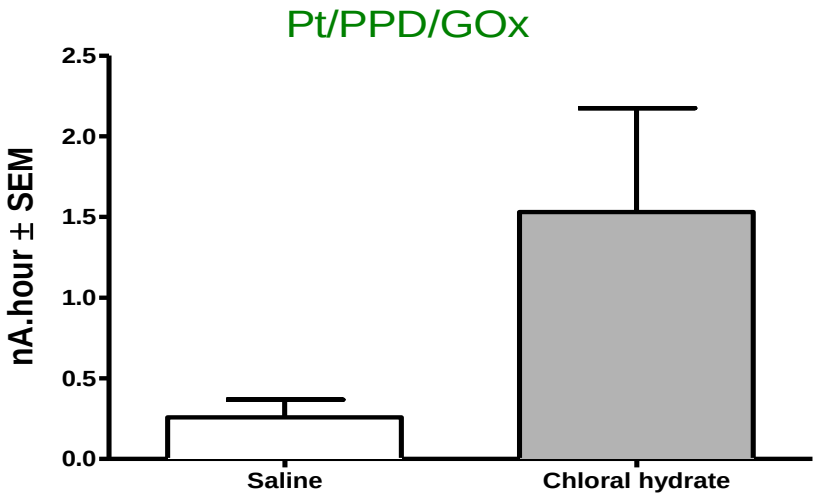

Figure 8.21: Effect of control and anaesthetic administrations on hippocampal glucose (Pt/PPD/GOx), showing the changes in area under the curve (AUC; nA.hour) for hippocampal glucose following saline and chloral hydrate injections.

Comparing the effects of saline and chloral hydrate treatment on hippocampal glucose, a 2 x 11 mixed factorial ANOVA with treatment (saline; chloral hydrate) as a between subject variable, and time (baseline and hours 1-10 post-injection) as a within subject variable on the normalised data showed that there was a significant effect for treatment (F = 4.894; df = 1, 120; P< 0.05), a significant effect for time (F = 2.964; df = 10, 120; P < 0.01) and a significant interaction effect (F = 3.512; df = 10, 120; P < 0.001). An unpaired t-test on the AUC-analysed data revealed that there was a non-significant increase of 1.12 ± 0.68 nA/min in hippocampal glucose (0-10 hours post-injection) compared to baseline (t = 1.801; df = 11; P > 0.05; Figure 8.21).

8.3.3.6 Basal concentrations of oxygen and glucose in the hippocampus

Caution needs to be applied when using *in vitro* electrode calibration data to estimate *in vivo* concentrations. This is primarily because of the differences between a free solution and a tissue matrix; factors such as capacitance current, diffusion, sensitivity, etc. need to be considered. However, it can be useful to estimate concentration data and with this in mind two time points were selected from each rat (n=10) on the second day of recording (one in the day, one in the night) in order to determine extracellular concentrations for comparisons

with previously reported work. The second day was chosen to allow time for sensors to settle and to allow for the expected post-implantation drop in sensitivity for biosensors (Hu *et al.*, 1994) and so that baseline levels were determined prior to any experimental interventions. The baseline current values were matched to the post-implantation calibration data for the CPE (average sensitivity to oxygen = -1.072 nA/µM) and the pre-implantation calibration data for Pt/PPD/GOx (average sensitivity to glucose = 1.560 nA/mM) as post-implantation calibration data is not available for Pt/PPD/GOx as the GOx component is lost during the explant procedure (Lowry *et al.*, 2002). It was determined that the basal oxygen concentration in the hippocampus is 100.26 ± 5.76 µM during the day and 99.37 ± 5.51 µM during the night. It was determined that the basal glucose concentration in the hippocampus is 0.60 ± 0.06 mM during the day and 0.57 ± 0.07 mM during the night. Paired *t*-tests revealed no significant differences between day and night for hippocampal oxygen ($t = 0.3361$; $df = 9$; $P > 0.05$) or for glucose ($t = 1.700$; $df = 9$; $P > 0.05$). However, it must be noted that hippocampal oxygen levels fluctuate based on activity (McHugh *et al.*, 2011) so it is difficult to determine a true basal concentration.

8.3.4 *+-Maze experiments*

Glucose has been measured in the hippocampus utilising the microdialysis technique by research groups such as McNay as discussed in Section 8.1, however, data using biosensors during the +-maze task has not been obtained. Hippocampal oxygen data has been presented during maze tasks (McHugh *et al.*, 2011) yet the simultaneous measurement of glucose and oxygen using sensors and biosensors has not been explored. This section examines the effect of glucose on performance in the +-maze task as well as the changes in glucose and oxygen levels for saline-treated and glucose-treated animals before, during and after the +-maze task (Section 3.7.7).

8.3.4.1 Effect of glucose treatment on performance in the +-maze task

It has been found that an i.p. injection of glucose has a cognitive enhancing effect (McNay *et al.*, 2000). A significant difference was found between the saline-treated control group and the glucose-treated group. Glucose-treated animals were shown to perform superiorly during the +-maze task compared to the control group. The cognitive enhancing effect for

glucose treatment was investigated. 30 min prior to being placed in the +-maze the control group was treated with saline (0.9 %; 1.0 ml/kg i.p.; *n*=5) and the other was treated with glucose (250 mg/kg; 1.0 ml/kg i.p.; *n*=6).

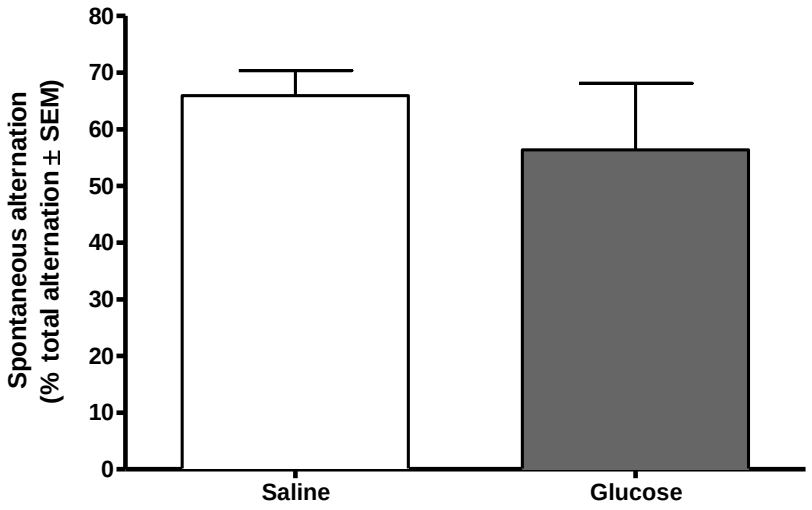

Figure 8.22: Spontaneous alternation scores (% total possible alternations ± SEM) for animals in the +-maze following treatment with either saline (0.9 % i.p.; *n* = 5) or glucose (250 mg/kg i.p.; *n* = 6).

From the results presented in Figure 8.22 it can be seen there was no significant difference between the percentage of spontaneous alternations performed by either group with a *P* value of 0.4620. It can be concluded that there is no cognitive enhancing effect for glucose-treated animals.

8.3.4.2 Effect of glucose treatment on hippocampal glucose, monitored using Pt/PPD/GOx electrodes

McNay and colleagues (2000) demonstrated that in addition to a cognitive enhancing effect for glucose treatment, such animals showed no performance-related reduction in hippocampal glucose levels. The saline-treated group showed a decrease in hippocampal glucose during the 20 min +-maze exploration trial. The administration of saline and glucose on hippocampal oxygen and glucose was measured using CPEs and Pt/PPD/GOx electrodes respectively. A typical raw data trace for each of these treatments is presented below in Figure 8.23.

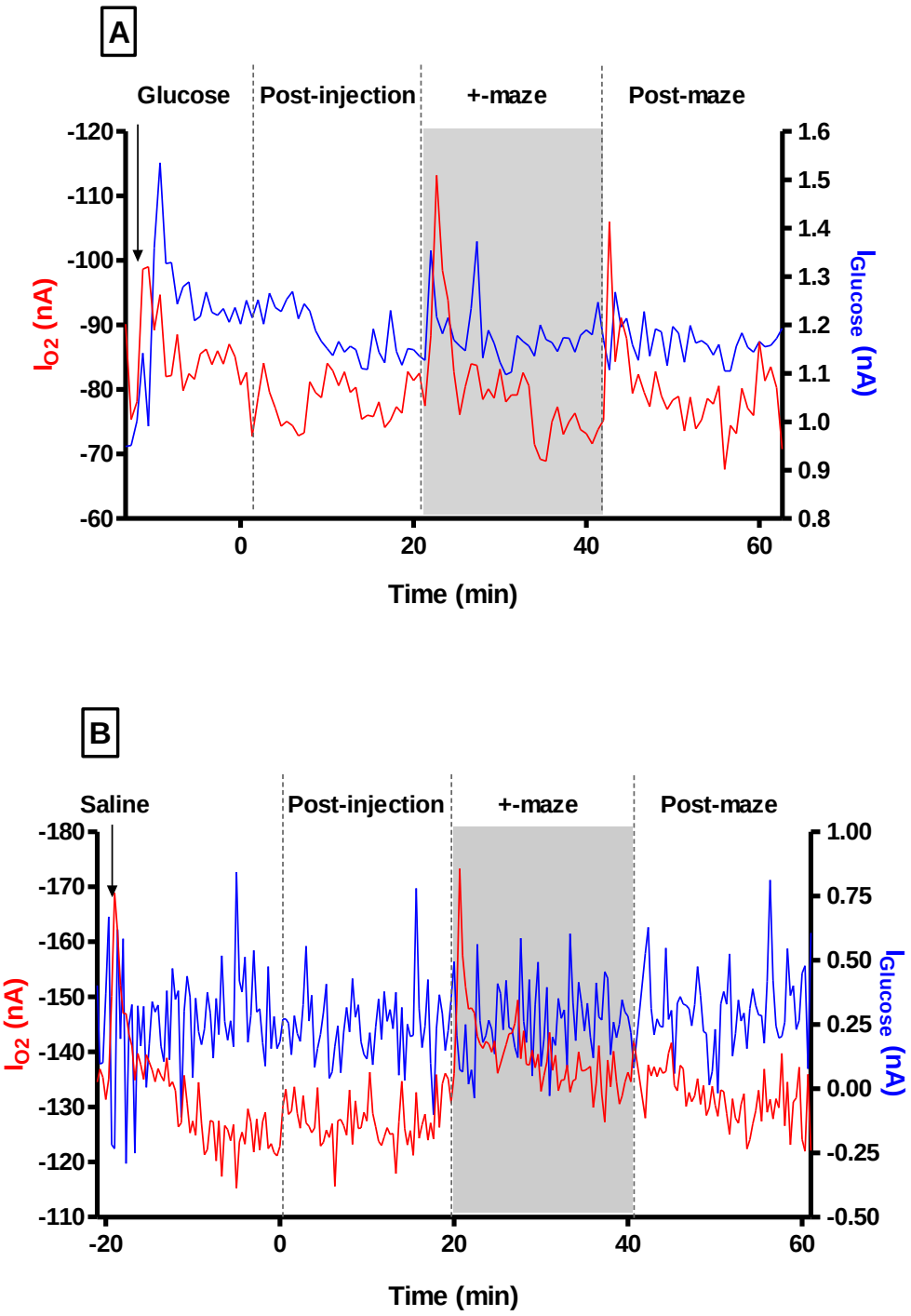

Figure 8.23: Typical raw data traces for oxygen and glucose from (A) an animal treated with saline (0.9 % i.p.) and (B) an animal treated with glucose (250 mg/kg i.p.) performing a +-maze task, monitored in the hippocampus using CPEs and Pt/PPD/GOx electrodes.

Data was averaged over 5 min periods to allow for direct comparisons to microdialysis data. Data was also averaged over 1 min periods to show the information that is lost over 5 min averaging, demonstrating the limitations of microdialysis. Data was normalised to the post-injection time period (the 20 min prior to the maze).

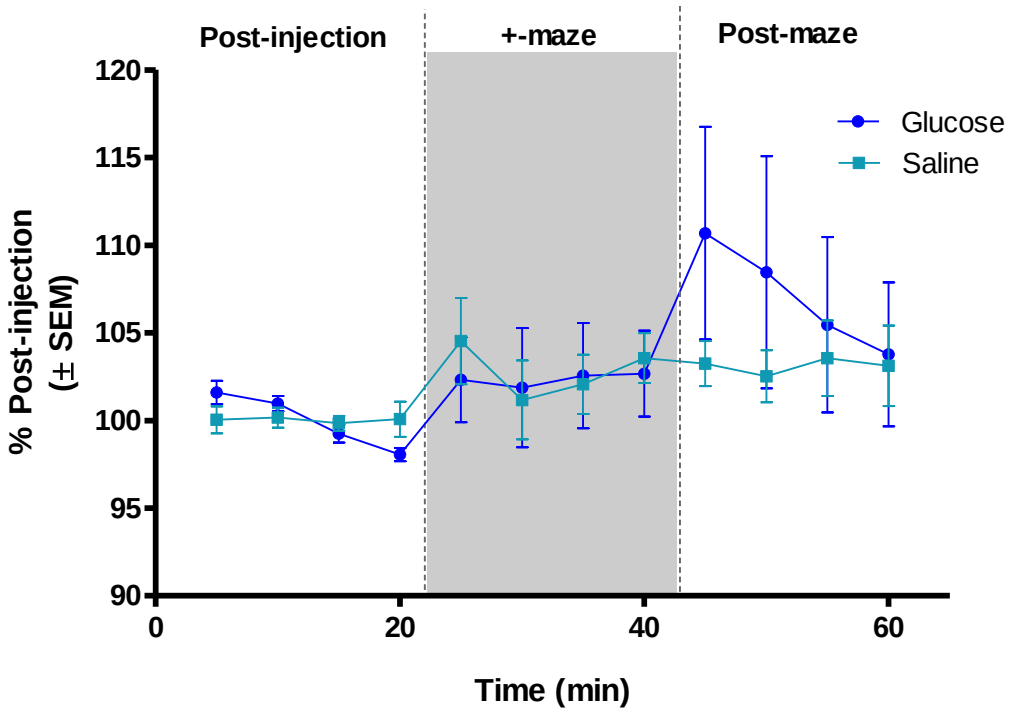

Figure 8.24: Hippocampal glucose monitored using Pt/PPD/GOx electrodes showing the average changes in glucose before, during and after a +-maze task with saline (*n*=5) and glucose (*n*=6) treated animals. Data averaged in 5 min time bins with all data normalised to baseline levels.

For data averaged over 5 min periods (Figure 8.24), a 2 x 12 repeated measures ANOVA showed that there was a significant effect for time on hippocampal glucose (F = 2.47; df = 11, 110; $P < 0.01$). There was no significant effect for drug treatment (F = 0.362; df = 1, 110; $P > 0.05$) and there was no interaction effect (F = 0.898; df = 11, 110; $P > 0.05$). A one way repeated ANOVA failed to show any significant differences between time points in either the saline-treated (F = 1.19; df = 11, 55; $P > 0.05$) or glucose-treated groups (F = 1.78; df = 11, 55; $P > 0.05$).

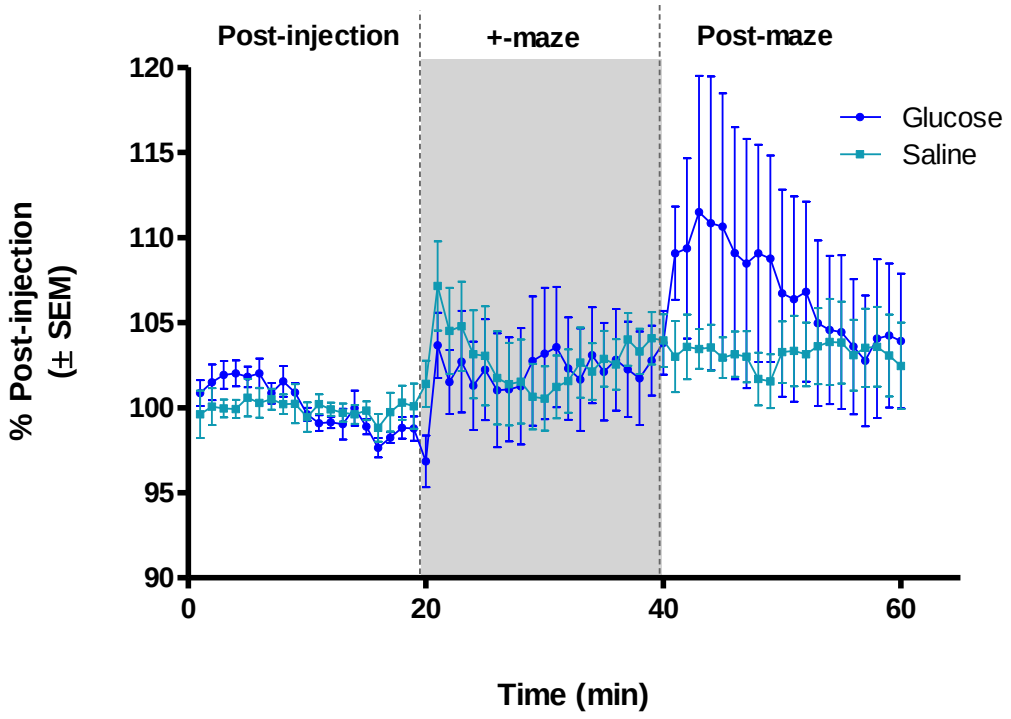

Figure 8.25: Hippocampal glucose monitored using Pt/PPD/GOx electrodes showing the average changes in glucose before, during and after a +-maze task with saline (*n*=5) and glucose (*n*=6) treated animals. Data averaged in 1 min time bins with all data normalised to baseline levels.

Data averaged over 1 min periods (Figure 8.25) also showed a significant effect for time on hippocampal glucose following a 2 x 60 repeated measures ANOVA (F = 2.07; df = 59, 590; $P < 0.001$). There was no significant effect for drug treatment (F = 0.338; df = 1, 590; $P > 0.05$) and there was no interaction effect (F = 0.796; df = 59, 590; $P > 0.05$). Unlike the data averaged over 5 min, a one way repeated ANOVA revealed that there was a significant difference between time points in the saline-treated group (F = 1.50; df = 59, 295; $P < 0.05$). From results presented in this section it can be seen that there is an increase in hippocampal glucose during exploration of the +-maze followed by a further increase when animals were returned to their home bowl therefore it can be determined that there is no performance related reduction in hippocampal glucose during the +-maze task.

8.3.4.3 Effect of glucose treatment on hippocampal O_2

The administration of saline and glucose on hippocampal oxygen was measured using CPEs during a +-maze task. Data was averaged over 5 min periods and over 1 min periods to allow comparisons to hippocampal glucose data presented in Section 8.3.4.2. Data was normalised to the post-injection time period (the 20 min prior to the maze).

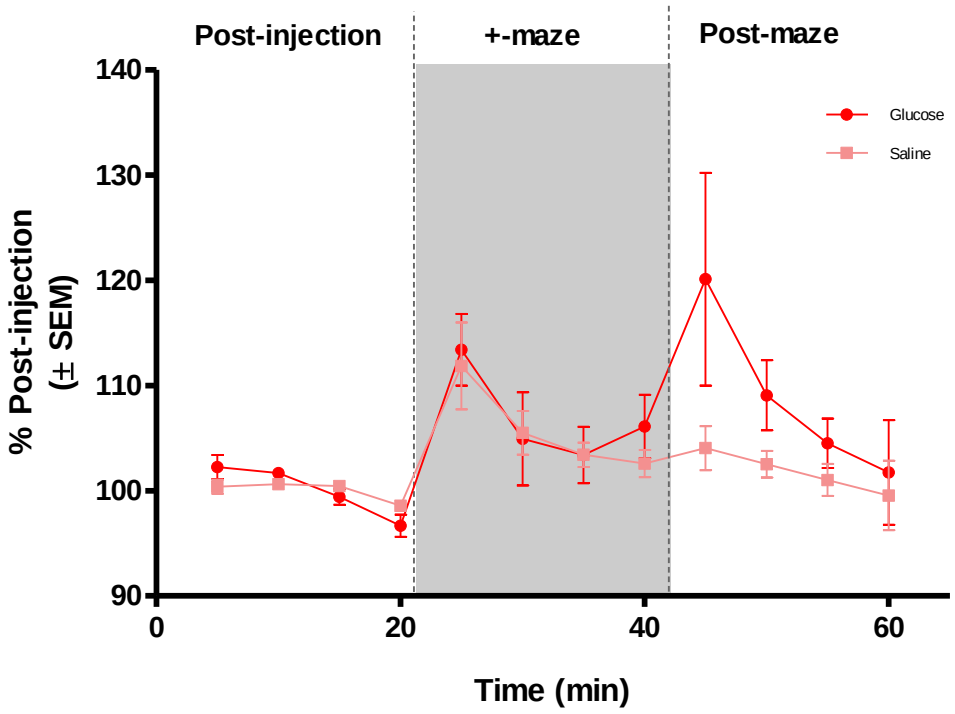

Figure 8.26: Hippocampal oxygen monitored using CPEs showing the average changes in oxygen before, during and after a +-maze task with saline (*n*=5) and glucose (*n*=6) treated animals. Data averaged in 5 min time bins with all data normalised to baseline levels.

For data averaged over 5 min periods (Figure 8.26), a 2 x 12 repeated measures ANOVA showed that there was a significant effect for time on hippocampal O_2 (F = 4.30; df = 11, 110; $P < 0.001$). There was no significant effect for drug treatment (F = 3.66; df = 1, 110; $P > 0.05$) and there was no interaction effect (F = 1.18; df = 11, 110; $P > 0.05$). One way repeated ANOVA showed significant differences between time points in the saline-treated group (F = 3.62; df = 11, 55; $P < 0.001$).

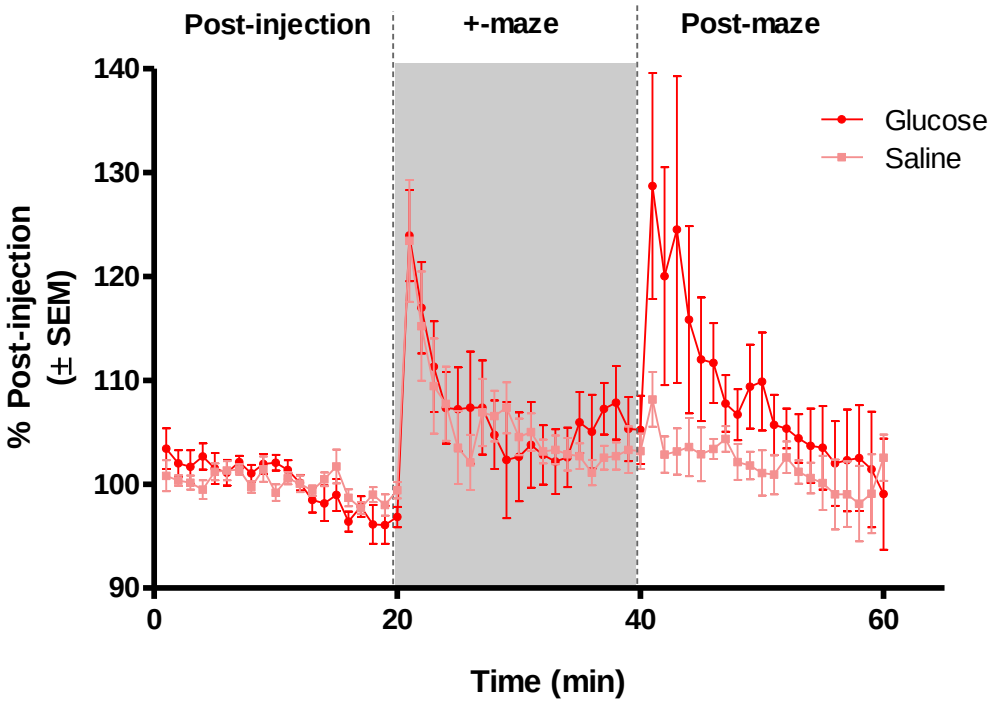

Figure 8.27: Hippocampal oxygen monitored using CPEs showing the average changes in oxygen before, during and after a +-maze task with saline (*n*=5) and glucose (*n*=6) treated animals. Data averaged in 1 min time bins with all data normalised to baseline levels.

Data averaged over 1 min periods (Figure 8.27) showed a significant effect for time on hippocampal O_2 following a 2 x 60 repeated measures ANOVA (F = 4.53; df = 59, 590; P < 0.001). There was no significant effect for drug treatment (F = 3.62; df = 1, 590; P > 0.05) and there was no interaction effect (F = 1.20; df = 59, 590; P > 0.05). A one way repeated ANOVA revealed that there was a significant difference between time points in the saline-treated group (F = 3.88; df = 59, 295; P < 0.001).

From results presented in this section it can be seen that there is a significant increase in hippocampal oxygen in the first minutes in the maze and the first minutes following the animal being returned to the home bowl following the +-maze task. As with the hippocampal glucose data (Section 8.3.4.3), there is some loss of accuracy by averaging over 5 min and the greater accuracy gained from using a smaller time resolution allows for a more complete picture of the changes occurring in the brain at any given time.

8.4 Conclusions

CPEs have been previously used to measure hippocampal oxygen during various behavioural tasks (McHugh *et al.*, 2011). Results presented in this chapter demonstrate the characterisation of hippocampal metabolism using CPEs and Pt/PPD/GOx electrodes and demonstrate that the temporal relationships between hippocampal oxygen and glucose levels vary during a number of different conditions.

As discussed previously there have been few studies in which sensors are used to measure hippocampal glucose as the popular choice is the microdialysis technique. Reported values for the glucose concentration in freely-moving rats in the hippocampus are between 1-1.5 mM: 1.00 ± 0.06 mM (McNay & Gold, 1999), 1.20 ± 0.03 mM (McNay et al., 2000), 1.05 ± 0.02 mM (McNay & Sherwin, 2004), 1.49 ± 0.05 mM (Rex et al., 2009) and 1.36 ± 0.04 mM (De Bundel et al., 2009) higher than our findings of 0.60 ± 0.06 mM. These studies utilise a zero net flux (ZNF) model of measuring glucose and there has been criticism of the use of this method to determine basal concentrations of analytes in the brain due to the trauma caused by the implantation of the microdialysis probe (Chen, 2003, 2005b, a, 2006). These criticisms are reinforced by the discrepancies observed between sensor recordings and microdialysis analysis due to the trauma caused by the much larger microdialysis probe (Khan & Michael, 2003). Our concentration may also be artificially lower than actual concentrations as it has been shown that enzyme-based sensors have a tendency to lose 20-50 % sensitivity when implanted into the brain (Hu et al., 1994). From these results and previous findings it is thought that the basal glucose concentration in the hippocampus is somewhere between our estimate and those of the microdialysis studies referenced above.

Reported values for oxygen levels in the hippocampus are 33.6 mm Hg (~52.8 µM) in the anaesthetised gerbil (Nair et al., 1987) and 20.3 mm Hg (~31.9 µM) in the anaesthetised rat (Cater *et al.*, 1961) much lower than our basal findings of 100.26 ± 5.78 µM. These findings are only an estimate since baseline levels are difficult to establish as it is hard to objectively determine what constitutes a baseline level of activity when considering the normal functions of a specific brain region, and overall changes in rCBF could impact on the oxygen levels.

Results presented in Section 8.3.3.2.1 show that neuronal activation in the form of a tail pinch cause an increase in hippocampal oxygen, similar to findings in the striatum (Bolger & Lowry, 2005). There was also an increase in hippocampal glucose, not consistent with findings in the striatum (Lowry *et al.*, 1998a) where a decrease in striatal glucose was reported during a tail pinch and post-tail pinch a increase in glucose higher than baseline levels. This effect of the tail pinch on striatal glucose has also been found using microdialysis (Fray *et al.*, 1996). Findings in this thesis show an overshoot in hippocampal oxygen following removal of the clip and glucose rapidly returning to baseline levels. It appears there is an increase in supply of hippocampal oxygen with a simultaneous increase in utlisation during the tail pinch. Evidence for this is derived from the increase in oxygen when the clip is removed, the utlisation of hippocampal oxygen decreases as neuronal activation decreases. However the supply remains elevated for several minutes upon removal of the clip thought to reflect an increase in the rCBF due to the stress induced increase in activity of the animal. This increase may be due to an increase in locomotor activity which has been shown to be closely associated to increases in the hippocampal oxygen signal (McHugh *et al.*, 2011). For hippocampal glucose an increase in its supply but not in utilisation is observed, as tissue levels increased during the tail pinch. This would suggest an alternative use for glucose during the tail pinch compared to the striatum. Differences in the brain regions are not unexpected as neuronal activation in the form of a tail pinch has been shown to increase striatal dopamine and ascorbic acid compared with and increase in 5-hydroxytryptamine and 5-hydroxyindole acetic acid in the hippocampus (Boutelle et al., 1990), possibly indicating different mechanisms and roles for the two regions.

An increase in hippocampal oxygen was observed following the administration of acetazolamide which is similar to findings in the striatum where the increase in striatal oxygen was correlated to rCBF (Bolger & Lowry, 2005). In order to administer acetazolamide the solvent DMSO was used as a vehicle for drug administration. From the data presented in Sections 8.3.3.3.2 and 8.3.3.4.1 it can be seen that DMSO treatment resulted in a significant increase in hippocampal glucose seen approximately 3 hours post-injection and this was also observed following acetazolamide treatment. Acetazolamide administration in the absence of DMSO is not associated with any changes in striatal

glucose (Dixon *et al.*, 2002), suggesting that acetazolamide has no effect on hippocampal glucose but the vehicle (DMSO) does. DMSO's effect on brain metabolism has been previously suggested. The application of DMSO to brain slices, increases glucose consumption and *in vitro* administration of DMSO has been shown to cause more varied dose-dependent in effects on glucose metabolism (Nasrallah *et al.*, 2008) Comparing our results to those of these other groups where with low concentrations of DMSO administered directly to brain tissue causes rapid changes in glucose metabolism in contrast to our findings where high concentrations of DMSO administered intraperitoneally caused a delayed but long-lasting increase in glucose concentration, perhaps reflecting a decrease in glucose consumption over longer time periods.

Results for the administration of the anaesthetic chloral hydrate (Section 8.3.3.5) show an increase in hippocampal oxygen during anaesthesia and an increase following return to consciousness. These results are similar to results found in the striatum (Bolger & Lowry, 2005). This increase in oxygen is associated with a decrease in neuronal activation and an increase in rCBF (Lowry et al., 1998a; Lowry & Fillenz, 2001). The suppression of neural activity by anaesthesia and its effects on glucose in the brain has been previously demonstrated using a number of different anaesthetic agents, including chloral hydrate (Fellows *et al.*, 1992; Fillenz & Lowry, 1998; Lowry *et al.*, 1998a; Lowry & Fillenz, 2001; Uematsu *et al.*, 2009; Horn & Klein, 2010). The increase in hippocampal glucose during anaesthesia has been observed with hippocampal microdialysis data (Horn & Klein, 2010), the striatum (Fellows et al., 1992) and also from glucose biosensor data in the cortex (Netchiporouk *et al.*, 2001). Conflicting results have also been reported using electrochemical detection in the striatum where the administration of chloral hydrate has been associated with a decrease in tissue glucose (Fillenz & Lowry, 1998; Lowry & Fillenz, 2001). It would be expected that a decrease in neuronal activity would result in an increase in tissue glucose due to decreased utilisation. This is supported by evidence to suggest that the brain switches between glucose and lactate as energy substrates during different levels of activity (Dienel & Hertz, 2001). The utilisation of glucose by the brain has been suggested to be dependent on neuronal activity (Serres *et al.*, 2005) and revealed that there is an increased utilisation of lactate during chloral hydrate anaesthesia, suggesting

that the brain switches to lactate as the energy source during this anaesthesia (Yamada *et al.*, 2009) and other anaesthetic conditions (Serres *et al.*, 2004; Horn & Klein, 2010).

Results presented in Section 8.3.4 show the simultaneous measurement of glucose and oxygen using Pt/PPD/GOx electrodes and CPEs respectively during a +-maze task. It has been shown that sensors and biosensors can be applied to maze experiments to allow for behavioural and electrochemical data to be simultaneously obtained in real-time. The cognitive enhancing effect for glucose treatment reported by McNay *et al.* (2000) and the performance related reduction in hippocampal glucose levels was investigated using glucose and oxygen electrodes. Our results show no cognitive enhancement for glucose-treated animals and no performance related reduction in hippocampal glucose during the +-maze task.

Results presented in this chapter demonstrate that neuronal activation (increased during tail pinch, restraint test and decreased during anaesthesia) can alter levels of hippocampal oxygen and glucose, and changes in hippocampal oxygen following administration of acetazolamide can be monitored. It has also been determined that hippocampal oxygen and glucose can be measured in freely-moving animals for behavioural experiments providing a valuable tool to enable real-time neurochemical data and behavioural data to be obtained simultaneously.

References

Antelman SM, Szechtman H, Chin P & Fisher AE. (1975). Tail pinch-induced eating, gnawing and licking behavior in rats: Dependence on the nigrostriatal dopamine system. *Brain Research* **99,** 319-337.

Barry DN & Commins S. (2011). Imaging spatial learning in the brain using immediate early genes: insights, opportunities and limitations. *Reviews in the Neurosciences* **22,** 131-142.

Bast T. (2011). The hippocampal learning-behavior translation and the functional significance of hippocampal dysfunction in schizophrenia. *Current Opinion in Neurobiology* **21,** 492-501.

Bliss TVP & Lømo T. (1973). Long-lasting potentiation of synaptic transmission in the dentate area of the anaesthetized rabbit following stimulation of the perforant path. *The Journal of Physiology* **232,** 331-356.

Bolger F & Lowry J. (2005). Brain Tissue Oxygen: *In Vivo* Monitoring with Carbon Paste Electrodes. *Sensors* **5,** 473-487.

Bolger FB, McHugh SB, Bennett R, Li J, Ishiwari K, Francois J, Conway MW, Gilmour G, Bannerman DM, Fillenz M, Tricklebank M & Lowry JP. (2011). Characterisation of carbon paste electrodes for real-time amperometric monitoring of brain tissue oxygen. *Journal of neuroscience methods* **195,** 135-142.

Bonilha L, Martz GU, Glazier SS & Edwards JC. (2012). Subtypes of medial temporal lobe epilepsy: Influence on temporal lobectomy outcomes? *Epilepsia* **53,** 1-6.

Boutelle MG, Zetterström T, Pei Q, Svensson L & Fillenz M. (1990). *In vivo* neurochemical effects of tail pinch. *Journal of neuroscience methods* **34,** 151-157.

Cater DB, Garattini S, Marina F & Silver IA. (1961). Changes of Oxygen Tension in Brain and Somatic Tissues Induced by Vasodilator and Vasoconstrictor Drugs. *Proceedings of the Royal Society of London Series B Biological Sciences* **155,** 136-158.

Chen KC. (2003). Insensitivity of the microdialysis zero-net-flux method to nonlinear uptake and release processes. *Neuroscience Research* **46,** 251-256.

Chen KC. (2005a). Evidence on extracellular dopamine level in rat striatum: implications for the validity of quantitative microdialysis. *Journal of Neurochemistry* **92,** 46-58.

Chen KC. (2005b). Preferentially impaired neurotransmitter release sites not their discreteness compromise the validity of microdialysis zero-net-flux method. *Journal of Neurochemistry* **92,** 29-45.

Chen KC. (2006). Effects of tissue trauma on the characteristics of microdialysis zero-net-flux method sampling neurotransmitters. *Journal of Theoretical Biology* **238,** 863-881.

Clark Jr L & Lyons C. (1965). Studies of a glassy carbon electrode for brain polarography with observations on the effect of carbonic anhydrase inhibition. *The Alabama Journal of Medical Sciences* **2,** 353.

Cloutier M, Bolger F, Lowry J & Wellstead P. (2009). An integrative dynamic model of brain energy metabolism using *in vivo* neurochemical measurements. *Journal of Computational Neuroscience* **27,** 391-414.

Cohen NJ, Ryan J, Hunt C, Romine L, Wszalek T & Nash C. (1999). Hippocampal system and declarative (relational) memory: summarizing the data from functional neuroimaging studies. *Hippocampus* **9,** 83-98.

Colgin LL & Moser EI. (2010). Gamma Oscillations in the Hippocampus. *Physiology* **25,** 319-329.

D'Hooge R & De Deyn PP. (2001). Applications of the Morris water maze in the study of learning and memory. *Brain Research Reviews* **36,** 60-90.

De Bundel D, Smolders I, Yang R, Albiston AL, Michotte Y & Chai SY. (2009). Angiotensin IV and LVV-haemorphin 7 enhance spatial working memory in rats: Effects on hippocampal glucose levels and blood flow. *Neurobiology of Learning and Memory* **92,** 19-26.

Dhikav V & Anand K. (2011). Potential Predictors of Hippocampal Atrophy in Alzheimers Disease. *Drugs & Aging* **28,** 1-11.

Dienel GA & Hertz L. (2001). Glucose and lactate metabolism during brain activation. *Journal of Neuroscience Research* **66,** 824-838.

Dixon BM, Lowry JP & O'Neill RD. (2002). Characterization *in vitro* and *in vivo* of the oxygen dependence of an enzyme/polymer biosensor for monitoring brain glucose. *Journal of neuroscience methods* **119,** 135-142.

Eacott MJ & Easton A. (2010). Episodic memory in animals: Remembering which occasion. *Neuropsychologia* **48,** 2273-2280.

Fellows LK, Boutelle MG & Fillenz M. (1992). Extracellular Brain Glucose Levels Reflect Local Neuronal Activity: A Microdialysis Study in Awake, Freely Moving Rats. *Journal of Neurochemistry* **59,** 2141-2147.

Fillenz M & Lowry J. (1998). The relation between local cerebral blood flow and extracellular glucose concentration in rat striatum. *Experimental Physiology* **83,** 233-238.

Fray AE, Forsyth RJ, Boutelle MG & Fillenz M. (1996). The mechanisms controlling physiologically stimulated changes in rat brain glucose and lactate: a microdialysis study. *The Journal of Physiology* **496,** 49-57.

Freund TF, Buzsáki G, Prohaska OJ, Leon A & Somogyi P. (1989). Simultaneous recording of local electrical activity, partial oxygen tension and temperature in the rat hippocampus with a chamber-type microelectrode. Effects of anaesthesia, ischemia and epilepsy. *Neuroscience* **28,** 539-549.

Gold PE. (2003). Acetylcholine modulation of neural systems involved in learning and memory. *Neurobiology of Learning and Memory* **80,** 194-210.

Gooney M, Shaw K, Kelly A, O'Mara S & Lynch M. (2002). Long-term potentiation and spatial learning are associated with increased phosphorylation of TrkB and extracellular signal-regulated kinase (ERK) in the dentate gyrus: evidence for a role for brain-derived neurotrophic factor. *Behavioral Neuroscience* **116,** 455.

Heckers S & Konradi C. (2010). Hippocampal pathology in schizophrenia. *Behavioral Neurobiology of Schizophrenia and Its Treatment***,** 529-553.

Horn T & Klein J. (2010). Lactate levels in the brain are elevated upon exposure to volatile anesthetics: A microdialysis study. *Neurochemistry international* **57,** 940-947.

Hu Y, Mitchell KM, Albahadily FN, Michaelis EK & Wilson GS. (1994). Direct measurement of glutamate release in the brain using a dual enzyme-based electrochemical sensor. *Brain Research* **659,** 117-125.

Hu Y & Wilson GS. (1997). Rapid Changes in Local Extracellular Rat Brain Glucose Observed with an *In Vivo* Glucose Sensor. *Journal of Neurochemistry* **68,** 1745-1752.

Khan AS & Michael AC. (2003). Invasive consequences of using micro-electrodes and microdialysis probes in the brain. *TrAC Trends in Analytical Chemistry* **22,** 503-508.

López-Pérez SJ, Morales-Villagrán A, Ventura-Valenzuela J & Medina-Ceja L. (2012). Short- and long-term changes in extracellular glutamate and acetylcholine concentrations in the rat hippocampus following hypoxia. *Neurochemistry international* **61,** 258-265.

Lowry JP, Boutelle MG & Fillenz M. (1997). Measurement of brain tissue oxygen at a carbon paste electrode can serve as an index of increases in regional cerebral blood flow. *Journal of neuroscience methods* **71,** 177-182.

Lowry JP, Boutelle MG, O'Neill RD & Fillenz M. (1996). Characterization of carbon paste electrodes *in vitro* for simultaneous amperometric measurement of changes in oxygen and ascorbic acid concentrations *in vivo*. *The Analyst* **121,** 761-766.

Lowry JP, Demestre M & Fillenz M. (1998a). Relation between Cerebral Blood Flow and Extracellular Glucose in Rat Striatum during Mild Hypoxia and Hyperoxia. *Developmental Neuroscience* **20,** 52-58.

Lowry JP & Fillenz M. (2001). Real-time monitoring of brain energy metabolism in vivo using microelectrochemical sensors: the effects of anesthesia. *Bioelectrochemistry* **54,** 39-47.

Lowry JP, McAteer K, El Atrash SS, Duff A & O'Neill RD. (1994). Characterization of Glucose Oxidase-Modified Poly(phenylenediamine)-Coated Electrodes *in vitro* and *in vivo*: Homogeneous Interference by Ascorbic Acid in Hydrogen Peroxide Detection. *Analytical Chemsitry* **66,** 1754-1761.

Lowry JP, Miele M, O'Neill RD, Boutelle MG & Fillenz M. (1998b). An amperometric glucose-oxidase/poly(*o*-phenylenediamine) biosensor for monitoring brain extracellular glucose: *in vivo* characterisation in the striatum of freely-moving rats. *Journal of neuroscience methods* **79,** 65-74.

Lowry JP, O'Neill RD, Boutelle MG & Fillenz M. (2002). Continuous monitoring of extracellular glucose concentrations in the striatum of freely moving rats with an implanted glucose biosensor. *Journal of Neurochemistry* **70,** 391-396.

Marlatt M & Lucassen P. (2010). Neurogenesis and Alzheimers Disease: Biology and Pathophysiology in Mice and Men. *Current Alzheimer Research* **7,** 113-125.

Martin S, Grimwood P & Morris R. (2000). Synaptic plasticity and memory: an evaluation of the hypothesis. *Annual review of neuroscience* **23,** 649-711.

McHugh SB, Fillenz M, Lowry JP, Rawlins JN & Bannerman DM. (2011). Brain tissue oxygen amperometry in behaving rats demonstrates functional dissociation of dorsal and ventral hippocampus during spatial processing and anxiety. *European Journal of Neuroscience* **33,** 322-337.

McNay EC, Fries TM & Gold PE. (2000). Decreases in rat extracellular hippocampal glucose concentration associated with cognitive demand during a spatial task. *Proceedings of the National Academy of Sciences USA* **97,** 2881-2885.

McNay EC & Gold PE. (1999). Extracellular Glucose Concentrations in the Rat Hippocampus Measured by Zero-Net-Flux. *Journal of Neurochemistry* **72,** 785-790.

McNay EC, McCarty RC & Gold PE. (2001). Fluctuations in Brain Glucose Concentration during Behavioral Testing: Dissociations between Brain Areas and between Brain and Blood. *Neurobiology of Learning and Memory* **75,** 325-337.

McNay EC & Sherwin RS. (2004). Effect of Recurrent Hypoglycemia on Spatial Cognition and Cognitive Metabolism in Normal and Diabetic Rats. *Diabetes* **53,** 418-425.

Minichiello L. (2009). TrkB signalling pathways in LTP and learning. *Nature Reviews Neuroscience* **10,** 850-860.

Morris R, Garrud P, Rawlins J & O'Keefe J. (1982). Place navigation impaired in rats with hippocampal lesions. *Nature* **297,** 681-683.

Morris RGM, Moser EI, Riedel G, Martin SJ, Sandin J, Day M & O'Carroll C. (2003). Elements of a neurobiological theory of the hippocampus: the role of activity-dependent synaptic plasticity in memory. *Philosophical Transactions of the Royal Society of London Series B: Biological Sciences* **358,** 773-786.

Nair PK, Buerk DG & Halsey J. (1987). Comparisons of oxygen metabolism and tissue PO_2 in cortex and hippocampus of gerbil brain. *Stroke* **18,** 616-622.

Nasrallah FA, Garner B, Ball GE & Rae C. (2008). Modulation of brain metabolism by very low concentrations of the commonly used drug delivery vehicle dimethyl sulfoxide (DMSO). *Journal of Neuroscience Research* **86,** 208-214.

Netchiporouk L, Shram N, Salvert D & Cespuglio R. (2001). Brain extracellular glucose assessed by voltammetry throughout the rat sleep–wake cycle. *European Journal of Neuroscience* **13,** 1429-1434.

O'Keefe J & Nadel L. (1978). *The Hippocampus as a Cognitive Map*. Clarendon Press, Oxford.

Rex A, Bert B, Fink H & Voigt JP. (2009). Stimulus-dependent changes of extracellular glucose in the rat hippocampus determined by *in vivo* microdialysis. *Physiology & behavior* **98,** 467-473.

Scoville WB & Milner B. (1957). Loss of recent memory after bilateral hippocampal lesions. *Journal of Neurology, Neurosurgery & Psychiatry* **20,** 11-21.

Serres S, Bezancon E, Franconi J-M & Merle M. (2004). *Ex Vivo* Analysis of Lactate and Glucose Metabolism in the Rat Brain under Different States of Depressed Activity. *Journal of Biological Chemistry* **279,** 47881-47889.

Serres S, Bezancon E, Franconi J-M & Merle M. (2005). *Ex vivo* NMR study of lactate metabolism in rat brain under various depressed states. *Journal of Neuroscience Research* **79,** 19-25.

Uematsu M, Takasawa M, Hosoi R & Inoue O. (2009). Uncoupling of flow and metabolism by chloral hydrate: a rat *in-vivo* autoradiographic study. *NeuroReport* **20,** 219-222

Yamada A, Yamamoto K, Imamoto N, Momosaki S, Hosoi R, Yamaguchi M & Inoue O. (2009). Lactate is an alternative energy fuel to glucose in neurons under anesthesia. *NeuroReport* **20,** 1538-1542

9. GENERAL CONCLUSIONS

9.1 Introduction

The field of neurochemical analysis using electrochemical techniques has advanced significantly over the last fifty years since the first design of an electrode for detection in brain tissue by Clarke *et al*. (Clark *et al.*, 1958; Clark Jr & Lyons, 1965). It was not until Adams and co-workers published their seminal paper in 1973, that voltammetric techniques were more widely incorporated as an analytical tool for monitoring electroactive species in the brain (Kissinger *et al.*, 1973). This work is the foundation for the research presented in this thesis which attempts to further understand brain energy metabolism via the development oxygen sensors for potential use in clinical environments, as well as in conjunction with pre-clinical fMRI imaging studies. The monitoring of glucose and oxygen in the hippocampus to determine how basic behavioural and pharmacological Chapter 4 details the *in vitro* characterisation of carbon paste electrodes (CPEs) and a Pt-based electrode modified with methyl-methacrylate (MMA) which is potentially suitable for use in the clinical environment as it is widely used in a wide variety of life science technologies i.e. hard contact lenses and dental fillings and can be easily sterilised. The effect of changes in temperature, pH, ions, convection, and implantation on the sensitivity of CPEs to O_2 was investigated. Pt-MMA electrodes were fully characterised *in vitro* by determining the sensitivity of the sensor to O_2 and the effects on the sensitivity following exposure to proteins, lipids and brain tissue. The effects of temperatures, pH, ions, convection, interferents and implantation were also examined along with the stability of the sensors in relation to time. It was concluded that Pt-MMA electrodes (-0.093 ± 0.003 $\mu Amm^{-2}\mu M^{-1}$ (n=64)) have a higher sensitivity to O_2 than CPEs (-0.033 ± 0.001 $\mu Amm^{-2}\mu M^{-1}$ (n=24)). The physiological temperature (37°C) affects the sensitivity of CPEs and Pt-MMA electrodes similarly and although convection experiments show that Pt-MMA electrodes are less affected by stirring than CPEs, these results only prove to be relevant for *in vitro* experiments. The effect of implantation of the sensors into the living brain showed that implantation has less of an effect on CPEs than Pt-MMA electrodes, although there was a difference in the implantation period of approximately 2 weeks. Our published data shows that CPEs have a stable baseline over 12 weeks (Bolger *et al.*, 2011b). These results indicate that Pt-MMA electrodes are an ideal choice for detection of brain tissue O_2 *in vivo*

over short periods of time due to their high sensitivity and small probe size (125 µm), but CPEs, given their excellent long-term stability, would be the sensor of choice for long-term monitoring of brain tissue O_2.

Following on from the previous chapter, Chapter 5 investigates and characterises the use of Pt-MMA electrodes for the detection of brain tissue O_2 in the striatum. Pt-based electrodes have been shown to be a potential alternative to CPEs to monitor brain tissue O_2 (Bolger *et al.*, 2011a). Comparisons between the Pt-MMA electrodes were made with striatal CPE data (Bolger & Lowry, 2005). It has been demonstrate that Pt-MMA electrodes have the ability to monitor changes in striatal O_2, evidenced by the response of the sensors to the administration of O_2 and N_2 gases to the animal's snout. The changes in tissue O_2 following neuronal activation in the form of a tail pinch, and the administrations of saline, DMSO, acetazolamide and chloral hydrate have also been demonstrated. Pt-MMA electrodes exhibit a greater change in O_2 current in terms of current density compared to CPEs when implanted in the striatum of freely-moving rats demonstrating that Pt-MMA electrodes provide a viable alternative to CPEs to monitor tissue O_2 in the brain. However, Pt-MMA electrodes are only suitable for short-term monitoring (established in Chapter 4) as there is a large reduction in sensitivity after 19 ± 3 days.

The aim of Chapter 6 was to fabricate a stable and reproducible metal-free electrode for use in conjunction with fMRI studies that can be characterised *in vitro* and *in vivo*. This follows on from work by (Lowry *et al.*) where BOLD fMRI and amperometric tissue O_2 data from rat cerebral cortex was obtained verifying that real-time metabolic information can be acquired during fMRI investigations and that the changes in the magnitude of the BOLD response can be directly correlated to changes in tissue O_2 concentrations. This technique provides an alternative to fMRI experiments as these O_2 sensors can be used in freely-moving animals eliminating the disadvantages of anaesthesia. Carbon fibre electrodes (CFEs) were utilised in this study but were not standardised in terms of manufacture. There were variations in both the amounts of carbon fibre strands that were used in each electrode and also the length of the carbon fibres. Due to the varying

dimensions of the carbon fibre bundle, reproducibility was difficult to obtain therefore hindering the characterisation of these sensors. The chapter initially explored the standardisation of the CFEs which proved not to be successful so the examination of carbon-based composite electrode incorporating a CF transducer was investigated. A carbon Rhoplex® composite electrode (CRCE) was developed and subsequently characterised *in vitro*. CRCEs were found to be biocompatible with no significant reduction in the sensitivity following exposure to proteins, lipids and brain tissue. However, the physiological temperature (37°C) affects the CRCEs causing a large increase in sensitivity. Changes in pH did have an effect on the sensitivity, though changes in ions showed no significant effect. The effect of implantation of the sensors into the living brain indicated that implantation has a detrimental effect on the sensitivity of the CRCEs which is thought to be due to fouling of the active surface of the electrodes. During preliminary acute *in vivo* experiments (Chapter 7) using the CRCE it was found that the electrodes background current did not reach a steady state quickly enough for experiments to take place. An fMRI compatible acute design was explored with an attempt at minimising the settling time which was unsuccessful. The original CRCE design was found to be the superior design. CRCEs can therefore be deemed suitable for use in chronic *in vivo* fMRI experiments for the detection of brain tissue O_2 with further modifications such as elimination of the majority of the CF wire and pre-conditioning the sensors before the acute *in vivo* experiments by applying a potential to the electrodes overnight prior to the acute implantation.

Chapter 7 investigated and characterised the use of CRCEs for the detection of brain tissue O_2 in the striatum of freely-moving animals, following on from the *in vitro* characterisation in the previous chapter. It has been demonstrated that CRCEs (freely-moving design) have the ability to monitor changes in striatal O_2, evidenced by the response of the sensors to the administration of O_2 and N_2 gases to the animal's snout. The changes in tissue O_2 following neuronal activation in the form of a restraint test, as well as the administrations of acetazolamide and chloral hydrate have also been demonstrated. These results compare well to CPE data (Bolger & Lowry, 2005). It can therefore be concluded that CRCEs provide a viable alternative to metal electrodes to monitor brain tissue O_2 but do not offer

any advantage in comparison to CPEs in terms of stability or biocompatibility. CRCEs are only suitable for short-term monitoring as there is a large reduction in sensitivity after 9 ± 2 days. The preliminary acute experiment using the CRCE full fMRI design performed in an anesthetised animal was not successful due to the background current not stabilising in time. An alternative design was investigated in Chapter 6, however, the original CRCE proved to be the best design in terms of settling time. Therefore an elimination of the CF wire, pre-conditioning the electrodes and alterations to the acute experimental set-up are thought to be the remedy to this problem.

Chapter 7 investigated and characterised the use of CRCEs for the detection of brain tissue O_2 in the striatum of freely-moving animals, following on from the *in vitro* characterisation in the previous chapter. It has been demonstrated that CRCEs (freely-moving design) have the ability to monitor changes in striatal O_2, evidenced by the response of the sensors to the administration of O_2 and N_2 gases to the animal's snout. The changes in tissue O_2 following neuronal activation in the form of a restraint test, as well as the administrations of acetazolamide and chloral hydrate have also been demonstrated. These results compare well to CPE data (Bolger & Lowry, 2005). It can therefore be concluded that CRCEs provide a viable alternative to metal electrodes to monitor brain tissue O_2 but do not offer any advantage in comparison to CPEs in terms of stability or biocompatibility. CRCEs are only suitable for short-term monitoring as there is a large reduction in sensitivity after 9 ± 2 days. The preliminary acute experiment using the CRCE full fMRI design performed in an anesthetised animal was not successful due to the background current not stabilising in time. An alternative design was investigated in Chapter 6, however, the original CRCE proved to be the best design in terms of settling time. Therefore an elimination of the CF wire, pre-conditioning the electrodes and alterations to the acute experimental set-up are thought to be the remedy to this problem.

Continuation of this body of work would involve the application and characterisation of the CRCEs in fMRI studies. This would allow for real-time metabolic information to be acquired during fMRI and allow for tissue O_2 concentrations to be monitored, and the relationship between BOLD and tissue O_2 when variations in metabolic demand are

induced by local stimulation. Although Long-term *In Vivo* Electrochemistry (LIVE) cannot substitute for imaging techniques such as fMRI in terms of providing whole brain information it might however be possible by implanting several electrodes at one time to measure the synchrony of activity between brain regions with a high temporal resolution. As LIVE can be applied to various neurochemicals the combination of these techniques may provide numerous possibilities for investigating the direct relationship between fMRI signal changes and the underlying neurochemistry across a range of different stimulation paradigms. In the case of monitoring tissue O_2 and glucose simultaneously in the hippocampus work is on-going in our group to compare hippocampal activity to different behaviours in a +-maze task. Making it a possibility that LIVE during behavioural tasks can be coupled with drug interventions such as induced disease states and the changes observed can be compared directly to more traditional methods such as electrophysiological recordings and microdialysis sampling.

References

Bolger F & Lowry J. (2005). Brain Tissue Oxygen: *In Vivo* Monitoring with Carbon Paste Electrodes. *Sensors* **5,** 473-487.

Bolger FB, Bennett R & Lowry JP. (2011a). An *in vitro* characterisation comparing carbon paste and Pt microelectrodes for real-time detection of brain tissue oxygen. *The Analyst* **136,** 4028-4035.

Bolger FB, McHugh SB, Bennett R, Li J, Ishiwari K, Francois J, Conway MW, Gilmour G, Bannerman DM, Fillenz M, Tricklebank M & Lowry JP. (2011b). Characterisation of carbon paste electrodes for real-time amperometric monitoring of brain tissue oxygen. *Journal of neuroscience methods* **195,** 135-142.

Clark Jr L & Lyons C. (1965). Studies of a glassy carbon electrode for brain polarography with observations on the effect of carbonic anhydrase inhibition. *The Alabama Journal of Medical Sciences* **2,** 353.

Clark LC, Misrahy G & Fox RP. (1958). Chronically implanted polarographic electrodes. *Journal of Applied Physiology* **13,** 85-91.

Kissinger PT, Hart JB & Adams RN. (1973). Voltammetry in brain tissue - a new neurophysiological measurement. *Brain Research* **55,** 209-213.

Lowry JP, Griffin K, McHugh SB, Lowe AS, Tricklebank M & Sibson NR. (2010). Real-time electrochemical monitoring of brain tissue oxygen: a surrogate for functional magnetic resonance imaging in rodents. *NeuroImage* **52,** 549-555.

Publications and Conferences

In preparation

- Kealy JR, Bennett R & Lowry JP. (2012). Simultaneous recording of hippocampal oxygen and glucose in real time using constant potential amperometry in the freely-moving rat. *Journal of neuroscience methods*, accepted.

Peer-reviewed publications

- Bolger FB, Bennett R & Lowry JP. (2011). An in vitro characterisation comparing carbon paste and Pt microelectrodes for real-time detection of brain tissue oxygen. *The Analyst* **136,** 4028-4035.

- Bolger FB, McHugh SB, Bennett R, Li J, Ishiwari K, Francois J, Conway MW, Gilmour G, Bannerman DM & Fillenz M. (2011). Characterisation of carbon paste electrodes for real-time amperometric monitoring of brain tissue oxygen. *Journal of neuroscience methods* **195,** 135-142.

-

Other publications

- Garry E. M., Kealy J., Russell D., Bennett R., Malpas S., Budgett D., Geoghegan R., Lowry J. (2011) Linking Brain to Behavior: Simultaneous behavioral tracking and continuous brain tissue oxygen monitoring with a fully implantable telemetry system in freely moving rats. *In 2011 Neuroscience Meeting Planner.* Washington, DC: Society for Neuroscience, 2011. Online.

- Bennett, R., Bolger, F.B., Lowry, J.P. (2011) Carbon-based composite electrode for the *in vivo* detection of tissue O_2 suitable for use in fMRI imaging studies. *In Neuroscience Ireland,* Coogan A., Commins S., Roche R., Lowry J.P. National University of Ireland, Maynooth, Co. Kildare, Ireland; pp.44.

- Kealy J., Bennett R., Craig J.D., Lowry J.P. (2011) Characterisation of real-time oxygen and glucose sensors in the hippocampus of freely moving rats. *In Neuroscience Ireland,* Coogan A., Commins S., Roche R., Lowry J.P. National University of Ireland, Maynooth, Co. Kildare, Ireland; pp.47.

- Bennett R., Bolger, F.B., Dalton M., Lowry J.P. (2011) *Characterisation of a Pt-modified sensor for detection of brain tissue oxygen.* Conference on Analytical Sciences Ireland 2011. Dublin City University, Dublin 9, Ireland; pp.73-74.

- Bennett, R., Bolger, F.B., Dalton, M. and Lowry, J.P. (2010) An *in vitro and in vivo* characterisation of a platinum modified sensor for detection of brain tissue oxygen. In *Monitoring Molecules in Neuroscience*, Westerink, B., Clinckers, R., Smolders, I., Sarre, S. and Michotte, Y. (Eds.) Vrije Universiteit Brussel, Brussels, Belgium; pp. 334-335.

- Bennett, R., Bolger, F.B., Lowry, J.P.(2009) Long-Term *In Vivo* Electrochemistry (LIVE): Real Time Monitoring of Brain Energy Metabolism. *DRHEA Module: Electroanalytical Chemistry Modern Techniques and Applications.* National University of Ireland, Maynooth, Co. Kildare, Ireland.

Conferences Attended

- Irish Neurosciences Discussion Group 2009, The Tullamore Court Hotel, Tullamore, Co. Offaly, Ireland.

- 61st Irish Universities Chemistry Research Colloquium 2009, Dublin Institute of Technology, Aungier St., Dublin 2, Ireland.

- 63rd Irish Universities Chemistry Research Colloquium 2011, University College Dublin, Belfield, Dublin 4, Ireland.

- 62nd Irish Universities Chemistry Research Colloquium, Queens University Belfast.